A REAL-TIME MOTION PLANNING FRAMEWORK FOR CONNECTED AND AUTOMATED VEHICLES: FROM THEORY TO SCALED EXPERIMENTS

by

Behdad Chalaki

A dissertation submitted to the Faculty of the University of Delaware in partial fulfillment of the requirements for the degree of Doctor of Philosophy in Mechanical Engineering

Summer 2022

A REAL-TIME MOTION PLANNING FRAMEWORK FOR CONNECTED AND AUTOMATED VEHICLES:

FROM THEORY TO SCALED EXPERIMENTS

by

Behdad Chalaki

Approved: _____

Ajay Prasad, Ph.D.
Chair of the Department of Mechanical Engineering

Approved: _____

Levi T. Thompson, Ph.D.
Dean of the College of Engineering

Approved: _____

Louis F. Rossi, Ph.D.
Vice Provost for Graduate and Professional Education and
Dean of the Graduate College

I certify that I have read this dissertation and that in my opinion it meets the academic and professional standard required by the University as a dissertation for the degree of Doctor of Philosophy.

Signed: _____

Andreas A. Malikopoulos, Ph.D.
Professor in charge of dissertation

I certify that I have read this dissertation and that in my opinion it meets the academic and professional standard required by the University as a dissertation for the degree of Doctor of Philosophy.

Signed: _____

Christos G. Cassandras, Ph.D.
Member of dissertation committee

I certify that I have read this dissertation and that in my opinion it meets the academic and professional standard required by the University as a dissertation for the degree of Doctor of Philosophy.

Signed: _____

Ioannis Poulakakis, Ph.D.
Member of dissertation committee

I certify that I have read this dissertation and that in my opinion it meets the academic and professional standard required by the University as a dissertation for the degree of Doctor of Philosophy.

Signed: _____

Ajay K. Prasad, Ph.D.
Member of dissertation committee

Dedicated to my parents, brother, and soulmate, Shadi

تقدیم به پدر، مادر، برادر و همراه همیشگی من شادی

ACKNOWLEDGEMENTS

As my adventurous yet joyful path toward Ph.D. is coming to an end, I want to thank and acknowledge the support I received throughout this journey. First, I need to express my deepest gratitude to Professor Andreas Malikopoulos for his outstanding support and being an excellent advisor and mentor. His being supportive and guiding me in the right direction while giving me the trust and autonomy to research the area of my interest have been an excellent catalyst for my growth both in academic and personal life.

I would like to sincerely thank Professor Ajay Prasad, Professor Ioannis Poulakakis, and Professor Christos Cassandras for serving on my committee. Indeed, this dissertation would not have been possible without their valuable and constructive feedback. I want to thank Professor Prasad since his different perspective has helped me look at my problem from a broader point of view and consider the big picture. I deeply appreciate Professor Poulakakis since I learned most of the concepts in the control theory through his classes. His passion for control theory and being mathematically rigorous has also shaped my perspective toward my research. Special and deepest thanks to Professor Cassandras for the detailed feedback and guidance he has provided me through several technical meetings and our fruitful discussions.

A great African proven says, "*If you want to go fast, go alone. If you want to go far, go together.*" Building upon this proverb, I would like to thank all information and decision science lab members who made this long journey possible. Specifically, I sincerely appreciate Logan and Ben, who spent so many long nights in the lab with me to get experiments working.

Finally, I dedicate this dissertation to my parents, brother, and soulmate, Shadi, for their sacrifices, constant support, love and encouragement. Their unquestionable support has empowered me and helped me believe in myself and keep going even in the toughest parts of this journey.

TABLE OF CONTENTS

LIST OF TABLES

LIST OF FIGURES

ABSTRACT

Traffic congestion has been persistently growing in the US from 1982 to 2020 since road capacity has not grown at the same pace as the population in urban areas. In 2019, traffic congestion in urban areas in the US caused drivers to spend an extra 8.7 billion hours on the road, purchasing an extra 3.5 billion gallons of fuel for a congestion cost of $\$190$ billion. Global climate change has also resulted in the pressing need for improved energy efficiency and reduced environmental impact on transportation. Additionally, traffic safety is another growing concern. In 2018, there were 5.2M traffic accidents in the US, resulting in more than 38K fatalities and 2.2M people injured. Equipped with capacities of computing capabilities and advanced communication and vehicle technologies, connected and automated vehicles (CAVs) provide novel and innovative opportunities to significantly reduce energy consumption, greenhouse gas emissions, and travel delays while improving passenger safety.

This dissertation goes through a journey from designing an optimal decentralized coordination framework for CAVs at different traffic bottlenecks to implementing and validating them in a scaled testbed. The dissertation consists of three main parts. In the first part, we develop two different bi-level approaches based on a scheduling and recursive algorithm for coordinating CAVs at multiple adjacent signal-free intersections. In the upper-level planning, each CAV computes the arrival time at each intersection along its path while ensuring lateral and rear-end safety. Given the output of the upper-level planning, in the low-level planning, we formulate an optimal control problem for each CAV with the interior-point constraints, the solution of which yields the energy optimal control input (acceleration/deceleration). Considering a signal-free intersection, we present a learning-based decentralized coordination framework consisting of a hysteretic Q-learning combined with a FIFO queuing policy to

minimize travel delay and improve fuel consumption while ensuring rear-end and lateral safety.

In the second part, we provide three different approaches that can extend our framework to consider uncertainty and address it appropriately. We first present a single-level coordination framework for CAVs, in which each CAV computes the optimal unconstrained control trajectory without activating any of the state, control, and safety constraints. We integrate a replanning mechanism into our coordination framework, which can be implemented in a time-driven or event-driven fashion. This embedded replanning aims at introducing indirect feedback into the coordination framework to respond to the unexpected changes in the system to some extent. Using the theory of the job-shop scheduling, we further enhance our decentralized coordination framework by introducing a priority-aware resequencing mechanism, which designates the order of decision making. We formulate a robust coordination framework by including the deviations from the nominal trajectories as uncertainty. We then employ Gaussian process regression to learn the uncertainty from the possibly noisy observation of CAVs' time trajectories. After obtaining the statistical knowledge about the deviation from nominal trajectories, we construct the confidence interval for time, position, and speed trajectories. Finally, we enhance the framework by employing control barrier functions to provide an additional safety layer and ensure the satisfaction of all constraints in the system. Using the proposed coordination framework in the motion planning module, each CAV first uses simple longitudinal dynamics to derive the optimal control trajectory without activating any constraint. We require a vehicle-level controller to track the resulting optimal trajectory in a real physical system. However, the system's constraints may become active due to the inherent deviations between the actual trajectory and the planned trajectory. We address this issue by introducing a barrier-certificate module based on more realistic dynamics as a safety middle layer between the vehicle-level tracking controller and physical vehicle to provide a reactive mechanism to guarantee constraint satisfaction.

In the last part, we introduce the Information and Decision Science Lab's Scaled Smart City (IDS^{3}C), a robotic scaled $(1{:}25)$ testbed capable of safely validating control approaches

beyond simulation in applications related to emerging mobility systems such as coordination of CAVs. Then, we demonstrate the effectiveness of coordination of CAVs at a multi-lane roundabout and show its scalability in a corridor consisting of a roundabout, an intersection, and a merging roadway.

These research contributions together result in a mathematically rigorous framework for the online coordination of CAVs in different traffic scenarios. This dissertation advances the state of the art in utilizing CAVs in real-world traffic scenarios to alleviate congestion, improve traffic throughput, and increase passenger safety.

Chapter 1

INTRODUCTION AND LITERATURE REVIEW

> Oh, come with old Khayyam, and leave the wise;
> To talk; one thing is certain, that life flies;
> One thing is certain, and the rest is lies;
> The flower that once has blown for ever dies.
>
> Omar Khayyam, *Rubaiyat of Omar Khayyam*, 1048–1131 CE

1.1 Motivation

Over the last few decades, the urban population of the world has proliferated. According to a report by the united nations [1], it is projected that 66 % of the population will reside in urban areas by 2050, and by 2030, there would be 41 Mega-cities, which have population over 10 M people. However, in urban areas road capacity has not grown at the same pace, and as a result of the increasing population and travel demand, traffic congestion has become a significant concern in big metropolitan areas around the world. Namely, people in large urban areas across the US have experienced the negative effects of traffic congestion on their daily life. Schrank et al. [2] reported that congestion in the US has been persistently growing from 1982 to 2020. In 2019, traffic congestion in urban areas in the US caused drivers to spend an extra 8.7 billion hours on the road, purchasing an extra 3.5 billion gallons of fuel for a congestion cost of $\$190$ billion. In addition, traffic congestion has a negative impact on traffic safety, in 2018, there were 5.2M traffic accidents in the US resulting in more than 38K fatalities and 2.2M people injured [3]. Singh [4] reported that the immediate reason for 94% of the crashes was assigned to the driver, with recognition errors accounted for about 41%, decision errors 33% and performance errors 11% of the crashes.

Emerging mobility systems, e.g., connected and automated vehicles (CAVs), shared mobility, and electric vehicles, mark a paradigm shift in which a numerous of opportunities exist for users to better monitor the transportation network conditions and make optimal operating decisions [5–7]. Equipped with capacities of computing capabilities and advanced communication and vehicle technologies, CAVs are expected to provide novel and innovative opportunities to transition our current transportation networks into energy-efficient mobility systems. The introduction of CAVs into the transportation system allows vehicles to make better decisions, leading to significant reductions of energy consumption, greenhouse gas emissions, and travel delays along with improvements to passenger safety [8–11]. The generation of massive amounts of vehicle data also creates significant opportunities to develop optimization algorithms for controlling large-scale behaviors for the entire urban transportation system. As we move to increasingly complex emerging mobility systems, new control approaches are needed to optimize the impact on system behavior of the interplay between vehicles at different traffic scenarios [12].

1.2 Literature Review

1.2.1 Coordination of Connected and Automated Vehicles

There have been two major approaches to utilizing connectivity and automation of vehicles, namely, platooning and traffic smoothing. A platoon is defined as a group of closely-coupled vehicles traveling to reduce their aerodynamic drag, especially at high cruising speeds. The concept of platoon formation is a popular system-level approach to address traffic congestion, which gained momentum in the 1980s and 1990s [13–15]. There has been a rich body of research exploring various methods of forming and/or utilizing platoons to improve transportation efficiency [16–30]. The second approach smooths the traffic flow to eliminate stop-and-go driving through optimal coordination through traffic scenarios [31], which gained attention after the seminal work of Levine and Athans [32, 33] on safely coordinating vehicles at merging-road ways. Assuming a given merging sequence, Levine and Athans formulated the merging problem as a linear optimal regulator [32] to control a single string of vehicles,

with the aim of minimizing the speed errors that will affect the desired headway between each consecutive pair of vehicles. Since then, substantial research efforts have been reported in the literature proposing optimal coordination of CAVs in different traffic scenarios such as merging roadways, roundabouts, speed reduction zones, and urban intersections.

According to Rios-Torres and Malikopoulos [34], approaches on coordination of CAVs can be categorized into two major groups, namely, centralized and decentralized. In centralized approaches, there is at least one task in the system that is globally decided for all CAVs by a single central controller. In decentralized approaches, CAVs are treated as autonomous agents that optimize specific performance criteria (e.g., fuel efficiency, travel time) through vehicle to vehicle (V2V) and/or vehicle to infrastructure (V2I) communication.

Centralized Framework

Some work has considered a reservation-based approach for coordination of CAVs at a signal-free intersection, which requires CAVs to reserve a space-time slot inside the intersection [35–42], and then a centralized controller accepts/rejects these requests according to some policy. Dresner and Stone [35, 36] first introduced this scheme based on a first-in-first-out (FIFO) queuing policy. In a sequel paper, Hausknecht et al. [37] extended this scheme to the network of interconnected intersections aimed at exploring the best route to navigate a CAV arriving at the intersection to minimize its delay through the network. Jin et al.[38] further developed the idea of a reservation-based scheme for signal-free intersection and relaxed the FIFO queuing policy. By relaxing FIFO, they showed that their approach resulted in better performance compared to the previous reservation-based schemes based on FIFO.

Several studies reported in the literature have addressed the coordination problem for CAVs using a centralized framework [43–50]. The authors in [43, 44] designed a controller to minimize the total length of overlapped trajectories of CAVs inside the intersection. Gregoire et al. [45] decomposed the coordination problem into a central priority assignment and trajectory planning. Given the priority assignment, they planned a safe trajectory with either

maximum or minimum control inputs. Bichiou and Rakha [46] considered minimizing travel time jointly with control efforts for M closest CAVs to the intersection. Although the authors showed improvement in fuel efficiency and travel time, their approach takes $2-5$ minutes to find the optimal control actions for $M=4$ rendering it inapplicable for real-time implementation. Xu et al. [47] presented a centralized controller to find vehicles' crossing order at a signal-free intersection based on the heuristic tree search methods. Borek et al. [48] presented the energy-optimal control for heavy-duty trucks, which employs an online MPC to track the optimal solution obtained off-line using dynamic programming. Du et al. [49] introduced a tri-level coordination framework for CAVs at multiple intersections. Employing a consensus algorithm, each intersection derives the desired speed limit at the top level to balance the traffic density over multiple intersections. In the middle level, the centralized controllers generate each vehicle's reference velocity, minimizing the deviation from the desired speed limit subject to lateral safety at the intersections. Finally, in the last level, each vehicle employs a fast MPC to track the reference velocity while avoiding rear-end collision.

Other research efforts have used scheduling theory to address the signal-free intersection problem [51–57]. Colombo and Del Vecchio [51] designed an intersection controller for a human driver which only intervenes and overrides the driver's control action when necessary, i.e., acting as a supervisory controller. They demonstrated that determining whether a state belongs to the maximal safe, controlled invariant set is equivalent to solving a scheduling problem. Ahn et al. [52] extended these results to include uncontrolled human drivers. In a sequel paper, Ahn and Del Vecchio [54] solved the supervisory problem for the first-order dynamics without considering the rear-end collision avoidance constraint using a mixed-integer linear program (MILP). Considering first-order dynamics and assuming an imposed speed inside the merging zone. Fayazi and Vahidi [55] proposed a framework based on the arrival time of CAVs at an intersection. Then, they converted the arrival time scheduling problem to a central MILP. Yu et al. [56] formulated the coordination problem of CAVs at multiple intersections as a centralized MILP, the solution of which yields the trajectory of each CAV, along with the lane-changing maneuver decision, minimizing total travel time.

Guney and Raptis [57] proposed a centralized scheduling framework for the coordination of CAVs crossing an intersection. In their approach, the intersection controller finds schedules based on the rule of first-come-first-serve (FCFS).

Decentralized Framework

To date, numerous papers have presented decentralized approaches for the coordination of CAVs at intersections. One of the early efforts was proposed by Makarem and Gillet [58] using a navigation function aimed at minimizing the energy consumption of each CAV. Wu et al. [59] presented an algorithm based on a mutual exclusion in which CAVs compete for the privilege of crossing the intersection through V2V communication. Focusing on V2V communication, Azimi et al. [60] proposed various intersection protocols to improve traffic throughput while avoiding collisions. In their approach, the control zone is considered a grid divided into small cells. In their most advanced protocol, when there is a potential conflict at a cell, a lower-priority CAV can either cross the conflicting cell or arrive at the cell after the higher-priority CAV has exited the cell. Hult et al. [61] presented a bi-level coordination scheme for CAVs crossing a signal-free intersection. The first level is a central controller, which yields the required arrival times for CAVs at the intersection along with CAVs' crossing orders. In the second level, the authors considered a local MPC given the arrival time computed from the first level. Other authors have also formulated a local MPC problem for each CAV with defined crossing priorities [62–64].

In decentralized coordination of CAVs, a number of research efforts have been reported in the literature using optimal control techniques to find closed-form solutions. Following a bi-level framework for addressing the throughput maximization and energy minimization problems, Malikopoulos et al. [65] presented a decentralized coordination framework for CAVs at a signal-free intersection. Using FIFO queuing policy, in the throughput maximization problem, each CAV computes its arrival time at the area of potential lateral collisions called merging zone. In the energy minimization problem, each CAV obtains its optimal acceleration/deceleration inside the control zone subject to speed and control constraints. The

authors considered no turning maneuvers at the intersection and restricted the CAVs to travel with constant speed inside the merging zone. The analytical solution without considering state and control constraints, was presented in [66–68] for coordinating online CAVs at highway on-ramps, in [69, 70] at two adjacent intersections, in [71] at roundabouts and in [72, 73] at a corridor. The solution of the unconstrained problem was also validated experimentally at a scaled testbed in [74] for a merging roadway scenario and in [75] at a corridor. Furthermore, the effectiveness of the decentralized coordination framework at a corridor was validated in a field test in [76]. In a follow-up paper to [65], Malikopoulos and Zhao [77] further enhanced the framework by presenting an analytical solution for the speed-dependent rear-end safety constraint. Relying on FIFO queuing policy, Zhang and Cassandras [78] presented a single-level decentralized coordination framework by formulating the objective function of each CAV to jointly minimize travel time and control effort with considering the minimum distance rear-end safety constraint. The authors provided the analytical solution for speed-dependent rear-end safety constraint in [79]. Following a similar single-level decentralized coordination framework, Xiao and Cassandras [80] derived explicit solutions for the unconstrained case with extensions to optimal trajectories with active constraints and coupled active constraints for CAVs at highway on-ramps.

Additionally, there have been several studies exploring the effects of decision-making sequence for the coordination of CAVs. Campos et al. [81] presented a heuristic approach to find a decision order for CAVs at an intersection based on their time to reach an unsafe set, i.e., the CAV can no longer stop before the intersection. Alrifaee et al. [82] proposed a graph-based approach to construct levels of parallelizable agents for non-cooperative decentralized MPC, in which agents on the same level solve the problem in parallel, sequentially after agents on the previous level. In [83], the authors presented a dynamic resequencing algorithm to relax the FIFO queuing policy by checking all feasible crossing sequences, and choosing the best one in terms of travel time. In a different approach, Xiao and Cassandras [84] relaxed the FIFO queuing policy by formulating a resequencing problem before the control zone. The authors assumed that after a CAV performs the resequencing, its speed remains constant until

it arrives at the control zone.

Owing to the fact that solving a constrained solution leads to solving a system of non-linear equations that might be hard to solve in real-time for some cases due to its iterative nature, different approaches have been proposed in the literature. Excluding cases with terminal speed and safety constraints, Mahbub and Malikopoulos [85, 86] have introduced a condition-based solution framework for the optimal coordination of CAVs, which leads to a closed-form analytical solution without this iterative procedure. The authors mathematically characterized the activation cases of different state and control constraint combinations, and provided a set of a priori conditions under which different constraint combinations can become active. The conditions under which the rear-end collision avoidance constraint never becomes active were discussed in [87]. For highway on-ramps, Xiao and Cassandras [88, 89] provided conditions to check whether the speed-dependent safety constraint and/or speed constraints remain inactive for each CAV. A different approach was proposed in [90, 91], and implemented at a roundabout in [92] and a corridor [93] consisting of a single optimization level aimed at both minimizing energy consumption and improving the traffic throughput. In this approach, each CAV computes the optimal exit time of the control zone corresponding to an unconstrained energy optimal trajectory that satisfies all the state, control, and safety constraints.

There are several other efforts which have used consensus [94], fuzzy logic [95], queuing theory [96], and game theory approach [97] to investigate coordination of CAVs at signal-free intersections. A thorough discussion of research efforts in the area of control and coordination of CAVs can be found in [34] and [98].

Reinforcement Learning Framework

The evolution of processing power and the generation of a massive amount of data have paved the way for machine learning techniques, particularly reinforcement learning (RL), to emerge as an alternative method for traffic control. RL approaches are used when an agent learns from interaction with an environment without requiring the complete models

of the environment. These approaches employ the Markov decision process framework to define the interaction between a learning agent and its environment [99]. Kiumarsi et al. [100] surveyed various RL-based techniques to solve optimal control problems in real-time using data measurement along the system trajectories.

An off-policy temporal difference learning called Q-learning is one of the simplest and most promising RL methods introduced by Watkins [101] in 1989. Since then, numerous studies have been reported in the literature to employ Q-learning in various transportation applications. El-Tantawy and Baher [102] presented a Q-learning-based traffic signal control with different state representations and tested the effectiveness of their model on a real-world multi-phase intersection. A group of papers employed a Q-learning-based approaches in ramp-metering control [103–106], lane-changing maneuvers [107], overtaking [108], and intersections management [109].

However, in large problems with many state-action pairs, to avoid Bellman's "curse of dimensionality," deep reinforcement learning methods (DRL), such as Deep Q-network (DQN) are used where the Q-function is replaced with a deep neural network. This method, which was first introduced by Mnih et al. [110] to learn control policies for computer games using only raw pixels, has been explored by researchers in various transportation applications. Seliman et al. [111] proposed a control strategy based on a Deep-Q-Network (DQN) Reinforcement learning (RL) for a single CAV to navigate through a congested lane-reduction zone. Isele and Cosgun [112] established a DQN framework for navigating a single CAV through a signal-free intersection and compared its performance with the baseline policy in a traffic simulator. Tram et al. [113] added a recurrent layer to the DQN for navigating a single CAV among human-driven vehicles with unknown intentions at an intersection. Instead of finding a policy with continuous control input, the authors used short-term goals as an action of the agent, in which the agent learns to keep a set speed, yield for a crossing car, or stop before the intersection. Several other efforts have considered using DQN in powertrain optimization of hybrid electric vehicles [114], eco-routing [115], and overtaking maneuver [116]. Few studies in the literature have applied DRL techniques to the problem of highway on-ramps. Wang and

Chan [117] presented a DRL formulation for the on-ramp merging of an autonomous vehicle using DQN. The same problem of freeway merging was addressed by Nishi et al. [118] using a combination of multi-policy decision making for choosing the possible spots to merge into and passive actor-critic method to learn the state value for choosing the policy to merge into the best spot. Nassef et al. [119] used a centralized trajectory recommendation framework for coordinating CAVs in a lane merging scenario. Ren et al. [120] addressed the CAV merging problem in the context of a lane drop caused by a highway work zone using a soft actor-critic algorithm where only the vehicles in the merging lane were considered as RL agents, while the vehicles on the main lane were controlled by a modified VISSIM driver model.

A survey of the state of the art on deep learning applications on control of CAVs and transportation research is given in [121] and [122].

1.2.2 Control of CAVs Under Uncertainty

One restrictive assumption that has been made in most of the existing work is neglecting any source of uncertainty in the system. This uncertainty can have a variety of sources, such as deviation from the nominal strategies, disturbances from the environment, noisy observations, uncertainties in the system dynamics, and delayed communications. Any framework for the coordination of CAVs that neglects this uncertainty is prone to suboptimality and can even lead to unsafe conditions.

Some research efforts in the literature have examined incorporating uncertainty in the control of CAVs in scenarios such as overtaking, collision avoidance, adaptive cruise control (ACC), and cooperative adaptive cruise control (CACC). Zhou et al. [123] proposed a centralized receding horizon stochastic optimal control strategy for ACC and CACC of platoons of vehicles to incorporate noise in the system dynamics and measurements. However, their computational time increases exponentially with respect to the prediction horizon and platoon size. Vitus and Tomlin [124] presented a control framework for the cooperation of CAVs in the presence of human-driven vehicles with uncertain behavior. They employed a chance-constrained formulation to avoid a traditional conservative solution resulting from

considering the worst-case scenario for human-driven vehicles. They used a sampling method to represent the system state and a convex bounding method to handle the chance constraints. Gao et al. [125] proposed a control algorithm for an automated vehicle to overtake a human-driven vehicle based on its aggressiveness/ non-aggressiveness.

Several studies reported in the literature have used various MPC architectures to include uncertainty in the design of controller for a single autonomous vehicle [126–135]. According to survey paper by Carvalho et al. [126] these designs are grouped into 1) tube-based robust MPC, 2) linear time-varying stochastic MPC, and 3) scenario-based MPC. In a tube-based robust MPC approach, the notion of robust positively invariant (RPI) sets is used, in which, if it is computed, robust constraint satisfaction can be guaranteed. However, the computation of the RPI set is generally difficult, and it can only be computed off-line for linear systems. For the linear time-varying stochastic MPC approaches, finding analytical solutions are restricted to linear systems with normally distributed additive disturbances. In scenario-based MPC, the intuition is to make the constraints of the MPC problem robustly safe in all of the scenarios. The benefits of sampling-based based MPC are flexibility in handling different types of uncertainties and easy implementation. Liu et al. [127] presented linear-time-varying stochastic MPC to correct the driver's steering wherever there is a risk of unintended roadway departures. They used a probabilistic safety constraint that accounts for uncertainty in the driver's behavior. Carvalho et al. [128] proposed stochastic MPC for uncertain environment modeling. To formulate a chance-constrained MPC, they employed an interacting multiple model Kalman filter to predict the positions of vehicles in the environment. Using constraint tightening and uncertainty propagation techniques, they solved the equivalent quadratic problem numerically. Katriniok et al. [129] presented a scenario-based MPC, which prescribed speed advice to a human driver while considering an uncertain delay in their response to the advised speed trajectory. Dunlap et al. [130] proposed a sampling-based MPC for planning a safe path for an autonomous vehicle. Berntorp and Cairano [131] presented a probabilistic framework for online planning and decision making for an autonomous vehicle using particle filtering. In a sequel paper, Berntorp et al. [132] validated the proposed particle

filtering strategy on a small-scale robotics platform for several different scenarios, such as collision avoidance, overtaking, and traffic-jam scenarios.

Recently in the control community, using the Gaussian process (GP) has gained attention. A GP is defined as a collection of random variables, any finite number of which have a joint Gaussian distribution, and can be used to describe a distribution over an infinite-dimensional space of functions [136]. Several research efforts in the literature have used GP for learning system dynamics which can be used in stochastic MPC [137] and Robust MPC [138, 139] setting. The authors in [140] employed GP to predict the future behavior of a lead vehicle for an overtaking scenario in autonomous racing and then used this to formulate a stochastic MPC. Hewing et al. [141] used GP to learn the dynamics of a racing car, and experimentally validated their proposed approach using a real race car in [142]. Some work has used GP to learn disturbance model [143, 144], which is then used for the path tracking algorithm. Similarly, the authors in [145, 146] used GP to learn disturbances in the dynamical system to design a safe learning-based controller. GP models have also been used in other control applications, including ship trajectory prediction [147] and modeling and control of buildings [148].

Numerous research efforts have sought the idea of employing control barrier functions (CBF) to ensure the satisfaction of constraints in a safety-critical system. The CBF approach handles constraints by rendering the safe sets forward invariant, which means that if the system initially starts in the safe set, it will stay in the safe set [149–151]. Ames et al. [149] presented a framework to unify safety constraints along with performance objectives of safety-critical system with affine control using CBFs and the control Lyapunov functions (CLFs), respectively. Under reasonable assumptions, the authors proved that CBF provides a necessary and sufficient condition on the forward invariance of a safe set. They demonstrated the performance of their approach on automotive applications such as adaptive cruise control and lane keeping. For systems with higher-relative degree constraints, in which the control input does not show up after taking the first derivative, exponential CBFs were proposed in [152], while a complete analysis of handling higher relative degree constraints in general

cases is given in [153]. A comprehensive discussion of the recent effort on CBFs and their use to verify and enforce safety in the context of safety-critical controllers is provided in [154].

More recently, there have been a series of papers initially proposed by Xiao et al. [155, 156] on using CBFs in the coordination of CAVs [155–161]. Xiao et al. [156], provided a joint CBF and CLF approach to respond to inevitable perturbation and noise in a highway on-ramps problem. The authors transformed the state and control constraints of the system into the corresponding CBF constraints and solved a quadratic program (QP) at each time step. Focusing on the highway merging problem in [155], the authors presented their two-step approach. First, using linearized dynamic and quadratic costs, they derived the unconstrained solution to the optimal control problem. Next, by formulating a QP at each time step, they tracked the optimal control trajectory using CLF and ensured the satisfaction of the constraints through CBF constraints. Additionally, the authors addressed the feasibility of the resulting QP by introducing an additional constraint in [159, 162]. Liu et al. [163] applied the formulation in [156] to a highway on-ramps problem with mixed-traffic, in which, human drivers were regarded as random disturbances to CAVs. Considering an intersection scenario, Khaled et al. [158] applied the formulation in [156] to a signal-free intersection, while Rodriguez and Fathi [157] employed the two-step formulation in [155] to an intersection with traffic lights. Focusing on the vehicle-level, Shivam et al. [160] proposed a tracking control problem based on CBFs to track the optimal trajectories generated in [65] for a signal-free intersection.

1.2.3 Experimental Validation in Scaled Testbeds

Although several studies have reported on the impact of coordination of CAVs in traffic scenarios, e.g., intersections, merging at roadways, and roundabouts, the effectiveness of these approaches has been primarily shown in the simulation. Evaluating the performance of CAVs in a simulation environment imposes limitations due to complexities arising from modeling the exact vehicle dynamics and driving behavior and data loss and transmission latency associated with connectivity and communication networks. As Grim et al. [164] stated, "*the problem with simulations is that they are doomed to succeed.*" Therefore, before deploying

the fleet of CAVs in different parts of a transportation network, a thorough evaluation of CAVs is required—ranging from numerical simulation to real-world public roads.

Assessment of the performance of CAVs in scaled testbeds has recently gained momentum due to the flexibility they offer to conduct quick, repeatable experiments that could go one step beyond simulation. Such testbeds can be used to conduct quick and repeatable experiments in an effort to go one step beyond simulation. Gulliver [165] and MOPED [166] have been the outcome of early efforts on developing scaled testbeds for robotic vehicles. Gulliver's focus is mainly on communication among vehicles, while MOPED is focused on low-level control of a single scaled vehicle. MIT's Duckietown [167] employs differential drive robots and Go-CHART [168] uses four-wheel skid-steer vehicles. Both testbeds focus primarily on local perception and autonomy. The Cambridge Minicars [169] is another testbed for emulating cooperative driving in highway traffic conditions. A general-purpose robotic testbed, called Robotarium, has been developed [170], which features differential drive robots. The Cyber-Physical Mobility Lab [171] has implemented another scaled testbed on decision-making policies and trajectory planning. For a review of such robotics testbeds, see [172].

1.3 Research Gaps and Contributions

On the basis of the presented literature review, several research gaps need to be addressed for establishing a real-time coordination framework for a fleet of CAVs. In what follows, we present these research gaps and summarize our contributions by showing how this dissertation advances the state of the art by addressing these gaps.

Multiple adjacent intersections

Although there have been many studies reporting on the coordination of CAVs at signal-free intersections, coordination of CAVs at multiple adjacent intersections has been assessed to a very limited extent. One of the main drawbacks of considering each intersection in isolation is neglecting the effects of the downstream intersection on the upstream intersection.

Namely, considering multiple intersections together with the same paradigm as of a single intersection results in unnecessary slowdowns of the CAVs. Therefore, for multiple adjacent intersections that are closely distanced, not only we should not consider each intersection in isolation, but we also need a new paradigm for coordinating CAVs in these traffic scenarios.

In Chapter 2, we present two different bi-level decentralized coordination approaches for CAVs at adjacent signal-free intersections consisting of the upper-level and low-level planning. The proposed framework advances the state of the art in the following ways. First, rather than investigating intersections in isolation [34, 65, 73, 173], our proposed framework considers the effects of intersections' interdependence methodically. Second, we ensure lateral safety through a decentralized upper-level planning, as opposed to a strict FIFO queuing policy [46, 65, 78, 79], or a centralized controller [36, 43, 47, 49, 50, 57, 61, 174]. Third, in contrast to the research efforts reported in the literature to date, in the upper-level planning, we allow lane-changing maneuvers. Fourth, our bi-level framework is enhanced to guarantee safety in the presence of a bounded steady-state error in tracking the positions of CAVs. Finally, our framework is not limited to straight paths [69] and does not exclude merging or splitting paths [173]. The results of this part were previously presented in the following publications:

- Behdad Chalaki and Andreas A Malikopoulos. Optimal control of connected and automated vehicles at multiple adjacent intersections. *IEEE Transactions on Control Systems Technology*, 30(3):972–984, 2022
- Behdad Chalaki and Andreas A Malikopoulos. Time-optimal coordination for connected and automated vehicles at adjacent intersections. *IEEE Transactions on Intelligent Transportation Systems*, 2021
- Behdad Chalaki and Andreas A Malikopoulos. An optimal coordination framework for connected and automated vehicles in two interconnected intersections. In *2019 IEEE Conference on Control Technology and Applications (CCTA)*, pages 888–893. IEEE, 2019

Decentralized RL-based coordination framework

Although there have been several research efforts reporting on Q-learning-based framework for different transportation applications, no paper has reported work on a decentralized RL-based coordination framework for CAVs at an intersection and its comparison with the optimal control method based on Pontryagin's minimum principle.

In Chapter 2, we establish a decentralized RL-based coordination framework for CAVs at a signal-free intersection to minimize travel time and improve fuel efficiency. We formulate the problem by employing a well-known RL approach enhanced with a coordination mechanism called a hysteretic Q-learning, in which two learning rates are considered. Additionally, we integrate a first-in-first-out (FIFO) queuing policy in our hysteretic Q-learning framework to improve the performance of our system. We show our proposed approach's effectiveness through simulation and comparison with the classical optimal control method based on Pontryagin's minimum principle. The proposed framework advances the state of the art in the following ways. First, rather than considering a single agent in the RL framework [111–113], we propose a decentralized multi-agent framework with 100% penetration rate of CAVs. Second, in contrast to [109, 112, 113], we incorporate energy consumption minimization into our framework in addition to traffic throughput improvement while ensuring both lateral and rear-end safety through our combined hysteretic Q-learning with FIFO framework. Third, in contrast to the research efforts reported in the literature to date, we compare the results of our proposed framework with the classical control method based on Pontryagin's minimum principle. The results of this part is based on the following publication:

- Behdad Chalaki and Andreas A Malikopoulos. A hysteretic q-learning coordination framework for emerging mobility systems in smart cities. In *2021 European Control Conferences (ECC)*, pages 17–22, 2021

Coordination of CAVs under uncertainty

Most of the research efforts reported on the coordination of CAVs at signal-free intersections, have neglected uncertainty or assumed a known bound on that uncertainty.

Following either of these approaches may result in an unsafe or overly conservative behavior. In Chapter 3, we build upon a single-level coordination framework for CAVs proposed in [91], and provide three different techniques to make the coordination framework uncertainty-aware.

First, we integrate a replanning mechanism into our coordination framework, which can be implemented in a time-driven or event-driven manner. This embedded replanning aims at introducing indirect feedback into the coordination framework to respond to the unexpected changes in the system to some extent. Additionally, we further enhance our framework by introducing a priority-aware resequencing mechanism, which designates the order of decision making. There have been limited studies in exploring the effects of decision-making sequence among CAVs in decentralized coordination framework. Our approach advances the state of the art in a way that relaxes the FCFS decision making sequence of the CAVs [57, 65].

Second, we reformulate the motion-planning framework for CAVs at a signal-free intersection as a robust coordination problem by including the deviations from the nominal trajectories as uncertainty. We adopt the data-driven approach, GP regression, to learn the uncertainty from the possibly noisy observation of CAVs' time trajectories. This work advances the state of the art in the following way. Rather than not considering uncertainty for the vehicle's trajectory planning [49, 57, 61–65, 78, 91] or assuming a known bound [175], we employ GP regression to model uncertainty and incorporate it in our coordination framework.

Finally, we enhance our framework through employing CBFs to provide an additional safety layer and ensure the satisfaction of all constraints in the system. By using the proposed framework in the motion planning module, each CAV first uses simple longitudinal dynamics to derive the optimal control trajectory without activating any constraint. A vehicle-level tracking controller employs a combined feedforward-feedback control law to track the resulting optimal trajectory from the motion planning module. Then, a barrier-certificate module, acting as a middle layer between the vehicle-level tracking controller and physical vehicle, receives the control law from the vehicle-level tracking controller and using realistic vehicle dynamics ensures that none of the state, control, and safety constraints becomes active.

Although several studies on coordination of CAVs at different traffic scenarios using CBFs have been reported in the literature, the approach reported in this dissertation advances the state of the art in the following ways. First, in contrast to other efforts which attempt to address satisfaction of all the constraints in the system through CBFs [88, 157, 158, 161], in this paper, the motion planning module yields an optimal unconstrained trajectory which guarantees that state, control, and safety constraints are satisfied, while barrier-certificate module only intervenes if the deviations from the nominal optimal trajectory lead to violating the constraints. Second, in several research efforts using CBFs, the lateral safety is handled through imposing a FIFO queuing policy [88, 155, 157, 158]. However, in our approach, we do not consider a FIFO queuing policy. Relaxing a FIFO queuing policy is not a trivial task since it introduces a constraint with a higher relative degree, which requires special analysis. The work in presented in this part appeared in the following publications:

- Behdad Chalaki and Andreas A. Malikopoulos. A priority-aware replanning and resequencing framework for coordination of connected and automated vehicles. *IEEE Control Systems Letters*, 6:1772–1777, 2022
- Behdad Chalaki and Andreas A Malikopoulos. Robust learning-based trajectory planning for emerging mobility systems. In *2022 American Control Conference (ACC)*, pages 2154–2159, 2022
- Behdad Chalaki and Andreas A Malikopoulos. A Barrier-Certified Optimal Coordination Framework for Connected and Automated Vehicles. *arXiv:2203.16418 (in review)*, 2022

Experimental validation

In Chapter 4, we introduce Information and Decision Science Lab's Scaled Smart City (IDS^{3}C), a robotic scaled (1:25) testbed capable of safely validating control approaches beyond simulation in applications related to emerging mobility systems such as coordination of CAVs. Then, we demonstrate the effectiveness of coordination of CAVs at a multi-lane roundabout and we show its scalability in a corridor consisting of a roundabout, an intersection, and a merging roadway.

There are several features that distinguish IDS^{3}C from other testbeds. First, unlike MIT's Duckietown [167] and GO-Chart [168], the CAVs in IDS^{3}C resemble full-scale vehicles by using four wheels, built-in suspension, and an Ackermann steering mechanism. Second, in contrast to the scaled testbeds reported in [167, 169–171], IDS^{3}C is equipped with driver emulation stations that interface directly with the robotic cars. These stations enable us to explore and study human driving behavior and their interactions with CAVs. Being able to study how CAVs can safely interact and co-exist with human-driven vehicles is of great importance since different penetration rates of CAVs can significantly alter transportation efficiency and safety. Third, rather than focusing on specific scenarios in a transportation network [165, 169] or a single individual vehicle [166], IDS^{3}C can accommodate almost every possible traffic scenario, including crossing three- and four-way intersections, merging at roadways and roundabouts, cruising in congested traffic, passing through speed reduction zones, and lane-merging or passing maneuvers. These features make IDS^{3}C a unique scaled robotic testbed to study problems in emerging mobility systems such as coordination of CAVs, shared-mobility, eco-routing, and first/last-mile delivery. Finally, only a few testbeds [167, 171] are equipped with a "digital twin." The digital twin of IDS^{3}C, called the Information and Decision Science Lab's Scaled Smart Digital City (IDS 3D City), is a Unity-based virtual simulation environment that can operate alongside the physical IDS^{3}C and interface with the existing control framework. The IDS 3D City provides the framework to develop and implement control algorithms for emerging mobility systems in simulation before moving to the physical IDS^{3}C for validation. More details about the IDS 3D City can be found in [181].

The results of this section were previously presented in the following publications:

- Behdad Chalaki, Logan E. Beaver, A M Ishtiaque Mahbub, Heeseung Bang, and Andreas A. Malikopoulos. A research and educational robotic testbed for real-time control of emerging mobility systems: From theory to scaled experiments. *IEEE Control Systems Magazine*, 2022 (in press)
- Behdad Chalaki, Logan E Beaver, and Andreas A Malikopoulos. Experimental validation of a real-time optimal controller for coordination of cavs in a multi-lane roundabout. In *31st IEEE Intelligent Vehicles Symposium (IV)*, pages 504–509, 2020

This dissertation primarily includes the main contributions of my research; however, there are several other publications listed as follows which were the outcomes of my research and collaborations with other colleagues

- A M Ishtiaque Mahbub, Behdad Chalaki, and Andreas A Malikopoulos. A constrained optimal control framework for vehicle platoons with delayed communication. *Network and Heterogeneous Media, Special Issue: Traffic and Autonomy*, 2022 (accepted)
- Heeseung Bang, Behdad Chalaki, and Andreas A Malikopoulos. Combined Optimal Routing and Coordination of Connected and Automated Vehicles. *IEEE Control Systems Letters*, 6:2749–2754, 2022
- Raymond M. Zayas, Logan E. Beaver, Behdad Chalaki, Heeseung Bang, and Andreas A. Malikopoulos. A digital smart city for emerging mobility systems. *arXiv:2109.02811*, 2021
- Meera Ratnagiri, Clare O'Dwyer, Logan E. Beaver, Behdad Chalaki, Heeseung Bang, and Andreas A. Malikopoulos. A scalable last-mile delivery service: From simulation to scaled experiment. *arXiv:2109.05995*, 2021
- Behdad Chalaki, Logan E Beaver, Ben Remer, Kathy Jang, Eugene Vinitsky, Alexandre Bayen, and Andreas A Malikopoulos. Zero-shot autonomous vehicle policy transfer: From simulation to real-world via adversarial learning. In *IEEE 16th International Conference on Control & Automation (ICCA)*, pages 35–40, 2020
- Kathy Jang, Eugene Vinitsky, Behdad Chalaki, Ben Remer, Logan Beaver, Andreas A Malikopoulos, and Alexandre Bayen. Simulation to scaled city: zero-shot policy transfer for traffic control via autonomous vehicles. In *Proceedings of the 10th ACM/IEEE International Conference on Cyber-Physical Systems*, pages 291–300, 2019
- Logan E Beaver, Behdad Chalaki, A M Mahbub, Liuhui Zhao, Ray Zayas, and Andreas A Malikopoulos. Demonstration of a Time-Efficient Mobility System Using a Scaled Smart City. *Vehicle System Dynamics*, 58(5):787–804, 2020

1.4 Dissertation Outline

In this chapter, we completed the literature review and identified some major research gaps along with the contributions of this dissertation. In the next chapter, we first present our bi-level coordination framework for CAVs at multiple adjacent intersections, and then proceed with our decentralized coordination framework for CAVs based on hysteretic Q-learning. In Chapter 3, we build upon a single-level coordination framework for CAVs proposed

in [91], and provide three different techniques both predictive and reactive, to enhance the coordination framework in the presence of uncertainty. In Chapter 4, we introduce Information and Decision Science Lab's Scaled Smart City (IDS^{3}C), a robotic scaled (1:25) testbed, and validate the effectiveness of our coordination framework for CAVs at a multi-lane roundabout and a corridor. Finally, in Chapter 4, we summarize the main contributions of this dissertation and provide some potential future directions.

Chapter 2

A DECENTRALIZED COORDINATION FRAMEWORK FOR CONNECTED AND AUTOMATED VEHICLES

> Mighty is the one who has knowledge
> By knowledge the old hearts grow young again
>
> Ferdowsi, *The Book of Kings*, 940–1020 CE

Among different traffic scenarios, intersections are the most challenging from a safety perspective, as an average of one-quarter of traffic fatalities and roughly half of all traffic injuries are attributed to intersections [186]. In this chapter, we establish a deterministic decentralized coordination framework for connected and automated vehicles (CAVs) at signal-free intersections.

We first provide a general modeling framework for a signal-free intersection in Section 2.1. In the sections 2.2 and 2.3, we study the problem of coordination of CAVs at multiple adjacent intersections. A closer look at the literature on coordination of CAVs at signal-free intersections reveals that only a limited number of papers address coordination of CAVs at adjacent intersections. Mahbub *et al.* [73] presented coordination of CAVs at a traffic corridor consisting of multiple traffic scenarios by considering each scenario in isolation. One of the main drawbacks of considering each intersection in isolation is neglecting the effects of the downstream intersection on the upstream intersection. Extending the single intersection results to the multiple intersections might be inefficient and sub-optimal. In this chapter, we show that applying first-in-first-out (FIFO) queuing policy [65, 78] to find the sequence of CAVs to enter the merging zone in a single intersection will result in unnecessary slowdowns of the CAVs at multiple intersections. In Section 2.2, we present a bi-level decentralized coordination framework for CAVs at multiple adjacent, multi-lane signal-free intersections

without considering left/right turns. In the upper-level planning, each CAV recursively computes the energy-optimal arrival time at each intersection on its path along with the optimal lane, while ensuring both lateral and rear-end safety. In the low-level planning, we formulate an optimal control problem for each CAV with interior-point constraints, the solution of which yields the energy optimal control input, given the time from the upper-level problem. In Section 2.3, we present a different bi-level decentralized coordination framework for CAVs at two adjacent intersections including every possible path. Focusing on minimizing travel time, in the upper level, we formulate a decentralized scheduling problem for each CAV, which can be solved by using mixed-integer linear program (MILP). The solution of the upper-level problem yields the minimum travel time while satisfying safety constraints. The solution of the upper-level problem becomes the inputs of the low-level problem. In the low level, we formulate an optimal control problem for each CAV, the solution of which yields the energy optimal control input. In Section 2.4, we study the problem of coordination of CAVs at a signal-free intersection by employing a well-known reinforcement learning approach enhanced with a coordination mechanism called a hysteretic Q-learning. Additionally, we integrate a FIFO queuing policy in our hysteretic Q-learning framework to improve the performance of our approach. Finally, in Section 2.5, we provide a summary of the chapter.

The primary contributions presented in this chapter are

- Section 2.2: (1) the development of a bi-level optimization framework to coordinate CAVs at multiple adjacent, multi-lane intersections aimed at decreasing stop-and-go driving and fuel consumption; (2) the enhancement of the upper-level planning layer to include the lane-changing maneuver to improve the traffic throughput; (3) a complete analysis of the low-level optimization problem including interior-point constraints; and (4) the enhancement of the bi-level framework to account for a bounded steady-state error in tracking the positions of CAVs. The results of this section were previously presented in the following publication:
  - [175] Behdad Chalaki and Andreas A Malikopoulos. Optimal control of connected and automated vehicles at multiple adjacent intersections. *IEEE Transactions on Control Systems Technology*, 30(3):972–984, 2022
- Section 2.3: (1) the establishment of a bi-level optimization framework to coordinate CAVs at two adjacent intersections considering all traffic movements aimed at decreasing both delay and travel time of each CAV; (2) a decentralized scheduling scheme for

the upper-level problem considering state and control constraints that relaxes the strict FIFO queuing policy; (3) a complete, closed-form solution of the low-level optimization problem including the speed-dependent rear-end safety constraint and state and control constraints; and (4) a demonstration of the effectiveness of our approach through extensive numerical simulations including all possible paths for CAVs in two adjacent intersections and comparison with signalized intersections, centralized scheduling, and FIFO queuing policy. The work in presented in this chapter appeared in the following publications:

  - [176] Behdad Chalaki and Andreas A Malikopoulos. Time-optimal coordination for connected and automated vehicles at adjacent intersections. *IEEE Transactions on Intelligent Transportation Systems*, 2021
  - [70] Behdad Chalaki and Andreas A Malikopoulos. An optimal coordination framework for connected and automated vehicles in two interconnected intersections. In *2019 IEEE Conference on Control Technology and Applications (CCTA)*, pages 888–893. IEEE, 2019

- Section 2.4: (1) the development of a hysteretic Q-learning optimal framework to coordinate CAVs at a signal-free intersection aimed at decreasing both travel time and fuel consumption of each CAV; (2) integrating FIFO queuing policy into our hysteretic Q-learning optimal framework; and (3) comparison of the proposed framework with the benchmark solution from the optimal control technique based on Pontryagin's minimum principle. The results of this sections is based on the material presented in the following publication:

  - [177] Behdad Chalaki and Andreas A Malikopoulos. A hysteretic q-learning coordination framework for emerging mobility systems in smart cities. In *2021 European Control Conferences (ECC)*, pages 17–22, 2021

2.1 Modeling Framework

We consider a symmetrical signal-free multi-lane intersection (Fig. 2.1) as a basis traffic scenario to describe our modeling framework. There is a *coordinator* that stores information about all intersections' geometric parameters and the planned trajectories of CAVs. The coordinator does not make any decision and it only acts as a *database* among the CAVs. The coordinator can be a physical infrastructure such as a drone, road site unit, or cloud storage. We define a *contol zone* in which the coordinator can communicate with the CAVs traveling inside the control zone. We call the area inside the control zone where a lateral collision may occur *merging zone*.

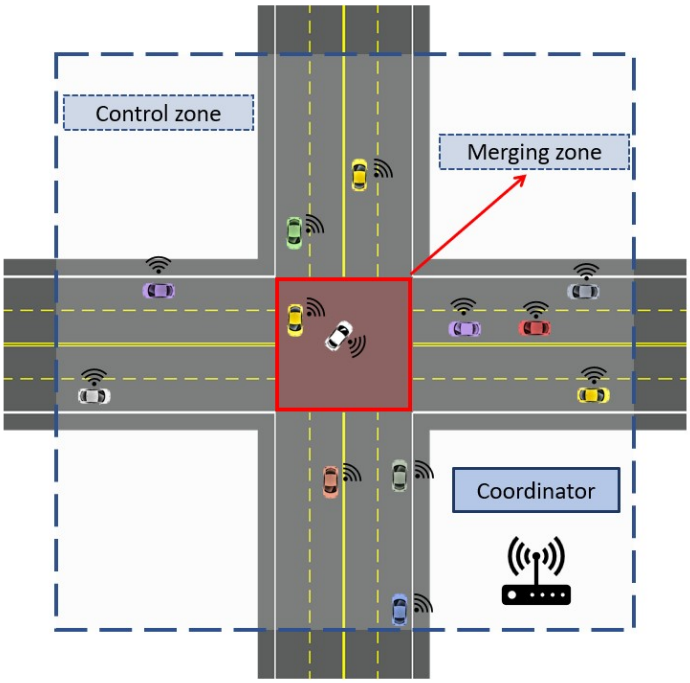

Figure 2.1: A signal-free intersection with a coordinator communicating with CAVs inside the control zone.

Let $N(t) \in \mathbb{N}$ be the total number of CAVs that have entered the control zone by the time $t \in \mathbb{R}_{\geq 0}$, and $\mathcal{N}(t) = \{1, \ldots, N(t)\}$ be the queue that designates the order that each CAV entered the control zone. Upon entering the control zone, the coordinator assigns each CAV an integer index equal to $N(t) + 1$. If two or more CAVs enter the control zone simultaneously, the CAV with the shorter path is assigned lower position in the queue; however, if the length of their paths is the same, then their positions are randomly chosen by the coordinator. The coordinator removes any CAV from $\mathcal{N}(t)$ when they exit the control zone. When there is no CAV inside the control zone, then $\mathcal{N}(t) = \emptyset$.

We model the longitudinal dynamics of each CAV $i \in \mathcal{N}(t)$ as a double integrator, i.e.,

$$\begin{aligned} \dot{p}_i(t) &= v_i(t), \\ \dot{v}_i(t) &= u_i(t), \end{aligned} \tag{2.1}$$

where $p_i(t) \in \mathcal{P}_i$, $v_i(t) \in \mathcal{V}_i$, and $u_i(t) \in \mathcal{U}_i$ denote position, speed, and acceleration at $t \in \mathbb{R}_{\geq 0}$, respectively. Let $\mathbf{x}_i(t) = [p_i(t), v_i(t)]^\top$ and $u_i(t)$ be the state and control input of the CAV i at time t, respectively, $t_i^0 \in \mathbb{R}_{\geq 0}$ be the time that CAV $i \in \mathcal{N}(t)$ enters the control zone, and $t_i^f > t_i^0 \in \mathbb{R}_{\geq 0}$ be the time that CAV i exits the control zone.

For each CAV $i \in \mathcal{N}(t)$ the control input and speed are bounded by

$$u_{i,\min} \leq u_i(t) \leq u_{i,\max}, \tag{2.2}$$

$$v_{\min} \leq v_i(t) \leq v_{\max}, \tag{2.3}$$

where $u_{i,\min}, u_{i,\max}$ are the minimum and maximum control inputs and $v_{\min}, v_{\max}$ are the minimum and maximum speed limit, respectively. Without loss of generality, we do not consider diversity among CAVs' maximum and minimum control input. Thus, to this end, we set $u_{i,\min} = u_{\min}$ and $u_{i,\max} = u_{\max}$. The sets $\mathcal{P}_i$, $\mathcal{V}_i$, and $\mathcal{U}_i$, $i \in \mathcal{N}(t)$, are complete and totally bounded subsets of $\mathbb{R}$.

Assumption 2.1.1. *None of the state, control, and safety constraints (defined in following sections) is active for each CAV $i \in \mathcal{N}(t)$ at the entry of the control zone.*

Assumption 2.1.2. *There are no errors or delays in the vehicle-to-vehicle and vehicle-to-infrastructure communication.*

The assumption 2.1.1 is imposed to ensure that the initial state and control input are feasible. This is a reasonable assumption since CAVs are automated, and so there is no compelling reason for them to activate any of the constraints by the time they enter the control zone. Although the assumption 2.1.2 is a strong assumption, it is relatively straightforward to relax this assumption as long as the noise or delays are bounded.

2.2 Optimal Control of Connected and Automated Vehicles at Multiple Adjacent Intersections

In this section, we establish a decentralized optimal control framework for CAVs crossing multiple adjacent, multi-lane signal-free intersections to minimize energy consumption and improve traffic throughput. Our framework consists of two layers of planning. In the upper-level planning, each CAV computes its optimal arrival time at each intersection recursively along with the optimal lane to improve the traffic throughput. In the low-level planning, we formulate an energy-optimal control problem with interior-point constraints, the solution of which yields the optimal control input (acceleration/deceleration) of each CAV to cross the intersections at the time specified by the upper-level planning. Moreover, we extend the results of the proposed bi-level framework to include a bounded steady-state error in tracking the optimal position of the CAVs. Finally, we demonstrate the effectiveness of the proposed framework through simulation for symmetric and asymmetric intersections , where the geometry of intersections might be different, and comparison with traditional signalized intersections.

This section is organized as follows. In subsection 2.2.1, we formulate the problem, while in subsections 2.2.2 and 2.2.3, we provide the upper-level planning and low-level planning with their corresponding solutions, respectively. In subsection 2.2.4, we enhance the framework to include the deviation from the nominal planned position. Finally, we provide simulation results in subsection 2.2.5.

2.2.1 Problem Formulation

We consider multiple adjacent intersections closely distanced from each other (see Fig. 2.2 for two adjacent intersections).

Definition 2.2.1. *The set of merging zones indexed uniquely in the control zone, is given by* $\mathcal{Z} \coloneqq \{1, \dots, n_z\},\ n_z \in \mathbb{N}$*, where* n_z *is the total number of merging zones in the control zone.*

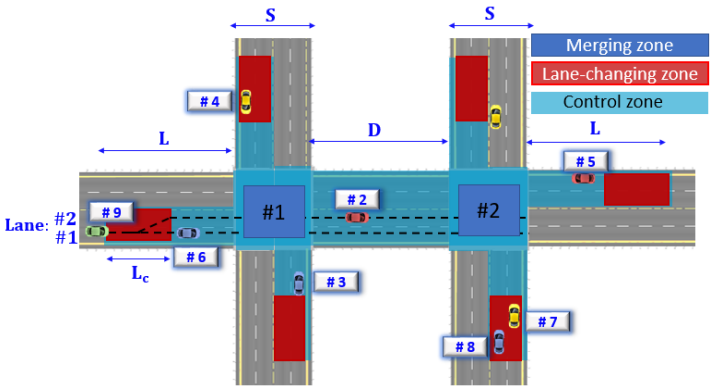

Figure 2.2: Bird-eye view of two interconnected intersections.

Definition 2.2.2. *The set of all same-directional lanes across all roads that are connected to the intersection, is given by* $\mathcal{L} \coloneqq \{1, \dots, n_\ell\},\ n_\ell \in \mathbb{N}$*, where* 1 *and* n_ℓ *are indices for the rightmost lane and leftmost lane, respectively (Fig. 2.2).*

Without loss of generality, in our analysis, we consider multiple intersections with two lanes on each road that is connected to an intersection, i.e., $\mathcal{L} \coloneqq \{1, 2\}$. We consider the distance between the two adjacent intersections to be D, and a merging zone of length $S = 4w$, where $w \in \mathbb{R}_{\geq 0}$ is the lane width. In this section, we limit our analysis to the cases where no left/right turns are allowed, and lane-change maneuver is only possible inside the lane-changing zone which we describe next.

Definition 2.2.3. *The lane-changing zone* Λ *is the interval with length* L_c *located at the entry of the control zone, where CAVs can change lanes (Fig. 2.2), i.e.,*

$$\Lambda \coloneqq [p_i(t_i^0),\ p_i(t_i^0) + L_c] \subset \mathcal{P}_i,\ i \in \mathcal{N}(t). \tag{2.4}$$

Definition 2.2.4. *The lane-changing occupancy interval* Γ_i *is the time interval that CAV* $i \in \mathcal{N}(t)$ *occupies the lane-changing zone, i.e.,*

$$\Gamma_i \coloneqq \left\{t \mid t > t_i^0,\ p_i(t) \leq L_c,\ t \in \mathbb{R}_{\geq 0}\right\}. \tag{2.5}$$

Definition 2.2.5. *For each CAV $i \in \mathcal{N}(t)$, $\ell_i^0,\ \ell_i^f \in \mathcal{L}$ denote the lane that CAV i occupies before and after the lane-changing zone, respectively.*

Definition 2.2.6. *Let $\mathcal{Z}_i \coloneqq \{z_1, \ldots, z_n\} \subseteq \mathcal{Z}$ be the set of merging zones that CAV $i \in \mathcal{N}(t)$ crosses, while z_1 and $z_n \in \mathcal{Z}_i,\ n \in \mathbb{N}$, denote the first and n'th merging zone that CAV i crosses along its path.*

Definition 2.2.7. *For each CAV $i \in \mathcal{N}(t)$, we denote $t_i^{z^*} \in \mathbb{R}_{\geq 0}$ and $\ell_i^{f^*} \in \mathcal{L}$ to be the optimal arrival time at the entry of zone $z \in \mathcal{Z}_i$ and the optimal lane occupied after the lane-changing zone, respectively.*

For CAV $i \in \mathcal{N}(t_i^0)$, CAV $j \in \mathcal{N}(t_i^0) \setminus \{i\}$, $j < i$, belongs to one of the following time-invariant subsets, determined upon CAV i's entrance at the control zone:

1. $\mathcal{A}_i^\ell, \ell \in \mathcal{L}$, is the set of all CAVs that travel on lane ℓ after a lane-changing zone with the same direction and destination as CAV i.
2. $\mathcal{B}_i^z, z \in \mathcal{Z}_i$, is the set of all CAVs which may cause collision with CAV i at the merging zone z at time $t \geq t_i^0$.
3. $\mathcal{C}_i$, is the set of all CAVs with a different origin-destination pair from CAV i, without any potential conflict for $t \geq t_i^0$.

For example, consider CAV #9 in Fig. 2.2. We have: $\mathcal{A}_9^1 = \{6\}$, $\mathcal{A}_9^2 = \{2\}$, $\mathcal{B}_9^1 = \{3, 4\}$, $\mathcal{B}_9^2 = \{7, 8\}$, $\mathcal{C}_9 = \{5\}$.

To ensure the absence of rear-end collision between CAV $i \in \mathcal{N}(t)$ and a preceding CAV $k \in \mathcal{N}(t) \setminus \{i\}$, we impose the following rear-end safety constraint

$$p_k(t) - p_i(t) \geq \delta, \tag{2.6}$$

where $\delta \in \mathbb{R}_{\geq 0}$ is a constant safe distance. Note that, since we study urban intersections, the average speed variation is not significant, thus considering a constant safe distance is reasonable. However, for scenarios in which the average speed variation is not negligible, one may consider speed-dependent safe distance discussed in [77, 79, 91, 176].

Definition 2.2.8. *The lane changing maneuver for CAV $i \in \mathcal{N}(t)$ is defined to be feasible, if upon arriving at the lane-changing zone, no other CAV occupies the lane-changing zone, i.e., $\{t_i^0\} \cap \Gamma_j = \emptyset$ for all $j \in \mathcal{A}_i^\ell$, $\ell \in \mathcal{L}$.*

Definition 2.2.9. *For each CAV $i \in \mathcal{N}(t)$, $\mathcal{T}_i^z$ is the set of optimal arrival times of CAVs at zone $z \in \mathcal{Z}_i$ that belong to $\mathcal{B}_i^z$, i.e.,*

$$\mathcal{T}_i^z := \{t_j^{z^*} \mid j \in \mathcal{B}_i^z\}. \tag{2.7}$$

2.2.2 Upper-level Planning

The objective of each CAV at the entry of the control zone is to derive the optimal control input (acceleration/deceleration) aimed at minimizing fuel consumption and improving traffic throughput by eliminating stop-and-go-driving. To achieve this aim, we establish a decentralized control framework consisting of two layers of planning. In the upper-level planning, each CAV $i \in \mathcal{N}(t)$ recursively computes the arrival time at each merging zone along its path with the optimal lane to occupy after lane-changing zone in order to improve traffic throughput and energy consumption. The outputs of the upper-level planning become the inputs for the low-level planning, which we describe in Section 2.2.3.

Definition 2.2.10. *For each CAV $i \in \mathcal{N}(t)$, v_{avg}^z is its average speed inside the merging zone $z \in \mathcal{Z}_i$, i.e.,*

$$v_{avg}^z = \frac{\int_{t_i^z}^{t_i^z + \Delta t_i^z} v_i(t) dt}{\Delta t_i^z}, \tag{2.8}$$

where t_i^z, $\Delta t_i^z \in \mathbb{R}^+$ are the arrival time at zone z and the time that it takes for CAV i to exit the merging zone z, respectively.

To increase safety and improve the throughput of CAV $i \in \mathcal{N}(t)$ while traveling inside the merging zone $z \in \mathcal{Z}_i$, we impose a constant average speed inside the merging zone equal to the speed that CAV i entered the control zone ($v_{\text{avg}}^z := v_i(t_i^0)$). This results in traveling at the merging zone with constant time $\Delta t_i^z = \dfrac{\Delta x_i^z}{v_{\text{avg}}^z}$, where Δx_i^z is the distance traveled at merging zone z for CAV i. As mentioned earlier, since no turn is allowed inside the merging

zone, Δx_i^z is the same for all CAVs, and it is equal to $S = 4w$ (see Fig. 2.2). It should be noted that, imposing desired average speed inside the merging zone is different from setting a constant speed as in [65], and thus it is less restrictive since CAV's speed can vary inside the merging zone as long as it satisfies the desired average speed. Moreover, to minimize the energy consumption of CAV $i \in \mathcal{N}(t)$ inside the control zone, we minimize transient engine operation, L^2-norm of the control input in $[t_i^0,\ t_i^f]$, which was shown to have direct benefit in fuel consumption and emission [187–189].

Lemma 2.2.11. *The arrival time of CAV $i \in \mathcal{N}$ at the merging zone of n'th intersection $z_n \in \mathcal{Z}_i$ along its path, without considering rear-end or lateral safety constraints, minimizing the energy-consumption is denoted by $\bar{t}_i^{z_n}$ and is computed recursively as follows*

$$\bar{t}_i^{z_n} = \begin{cases} t_i^0 + \dfrac{L}{v_i(t_i^0)}, & \text{for } z_1, \\ t_i^{z_{n-1}^*} + \Delta t_i^{z_{n-1}} + \dfrac{D}{v_i(t_i^0)}, & \text{otherwise.} \end{cases} \tag{2.9}$$

Proof. There are two cases to consider: Case 1: z_1 and Case 2: z_n.

Case 1: Suppose CAV $i \in \mathcal{N}(t)$ enters the control zone at $t = t_i^0$, and let the arrival time at merging zone of the first intersection $z_1 \in \mathcal{Z}_i$ along its path be $t_i^{z_1}$. Let $\bar{t}_i^{z_1}$ be the arrival time at $z_1 \in \mathcal{Z}_i$ minimizing the following cost function $J_i(u_i(t), t_i^{z_1}) = \dfrac{1}{2}\displaystyle\int_{t_i^0}^{t_i^{z_1}} u_i(t)^2 dt$, without considering rear-end safety or lateral safety constraints. For the unconstrained case, the Hamiltonian is

$$H_i(t, p_i(t), v_i(t), u_i(t)) = \frac{1}{2}u_i(t)^2 + \lambda_i^p v_i(t) + \lambda_i^v u_i(t), \tag{2.10}$$

where λ_i^p and λ_i^v are costates. Applying the Euler-Lagrange optimality conditions, the optimal control input minimizing the cost function $J_i(u_i(t), t_i^{z_1})$ is $u_i^*(t) = -\lambda_i^{v*} = a_i t + b_i$ [65], where a_i and b_i are constants of integration. We also have $\lambda_i^{p*} = a_i$. Since the speed at $t = \bar{t}_i^{z_1}$ is not specified, we have $\lambda_i^v(\bar{t}_i^{z_1}) = 0$. In addition, since $t_i^{z_1}$ is not defined, we have the following transversality condition $H_i(\bar{t}_i^{z_1}, p_i^*(t), v_i^*(t), u_i^*(t)) = 0$. From the transversality

condition, we have $H_i(\bar{t}_i^{z_1}, p_i^*(t), v_i^*(t), u_i^*(t)) = \lambda_i^{p*} v_i^*(\bar{t}_i^{z_1}) = 0$, and because $v_i^*(\bar{t}_i^{z_1}) \neq 0$, we get

$$\lambda_i^{p*} = 0 \Rightarrow u_i^*(t) = 0, \ \forall\, t \in [t_i^0, \bar{t}_i^{z_1}]. \tag{2.11}$$

Hence, CAV i cruises with $v_i(t_i^0)$, and $\bar{t}_i^{z_1} = t_i^0 + \dfrac{L}{v_i(t_i^0)}$.

Case 2: For the n'th merging zone, $z_n \in \mathcal{Z}_i$, let us consider the optimal arrival time at the upstream merging zone, $z_{n-1} \in \mathcal{Z}_i$, to be $t_i^{z_{n-1}^*}$. Let $\bar{t}_i^{z_n}$ be the energy-efficient arrival time at $z_n \in \mathcal{Z}_i$ without considering rear-end safety or lateral safety constraint. As it was shown in Case 1, by neglecting the safety constraint, CAV $i \in \mathcal{N}(t)$ cruises with $v_i(t_i^0)$ to minimize the energy consumption. Thus, $\bar{t}_i^{z_n} = t_i^{z_{n-1}^*} + \Delta t_i^{z_{n-1}} + \dfrac{D}{v_i(t_i^0)}$. □

Remark 2.2.12. *To consider the impact of the upstream merging zone z_{n-1} on the merging zone z_n for CAV $i \in \mathcal{N}(t)$, we need a recursive formulation to relate the arrival time at z_n to the optimal arrival time at z_{n-1}.*

In order for CAV $i \in \mathcal{N}(t)$ to avoid the lateral collision with CAV $j \in \mathcal{B}_i^z$, it can either arrive at merging zone $z \in \mathcal{Z}_i$ after CAV j exits the merging zone z, or exit the merging zone z before CAV j enters the merging zone z. This is formulated as either

$$t_i^{z^*} \geq t_j^{z^*} + \Delta t_j^z, \tag{2.12}$$

or

$$t_i^{z^*} + \Delta t_i^z \leq t_j^{z^*}. \tag{2.13}$$

Let CAV $k \in \mathcal{A}_i^l,\ l = l_i^{f^*}$, be the vehicle immediately ahead of CAV $i \in \mathcal{N}(t)$ at lane $l_i^{f^*} \in \mathcal{L}$. In order for CAV i to avoid the rear-end collision at the merging zone $z \in \mathcal{Z}_i$,

$$t_i^{z^*} \geq t_k^{z^*} + \rho_k^z, \tag{2.14}$$

where $\rho_k^z \in \mathbb{R}^+$ is the time that it takes for CAV k to travel a safe distance δ inside the merging zone z.

As we mentioned earlier, in the upper-level planning, we relax the FIFO queuing policy to improve the traffic throughput in multiple intersections. Upon arrival at the control zone, each CAV $i \in \mathcal{N}(t)$ recursively computes the energy-optimal arrival time for each merging zone along its path ensuring the lateral safety in conjunction with the lane that it should occupy using the Algorithms 1 and 2. Given ℓ_i^f, the lane that CAV i needs to follow after lane changing zone, CAV i employs Algorithm 1 to find the energy-optimal arrival time for all merging zones $z \in \mathcal{Z}_i$.

Algorithm 1 Recursive upper-level planning

Input: ℓ_i^f
Output: Arrival time at merging zones $\mathcal{Z}_i = \{z_1, \ldots, z_n\}$

1: **for** $z \in \mathcal{Z}_i$ **do**
2: $k = \max\{j \mid j \in \mathcal{A}_i^\ell,\ \ell = \ell_i^f\}$
3: $t_i^{z^*} \leftarrow \max\left\{\bar{t}_i^z, t_k^{z^*} + \rho_k^z\right\}$
4: `Sort` $\mathcal{T}_i^z$ `increasingly`
5: **for** $t_j^{z^*} \in \mathcal{T}_i^z$ **do**
6: **if** $t_j^{z^*} + \Delta t_j^z \le t_i^{z^*}$ **then**
7: `continue` ▷ CAV j exits before CAV i enters
8: **end if**
9: **if** $t_i^{z^*} + \Delta t_i^z \le t_j^{z^*}$ **then**
10: `break` ▷ CAV i exits before CAV j enters
11: **else** ▷ CAV i has conflict with CAV j
12: $t_i^{z^*} \leftarrow t_j^{z^*} + \Delta t_j^z$
13: **end if**
14: **end for**
15: **end for**
16: **return** $\{t_i^{z^*} \mid z \in \mathcal{Z}_i\}$

Theorem 2.2.13. *For a given lane $\ell_i^f \in \mathcal{L}$, CAV $i \in \mathcal{N}(t)$ recursively computes the energy-optimal arrival time at merging zone $z \in \mathcal{Z}_i$, which minimizes the energy consumption of CAV $i \in \mathcal{N}(t)$ inside the control zone, subject to the constraints (2.12)-(2.14) using Algorithm 1.*

Proof. For a given lane ℓ_i^f after lane-changing zone, there are four cases to consider.

Case 1: If $\mathcal{N}(t_i^0) = \mathcal{C}_i$, then we have: $\mathcal{B}_i^z = \emptyset$ for all $z \in \mathcal{Z}_i$ and $\mathcal{A}_i^\ell = \emptyset$ for all $\ell \in \mathcal{L}$. Thus, there is no leading vehicle (in line 2, $k = \emptyset$), and $\mathcal{T}_i^z = \emptyset$. Thus, we have $t_i^{z^*} = \bar{t}_i^z$ for all $z \in \mathcal{Z}_i$, and from Lemma 2.2.11, $\bar{t}_i^z$ is the energy-optimal arrival time.

Case 2: If $\mathcal{N}(t_i^0) = \mathcal{A}_i^\ell,\ \ell = \ell_i^f \in \mathcal{L}$, there exists a CAV $k \in \mathcal{A}_i^\ell,\ \ell = \ell_i^f$, which is

immediately ahead of CAV i at lane ℓ_i^f (in line 2, $k \neq \emptyset$). Similarly, we have: $\mathcal{B}_i^z = \emptyset$ for all $z \in \mathcal{Z}_i$ and $\mathcal{C} = \emptyset$. To ensure rear-end safety, we have

$$\max\left\{\bar{t}_i^z, t_k^{z^*} + \rho_k^z\right\} \leq t_i^{z^*}, \ \forall z \in \mathcal{Z}_i. \tag{2.15}$$

Selecting the lower bound in the above equation, CAV i computes the energy-optimal arrival time at the merging zone $z \in \mathcal{Z}_i$ satisfying the rear-end safety constraint (2.14) (line 3).

Case 3: If $\mathcal{N}(t_i^0) = \bigcup_{z \in \mathcal{Z}_i} \mathcal{B}_i^z$, then we have: $\mathcal{C} = \emptyset$ and $\mathcal{A}_i^\ell = \emptyset$ for all $\ell \in \mathcal{L}$. Since for CAV i, $\bar{t}_i^z$ is the energy-optimal arrival time at merging zone $z \in \mathcal{Z}_i$ without considering safety (Lemma 2.2.11), we use $\bar{t}_i^z$ as a lower bound (line 6-8). CAV i determines $t_i^{z^*} \in [\bar{t}_i^z, \infty]$ to be the smallest time satisfying lateral safety constraints in (2.12) or (2.13) (line 5 -14).

Case 4: Similarly, for other cases that $\mathcal{A}_i^\ell \neq \emptyset$, $\ell \in \mathcal{L}$, $\mathcal{B}_i^z \neq \emptyset$ $z \in \mathcal{Z}_i$, and $\mathcal{C}_i \neq \emptyset$, the energy-optimal arrival time at the merging zone $z \in \mathcal{Z}_i$, $t_i^{z^*} \in [\bar{t}_i^z, \infty]$ is the smallest time satisfying the lateral safety constraints in (2.12) or (2.13) (line 5 -14), and rear-end safety constraint (2.14) (line 3). □

Algorithm 2 Lane-changing decision

1: occupancy $\leftarrow \bigcup_{j \in \mathcal{A}_i^\ell, \ell \in \mathcal{L}} [t_i^0, \infty) \cap \Gamma_j$
2: $\ell_i^{f^*} \leftarrow \ell_i^0$
3: $t_i^{z_n^*} \leftarrow$ Find arrival time at z_n, given $\ell_i^{f^*}$
4: **if** occupancy $= \emptyset$ **then**
5: **for** $\ell \in \mathcal{L} \setminus \ell_i^0$ **do**
6: $\ell_i^f \leftarrow \ell$
7: $t_i^{z_n} \leftarrow$ Find arrival time at z_n, given ℓ_i^f
8: **if** $t_i^{z_n} < t_i^{z_n^*}$ **then**
9: $\ell_i^{f^*} \leftarrow \ell$
10: $t_i^{z_n^*} \leftarrow t_i^{z_n}$
11: **end if**
12: **end for**
13: **end if**
14: **return** $\ell_i^{f^*}$

Using Algorithm 2, CAV $i \in \mathcal{N}(t)$ investigates the feasibility of the lane-changing maneuver (line 1). If such a maneuver is not feasible, CAV i exits from the lane-changing

zone with the same lane that it entered the control zone, $\ell_i^{f^*} = \ell_i^0 \in \mathcal{L}$, and no lane-change maneuver is performed. Otherwise, CAV i selects the optimal lane $\ell_i^{f^*} \in \mathcal{L}$ yielding the minimum travel time, i.e., the arrival time at the last merging zone.

2.2.3 Low-level Planning

In our decentralized framework, the outputs of the upper-level planning for CAV $i \in \mathcal{N}(t)$, which are the optimal arrival time, $t_i^{z^*}$, at merging zone $z \in \mathcal{Z}_i$ along with the optimal lane to occupy, $\ell_i^{f^*}$, become inputs for the low-level planning. In particular, in the low-level planning, CAV $i \in \mathcal{N}(t)$ formulates the optimal control problem with interior-point constraints defined at the entry and exit of each merging zone, the solution of which minimizes the engine control effort, and energy consumption correspondingly. In addition, if the optimal lane after the lane-changing zone, $\ell_i^{f^*} \neq \ell_i^0$, CAV i needs to perform the lane-changing maneuver. If so, CAV $i \in \mathcal{N}(t)$ first travels a distance $\delta \in \mathbb{R}_{\geq 0}$ on the lane that it entered, $\ell_i^0 \in \mathcal{L}$, and then travels on a triangle with the hypotenuse $ds \in \mathbb{R}_{\geq 0}$ and sides $Lc - \delta$ and $w \in \mathbb{R}_{\geq 0}$, respectively, to reach lane $\ell_i^{f^*}$ (see Fig. 2.3). Since $w \ll L_c - \delta$, we approximate $ds \approx L_c - \delta$.

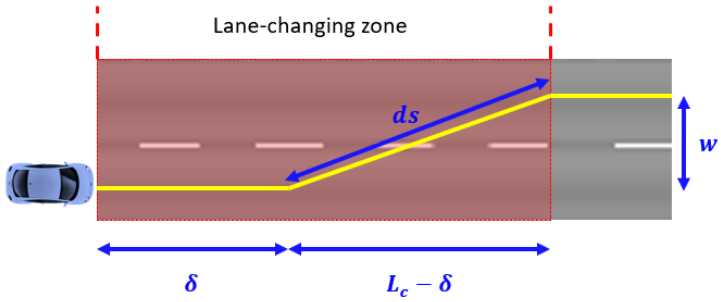

Figure 2.3: Lane-changing maneuver.

For CAV $i \in \mathcal{N}(t)$ the control-effort minimization with interior-point constraints at the boundary of each merging zone $z \in \mathcal{Z}_i$ is formulated as follows

Problem 2.2.14. *Control-effort minimization*

$$\begin{aligned} \min_{u_i \in \mathcal{U}_i} \quad & J_i(u_i(t)) = \frac{1}{2}\int_{t_i^0}^{t_i^f} u_i(t)^2 dt, \\ \text{subject to:} \quad & (2.1), (2.2), (2.3), (2.6), \\ \text{given} \quad & p_i(t_i^0), v_i(t_i^0), \\ & p_i(t_i^{z^*}), p_i(t_i^{z^*} + \Delta t_i^z), \ \ \forall z \in \mathcal{Z}_i. \end{aligned} \tag{2.16}$$

Recall that t_i^f is the time that CAV i exits the control zone, i.e., the merging zone of the last intersection along its path, $t_i^f = t_i^{z_n^*} + \Delta t_i^{z_n}$.

Solution of the Control-Effort Minimization

To derive the solution of the control-effort minimization (Problem 2.2.14), we apply Hamiltonian analysis. After solving the upper-level problem for CAV $i \in \mathcal{N}(t)$, the entry and exit time of merging zones $z \in \mathcal{Z}_i$ are the interior-point constraints for the low-level problem. First, we adjoin the control inequality constraints (2.2) along with the qth-order state variable inequality constraints to the Hamiltonian function. The qth-order state variable inequality constraint can be found by taking the successive total time derivative of constraint and substitute (2.1), until we obtain an expression that is explicitly dependent on the control variable [190]. For each CAV $i \in \mathcal{N}(t)$, with CAV $k \in \mathcal{A}_i^\ell, \ \ell = \ell_i^{f^*}$, physically located ahead of it, the Hamiltonian given by

$$\begin{aligned} H_i(t, p_i(t), v_i(t), u_i(t)) &= \frac{1}{2}u_i(t)^2 + \lambda_i^p v_i(t) + \lambda_i^v u_i(t) \\ &+\mu_i^a(u_i(t) - u_{i,\max}) + \mu_i^b(u_{i,\min} - u_i(t)) \\ &+\mu_i^c(u_i(t)) + \mu_i^d(-u_i(t)) \\ &+\mu_i^s(u_i(t) - u_k^*(t)), \end{aligned} \tag{2.17}$$

where λ_i^p and λ_i^v are costates, and $\mu_i^\top = [\mu_i^a, \mu_i^b, \mu_i^c, \mu_i^d, \mu_i^s]$ is a vector of Lagrange multipliers. It should be noted that $u_k^*(t)$ is the optimal control input for CAV $k \in \mathcal{A}_i^\ell, \ \ell = \ell_i^{f^*}$, which

is available information to CAV i through the coordinator. The Euler-Lagrange equations become:

$$\dot{\lambda}_i^p = -\frac{\partial H_i}{\partial p_i} = 0, \tag{2.18}$$

$$\dot{\lambda}_i^v = -\frac{\partial H_i}{\partial v_i} = -\lambda_i^p, \tag{2.19}$$

$$\frac{\partial H_i}{\partial u_i} = u_i + \lambda_i^v + \mu_i^a - \mu_i^b + \mu_i^c - \mu_i^d + \mu_i^s = 0. \tag{2.20}$$

Since the speed of CAV i is not specified at the fixed terminal time t_i^f, we have [190]

$$\lambda_i^v(t_i^f) = 0. \tag{2.21}$$

Since the arrival time of CAV $i \in \mathcal{N}(t)$ at the entry and exit of each merging zone $z \in \mathcal{Z}_i$, is specified, for each interior-point constraint at specified time t_1, we have the following condition

$$\mathbf{N}(\mathbf{x}_i(t), t) = \begin{bmatrix} p_i(t) - C \\ t - t_1 \end{bmatrix} = 0, \tag{2.22}$$

where C is the position at the specified time t_1 (i.e., entry/exit of merging zone). In addition, the costates and the Hamiltonian should satisfy the following jump conditions at t_1^- and t_1^+, [190]

$$\lambda_i^\top(t_1^-) = \lambda_i^\top(t_1^+) + \pi^\top \frac{\partial \mathbf{N}}{\partial \mathbf{x}_i}|_{t=t_1}, \tag{2.23}$$

$$H_i(t_1^-) = H_i(t_1^+) - \pi^\top \frac{\partial \mathbf{N}}{\partial t}|_{t=t_1}. \tag{2.24}$$

where $\lambda_i^\top = [\lambda_i^p, \lambda_i^v]$, $\pi^\top = [\pi_1, \pi_2]$, $\frac{\partial \mathbf{N}}{\partial x_i} = \begin{bmatrix} 1 & 0 \\ 0 & 0 \end{bmatrix}$ and $\frac{\partial \mathbf{N}}{\partial t} = [0, 1]^\top$. Hence,

$$\lambda_i^p(t_1^-) = \lambda_i^p(t_1^+) + \pi_1, \tag{2.25}$$

$$\lambda_i^v(t_1^-) = \lambda_i^v(t_1^+), \tag{2.26}$$

$$H_i(t_1^-) = H_i(t_1^+) - \pi_2. \tag{2.27}$$

Note that $\pi^\top$ is a 2-component vector of constant Lagrange multipliers, determined so that the interior-point constraint (2.22) is satisfied.

Unconstrained Solution Without Interior-point Constraints

If the state and control constraints never become active, $\mu_i^a = \mu_i^b = \mu_i^c = \mu_i^d = \mu_i^s = 0$ the solution, see [65], is

$$u_i^*(t) = a_i t + b_i, \tag{2.28}$$

by substituting (2.28) in (2.1), we have

$$v_i^*(t) = \frac{1}{2} a_i t^2 + b_i t + c_i, \tag{2.29}$$

$$p_i^*(t) = \frac{1}{6} a_i t^3 + \frac{1}{2} b_i t^2 + c_i t + d_i. \tag{2.30}$$

In the above equations a_i, b_i, c_i, d_i are constants of integration, which are found by substituting the initial and final conditions $p_i^*(t_i^0), v_i^*(t_i^0), p_i^*(t_i^f)$ and $u_i^*(t_i^f) = 0$.

Unconstrained Solution With Interior-point Constraints

To find the analytical solution for CAV $i \in \mathcal{N}(t)$ including the interior-point constraints at the entry and exit of merging zone $z \in \mathcal{Z}_i$ (recall that z_1 and z_n are the first and last merging zones that CAV i crosses, respectively, Definition 2.2.6), we need to satisfy $2n - 1$ interior-point constraints (t_i^f is excluded, since it is a boundary condition).

Lemma 2.2.15. *The optimal control input $u_i^*(t)$ when none of the constraints is active at the interior-point constraint $N_j,\ j \in \{1, \dots, 2n-1\}$, where n is the total number of merging zones in CAV i's path, is continuous.*

Proof. Let t_j be the time that we have an interior-point constraint $N_j,\ j \in \{1, \dots, 2n-1\}$. From (2.26), we know λ_i^v is continuous t_j, i.e.,

$$\lambda_i^v(t_j^-) = \lambda_i^v(t_j^+), \tag{2.31}$$

Since none of the state or control inequality constraints is active, we have $\mu_i^a = \mu_i^b = \mu_i^c = \mu_i^d = \mu_i^s = 0$ and from (2.20), we have $\lambda_i^v(t) = -u_i(t)$ which gives

$$u_i(t_j^-) = u_i(t_j^+). \tag{2.32}$$

□

Theorem 2.2.16. *The unconstrained solution of Problem 2.2.14 for CAV $i \in \mathcal{N}(t)$ with n merging zones, is a continuous piecewise linear function.*

Proof. For CAV $i \in \mathcal{N}(t)$, we first divide $[t_i^0, t_i^f]$ (recall that $t_i^f = t_i^{z_n^*} + \Delta t_i^{z_n}$) into $2n$ sub-intervals with corresponding optimal control input as follows:

$$u_i^*(t) = \begin{cases} u_i^{(1)}(t), & \text{if} \quad t_i^0 \le t < t_i^{z_1^*}, \\ u_i^{(2)}(t), & \text{if} \quad t_i^{z_1^*} \le t \le t_i^{z_1^*} + \Delta t_i^{z_1}, \\ & \vdots \\ u_i^{(2n-1)}(t), & \text{if} \quad t_i^{z_{n-1}^*} + \Delta t_i^{z_{n-1}} \le t \le t_i^{z_n^*}, \\ u_i^{(2n)}(t), & \text{if} \quad t_i^{z_n^*} \le t \le t_i^f. \end{cases} \tag{2.33}$$

Integrating (2.18) and (2.19) at each time-interval $j \in \{1, \dots, 2n\}$ and using (2.20), we get a linear form for $u_i^{(j)}(t)$. From Lemma 2.2.15, we have continuity of control input at each interior point, thus the control input is a continuous piecewise linear function. □

Corollary 2.2.17. *For CAV $i \in \mathcal{N}(t)$, let $\pi^{(j)} = [\pi_1^{(j)}, \pi_2^{(j)}]^\top$ be the constant Lagrange multipliers for the interior-point constraint $N_j,\ j \in \{1, \ldots, 2n-1\}$ at time t_j, where n is the total number of merging zones in CAV i's path. Then, we have*

$$\pi_2^{(j)} = -\pi_1^{(j)} v_i(t_j). \tag{2.34}$$

Proof. From (2.27) and (2.17), we have

$$\begin{aligned} &\frac{1}{2}u_i(t_j^-)^2 + \lambda_i^p(t_j^-)v_i(t_j^-) + \lambda_i^v(t_j^-)u_i(t_j^-) = \\ &\frac{1}{2}u_i(t_j^+)^2 + \lambda_i^p(t_j^+)v_i(t_j^+) + \lambda_i^v(t_j^+)u_i(t_j^+) - \pi_2, \end{aligned} \tag{2.35}$$

and by substituting (2.25) and $\lambda_i^v(t) = -u_i(t)$ into (2.35), we get

$$\begin{aligned} &-\frac{1}{2}u_i(t_j^-)^2 + \left(\lambda_i^p(t_j^+) + \pi_1^{(j)}\right) v_i(t_j^-) = \\ &\quad -\frac{1}{2}u_i(t_j^+)^2 + \lambda_i^p(t_j^+)v_i(t_j^+) - \pi_2^{(j)}. \end{aligned} \tag{2.36}$$

Using continuity of speed at the interior-point, i.e., $v_i(t_j^-) = v_i(t_j^+) = v_i(t_j)$ and rearranging (2.36), we get

$$-\frac{1}{2}u_i(t_j^-)^2 + \pi_1^{(j)} v_i(t_j) = -\frac{1}{2}u_i(t_j^+)^2 - \pi_2^{(j)}. \tag{2.37}$$

From Lemma (2.2.15), we have $u_i(t_j^-) = u_i(t_j^+)$. Therefore $\pi_2^{(j)} = -\pi_1^{(j)} v_i(t_j)$, and the proof is complete. □

The unconstrained solution with interior-point constraints for CAV $i \in \mathcal{N}(t)$ with n merging zones, consists of $2n$ unconstrained arcs as follows:

$$u_i^*(t) = \begin{cases} a_i^{(1)}t + b_i^{(1)}, & \text{if} \quad t_i^0 \le t < t_i^{z_1^*}, \\ a_i^{(2)}t + b_i^{(2)}, & \text{if} \quad t_i^{z_1^*} \le t \le t_i^{z_1^*} + \Delta t_i^{z_1}, \\ & \vdots \\ a_i^{(2n-1)}t + b_i^{(2n-1)}, & \text{if} \quad t_i^{z_{n-1}^*} + \Delta t_i^{z_{n-1}} \le t \le t_i^{z_n^*}, \\ a_i^{(2n)}t + b_i^{(2n)}, & \text{if} \quad t_i^{z_n^*} \le t \le t_i^f, \end{cases} \tag{2.38}$$

Initial conditions $p_i(t_i^0)$ and $v_i(t_i^0)$, final conditions $p_i(t_i^f)$ and $u_i(t_i^f)$, (4 equations), continuity of state and control at interior-point constraints ($3 \cdot (2n-1)$ equations), position at interior-point constraints ($2n-1$ equations), and jump conditions on λ_i^p at interior-point constraints ($2n-1$ equations) result in $10n-1$ equations, which form a system of linear equations that yields the optimal trajectory.

Remark 2.2.18. *After finding the optimal trajectory, along with $\pi_1^{(j)}, j \in \{1, \dots, 2n-1\}$, one can use Corollary 2.2.17 to find $\pi_2^{(j)}$ which satisfies (2.27).*

Theorem 2.2.19. *For the cases that none of the state/control inequality constraints becomes active, the control effort minimization problem with interior-point constraints always has a unique solution.*

Proof. The analytical solution for the unconstrained case with interior-point constraints is found by solving a system of linear equations in the classical form $AX = B$, where $A \in \mathbb{R}^{(10n-1)\times(10n-1)}$ is the coefficients matrix, $X \in \mathbb{R}^{(10n-1)\times 1}$ is the vector of $10n-1$ unknowns and $b \in \mathbb{R}^{(10n-1)\times 1}$ is the constant vector. Since there are $10n-1$ linearly independent equations, which forms row vectors in $AX = B$, we have $\text{rank}(A) = \text{rank}(A|B) = 10n-1$, and the proof is complete. □

Constrained solution

Using (2.38), we first start with the unconstrained solution of Problem 2.2.14. If the solution violates any of the speed (2.3) or control (2.2) constraints, then the unconstrained arc is pieced together with the arc corresponding to the violated constraint at unknown time τ_1, and we re-solve the problem with the two arcs pieced together. The two arcs yield a set of algebraic equations which are solved simultaneously using the boundary and interior conditions at τ_1. If the resulting solution violates another constraint, then the last two arcs are pieced together with the arc corresponding to the new violated constraint, and we re-solve the problem with the three arcs pieced together at unknown times τ_1 and τ_2. The three arcs will yield a new set of algebraic equations that need to be solved simultaneously using the

boundary and interior conditions at τ_1 and τ_2. The process is repeated until the solution does not violate any other constraints, [65, 176]. In the following section, we show the analysis for the case where the rear-end safety constraint becomes active.

Rear-end safety constraint becomes active

Suppose for CAV $i \in \mathcal{N}(t)$, at some time $t = \tau_1$, the rear-end safety constraint with the vehicle k becomes active until $t = \tau_2$, $p_k(t) - p_i(t) = \delta$ for all $t \in [\tau_1, \tau_2]$, in this case $\mu_i^s \neq 0$. At the entry of the constrained arc, we have the following tangency conditions

$$\mathbf{N}(\mathbf{x}_i(t), t) = \begin{bmatrix} p_i(t) - p_k^*(t) + \delta \\ v_i(t) - v_k^*(t) \end{bmatrix} = 0. \tag{2.39}$$

Since $\mathbf{N}(t, \mathbf{x}_i(t)) = 0$ for $t \in [\tau_1, \tau_2]$, its first derivative, which is dependent on the optimal control input, should vanish in $t \in [\tau_1, \tau_2]$, i.e.,

$$\mathbf{N}^{(1)}(t, \mathbf{x}_i(t)) = u_i^*(t) - u_k^*(t) = 0. \tag{2.40}$$

From (2.40), the optimal control input of CAV $i \in \mathcal{N}(t)$, when rear-end safety constraint is active, can be found $u_i^*(t) = u_k^*(t)$ The optimal solution needs to satisfy the following jump conditions on costates upon entry to the constrained arc at $t = \tau_1$,

$$\lambda_i^p(\tau_1^-) = \lambda_i^p(\tau_1^+) + [\pi_1, \pi_2]\frac{\partial \mathbf{N}}{\partial p_i} = \lambda_i^p(\tau_1^+) + \pi_1, \tag{2.41}$$

$$\lambda_i^v(\tau_1^-) = \lambda_i^v(\tau_1^+) + [\pi_1, \pi_2]\frac{\partial \mathbf{N}}{\partial v_i} = \lambda_i^v(\tau_1^+) + \pi_2, \tag{2.42}$$

$$H_i(\tau_1^-) = H_i(\tau_1^+) - [\pi_1, \pi_2]\frac{\partial \mathbf{N}}{\partial t} = H_i(\tau_1^+) + \pi_1 v_k^*(t) + \pi_2 u_k^*(t), \tag{2.43}$$

where π_1 and π_2 are constant Lagrange multipliers, determined so that (2.39) is satisfied. At the exit point of the constrained arc, we have

$$\lambda_i^p(\tau_2^-) = \lambda_i^p(\tau_2^+), \quad \lambda_i^v(\tau_2^-) = \lambda_i^v(\tau_2^+), \quad H_i(\tau_2^-) = H_i(\tau_2^+). \tag{2.44}$$

As described earlier, the three arcs need to be solved simultaneously using initial and final conditions (speed and position), interior-point constraints (2.22), and interior conditions at unknown times τ_1 and τ_2 (continuity of speed and position, jump conditions (2.39)-(2.44)).

2.2.4 Deviation From Nominal Planned Position

We extend the previous results to include a bounded steady-state error in CAV's position, which can be originated from the vehicle-level controller tracking the optimal trajectory. Namely, suppose that CAV i's actual position deviates from the nominal $p_i^*(t)$, which is the optimal solution of the Problem 2.2.14, and it takes values in $[p_i^*(t) - \epsilon\ , p_i^*(t) + \epsilon]$, where $\epsilon \in \mathbb{R}_{\geq 0}$ is the maximum deviation from the nominal path. To guarantee longitudinal and lateral safety, we consider the worst-case scenario in our upper-level and low-level planning analysis.

Low-level Safety

To guarantee rear-end safety between CAV $i \in \mathcal{N}(t)$ and CAV $k \in \mathcal{N}(t)$, where CAV $k \in \mathcal{A}_i^l,\ l = l_i^{f^*}$ is the vehicle immediately ahead of CAV i, we modify the rear-end safety constraint (2.6) as $(p_k(t) - \epsilon) - (p_i(t) + \epsilon) \geq \delta$, where it simplifies to $p_k(t) - p_i(t) \geq \delta + 2\epsilon$.

Thus, considering the worst-case scenario in the low-level planning results in increasing the rear-end safety distance $\delta_{\text{new}} = \delta + 2\epsilon$. However, this might be a conservative causing the rear-end safety constraint becomes active without being necessary and thus results in higher fuel consumption.

Upper-level Safety

In the low-level problem, we modified the rear-end safety constraint to guarantee safety in the worst-case scenario in the presence of a bounded steady-state error in the position. In addition, to ensure safety in the upper-level problem, we need to consider the error's effects in order to avoid lateral collision. By introducing the idle-time t_{idle}, acting as a safety buffer

in the presence of a bounded steady-state error in position, we modify the lateral safety constraints with idle-time as follows

$$t_i^{z^*} \geq t_j^{z^*} + \Delta t_j^z + t_{\text{idle}}, \tag{2.45}$$

or

$$t_i^{z^*} + \Delta t_i^z + t_{\text{idle}} \leq t_j^{z^*}, \tag{2.46}$$

where in (2.45), merging zone should be idle after CAV j's planned exit time and in (2.46) merging zone should be idle before CAV j's planned arrival time. To consider rear-end safety at entry of each merging zone, (2.14) is being adjusted as follows

$$t_i^{z^*} \geq t_k^{z^*} + \rho_k^z + t_{\text{idle}}. \tag{2.47}$$

The worst-case scenario for computing t_{idle} can be computed as follows

$$t_{\text{idle}} = \frac{2\epsilon}{v_{\min}}. \tag{2.48}$$

It should be noted that t_{idle} computed from (2.48) is very conservative, since it assumes that both vehicles cross the merging zone with minimum speed. Algorithm 3 can be employed to consider the deviation from the nominal planned position.

2.2.5 Simulation Results

To evaluate the effectiveness of the proposed framework in reducing fuel consumption and improving traffic throughput, we investigate the coordination of CAVs at three adjacent intersections in two scenarios under different traffic volumes, and then compare the results with a baseline scenario consisting of two-phase traffic signals. We construct the baseline scenario with two-phase fixed-time traffic signals in PTV-VISSIM [191], which is a commercial microscopic multi-modal traffic flow simulation software, by considering all vehicles as human-driven and without V2V communication. To emulate human-driven vehicles' driving

Algorithm 3 Recursive upper-level planning with idle-time

Input: ℓ_i^f
Output: Arrival time at merging zones $\mathcal{Z}_i = \{z_1, \ldots, z_n\}$

for $z \in \mathcal{Z}_i$ **do**
  $k = \max\{j \mid j \in \mathcal{A}_i^\ell\ ,\ \ell = \ell_i^f\}$
  $t_i^{z^*} \leftarrow \max\left\{\bar{t}_i^z, t_k^{z^*} + \rho_k^z + t_{\text{idle}}\right\}$
  `Sort` $\mathcal{T}_i^z$ `increasingly`
  for $t_j^{z^*} \in \mathcal{T}_i^z$ **do**
    if $t_j^{z^*} + \Delta t_j^z + t_{\text{idle}} \leq t_i^{z^*}$ **then**
      `continue`
    end if
    if $t_i^{z^*} + \Delta t_i^z + t_{\text{idle}} \leq t_j^{z^*}$ **then**
      `break`
    else
      $t_i^{z^*} \leftarrow t_j^{z^*} + \Delta t_j^z + t_{\text{idle}}$;
    end if
  end for
end for
return $\{t_i^{z^*} \mid z \in \mathcal{Z}_i\}$

behavior, we use a built-in car-following model (Wiedemann [192]) in PTV-VISSIM with default parameters. In the optimal-scenario, we use a dynamic-link library in PTV-VISSIM to simulate our framework. Videos from our simulation analysis can be found at the supplemental site, https://sites.google.com/view/ud-ids-lab/OCMI.

For the first scenario, we construct three symmetric adjacent intersections. We consider the length of each road connecting to the intersections to be $L = 150$ m, the length of the merging zones to be $S = 15$ m, and the distance between each intersection to be $D = 75$ m (see Fig. 2.4). The CAVs enter the control zone with initial speed uniformly distributed between 11 m/s to 13 m/s from each entry with equal traffic volumes.

Table 2.1 shows the average travel time of all CAVs inside the control zone for the baseline and optimal cases, respectively, at different traffic volumes ranging from 600 veh/h to 1,400 veh/h per lane for each entry. For each traffic volume, we performed five simulations with different random seeds and averaged the results. Within our proposed framework, average travel time has been decreased by $11\% - 24\%$ compared to the baseline scenario with two-phase traffic signals. Relative frequency histogram of travel time of each CAV for traffic volume 1,400 veh/h for one of the selected seed, which includes 119 vehicles, for the baseline

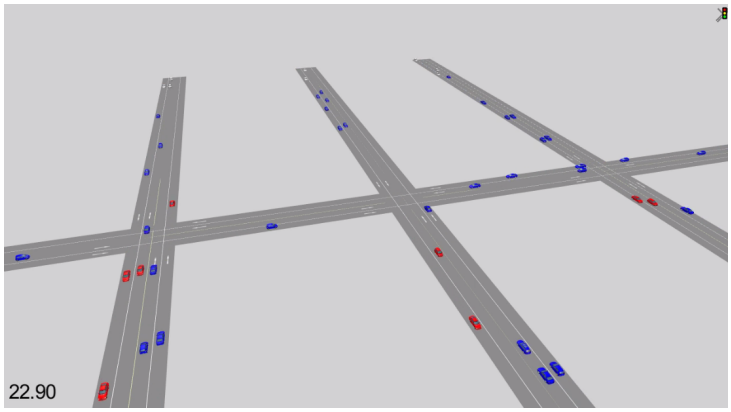

Figure 2.4: Snap-shot of the three multi-lane adjacent intersections in the first scenario.

and optimal scenarios are shown in Fig. 2.5. As it can be seen in Fig. 2.5, travel times for all CAVs are less than 40 s for the optimal scenario, whereas, in the baseline scenario, 23% of vehicles have travel time higher than 40 s. For the scenario shown in Fig. 2.5, the average travel time has been reduced by 17.62%.

Table 2.1: Average travel time of vehicles in the first scenario for the optimal and baseline cases under different traffic volumes.

Flow (veh/h)	Average number of vehicles	Average travel time (s)		
		Baseline	Optimal	%
600	44	25.51	19.41	24
800	61	25.14	20.23	20
1,000	76	26.03	20.59	21
1,200	91	26.26	21.99	16
1,400	110	27.27	24.30	11

To investigate the computational complexity of our approach, for each traffic flow in each seed, the time that it takes for a CAV to compute the optimal trajectory is recorded, and then averaged across all the CAVs. For each traffic flow, we choose the seed with a maximum mean of computation time to report. The mean and standard deviation of computation times of CAVs in our optimal proposed framework for different traffic volumes are listed in Table 2.2. It shows that our approach is computationally feasible and does not grow exponentially with increasing the traffic volume. Note that since our scheme is decentralized, there is not a relation between the traffic flow and computation times.

Table 2.2: The mean and standard deviation of computation times of CAVs in the first scenario.

Traffic volume	600	800	1,000	1,200	1,400
Mean (ms)	0.21	0.19	0.18	0.18	0.17
Standard deviation (ms)	0.14	0.14	0.13	0.13	0.13

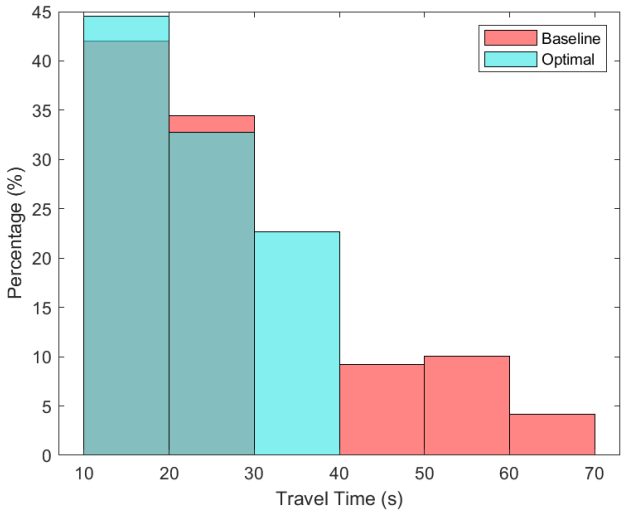

Figure 2.5: A travel time of each vehicle for the first scenario in the baseline and optimal cases under traffic volume $1{,}400$ veh/h.

Our next measure of effectiveness is time-delay, which is computed as a difference between the vehicle's travel time, and the time that it would have taken for the vehicle to cruise with the same speed as the one that it entered the control zone. For CAV $i \in \mathcal{N}(t)$, the time-delay is denoted by t_i^{delay} and given by

$$t_i^{\text{delay}} = (t_i^f - t_i^0) - \frac{p_i(t_i^f) - p_i(t_i^0)}{v_i(t_i^0)}. \tag{2.49}$$

Average delay of all CAVs inside the control zone for the baseline and optimal scenarios at different traffic volumes ranging from 600 veh/h to $1{,}400$ veh/h per lane for each entry, along with the percentage of improvement are illustrated in Fig. 2.6. As shown in Fig. 2.6, in our proposed framework the average delay has been reduced 47% - 85% compared to the baseline scenario.

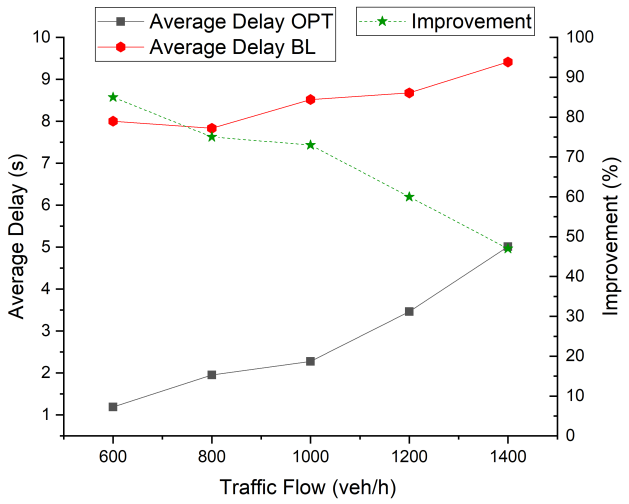

Figure 2.6: Average delay of vehicles in the first scenario for the baseline and optimal cases.

The instantaneous average, maximum, and minimum speed of CAVs inside the control zone for the baseline and optimal scenarios with traffic volume 600 veh/h, $1{,}000$ veh/h, and $1{,}400$ veh/h for three randomly selected seeds are shown in Fig. 2.7. The average speed for the optimal scenario is higher than the average speed in the baseline scenario most of the time, which shows improved traffic throughput. The instantaneous minimum speed for all traffic volumes in the optimal scenario is positive indicating smooth traffic flow, compared to the baseline scenario, which experiences much stopping due to the traffic lights. The position, speed, and control input for a CAV entering the control zone from the east are shown in Fig. 2.8 for the optimal proposed framework, and in Fig. 2.9 for the baseline scenario. As it was shown earlier (Theorem 2.2.16), the control input is a continuous piecewise linear function. We can see in Fig. 2.8 that the CAV needs to accelerate to satisfy the imposed average speed at each merging zone. Choosing the optimal speed for v^z_{avg} may reduce this oscillation, and potentially improve the system's efficiency.

To evaluate fuel efficiency improvement achieved by our proposed framework, we use a polynomial meta-model proposed in [193], which approximates the fuel consumption in ml/s as a function of speed and control input of a CAV and coefficients obtained from an engine torque-speed-efficiency map of a typical car. Table 2.3 summarizes the average

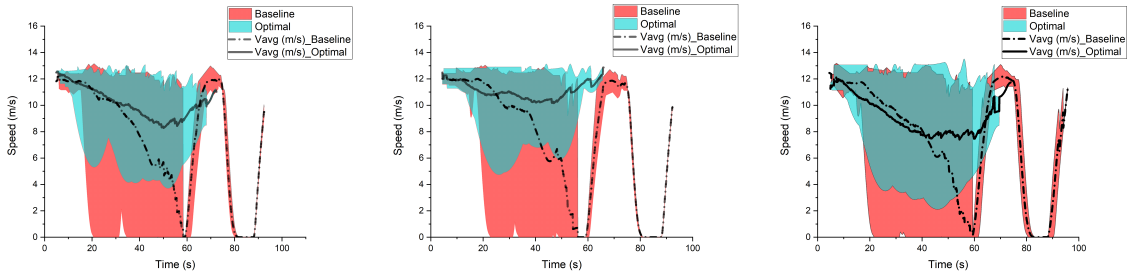

(a) (b) (c)

Figure 2.7: The instantaneous average, maximum and minimum speed of CAVs inside the control zone in the first scenario for the baseline and optimal cases with traffic volume (a) 600 veh/h, (b) 1,000 veh/h and (c) 1,400 veh/h.

fuel consumption and the average cumulative fuel consumption for the optimal and baseline scenarios at different traffic volumes for which five simulations with different random seeds were performed, and the results were averaged. It can be noted that our optimal framework results in better fuel efficiency compared to the baseline scenario. Within our optimal framework, the average cumulative fuel consumption has been improved by 32% - 55% compared to the baseline scenario with two-phase traffic signals.

Table 2.3: Average fuel consumption and average cumulative fuel consumption in first scenario for the optimal and baseline cases under different traffic volumes.

Flow	Average fuel consumption (ml/s)		Average cumulative fuel consumption (ml)		
(veh/h)	Baseline	Optimal	Baseline	Optimal	%
600	0.32	0.19	8.87	3.89	55
800	0.33	0.21	8.91	4.58	48
1,000	0.34	0.23	9.46	4.92	48
1,200	0.34	0.25	9.54	5.80	39
1,400	0.34	0.27	10.01	6.79	32

In the second scenario, we consider an asymmetric corridor in W 4th street in Wilmington, Delaware consisting of three adjacent intersections with N Orange street, N Shipley street, and N Market street (see Fig. 2.10). In terms of geometry, this is an asymmetric scenario since it consists of one way and two-way roads. The incoming traffic flows are also not symmetric, since one of the streets has two incoming lanes. We consider the length of

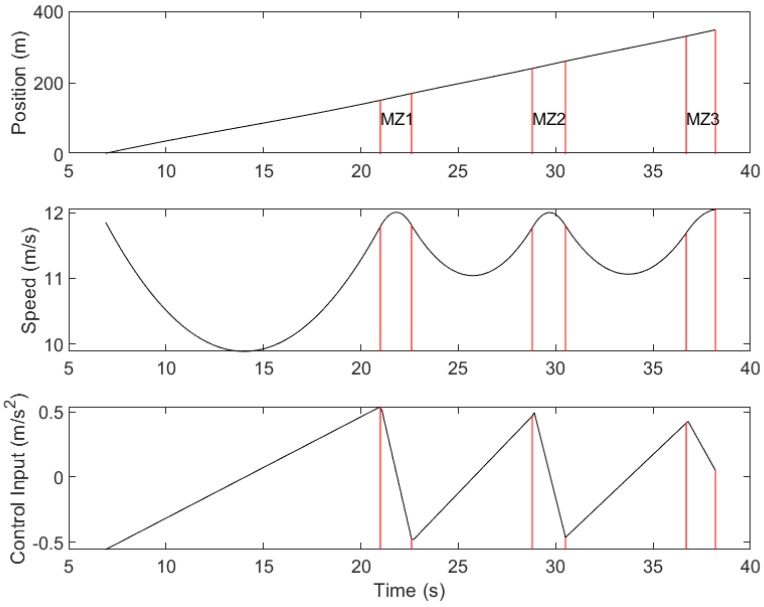

Figure 2.8: The position, speed and control input for a CAV entering the control zone from east for the optimal case in the first scenario.

each road connecting to the intersections to be $L = 150$ m. The vehicles enter the control zone with initial speed uniformly distributed between 8 m/s to 11 m/s from each entry with equal traffic volumes. For each traffic volume, we performed five simulations with different random seeds and averaged the results.

Table 2.4 contains the average travel time and average delay of all CAVs inside the control zone for the baseline and optimal cases, respectively, at different traffic volumes ranging from 600 veh/h to $1{,}400$ veh/h per lane for each entry. The results indicate that three is $21\% - 35\%$ reduction in the average travel time, and $57\% - 84\%$ decrease in the average delay compared to the baseline scenario with two-phase traffic signals.

Table 2.5 shows the average fuel consumption and the average cumulative fuel consumption for the optimal and baseline cases at different traffic volumes. The results further support the improvement in fuel efficiency by using the optimal framework. Namely, the average cumulative fuel consumption has been improved by 54% - 62% compared to the baseline scenario with two-phase traffic signals.

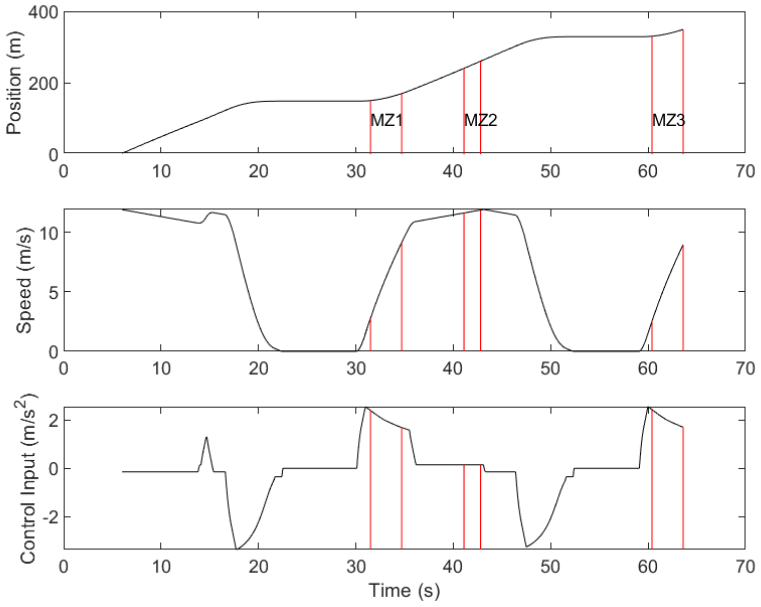

Figure 2.9: The position, speed, and control input for a CAV entering the control zone from east for the baseline case in the first scenario.

2.3 Time-Optimal Coordination for Connected and Automated Vehicles at Adjacent Intersections

In this section, we provide a different bi-level coordination framework for CAVs at two adjacent intersections. This framework consists of an upper-level scheduling problem and a low-level optimal control problem. By partitioning the area around two adjacent intersections into different zones, we formulate a scheduling problem for each individual CAV aimed at minimizing its total travel time. For each CAV, the solution of the upper-level problem designates the arrival times at each zones on its path which becomes the inputs of the low-level problem. The solution of the low-level problem yields the optimal control input (acceleration/deceleration) of each CAV to exit the intersections at the time specified in the upper-level scheduling problem. We validate the performance of our proposed hierarchical framework through extensive numerical simulations and comparison with signalized intersections, centralized scheduling, and FIFO queuing policy.

We organize this section as follows. In subsection 2.3.1, we provide a detailed

Figure 2.10: An asymmetric corridor in W 4th street in Wilmington, Delaware, second scenario.

Table 2.4: Average travel time and delay of vehicles in in the second scenario for the optimal and baseline cases under different traffic volumes.

Flow	Avg. travel time (s)			Avg. delay (s)		
(veh/h)	Baseline	Optimal	%	Baseline	Optimal	%
600	37.72	24.53	35	15.92	2.56	84
800	39.67	25.89	35	17.80	3.47	80
1,000	40.10	28.65	29	18.17	5.42	70
1,200	40.69	30.38	25	18.57	6.52	65
1,400	42.25	33.38	21	19.98	8.68	57

exposition of the formulation of both low-level and upper-level optimization problems, while in subsection 2.3.4, we derive the corresponding solutions. Finally, we demonstrate the effectiveness of our approach through simulation in subsection 2.3.5.

2.3.1 Problem Formulation

We consider two adjacent intersections shown in Fig. 2.11 which are closely distanced from each other. We partition the roads around the intersections into $n_z \in \mathbb{N}$ zones where each zone has a unique integer index that belongs to the set $\mathcal{M} = \{1, \ldots, n_z\}$. Although the number n_z of partitions is arbitrary, choosing a big number increases the burden of computation for the scheduling problem since each CAV $i \in \mathcal{N}(t)$ needs to find its arrival time at each zone. We consider each road connecting to the merging zone to be a single zone.

Table 2.5: Average fuel consumption and average cumulative fuel consumption in second scenario for the optimal and baseline cases under different traffic volumes.

Flow (veh/h)	Average fuel consumption (ml/s)		Average cumulative fuel consumption (ml)		
	Baseline	Optimal	Baseline	Optimal	%
600	0.25	0.14	9.36	3.86	59
800	0.25	0.13	9.74	3.73	62
1,000	0.24	0.13	9.79	4.14	58
1,200	0.24	0.13	9.96	4.44	55
1,400	0.24	0.14	10.18	4.73	54

Similarly, we partition each merging zone into four smaller zones (Fig. 2.11). Without being restrictive in our analysis, the total number of zones in the two intersections considered here (Fig. 2.11) is $n_z = 22$. We should note that zones are numbered arbitrarily.

Definition 2.3.1. *When CAV $i \in \mathcal{N}(t)$ enters the control zone, it creates a tuple of the zones $\mathcal{I}_i := [m_1, \ldots, m_n]$, $m_n \in \mathcal{M}$, $n \in \mathbb{N}$, defined as the "path" of CAV i, where m_1 and m_n denote the first and last zone on its path respectively, that i needs to cross until it exits the control zone.*

Definition 2.3.2. *For each CAV $i \in \mathcal{N}(t)$ upon entering the control zone, we define the set $\mathcal{C}_{i,j}$ of conflict zones with CAV $j \in \mathcal{N}(t) \setminus \{i\}$, which is present in the control zone ($j < i$),*

$$\mathcal{C}_{i,j} = \{m \mid m \in \mathcal{M},\ m \in \mathcal{I}_i\ ,\ m \in \mathcal{I}_j\}. \tag{2.50}$$

For example in Fig. 2.11, CAV #3 has the following conflict tuples with CAV #1 and #2 respectively: $\mathcal{C}_{3,1} = \{7\}$ and $\mathcal{C}_{3,2} = \{4, 13, 7, 8, 19\}$.

Definition 2.3.3. *Let CAV $k \in \mathcal{N}(t) \setminus \{i\}$ be the preceding vehicle of CAV $i \in \mathcal{N}(t)$ in zone $m \in \mathcal{M}$. The distance, $d^m(p_k(t), p_i(t))$, between i and k in zone m is defined as*

$$d^m(p_k(t), p_i(t)) = (p_k(t) - p_k(T_k^m)) - (p_i(t) - p_i(T_i^m)), \tag{2.51}$$

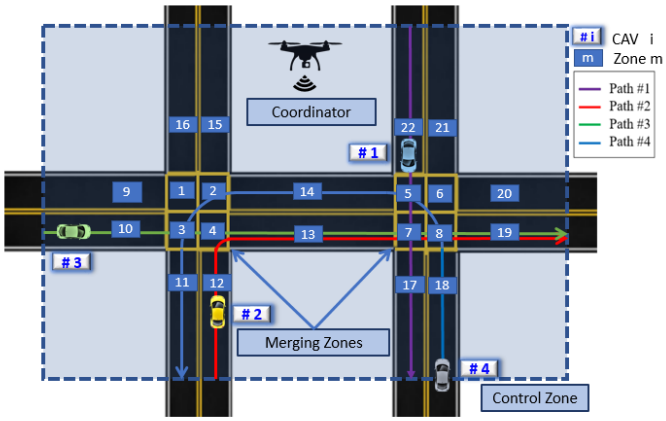

Figure 2.11: Two interconnected intersections with a drone as a coordinator. Zones numbered topologically and the fixed path for each CAV is shown.

where $p_k(T_k^m), p_i(T_i^m) \in \mathbb{R}_{\geq 0}$ *correspond to the distances from the entry point of the control zone to the entry point of the conflict zone* m *for CAV* k *and* i *respectively. If no such CAV* k *leads CAV* i *at zone* m*, then we let* $d^m(\cdot) \to \infty$*. Note that,* $p_k(T_k^m)$ *and* $p_i(T_i^m)$ *depends on the geometry of the control zone and intersections.*

To ensure the absence of rear-end collision between CAV $i \in \mathcal{N}(t)$ and the preceding CAV $k \in \mathcal{N}(t) \setminus \{i\}$ in zone $m \in \mathcal{I}_i$, while $m \in \mathcal{I}_k$, we impose the following rear-end safety constraint

$$d^m(p_k(t), p_i(t)) \geq \delta_i(t), \ t \in [T_i^m, T_i^{m'}], \tag{2.52}$$

where T_i^m and $T_i^{m'}$ are the entry time at and exit time from from zone m of CAV i respectively, and $\delta_i(t)$ is a predefined safe distance. The minimum safe distance $\delta_i(t)$ is a function of speed

$$\delta_i(t) = \gamma + \varphi \cdot v_i(t), \ t \in [T_i^m, T_i^{m'}], \tag{2.53}$$

where γ is the standstill distance, and φ is the reaction time.

In our modeling framework described above, we impose the following assumption

Assumption 2.3.4. *The speed of each CAV* $i \in \mathcal{N}(t)$ *at the boundary of zone* $m \in \mathcal{M}$ *in the merging zones is given and is equal to* v_{merge}*.*

This assumption can be relaxed by estimating the speed at the boundaries of each zone in the upper-level problem.

2.3.2 Upper-level Problem: Scheduling

The objective of each CAV inside the control zone is to derive the optimal control input (acceleration/deceleration) aimed at minimizing travel time and improving traffic throughput. In the upper-level scheduling problem, each CAV $i \in \mathcal{N}(t)$ computes its arrival time to each zone $m \in \mathcal{I}_i$ that minimizes its total travel time inside the control zone and guarantees lateral safety constraints.

Scheduling is a decision-making process that addresses the optimal allocation of resources to tasks over given time periods [194]. Thus, in what follows, we use scheduling theory to find the time that CAV $i \in \mathcal{N}(t)$ has to reach the zone $m \in \mathcal{I}_i$. Each zone $m \in \mathcal{M}$ represents a "resource," and CAVs crossing this zone are the "jobs" assigned to the resource.

Definition 2.3.5. *The time that a CAV $i \in \mathcal{N}(t)$ enters a zone $m \in \mathcal{I}_i$ is called "schedule" and is denoted by $T_i^m \in \mathbb{R}_{\geq 0}$. For CAV $i \in \mathcal{N}(t)$, we define a "schedule tuple,"*

$$\mathcal{T}_i = [T_i^m \mid m \in \mathcal{I}_i]. \tag{2.54}$$

For example, the schedule tuple of CAV #1 in Fig. 2.11 is $\mathcal{T}_1 = [T_1^{22}, T_1^5, T_1^7, T_1^{17}]$. For each zone $m \in \mathcal{I}_i$, $i \in \mathcal{N}(t)$, the schedule $T_i^m \in \mathbb{R}_{\geq 0}$ is bounded by

$$T_i^{\underline{m}} + R_i^m \leq T_i^m \leq T_i^{\underline{m}} + D_i^m, \tag{2.55}$$

where $\underline{m} \in \mathcal{I}_i$ is the zone right before zone $m \in \mathcal{I}_i$, $T_i^{\underline{m}}$ is the time that CAV i enters the zone $\underline{m}$, and $R_i^m \in \mathbb{R}_{\geq 0}$ and $D_i^m \in \mathbb{R}_{\geq 0}$ are the shortest and latest feasible times that it takes for CAV $i \in \mathcal{N}(t)$ to travel through the zone $\underline{m}$ respectively. $R_i^m \in \mathbb{R}_{\geq 0}$ and $D_i^m \in \mathbb{R}_{\geq 0}$ are called the *release time* and the *deadline* of the job respectively.

Remark 2.3.6. *The exit time, $T_i^{m'}$, of CAV $i \in \mathcal{N}(t)$ from zone $m \in \mathcal{I}_i$ is equal to the entry time to zone $\bar{m} \in \mathcal{I}_i$, which is the zone that CAV i crosses right after zone m.*

$$T_i^{m'} = T_i^{\bar{m}}. \tag{2.56}$$

Definition 2.3.7. *For each CAV $i \in \mathcal{N}(t)$, we define the set Γ_i of all feasible time headways which do not violate the rear-end safety constraint (2.52) at the entry of all zones $m \in \mathcal{I}_i$.*

Definition 2.3.8. *For each CAV $i \in \mathcal{N}(t)$ and $j \in \mathcal{N}(t) \setminus \{i\}$, $j < i$, the safety constraint at the entry of zone $m \in \mathcal{C}_{i,j}$ can be restated as*

$$|T_i^m - T_j^m| \geq t_h, \tag{2.57}$$

where $t_h \in \Gamma_i$ is the minimum time headway to avoid lateral collision.

Remark 2.3.9. *Definition 2.3.8 relaxes the FIFO queuing policy for entering zone $m \in \mathcal{M}$ by restricting the absolute value of the difference between the two schedules, rather than just enforcing $T_i^m - T_j^m \geq t_h$.*

Problem 2.3.10. *(Scheduling problem) For each CAV $i \in \mathcal{N}(t)$ with schedule tuple $\mathcal{T}_i$ and minimum time headway $t_h \in \Gamma_i$, the scheduling problem is formulated as follows*

$$\begin{aligned} \min_{\mathcal{T}_i} \quad & J_i^{[1]}(\mathcal{T}_i) = t_i^f(\mathcal{T}_i), \\ \text{subject to: } & (2.55), (2.57). \end{aligned} \tag{2.58}$$

Remark 2.3.11. *In Problem 2.3.10, the time t_i^f that each CAV i exits the control zone is a function of the schedule tuple $\mathcal{T}_i$ as implied by (2.55), which relates the arrival time at each zone to the arrival time at its previous zone.*

Upon entering the control zone, CAV i solves the scheduling problem that yields its time-optimal arrival time at each zone. Then, it shares the schedule tuples with the drone.

Consider, for example (see Fig. 2.11), CAV #3 with $\mathcal{I}_3 = [10, 3, 4, 13, 7, 8, 19]$, $\mathcal{C}_{3,1} = \{7\}$ and $\mathcal{C}_{3,2} = \{4, 13, 7, 8, 19\}$. The constraint (2.55) for each zone $m \in \mathcal{I}_3$ is

$$t_3^0 + R_3^{10} \leq T_3^3 \leq t_3^0 + D_3^{10}, \qquad T_3^3 + R_3^3 \leq T_3^4 \leq T_3^3 + D_3^3, \tag{2.59}$$

$$T_3^4 + R_3^4 \leq T_3^{13} \leq T_3^4 + D_3^4, \qquad T_3^{13} + R_3^{13} \leq T_3^7 \leq T_3^{13} + D_3^{13}, \tag{2.60}$$

$$T_3^7 + R_3^7 \leq T_3^8 \leq T_3^7 + D_3^7, \qquad T_3^8 + R_3^8 \leq T_3^{19} \leq T_3^8 + D_3^8, \tag{2.61}$$

$$T_3^{19} + R_3^{19} \leq t_3^f \leq T_3^{19} + D_3^{19}. \tag{2.62}$$

Note that the time CAV #3 enters the zone $\#10$, T_3^{10} is equal to the time that CAV $\#$ 3 enters the control zone t_3^0. From the safety constraint (2.57) for $m \in \mathcal{C}_{3,1}$ and $m \in \mathcal{C}_{3,2}$ we have

$$|T_3^7 - T_1^7| \geq t_h, \qquad |T_3^4 - T_2^4| \geq t_h, \qquad |T_3^{13} - T_2^{13}| \geq t_h, \tag{2.63}$$

$$|T_3^7 - T_2^7| \geq t_h, \qquad |T_3^8 - T_2^8| \geq t_h, \qquad |T_3^{19} - T_2^{19}| \geq t_h, \tag{2.64}$$

where the schedule tuples of CAV #1 and #2 are accessible through the drone. CAV $i \in \mathcal{N}(t)$ derives the release time and the deadline of each zone $m \in \mathcal{I}_i$ prior to solving the scheduling problem (Problem 2.3.10). CAV #3 above, for example, computes R_3^m and D_3^m for all $m \in \mathcal{I}_3$, and then it solves the scheduling problem, the solution of which yields the tuple $\mathcal{T}_3$. Next, we formulate the problems that yield the release time and deadline respectively.

Problem 2.3.12. *(Release time problem) For each CAV $i \in \mathcal{N}(t)$ and each zone $m \in \mathcal{I}_i$, the release time R_i^m is derived by the following optimization problem*

$$\begin{aligned} &\min_{u_i \in \mathcal{U}_i} J_i^{[2]}(u_i(t)) = t_i^{e,m}(u_i(t)) - t_i^{s,m}, \\ &\text{subject to: (2.1), (2.2), (2.3),} \\ &\text{given } \ p_i(t_i^{s,m}), v_i(t_i^{s,m}), p_i(t_i^{e,m}), v_i(t_i^{e,m}), \end{aligned} \tag{2.65}$$

where $t_i^{s,m}$ and $t_i^{e,m}$ are the time that CAV $i \in \mathcal{N}(t)$ enters and exits the zone $m \in \mathcal{I}_i$ respectively. The optimal solution $u_i^*(t)$ of Problem 2.3.12 yields the release time, $R_i^m = t_i^{e,m}(u_i^*(t)) - t_i^{s,m}$, which is the shortest feasible time that it takes for CAV i to travel through

zone m without considering safety.

Problem 2.3.13. *(Deadline problem) For each CAV $i \in \mathcal{N}(t)$ and each zone $m \in \mathcal{I}_i$, the deadline D_i^m is derived by the following optimization problem*

$$\begin{aligned} &\max_{u_i \in \mathcal{U}_i} \ J_i^{[3]}(u_i(t)) = t_i^{e,m}(u_i(t)) - t_i^{s,m}, \\ &\text{subject to: } (2.1), (2.2), (2.3), \\ &\text{given } \ p_i(t_i^{s,m}), v_i(t_i^{s,m}), p_i(t_i^{e,m}), v_i(t_i^{e,m}). \end{aligned} \tag{2.66}$$

The optimal solution $u_i^*(t)$ of Problem 2.3.13 yields the deadline, $D_i^m = t_i^{e,m}(u_i^*(t)) - t_i^{s,m}$, which is the latest feasible time that it takes for CAV i to travel through zone m without considering safety.

Remark 2.3.14. *Note that in Problems 2.3.12 and 2.3.13, we do not consider safety constraints. The only objective of these two problems is to find the feasible bound for arrival time at each zone m in (2.55), to form the scheduling problem (Problem 2.3.10).*

2.3.3 Low-level Problem: Energy Minimization

After solving the upper-level scheduling problem, the low-level problem yields for each CAV the minimum control input at each zone (acceleration/deceleration) that satisfies the schedule resulted from the upper-level problem. We demonstrate the system architecture in Fig. 2.12

Problem 2.3.15. *For each CAV $i \in \mathcal{N}(t)$ and each zone $m \in \mathcal{I}_i$, the energy minimization problem is*

$$\begin{aligned} &\min_{u_i \in \mathcal{U}_i} J_i^{[4]}(u_i(t), T_i^m, T_i^{\bar{m}}) = \frac{1}{2} \int_{T_i^m}^{T_i^{\bar{m}}} u_i^2(t)\, dt, \\ &\text{subject to: } (2.1), (2.2), (2.3), (2.52), \\ &\text{given } \ p_i(T_i^m), v_i(T_i^m), p_i(T_i^{\bar{m}}), v_i(T_i^{\bar{m}}), T_i^m, T_i^{\bar{m}}, \end{aligned} \tag{2.67}$$

where T_i^m and $T_i^{\bar{m}}$ are the entry and exit time of CAV $i \in \mathcal{N}(t)$ from zone $m \in \mathcal{I}_i$, determined by the upper-level scheduling problem.

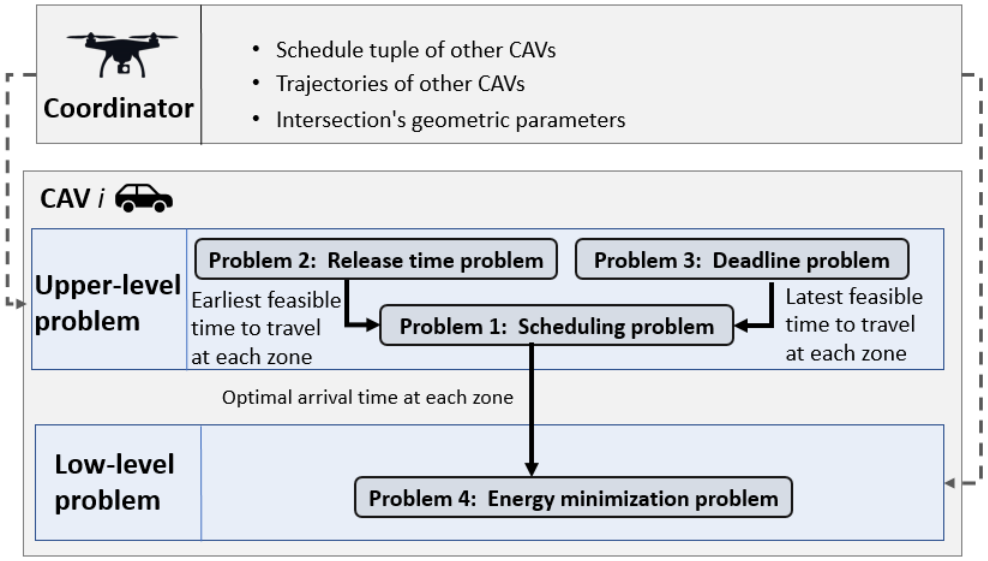

Figure 2.12: The hierarchical system architecture for CAV i and drone (coordinator)

2.3.4 Solution of Low-level and Upper-level Problems

In the previous subsection, we described the bi-level optimization framework that consists of three upper-level problems and one low-level problem. Upon entering the control zone, each CAV is added to the queue $\mathcal{N}(t)$, and it solves the upper-level problems (Problems 2.3.10, 2.3.12 and 2.3.13) the solutions of which designate the optimal entry time to each zone along its path. In the upper-level problems, each CAV first derives the release time and deadline (Problems 2.3.12 and 2.3.13) for each zone prior to solving the scheduling problem (Problem 2.3.10). The outcome of the upper-level scheduling problem becomes the input of the low-level problem (Problem 2.3.15). In particular, in the low-level problem (Problem 2.3.15), each CAV derives the optimal control input (acceleration/deceleration) that minimizes energy consumption at each zone of its path at the times specified in the upper-level (Problem 2.3.10).

To this end, to simplify notation, we use p_i^s, v_i^s, p_i^e and v_i^e instead of $p_i(t_i^{s,m})$, $v_i(t_i^{s,m})$, $p_i(t_i^{e,m})$ and $v_i(t_i^{e,m})$ respectively.

Analytical solution of the release time and the deadline

Here, we provide the analytical closed-form solutions to Problems 2.3.12 and 2.3.13, which each CAV $i \in \mathcal{N}(t)$ uses to formulate the scheduling problem (Problem 2.3.10). One of the main advantages of deriving analytical solutions to Problem 2.3.12 and 2.3.13 is to improve the computational effort in the upper-level problem. For the analytical solution of the release time problem (Problem 2.3.12), we apply Hamiltonian analysis. For each CAV $i \in \mathcal{N}(t)$ the Hamiltonian function with the state and control constraints adjoined is

$$\begin{aligned} &H_i(t, p_i(t), v_i(t), u_i(t), \lambda_i(t)) = 1 + \lambda_i^p v_i(t) + \lambda_i^v u_i(t) + \mu_i^a(u_i(t) - u_{\max}) \\ &+\mu_i^b(u_{\min} - u_i(t)) + \mu_i^c(v_i(t) - v_{\max}) + \mu_i^d(v_{\min} - v_i(t)), \end{aligned} \tag{2.68}$$

where λ_i^p and λ_i^v are costates, and $\mu_i^\top = [\mu_i^a, \mu_i^b, \mu_i^c, \mu_i^d, \mu_i^s]$ is a vector of Lagrange multipliers.

The Euler-Lagrange equations become:

$$\dot{\lambda_i^p} = -\frac{\partial H_i}{\partial p_i} = 0, \qquad \dot{\lambda_i^v} = -\frac{\partial H_i}{\partial v_i} = -\lambda_i^p - \mu_i^c + \mu_i^d. \tag{2.69}$$

Similarly for the deadline problem (Problem 2.3.13), the Hamiltonian function is

$$\begin{aligned} &H_i(t, p_i(t), v_i(t), u_i(t), \lambda_i(t)) = -1 + \lambda_i^p v_i(t) + \lambda_i^v u_i(t) + \mu_i^a(u_i(t) - u_{\max}) \\ &+\mu_i^b(u_{\min} - u_i(t)) + \mu_i^c(v_i(t) - v_{\max}) + \mu_i^d(v_{\min} - v_i(t)). \end{aligned} \tag{2.70}$$

State constraints are not active

First, we consider the case where the state constraint (2.3) does not become active, hence $\mu_i^c = \mu_i^d = 0$.

Lemma 2.3.16. *The sign of the optimal control input of the release time problem (Problem 2.3.12) for zone m, when the state constraint is not active, can change at most once, and it is equal to either: (1) $u_i(t) = u_{\min}$, or (2) $u_i(t) = u_{\max}$, or (3) $u_i(t) = u_{\max}$ and then it switches to $u_i(t) = u_{\min}$.*

Proof. If the state constraints for the release time problem (Problem 2.3.12) are not active, this implies that $\mu_i^c = \mu_i^d = 0$. Solving (2.69), we have $\lambda_i^{p^*}(t) = a_i$ and $\lambda_i^{v^*}(t) = -a_i t + b_i$, where a_i, b_i are the constants of integration. From Pontryagin's minimum principle, the optimal control input should satisfy the following condition

$$H(t, p_i^*(t), v_i^*(t), u_i^*(t), \lambda_i^*(t)) \leq H(t, p_i^*(t), v_i^*(t), u_i(t), \lambda_i^*(t)). \tag{2.71}$$

Substituting (2.68) in above equation, and simplifying yields $\lambda_i^{v^*}(t)\ u_i^*(t) \leq \lambda_i^{v^*}(t)\ u_i(t)$. Therefore, $u^*(t)$ is found as follows

$$u_i^*(t) = \begin{cases} u_{\min}, & \text{if} \quad \lambda_i^{v^*}(t) > 0 \\ u_{\max}, & \text{if} \quad \lambda_i^{v^*}(t) < 0 \end{cases}. \tag{2.72}$$

It follows immediately from the linearity of $\lambda_i^{v^*}(t)$ that its sign can change at most once. For the second statement, we use the fact that we can have at most one switching point. There are four cases that we should consider: Case 1: $u_i^*(t) = u_{\min}$, Case 2: $u_i^*(t) = u_{\max}$, Case 3: $u_i^*(t) = u_{\max}$ and then it switches to $u_i^*(t) = u_{\min}$, and Case 4: $u_i^*(t) = u_{\min}$ and then it switches to $u_i^*(t) = u_{\max}$. The initial and final states, denoted by $[p_i^s, v_i^s]^\top$ and $[p_i^e, v_i^e]^\top$ respectively, are known.

Case 1: If CAV $i \in \mathcal{N}(t)$ decelerates with $u_{\min}$, then from (2.1) its final speed is $v_i^f = \sqrt{2u_{\min} \cdot (p_i^e - p_i^s) + v_i^{s2}}$.

Case 2: If CAV $i \in \mathcal{N}(t)$ accelerates with $u_{\max}$, similarly from (2.1) its final speed is $v_i^f = \sqrt{2u_{\max} \cdot (p_i^e - p_i^s) + v_i^{s2}}$.

Case 3: We have $u_{\max}$ then $u_{\min}$, this implies the following:

$$\lambda_i^{v^*}(t) = \begin{cases} - & \text{, if} \quad t_i^{s,m} \leq t < t_i^{c,m} \\ 0 & \text{, if} \quad t = t_i^{c,m} \\ + & \text{, if} \quad t_i^{c,m} < t \leq t_i^{e,m} \end{cases}, \tag{2.73}$$

where $t_i^{c,m}$ is the time that the control input changes sign, and $\dot{\lambda_i^{v^*}}(t) = -\lambda_i^{p^*} = -a_i > 0$. Evaluating the Hamiltonian along the optimal control at $t_i^{c,m}$ yields

$$H_i(t_i^{c,m}, p_i^*(t_i^{c,m}), v_i^*(t_i^{c,m}), u_i^*(t_i^{c,m}), \lambda_i^*(t_i^{c,m})) = 1 + \lambda_i^{p^*} v_i^*(t_i^{c,m}). \tag{2.74}$$

Since the final time $t = t^{e,m}$ is not specified, the transversality condition gives

$$H_i(t_i^{e,m}, p_i^*(t_i^{e,m}), v_i^*(t_i^{e,m}), u_i^*(t_i^{e,m}), \lambda_i^*(t_i^{e,m})) = 0. \tag{2.75}$$

Additionally, the Hamiltonian (2.68) must be constant along the optimal solution, since it is not an explicit function of time

$$1 + \lambda_i^{p^*} v_i^*(t_i^{c,m}) = 0. \tag{2.76}$$

Hence, $v_i^*(t_i^{c,m}) = -\dfrac{1}{\lambda_i^{p^*}} > 0$.

Case 4 : Similarly to Case 3, it can be shown that $\lambda_i^{p^*} = a_i > 0$. Solving (2.76) for $v_i^*(t_i^{c,m})$, we have $v_i^*(t_i^{c,m}) = -\dfrac{1}{\lambda_i^{p^*}} < 0$. Hence, this case cannot be a feasible solution. □

Lemma 2.3.17. *In Problem 2, let* $\mathbf{x}_i^s = [p_i^s, v_i^s]^\top$ *and* $\mathbf{x}_i^e = [p_i^e, v_i^e]^\top$ *be the initial and final states of CAV* $i \in \mathcal{N}(t)$ *traveling in zone* $m \in \mathcal{I}_i$. *Let* $\mathbf{x}_i^c = [p_i^c, v_i^c]^\top$ *be the intermediate state at the time* $t_i^{c,m}$ *that the control input changes sign. Then,*

$$p_i^c = \frac{v_i^{e2} - v_i^{s2} + 2(u_{\max} p_i^s - u_{\min} p_i^e)}{2(u_{\max} - u_{\min})}, \tag{2.77}$$

$$v_i^c = \sqrt{v_i^{s2} + 2u_{\max} \cdot (p_i^c - p_i^s)}. \tag{2.78}$$

Proof. From (2.1) and Lemma 2.3.16, the intermediate states are found by solving the following system of equations

$$\begin{cases} v_i^{c2} - v_i^{s2} = 2u_{\max} \cdot (p_i^c - p_i^s) \\ v_i^{e2} - v_i^{c2} = 2u_{\min} \cdot (p_i^e - p_i^c) \end{cases}, \tag{2.79}$$

which yields (2.77) and (2.78). □

Proposition 2.3.18. *The release time of CAV $i \in \mathcal{N}(t)$ traveling in zone $m \in \mathcal{I}_i$, when the state constraint is not active, is*

$$R_i^m = \frac{v_i^c - v_i^s}{u_{\max}} + \frac{v_i^e - v_i^c}{u_{\min}}. \tag{2.80}$$

Proof. When $u_i(t) = u_{\max}$ for all $t \in [t_i^{s,m}, t_i^{c,m}]$ and $u_i(t) = u_{\min}$ for all $t \in [t_i^{c,m}, t_i^{e,m}]$, where $t_i^{c,m}$ is the time that the control input changes sign, the total time traveled inside the zone m can be found by integrating (2.1), hence

$$\begin{aligned} v_i^c - v_i^s &= u_{\max} \cdot (t_i^{c,m} - t_i^{s,m}), \quad \forall\, t \in [t_i^{s,m}, t_i^{c,m}], \\ v_i^e - v_i^c &= u_{\min} \cdot (t_i^{e,m} - t_i^{c,m}), \quad \forall\, t \in [t_i^{c,m}, t_i^{e,m}]. \end{aligned} \tag{2.81}$$

Solving (2.81) for $t_i^{c,m}$ and $t_i^{e,m}$, we have

$$t_i^{c,m} = \frac{v_i^c - v_i^s}{u_{\max}} + t_i^{s,m}, \quad t_i^{e,m} = \frac{v_i^c - v_i^s}{u_{\max}} + \frac{v_i^e - v_i^c}{u_{\min}} + t_i^{s,m}. \tag{2.82}$$

Substituting $t_i^{e,m}$ into $R_i^m = t_i^{e,m} - t_i^{s,m}$ yields (2.80). □

Lemma 2.3.19. *The optimal control input of the deadline problem (Problem 2.3.13) for zone $m \in \mathcal{I}_i$, when the state constraint is not active, changes sign at most once, and it is equal to either: (1) $u_i(t) = u_{\min}$, or (2) $u_i(t) = u_{\max}$, or (3) $u_i(t) = u_{\min}$ and then it switches to $u_i(t) = u_{\max}$.*

Proof. The proof is similar to the proof of Lemma 2.3.16, and thus, it is omitted. □

Proposition 2.3.20. *Let $\mathbf{x}_i^s = [p_i^s, v_i^s]^\top$ and $\mathbf{x}_i^e = [p_i^e, v_i^e]^\top$ be the initial and final states of CAV $i \in \mathcal{N}(t)$ traveling in zone $m \in \mathcal{I}_i$. Let $\mathbf{x}_i^c = [p_i^c, v_i^c]^\top$ be the intermediate state at the*

time $t_i^{c,m}$ that the control input changes sign. Then, the deadline of CAV i traveling in zone $m \in \mathcal{I}_i$ for the unconstrained case is

$$D_i^m = \frac{v_i^c - v_i^s}{u_{\min}} + \frac{v_i^e - v_i^c}{u_{\max}}, \tag{2.83}$$

$$p_i^c = \frac{v_i^{e2} - v_i^{s2} + 2(u_{\min} p_i^s - u_{\max} p_i^e)}{2(u_{\max} - u_{\min})}, \quad v_i^c = \sqrt{v_i^{s2} + 2u_{\min} \cdot (p_i^c - p_i^s)}. \tag{2.84}$$

Proof. The control input of $i \in \mathcal{N}(t)$ in zone $m \in \mathcal{I}_i$ consists of two arcs, i.e., decelerating with $u_i(t) = u_{\min}$ and accelerating with $u_i(t) = u_{\max}$. Following similar arguments to Lemma 2.3.17, we derive (2.84). The total time traveled inside the zone m can be found by integrating (2.1), hence

$$\begin{aligned} v_i^c - v_i^s &= u_{\min} \cdot (t_i^{c,m} - t_i^{s,m}), \quad \forall\, t \in [t_i^{s,m}, t_i^{c,m}], \\ v_i^e - v_i^c &= u_{\max} \cdot (t_i^{e,m} - t_i^{c,m}), \quad \forall\, t \in [t_i^{c,m}, t_i^{e,m}]. \end{aligned} \tag{2.85}$$

Solving (2.85) for $t_i^{c,m}$ and $t_i^{e,m}$, we have $t_i^{c,m} = \frac{v_i^c - v_i^s}{u_{\min}} + t_i^{s,m}$, $t_i^{e,m} = \frac{v_i^c - v_i^s}{u_{\min}} + \frac{v_i^e - v_i^c}{u_{\max}} + t_i^{s,m}$. Substituting $t_i^{e,m}$ into $D_i^m = t_i^{e,m} - t_i^{s,m}$ (2.83) follows. □

State constraints are active

Next, we consider the cases where the speed constraints become active.

Theorem 2.3.21. *In Problems 2.3.12 and 2.3.13, if there is no change on the sign of the control input, then none of the speed constraints becomes active.*

Proof. We consider the two cases that there is no change on the sign of the control input, i.e., case 1: $u_i(t) = u_{\min}$, case 2: $u_i(t) = u_{\max}$. Case 1: For all $t < t' \in [t_i^{s,m}, t_i^{e,m}]$, we have $v_i(t) > v_i(t')$. Hence, the minimum and maximum speed can only occur at $t_i^{e,m}$ and $t_i^{s,m}$ respectively, namely $v_i^e \leq v_i(t)$, and $v_i(t) \leq v_i^s$. However, from the Assumptions 2.3.4 and 2.1.1, we have $v_{\min} < v_i^e \leq v_i(t) \leq v_i^s < v_{\max}$.

Case 2: Following similar arguments to Case 1, we have $v_{\min} < v_i^s \leq v_i(t) \leq v_i^e < v_{\max}$ □

Corollary 2.3.22. *For CAV $i \in \mathcal{N}(t)$ in zone $m \in \mathcal{I}_i$, the unconstrained solution of the release time problem (Problem 2.3.12) can not activate the constrained arc $v_i(t) = v_{\min}$.*

Proof. From Theorem 2.3.21, we know that if there is no change on the sign of the control input, then none of the speed constraints becomes active. Let's consider that the control input changes sign at $t_i^{c,m} \in [t_i^{s,m}, t_i^{e,m}]$, thus

$$u_i(t) = u_{\max} > 0 \Rightarrow v_i^s \leq v_i(t), \ \forall\, t \in [t_i^{s,m}, t_i^{c,m}], \tag{2.86}$$

$$u_i(t) = u_{\min} < 0 \Rightarrow v_i^e \leq v_i(t), \ \forall\, t \in [t_i^{c,m}, t_i^{e,m}]. \tag{2.87}$$

It follows that the minimum speed of CAV i for all $t \in [t_i^{s,m}, t_i^{e,m}]$ is either v_i^e or v_i^s. From the Assumptions 2.3.4 and 2.1.1, state constraints are not active at the entry and exit of the zones, and the proof is complete. □

One can verify whether the unconstrained solution of CAV i leads to violation of the speed constraint $v_i(t) \leq v_{\max}$ in zone m, by checking the speed at the interior point v_i^c found from (2.78). If the unconstrained solution violates the speed constraint $v_i(t) \leq v_{\max}$, then the solution exits the unconstrained arc at time τ_1, and enters the constrained arc $v_i(t) = v_{\max}$. Then the unconstrained arc is pieced together with the constrained arc $v_i(t) = v_{\max}$, and we re-solve the problem with the two arcs pieced together. The two arcs yield a set of algebraic equations that are solved simultaneously using the boundary conditions and interior conditions between the arcs. Since the speed at the boundary of zones do not activate the speed constraint, the solution cannot stay at the constrained arc $v_i(t) = v_{\max}$ and it must exit the constrained arc $v_i(t) = v_{\max}$ at time τ_2. The unconstrained and constrained arcs are pieced together, and we re-solve the problem consisting of the three arcs.

Theorem 2.3.23. *The release time of CAV $i \in \mathcal{N}(t)$ traveling in zone $m \in \mathcal{I}_i$ when the constraint $v_i(t) = v_{\max}$ is active is*

$$R_i^m = \frac{a_i + b_i}{2u_{\min}\, u_{\max}\, v_{\max}}, \tag{2.88}$$

where

$$a_i = v_i^{s2}\, u_{\min} - v_i^{e2}\, u_{\max} + (u_{\min} - u_{\max})\, v_{\max}^2, \tag{2.89}$$

$$b_i = 2u_{\min}\, u_{\max}(p_i^e - p_i^s) + 2v_{\max}\, (v_i^e\, u_{\max} - v_i^s\, u_{\min}). \tag{2.90}$$

Proof. Let CAV $i \in \mathcal{N}(t)$ enter and exit the zone $m \in \mathcal{I}_i$ at t_i^s and t_i^e respectively. From the boundary conditions, we have $p_i(t_i^s) = p_i^s$, $v_i(t_i^s) = v_i^s$, $p_i(t_i^e) = p_i^e$ and $v_i(t_i^e) = v_i^e$. CAV i cruises with $u_i(t) = u_{\max}$, and then it enters the constrained arc $v_i(t) = v_{\max}$ at time τ_1. It stays at the constrained arc with $u_i(t) = 0$ until time τ_2. After exiting the constrained arc, it decelerates with $u_i(t) = u_{\min}$. Substituting the optimal control input in (2.1) yields the following optimal state equations:

$$\begin{aligned}
p_i^*(t) =& \frac{1}{2}u_{\max}(t^2 - t_i^{s2}) - u_{\max}t_i^s(t - t_i^s) + v_i^s(t - t_i^s) + p_i^s,\\
v_i^*(t) =& u_{\max}(t - t_i^s) + v_i^s, \quad \forall\, t \in [t_i^s, \tau_1^-].\\
p_i^*(t) =& v_{\max}(t - \tau_1) + p_i^*(\tau_1^+), \quad v_i^*(t) = v_{\max}, \quad \forall\, t \in [\tau_1^+, \tau_2^-].\\
p_i^*(t) =& \frac{1}{2}u_{\min}(t^2 - \tau_2^2) - u_{\min}\tau_2(t - \tau_2) + v_i^*(\tau_2^+)(t - \tau_2) + p_i^*(\tau_2^+),\\
v_i^*(t) =& u_{\min}(t - \tau_2) + v_i^*(\tau_2^+), \quad \forall\, t \in [\tau_2^+, t_i^e].
\end{aligned} \tag{2.91}$$

The states of CAV are continuous at τ_1 and τ_2, thus

$$p_i^*(\tau_1^-) = p_i^*(\tau_1^+), \qquad v_i^*(\tau_1^-) = v_i^*(\tau_1^+), \tag{2.92}$$

$$p_i^*(\tau_2^-) = p_i^*(\tau_2^+), \qquad v_i^*(\tau_2^-) = v_i^*(\tau_2^+). \tag{2.93}$$

From (2.92)-(2.93) and the boundary conditions, piecing the unconstrained and constrained

arcs together, we have

$$
\begin{aligned}
p_i^*(\tau_1) &= \frac{1}{2}u_{\max}(\tau_1^2 - t_i^s) - u_{\max}t_i^s(\tau_1 - t_i^s) + v_i^s(\tau_1 - t_i^s) + p_i^s,\\
\tau_1 &= \frac{v_{\max} - v_i^s}{u_{\max}} + t_i^s,\\
p_i^*(\tau_2) &= v_{\max}(\tau_2 - \tau_1) + p_i^*(\tau_1), \quad v_i^*(\tau_2) = v_{\max},\\
p_i^e &= \frac{1}{2}u_{\min}(t_i^{e2} - \tau_2^2) - u_{\min}\tau_2(t_i^e - \tau_2), + v_i^*(\tau_2)(t_i^e - \tau_2) + p_i^*(\tau_2),\\
v_i^e &= u_{\min}(t_i^e - \tau_2) + v_i^*(\tau_2).
\end{aligned}
$$

Solving the system of equations above yields (2.88). □

Remark 2.3.24. *Similar to Corollary 2.3.22, for CAV $i \in \mathcal{N}(t)$ in zone $m \in \mathcal{I}_i$, the unconstrained solution of the deadline problem (Problem 2.3.13) can not activate the constrained arc $v_i(t) = v_{\max}$.*

Proposition 2.3.25. *Let τ_1 and τ_2 be the time that CAV $i \in \mathcal{N}(t)$ enters the constrained arc $v_i(t) = v_{\min}$, while it is in zone $m \in \mathcal{I}_i$. Let $[p_i^s, v_i^s]^\top$ and $[p_i^e, v_i^e]^\top$ be the initial and final states of CAV i in zone m respectively. Then, the deadline of CAV i to exit zone m is*

$$
D_i^m = \frac{v_i^e - v_{\min}}{u_{\max}} + \tau_2 - t_i^{s,m}, \tag{2.94}
$$

where

$$
\tau_2 = \frac{p_i(\tau_2) - p_i(\tau_1)}{v_{\min}} + \tau_1, \qquad p_i(\tau_2) = \frac{v_{\min}^2 - v_i^{e2}}{2\,u_{\max}} + p_i^e, \tag{2.95}
$$

$$
p_i(\tau_1) = \frac{v_{\min}^2 - v_i^{s2}}{2\,u_{\min}} + p_i^s, \qquad \tau_1 = \frac{-v_i^s + v_{\min}}{u_{\min}} + t_i^{s,m}. \tag{2.96}
$$

Proof. The proof is similar to the proof of Theorem 2.3.23, and thus, it is omitted. □

Solution of the scheduling problem (Problem 2.3.10)

As we described earlier, at the entry of the control zone, CAV $i \in \mathcal{N}(t)$ computes the release time and deadline for each zone $m \in \mathcal{I}_i$. Then, it solves the scheduling problem (Problem 2.3.10), the solution of which determines the schedule tuple $\mathcal{T}_i$ (Definition 2.3.5) aimed at minimizing the time t_i^f that i exits the control zone. In the scheduling problem (Problem 2.3.10) of CAV i, for each zone m which belongs to the conflict set $\mathcal{C}_{i,j}$ where $j < i \in \mathcal{N}(t)$, we impose the safety constraint (2.57) (Definition 2.3.8) stated as

$$T_i^m - T_j^m \geq t_h \quad \text{OR} \quad -(T_i^m - T_j^m) \geq t_h, \tag{2.97}$$

which is a disjunctive constraint due to the OR statement, and also determines the order of entry at zone m. By introducing a binary variable $B_{i,j}^m \in \{0,1\}$ and big number $M \in \mathbb{R}_{\geq 0}$ [195], we rewrite the disjunctive constraints (2.57) as two separate constraints as following

$$(T_i^m - T_j^m) + B_{i,j}^m \cdot M \geq t_h, \tag{2.98}$$

$$-(T_i^m - T_j^m) + (1 - B_{i,j}^m) \cdot M \geq t_h. \tag{2.99}$$

However, there are two cases to consider in handling the safety constraint; case 1: CAV i and CAV j follow the same path (Fig. 2.13), and case 2: CAV i and CAV j have different paths that merge together (Fig. 2.14). In case 1, we have $\mathcal{C}_{i,j} = \mathcal{I}_i = \mathcal{I}_j$ implying that they conflict on each zone of their path. Since CAV i entered the control zone later, it cannot arrive at any zone earlier than CAV j, thus, we have $B_{i,j}^m = 0$ for all $m \in \mathcal{C}_{i,j}$. For the second case, let $\mathcal{C}_{i,j} = \{m_a, \ldots, m_b\}$ be the conflict set between CAV i and j, which have merging paths, m_a be the first zone that there is a potential lateral collision, and m_b be their last conflict zone with the potential rear-end collision. Since we relaxed the FIFO queuing policy, CAV i can arrive at zone m_1 either before ($B_{i,j}^{m_1} = 1$), or after CAV j ($B_{i,j}^{m_1} = 0$). However, to ensure the absence of the rear-end safety in the following zones after m_a, we need to have all the binary variables equal to $B_{i,j}^{m_a}$, i.e., $B_{i,j}^{m_a} = \cdots = B_{i,j}^{m_b}$, $B_{i,j}^{m_a} \in \{0,1\}$.

In addition, the arrival time at each zone m is lower bounded with the arrival time

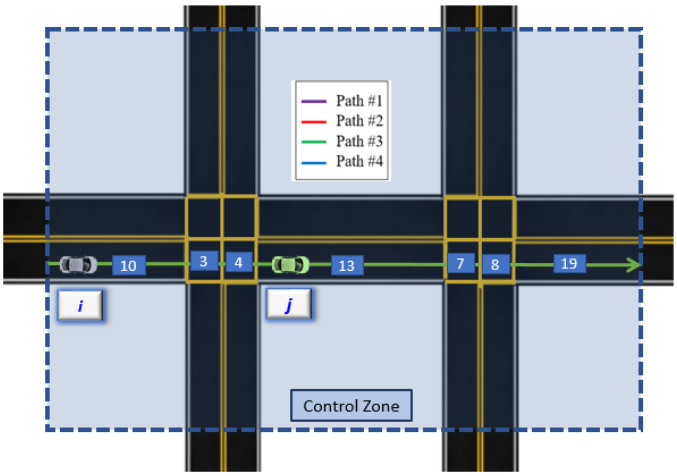

Figure 2.13: CAV i and CAV j follow the same path.

and release time, and upper-bounded with arrival time and deadline of the previous zone m. Similarly, the exit time from the control zone t_i^f is bounded by the arrival time, release time, and deadline of the last zone.

After transforming each safety constraint to two separate constraints augmented with a binary variable, we use a mixed-integer linear program (MILP) (IBM ILOG CPLEX [196]) to solve the scheduling problem. We discuss the implications on the computation effort of solving the MILP in subsection 2.3.5.

Analytical solution of the energy minimization problem (Problem 2.3.15)

Similar to (2.17), we adjoin the qth-order state variable inequality constraint to the Hamiltonian function. For each CAV $i \in \mathcal{N}(t)$, with CAV $k \in \mathcal{N}(t)$ positioned immediately in front of it, the Hamiltonian is

$$H_i(t, p_i(t), v_i(t), u_i(t), \lambda(t)) = \frac{1}{2}u_i(t)^2 + \lambda_i^p v_i(t) + \lambda_i^v u_i(t) + \mu_i^a(u_i(t) - u_{\max})$$
$$+\mu_i^b(u_{\min} - u_i(t)) + \mu_i^c(u_i(t)) + \mu_i^d(-u_i(t)) + \mu_i^s(v_i(t) - v_k(t) + \varphi u_i(t)), \qquad (2.100)$$

where λ_i^p and λ_i^v are the costates, and $\mu^\top$ is a vector of Lagrange multipliers.

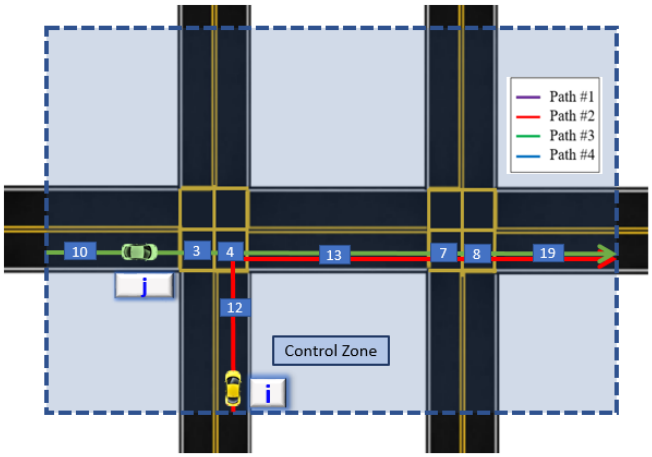

Figure 2.14: CAV i and CAV j have different paths that merge together.

State and control constraints are not active

If the state and control constraints are not active, $\mu_i^a = \mu_i^b = \mu_i^c = \mu_i^d = \mu_i^s = 0$ and from [65] the solution is

$$u_i^* = a_i t + b_i, \tag{2.101}$$

by substituting (2.101) in (2.1) we have

$$v_i^* = \frac{1}{2}a_i t^2 + b_i t + c_i, \quad p_i^* = \frac{1}{6}a_i t^3 + \frac{1}{2}b_i t^2 + c_i t + d_i. \tag{2.102}$$

In the above equations a_i, b_i, c_i, d_i are constants of integration, which are found by substituting the initial and final states $p_i(T_i^m), v_i(T_i^m), p_i(T_i^{\bar{m}})$ and $v_i(T_i^{\bar{m}})$ in zone $m \in \mathcal{I}_i$. Thus, a system of equations in the form of $\mathbf{T}_i\mathbf{b}_i = \mathbf{q}_i$, is

$$\begin{bmatrix} \frac{1}{6}\left(T_i^m\right)^3 & \frac{1}{2}(T_i^m)^2 & T_i^m & 1 \\ \frac{1}{2}\left(T_i^m\right)^2 & T_i^m & 1 & 0 \\ \frac{1}{6}\left(T_i^{\bar{m}}\right)^3 & \frac{1}{2}\left(T_i^{\bar{m}}\right)^2 & T_i^{\bar{m}} & 1 \\ \frac{1}{2}\left(T_i^{\bar{m}}\right)^2 & T_i^{\bar{m}} & 1 & 0 \end{bmatrix} \cdot \begin{bmatrix} a_i \\ b_i \\ c_i \\ d_i \end{bmatrix} = \begin{bmatrix} p_i(T_i^m) \\ v_i(T_i^m) \\ p_i(T_i^{\bar{m}}) \\ v_i(T_i^{\bar{m}}) \end{bmatrix}. \tag{2.103}$$

Note that since (2.103) can be computed online, the controller may re-evaluate the four constants at any time $t \in [T_i^m, T_i^{\bar{m}}]$ and update (2.101).

There are different cases that can happen and activate either the state or control constraints. Next, we consider the cases that CAV only travels on the constrained arcs except the rear-end safety (2.52).

CAV travels on different constrained arcs

Case 1: CAV $i \in \mathcal{N}(t)$ enters the constrained arc $u_i(t) = u_{\max}$ at T_i^m. Then, it moves to the constrained arc $u_i(t) = u_{\min}$ at τ_1 and stays on it until $T_i^{\bar{m}}$.

Theorem 2.3.26. *Let T_i^m and $T_i^{\bar{m}}$ be the schedules of CAV $i \in \mathcal{N}(t)$ for zones $m, \bar{m} \in \mathcal{I}_i$ respectively, where zone $\bar{m}$ is right after m. In zone m, the CAV i first enters the constrained arc $u_i(t) = u_{\max}$ and then the arc $u_i(t) = u_{\min}$, if the speed constraint does not become active in zone m and*

$$T_i^{\bar{m}} - T_i^m = R_i^m. \tag{2.104}$$

Proof. Let CAV $i \in \mathcal{N}(t)$ enter and and exit the zone $m \in \mathcal{I}_i$ at T_i^m and $T_i^{m'}$ respectively. Substituting (2.56) into $T_i^{\bar{m}} - T_i^m = R_i^m$, we have $T_i^{m'} - T_i^m = R_i^m$. Thus, CAV i is traveling at the earliest feasible time in zone m. Since the speed constraint is not active, the solution is equivalent to the solution of the release time problem (Problem 2.3.12) when the speed constraint is not active. □

In the above case, the optimal control input is

$$u_i^*(t) = \begin{cases} u_{\max} & \text{, if} \quad T_i^m \leq t < \tau_1 \\ u_{\min} & \text{, if} \quad \tau_1 \leq t \leq T_i^{\bar{m}} \end{cases}. \tag{2.105}$$

Substituting (2.105) in (2.1), we have

$$p_i^*(t) = \frac{1}{2}u_{\max}t^2 + b_i t + c_i, \qquad v_i^*(t) = u_{\max}t + b_i, \qquad \forall\, t \in [T_i^m, \tau_1^-], \tag{2.106}$$

$$p_i^*(t) = \frac{1}{2}u_{\min}t^2 + d_i t + e_i, \qquad v_i^*(t) = u_{\min}t + d_i, \qquad \forall\, t \in [\tau_1^+, T_i^{\bar{m}}], \tag{2.107}$$

where b_i, c_i, d_i and e_i are constants of integration, which are found by using initial conditions $p_i(T_i^m), v_i(T_i^m)$ and final conditions $p_i(T_i^{\bar{m}}), v_i(T_i^{\bar{m}})$ of the CAV in zone $m \in \mathcal{I}_i$. The switching point τ_1 can be found from (2.82).

Case 2: CAV i enters the constrained arc $u_i(t) = u_{\max}$ at T_i^m, then it moves to the constrained arc $v_i(t) = v_{\max}$ at $t = \tau_1$. It exits the constrained arc $v_i(t) = v_{\max}$ at $t = \tau_2$, and it enters the constrained arc $u_i(t) = u_{\min}$ and stays on it until $T_i^{\bar{m}}$.

Corollary 2.3.27. *Case 2 is realized for CAV $i \in \mathcal{N}(t)$ travelling in zone $m \in \mathcal{I}_i$, if the speed constraint becomes active and (2.104) holds.*

Proof. The proof is similar to the proof of Theorem 2.3.26, and thus, it is omitted. □

In this case, the optimal control input is

$$u_i^*(t) = \begin{cases} u_{\max} & \text{, if} \quad T_i^m \le t < \tau_1 \\ 0 & \text{, if} \quad \tau_1 \le t \le \tau_2 \\ u_{\min} & \text{, if} \quad \tau_2 \le t \le T_i^{\bar{m}} \end{cases}. \tag{2.108}$$

Substituting (2.108) in (2.1), we have

$$p_i^*(t) = \frac{1}{2}u_{\max}t^2 + b_i t + c_i, \qquad v_i^*(t) = u_{\max}t + b_i, \qquad \forall\, t \in [T_i^m, \tau_1^-], \tag{2.109}$$

$$p_i^*(t) = v_{\max}t + d_i, \qquad v_i^*(t) = v_{\max}, \qquad \forall\, t \in [\tau_1^+, \tau_2^-], \tag{2.110}$$

$$p_i^*(t) = \frac{1}{2}u_{\min}t^2 + e_i t + f_i, \qquad v_i^*(t) = u_{\min}t + e_i, \qquad \forall\, t \in [\tau_2^+, T_i^{\bar{m}}], \tag{2.111}$$

where b_i, c_i, d_i, e_i and f_i are constants of integration, and time τ_1 and τ_2 are times that we move from one arc to another arc, which are found by using initial and final conditions in zone m and continuity of states at τ_1 and τ_2.

Case 3: CAV $i \in \mathcal{N}(t)$ enters the constrained arc $u_i(t) = u_{\min}$ at T_i^m. Then, it moves to the constrained arc $u_i(t) = u_{\max}$ at τ_1 and stays on it until $T_i^{\bar{m}}$.

Theorem 2.3.28. *Let T_i^m and $T_i^{\bar{m}}$ be the schedules of CAV $i \in \mathcal{N}(t)$ for zones $m, \bar{m} \in \mathcal{I}_i$ respectively, where zone $\bar{m}$ is right after zone m. In zone m, CAV i first enters the constrained arc $u_i(t) = u_{\min}$, and then the constrained arc $u_i(t) = u_{\max}$, if the speed constraint does not become active in zone m and*

$$T_i^{\bar{m}} - T_i^m = D_i^m. \tag{2.112}$$

Proof. The proof is similar to the proof of Theorem 2.3.26, and thus, it is omitted. □

In this case, the optimal control input is

$$u_i^*(t) = \begin{cases} u_{\min} & \text{, if} \quad T_i^m \leq t < \tau_1 \\ u_{\max} & \text{, if} \quad \tau_1 \leq t \leq T_i^{\bar{m}} \end{cases}. \tag{2.113}$$

Substituting (2.113) in (2.1), we have

$$p_i^*(t) = \frac{1}{2}u_{\min}t^2 + b_i t + c_i, \qquad v_i^*(t) = u_{\max}t + b_i, \quad \forall\, t \in [T_i^m, \tau_1^-], \tag{2.114}$$

$$p_i^*(t) = \frac{1}{2}u_{\max}t^2 + d_i t + e_i, \qquad v_i^*(t) = u_{\min}t + d_i, \quad \forall\, t \in [\tau_1^+, T_i^{\bar{m}}], \tag{2.115}$$

where b_i, c_i, d_i, and e_i are integration constants, which can be computed by using initial and final conditions of CAV in zone $m \in \mathcal{I}_i$ respectively. The switching point τ_1 can be found from (2.83).

Case 4: CAV i enters the constrained arc $u_i(t) = u_{\min}$ at T_i^m, then it moves to the constrained arc $v_i(t) = v_{\min}$ at $t = \tau_1$. It exits the constrained arc $v_i(t) = v_{\min}$ at $t = \tau_2$, and it enters the constrained arc $u_i(t) = u_{\max}$ and stays on it until $T_i^{\bar{m}}$.

Corollary 2.3.29. *Case* 4 *is realized for CAV* $i \in \mathcal{N}(t)$ *travelling in zone* $m \in \mathcal{I}_i$*, if the speed constraint becomes active in zone* m *and* (2.112) *holds.*

Proof. The proof is similar to the proof of Theorem 2.3.26, and thus, it is omitted. □

In this case, the optimal control input is

$$u_i^*(t) = \begin{cases} u_{\min} & \text{, if} \quad T_i^m \leq t < \tau_1 \\ 0 & \text{, if} \quad \tau_1 \leq t \leq \tau_2 \\ u_{\max} & \text{, if} \quad \tau_2 \leq t \leq T_i^{\bar{m}} \end{cases}. \tag{2.116}$$

Substituting (2.116) in (2.1), we have

$$p_i^*(t) = \frac{1}{2}u_{\min}t^2 + b_i t + c_i, \qquad v_i^*(t) = u_{\min}t + b_i, \qquad \forall\, t \in [T_i^m, \tau_1^-], \tag{2.117}$$

$$p_i^*(t) = v_{\min}t + d_i, \qquad v_i^*(t) = v_{\min}, \qquad \forall\, t \in [\tau_1^+, \tau_2^-], \tag{2.118}$$

$$p_i^*(t) = \frac{1}{2}u_{\max}t^2 + e_i t + f_i, \qquad v_i^*(t) = u_{\max}t + e_i, \qquad \forall\, t \in [\tau_2^+, T_i^{\bar{m}}]. \tag{2.119}$$

CAV travels on a combination of constrained and unconstrained arcs

Using (2.1), we first start with the unconstrained solution of Problem 2.3.15. If the solution violates any of the speed (2.3) or control (2.2) constraints, then we piece the arcs together as it was described in 2.2.3.

CAV enters the safety constrained arc

Let CAV i enter and exit zone $m \in \mathcal{I}_i$ at T_i^m and $T_i^{\bar{m}}$ respectively. CAV $k \in \mathcal{N}(t) \setminus \{i\}$ is immediately positioned in front of CAV i in zone m, and CAV i activates the rear-end safety constraint (2.52) at time $\tau_1 \in [T_i^m, T_i^{\bar{m}}]$. We have two cases to consider: Case 1: CAV i remains in the constrained arc until $T_i^{\bar{m}}$ or Case 2: CAV i exits the constrained arc at $\tau_2 \in [\tau_1, T_i^{\bar{m}}]$.

Lemma 2.3.30. *Let CAV $i \in \mathcal{N}(t)$ and $k \in \mathcal{N}(t) \setminus \{i\}$ enter zone m at time T_i^m and T_k^m respectively. Let CAV k be immediately ahead of i. Then the rear-end safety constraint for CAV i does not become active at the entry of zone m, if the minimum time headway $t_h \in \Gamma_i$, where*

$$\Gamma_i = \{t \mid \frac{1}{2}u_{\min}t^2 + v_k(T_k^m)t - \varphi v_i(T_i^m) - \gamma_i > 0,\ \forall\, t \in \mathbb{R}_{\geq 0}\}. \tag{2.120}$$

Proof. Since CAV i and k cruise on the same lane, (2.57) simplifies to $T_i^m \geq T_k^m + t_h$. For CAV k we have

$$p_k(t) < p_k(t'), \quad \forall\, t < t' \in \mathbb{R}_{\geq 0}, \tag{2.121}$$

$$\inf(p_k(T_i^m)) = p_k(T_k^m + t_h), \quad T_i^m \geq T_k^m + t_h. \tag{2.122}$$

Evaluating the (2.52) at time T_i^m yields

$$(p_k(T_i^m) - p_k(T_k^m)) - (p_i(T_i^m) - p_i(T_i^m)) \geq \gamma_i + \varphi v_i(T_i^m). \tag{2.123}$$

Then, we have

$$(p_k(T_i^m) - p_k(T_k^m)) \geq \gamma_i + \varphi v_i(T_i^m), \tag{2.124}$$

$$(p_k(T_i^m) - p_k(T_k^m)) \geq \inf((p_k(T_i^m) - p_k(T_k^m))), \tag{2.125}$$

where $\inf((p_k(T_i^m) - p_k(T_k^m))) = p_k(T_k^m + t_h) - p_k(T_k^m)$. If

$$p_k(T_k^m + t_h) - p_k(T_k^m) > \gamma_i + \varphi v_i(T_i^m) \tag{2.126}$$

holds, then (2.124) also holds, and the rear-end safety constraint never becomes active at $t = T_i^m$.

The LHS of (2.126) corresponds to the distance that CAV k travelled after t_h seconds

from its entry in the zone m, denoted by $\Delta_k^m(t_h, u_i(t))$. Thus,

$$\underset{u_i(t)}{\operatorname{argmin}} \Delta_k^m(t_h, u_i(t)) = u_{\min}. \tag{2.127}$$

Substituting (2.127) and $t = t_h$ into (2.1), we have

$$\Delta_k^m = \frac{1}{2} u_{\min} t_h^2 + v_i(T_k^m) t_h. \tag{2.128}$$

If (2.128) is greater than $\gamma_i + \varphi v_i(T_i^m)$, it yields (2.126), and the proof is complete. □

Lemma 2.3.31. *If the rear-end safety constraint becomes active for CAV $i \in \mathcal{N}(t)$ at $\tau_1 \in (T_i^m, T_i^{\bar{m}})$, then it must exit the rear-end safety constrained arc at $\tau_2 \in [\tau_1, T_i^{\bar{m}})$.*

Proof. From Lemma 2.3.30, the rear-end safety constraint of CAV i with a schedule $T_i^m \in \mathcal{T}_i$ does not become active at the entry of zone $m \in \mathcal{I}_i$. Thus, if the rear-end safety constraint of CAV i becomes active at τ_1, it must exit the constrained arc before it exits zone m. □

Suppose CAV $i \in \mathcal{N}(t)$ enters the zone m at time $t = T_i^m$ and at some time $t = \tau_1$, the rear-end safety constraint with the vehicle k becomes active until $t = \tau_2$, $d^m(p_k(t), p_i(t)) = \delta_i(t)$ for all $t \in [\tau_1, \tau_2]$, in this case $\mu_i^s \neq 0$. Let $N_i(t, \mathbf{x}_i(t)) = (p_i^*(t) - p_i^*(T_i^m)) - (p_k^*(t) - p_k^*(T_k^m)) + \gamma + v_i^*(t)$. Note that, $p_i^*(T_i^m)$ and $p_k^*(T_k^m)$ are time-invariant and we can simplify the notation by defining $\bar{\gamma} = -p_i^*(T_i^m) + p_k^*(T_k^m) + \gamma$. Thus, we have

$$N_i(t, \mathbf{x}_i(t)) = p_i^*(t) - p_k^*(t) + \bar{\gamma} + \varphi v_i^*(t). \tag{2.129}$$

Since $N_i(t, \mathbf{x}_i(t)) = 0$ for $t \in [\tau_1, \tau_2]$, its first derivative, which is dependent on the optimal control input, should vanish in $t \in [\tau_1, \tau_2]$

$$N_i^{(1)}(t, \mathbf{x}_i(t)) = v_i^*(t) - v_k^*(t) + \varphi u_i^*(t) = 0. \tag{2.130}$$

By taking a time derivative from (2.130), the optimal control input of CAV i, when rear-end safety constraint is active can be found from solving the following ODE.

$$\dot{u}_i^*(t) + \frac{1}{\varphi} u_i^*(t) - \frac{1}{\varphi} u_k^*(t) = 0, \ \forall\, t \in [\tau_1, \tau_2]. \tag{2.131}$$

The optimal solution need to satisfy the following jump conditions on costates upon entry the constrained arc at $t = \tau_1$

$$\lambda_i^p(\tau_1^-) = \lambda_i^p(\tau_1^+) + \pi_i \frac{\partial N_i}{\partial p_i} = \lambda_i^p(\tau_1^+) + \pi_i, \tag{2.132}$$

$$\lambda_i^v(\tau_1^-) = \lambda_i^v(\tau_1^+) + \pi_i \frac{\partial N_i}{\partial v_i} = \lambda_i^v(\tau_1^+) + \varphi \pi_i, \tag{2.133}$$

$$H_i(\tau_1^-) = H_i(\tau_1^+) - \pi_i \frac{\partial N_i}{\partial t} = H_i(\tau_1^+) + \pi_i v_k^*(t), \tag{2.134}$$

where π_i is a constant Lagrange multipliers, determined so that $N_i(\tau_1, \mathbf{x}_i(\tau_1)) = 0$. At the exit point of the constrained arc we have

$$\lambda_i^p(\tau_2^-) = \lambda_i^p(\tau_2^+), \quad \lambda_i^v(\tau_2^-) = \lambda_i^v(\tau_2^+), \quad H_i(\tau_2^-) = H_i(\tau_2^+). \tag{2.135}$$

As described earlier, the three arcs need to be solved simultaneously using initial and final conditions (speed and position), and interior conditions at unknown time τ_1 and τ_2 (continuity of speed and position, jump conditions (2.129)-(2.135)). The complete analytical solution when the rear-end safety constraint becomes active has been presented in [77, 91].

2.3.5 Simulation Results

To evaluate the effectiveness of the proposed framework to improve travel time and the traffic throughput, we investigate coordination of CAVs at two adjacent intersections considering different traffic volumes, and then compare the results with the baseline scenario consisting of two-phase traffic signals. We consider two adjacent intersections which are 100 m apart. In addition, the length of each road connecting to the intersections is 300 m, and the length of the merging zones are 30 m. We used the following parameters for the simulation:

$t_h = 1.5$ s, $v_{\min} = 5$ m/s, $v_{\max} = 25$ m/s, $v_{\text{merge}} = 15$ m/s $u_{\min} = -1$ m/s^2, $u_{\max} = 1$ m/s^2, $\gamma = 5$ m, and $\varphi = 0.2$ s.

For the first scenario, we consider CAVs enter the control zone with initial speed uniformly distributed between 13 m/s to 16 m/s from four conflicting paths shown in figure 2.11 with equal traffic volumes. We construct the baseline scenario with two-phase fixed-time traffic signals in PTV-VISSIM by considering all vehicles as human-driven and without any vehicle-to-vehicle communication. We use VISSIM built-in traffic signal optimizer to obtain the traffic signal timing. To emulate the driving behavior of real human-driven vehicles, we use a built-in car-following model (Wiedemann [192]) in PTV-VISSIM with default parameters. We let the speed limit for the baseline scenario to be $v_{\max}$. In the optimal scenario, we use MATLAB to simulate our framework. To compare the optimal scenario with the baseline scenario, CAVs enter the control zone at the same time, speed, and path that they entered in the baseline scenario. Videos of the experiment can be found at the supplemental site, https://sites.google.com/view/ud-ids-lab/TITS.

Table 2.6 presents the average travel time of all CAVs inside the control zone for the baseline and optimal scenarios at different traffic volumes ranging from 400 veh/h to 1200 veh/h per path. For each traffic volume, we performed five simulations with different random seeds and averaged the results. Within our proposed framework, average travel time has been decreased by $21\% - 33\%$ compared to the baseline scenario. Relative frequency histogram of travel time of each CAV for traffic volume 1200 veh/h for a randomly selected seed for the baseline and optimal scenarios are shown in Fig. 2.15. The optimal scenario has a high relative frequency of lower travel time compared to the baseline scenario. Travel time for 65% of CAVs lies in the range [40s-50s] for the optimal scenario, whereas travel time of vehicles for the baseline scenario has a higher variation, and only 20% of vehicles' travel time is in the range [20s-50s]. In the optimal scenario, maximum travel time is in the range [60s-70s] compared to the maximum range [120s-130s] for the baseline scenario. Although we used VISSIM built-in traffic signal optimizer to obtain the traffic signal-timing in the baseline scenario, it is worth mentioning that one potential direction to explore is to construct

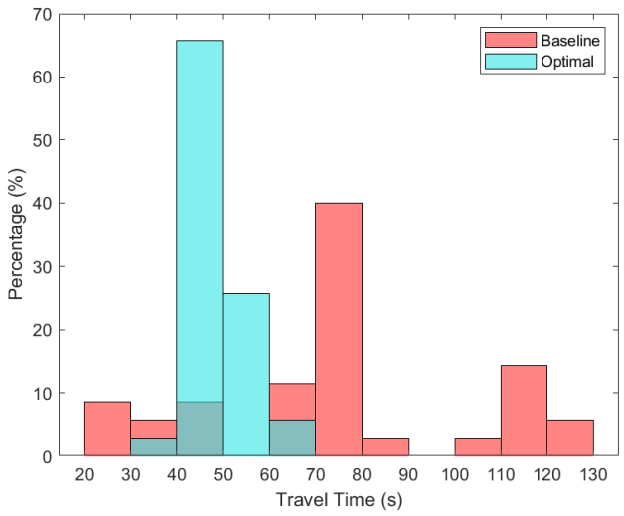

Figure 2.15: A relative frequency histogram for travel time of each vehicle for the baseline and optimal scenarios with traffic volume 1200 veh/h.

the baseline case such that human-driven vehicles cross a multiple signal-free intersections using a standard car-following model. This approach allows a fairer comparison since the vehicles do not have to come to a full stop due to a traffic light.

Table 2.6: Average travel time of vehicles in the optimal and baseline scenarios for different traffic volumes.

Traffic volume (veh/h)	Average number of vehicles	Average travel time (s)		Decrease
		Baseline	Optimal	%
400	14	51.89	40.81	21
600	18	57.52	41.86	27
800	25	63.30	43.26	32
1000	31	68.82	46.59	32
1200	36	72.15	48.53	33

The instantaneous average, maximum and minimum speed of CAVs inside the control zone for the baseline and optimal scenarios with traffic volume 600 veh/h, 1000 veh/h, and 1200 veh/h for a randomly selected seed are illustrated in Fig 2.16. The instantaneous minimum speed for all traffic volumes in the optimal scenario is positive and higher than $v_{\min}$ indicating smooth traffic flow, compared to the baseline scenario, which experiences much stopping due to the traffic lights. Relative frequency histogram of the average speed of each

CAV for traffic volume 1200 veh/h for the baseline and optimal scenarios are plotted in Fig. 2.17 on top of each other. Figure 2.17 shows that, in the baseline scenario, the average speed of almost all CAVs are lower than the optimal scenario, and that the CAVs in the optimal scenario speed up and 70% of CAVs achieve mean speed higher than 14 m/s, whereas in the baseline scenario vehicles decrease their speed while 75% of the vehicles have mean speed less than 12 m/s.

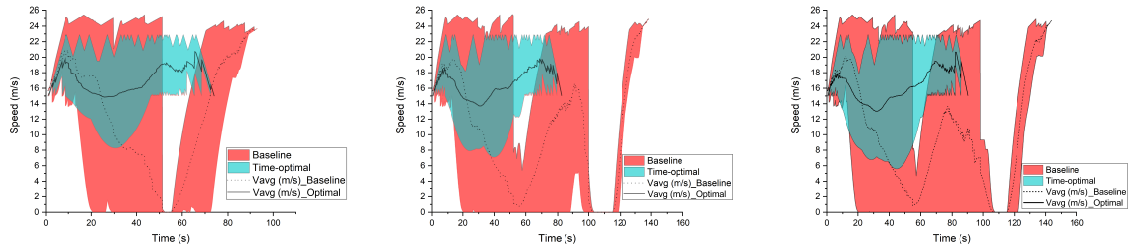

(a) (b) (c)

Figure 2.16: The instantaneous average, maximum and minimum speed of CAVs inside the control zone for the baseline and optimal scenarios with traffic volume (a) 600 veh/h, (b) 1000 veh/h and (c) 1200 veh/h.

To evaluate the fuel efficiency improvement through our framework, we use a polynomial meta-model proposed in [193], which approximates the fuel consumption in ml/s as a function of speed and control input of a CAV and coefficients obtained from an engine torque-speed-efficiency map of a typical car. Table 2.7 summarizes the average fuel rate and fuel consumption for the optimal and baseline scenarios at different traffic volumes for which five simulations with different random seeds were performed, and the results were averaged. Although our time-optimal framework results in higher average fuel rate compared to the baseline scenario, it leads to smaller fuel consumption as the traffic flow gets higher. A higher fuel rate in our approach is the result of speeding to reach the speed imposed at the boundaries of zones in the merging zones, i.e., v_{merge}. Similarly, setting v_{merge} at the boundaries of zones may lead to a discontinuity of the control input at these points, which can cause a higher fuel rate, and passenger discomfort. As it can be seen, there is a trade-off between minimizing travel time and energy consumption. One may consider minimizing them jointly by formulating a multi-objective cost function as proposed by [78, 79] for a

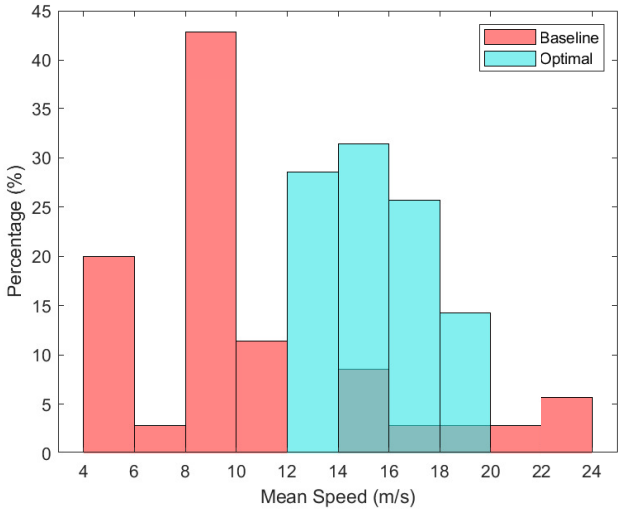

Figure 2.17: A relative frequency histogram for mean speed of each vehicle for the baseline and optimal scenarios with traffic volume 1200 veh/h.

single intersection, or using a recursive structure for the upper-level problem in [65] to trade off between the energy minimization and throughput maximization indirectly.

Table 2.7: Average fuel rate, and fuel consumption of vehicles in the optimal and baseline scenarios for different traffic volumes.

Traffic volume (veh/h)	Average fuel rate (ml/s)		Average fuel consumption (l)	
	Baseline	Optimal	Baseline	Optimal
400	1.53	2.03	0.076	0.083
600	1.45	1.92	0.079	0.080
800	1.35	1.80	0.079	0.077
1000	1.29	1.62	0.079	0.074
1200	1.24	1.57	0.077	0.075

The mean and standard deviation of computation times of CAVs in solving the MILP in the scheduling problem (Problem 2.3.10) for different traffic volumes is listed in Table 2.8. For each traffic flow, we choose the seed with a maximum mean of computation time to report. It shows that the scheduling problem is computationally feasible and does not grow exponentially with increasing the traffic volume and number of CAVs. The mean computation time of CAVs in different traffic volumes is in the range [21 ms - 25.4 ms] with a very small standard deviation.

In the second scenario, we further evaluate the performance of our upper-level scheduling approach compared to the centralized scheduling and FIFO queuing policy. Namely, we consider all different possible paths in two adjacent intersections. We have six different origins or destination for vehicles, including northbound 1 (NB1), northbound 2 (NB2), eastbound (EB), westbound (WB), southbound 1 (SB1), and southbound 2 (SB2) (Fig. 2.18). There are five possible paths for each origin, which in total would be 30 possible paths. We assume that CAVs enter the control zone based on a Poisson process with a rate of 1 second. We performed five simulations with random seeds for different numbers of vehicles and averaged the results.

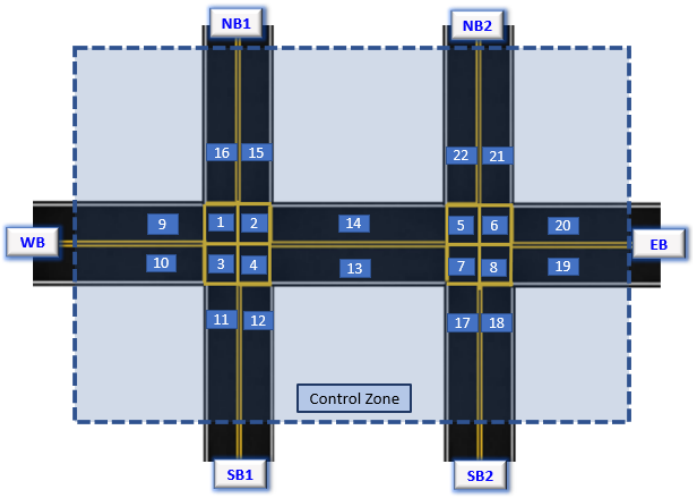

Figure 2.18: Two interconnected intersections with origins and destinations.

To obtain the maximum possible performance of the system in the centralized scheduling, we consider that the initial conditions of all CAVs, including their arrival time and their initial speed at the control zone, are known to the central controller. We then formulated a centralized scheduling problem aimed at minimizing the average travel time of all CAVs subject to the constraints (2.55) and (2.57). The solution to the centralized scheduling problem is schedule tuples of all CAVs, which then can be used as inputs for the low-level problem. On the other hand, in our upper-level scheduling formulation, each CAV solves the scheduling problem upon entering the control zone, and once the solution is derived, then the schedule tuple of the CAV does not change. When a new CAV i enters the control zone, the schedule

tuples of other CAVs are fixed since they entered earlier, and they have already obtained their optimal schedule tuples. Using this sequential decision-making approach, we may sacrifice optimality in terms of minimizing total travel time since we assume that when a new vehicle arrives, it cannot change the schedule of the vehicles that arrived earlier. However, the optimality gap between the centralized and decentralized solution may be reduced by introducing a re-planning framework to update the schedules of the vehicles as new vehicle arrives.

Figure 2.19 illustrates the average travel time of all CAVs and computation time for our decentralized scheduling approach, centralized scheduling, and FIFO queuing policy. As it can be seen, there is a close gap between the average travel time achieved by our decentralized scheduling problem and the centralized scheduling problem. However, the computation complexity of the centralized scheduling problem renders it inapplicable for real-time implementation. Moreover, there are significant delays in travel time caused by the strict FIFO queuing policy leading into sub-optimal solutions for two adjacent intersections. Note that, by increasing the number of vehicles from 15 to 75, average travel time is changed from 41 s to 44.6 s, and from 40 s to 42.9 s for decentralized and centralized scheduling, respectively. However, this is not a significant change since the vehicles arrive at the control zone at the fixed flow rate based on the Poisson process with a rate of 1 second.

To demonstrate the effects of flow rate on the performance of our approach, we evaluate the coordination of 30 vehicles arriving at all possible paths under different Poisson process arrival rates compared to the centralized scheduling and FIFO queuing policy. Similar to the previous scenarios, we performed 5 simulations with random seeds for different arrival rates and averaged the results. Figure 2.20 shows the average travel time and average computation time for decentralized scheduling, centralized scheduling, and FIFO queuing policy. In Fig. 2.20, smaller Poisson arrival rates correspond to the higher traffic volumes. In all three approaches, by decreasing traffic volume, average travel time increases; however, this change is more significant in the FIFO queuing policy. In the centralized scheduling approach, the computation complexity increases with the increase in traffic volume, making it difficult for

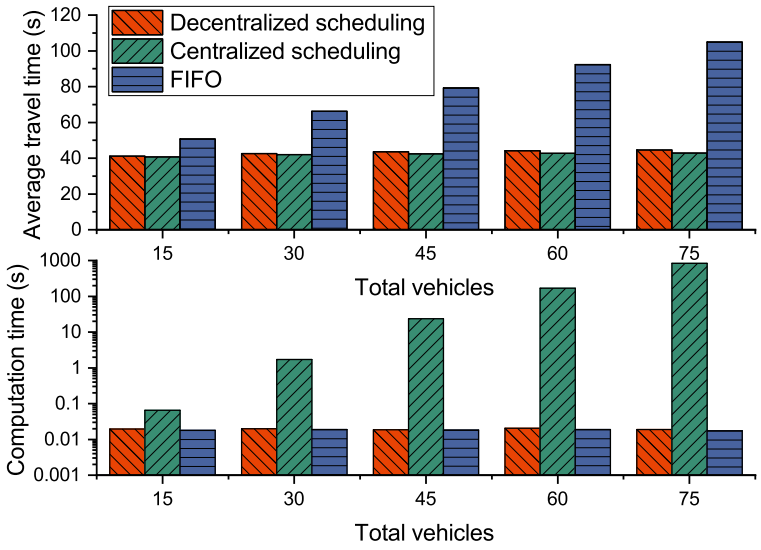

Figure 2.19: Average travel time and computation time of decentralized scheduling, centralized scheduling, and FIFO queuing policy for different numbers of vehicles.

real-time implementation.

Since v_{merge} is imposed a priori, upon entering the control zone CAV i might find the scheduling problem (Problem 2.3.10) infeasible. In this case, CAV i searches for the largest speed less than v_{merge}, in which the scheduling problem has a feasible solution. Note that due to the cheap computation cost of solving the scheduling problem (Table 2.8), this can be achieved in real time. However, if there is a scenario of high-traffic volume and $v_{\min} > 0$, the scheduling problem may still have not a feasible solution. To address this problem, it is required to set $v_{\min} = 0$, implying that the latest feasible time for CAV i to travel at zone $m \in \mathcal{I}_i$ is infinity. Thus, to satisfy the safety constraint, the arrival time at zone m might be too big resulting in CAV i reaches to a full stop if the road reaches its maximum capacity.

2.4 A Hysteretic Q-learning Coordination Framework for Emerging Mobility Systems in Smart Cities

In this section, we provide a decentralized coordination framework for CAVs at a signal-free intersection to minimize travel time and improve fuel efficiency. We employ

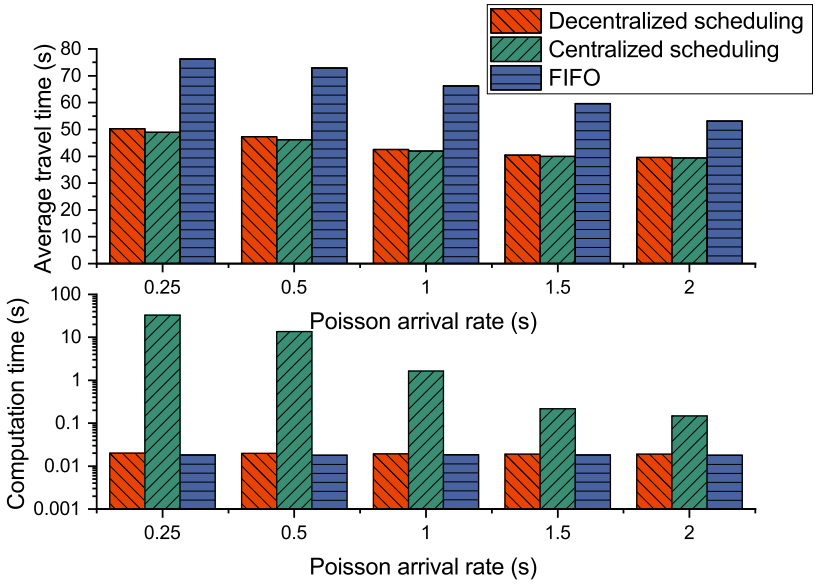

Figure 2.20: Average travel time and computation time of decentralized scheduling, centralized scheduling, and FIFO queuing policy for 30 vehicles with different Poisson arrival rates.

Table 2.8: The mean, and standard deviation of computation times of CAVs in solving the MILP.

Traffic volume (veh/h)	Total vehicles	Mean (ms)	Standard deviation (ms)
400	16	21.0	2.9
600	19	21.3	1.6
800	25	23.8	2.3
1000	29	24.1	2.2
1200	35	25.4	1.9

a simple yet powerful reinforcement learning approach, an off-policy temporal difference learning called Q-learning, enhanced with a coordination mechanism to address this problem. Then, we integrate a FIFO queuing policy to improve the performance of our system. We demonstrate the efficacy of our proposed approach through simulation and comparison with the classical optimal control method based on Pontryagin's minimum principle.

The rest of this section is structured as follows. In subsection 2.4.1, we introduce the problem formulation which includes main elements of the proposed framework, FIFO queuing policy, and combined hysteretic Q-learning with FIFO framework. We present the simulation framework in subsection 2.4.2, and the corresponding results in subsection 2.4.3.

2.4.1 Problem Formulation

We consider a single-lane signal-free intersection where the distance from the entry of the control zone to the entry of the merging zone is $L \in \mathbb{R}_{>0}$. The length of the merging zone is denoted by $D \in \mathbb{R}_{>0}$. We limit our analysis to the cases where left/right turns and lane-changing maneuvers are not allowed.

We formulate this problem as a multi-agent Markov decision process $\langle n,\ \mathcal{S},\ \mathcal{U},\ P, R, \gamma\rangle$, where $n \in \mathbb{N}$ is total number of CAVs, $\mathcal{S} \coloneqq \times_{i=1}^{n}\mathcal{S}^i$ is a finite set of states of all CAVs, $\mathcal{U} \coloneqq \times_{i=1}^{n}\mathcal{U}^i$ is the joint action space, where $\mathcal{U}^i,\ i \in \{1, 2, \ldots, n\}$ is the finite set of actions of CAV i, $P \coloneqq \mathcal{S} \times \mathcal{U} \times \mathcal{S} \to [0, 1]$ is the state transition probability which defines the transition probability between states, $R \coloneqq \mathcal{S} \times \mathcal{U} \to \mathbb{R}$ is the reward function for all CAVs, R^i is the reward function for CAV i, and $\gamma \in [0, 1]$ is a discount factor.

Next, we briefly explain different approaches to formulate the Q-learning updates along with advantages and disadvantages of each approach. For CAV i, we use s_k^i and u_k^i to denote the state and action that CAV i takes at time step $k \in \mathbb{N}$, respectively. Taking action $u_k^i \in \mathcal{U}^i$, CAV i transitions from $s_k^i \in \mathcal{S}^i$ to $s_{k+1}^i \in \mathcal{S}^i$ and receives the reward $r_k^i = R^i(s_k^i, u_k^i)$. In the centralized update rule, the multi-agent system is viewed as a whole and is solved as a single-agent learning task, in which there is only a single Q-function. The

update rule is

$$Q(s_k, u_k^1, \ldots, u_k^n) \leftarrow (1-\alpha) Q(s_k, u_k^1, \ldots, u_k^n) + \alpha \left[r_k + \gamma \max_{u_{k+1}^1, \cdots, u_{k+1}^n} Q(s_{k+1}, u_{k+1}^1, \ldots, u_{k+1}^n) \right], \tag{2.136}$$

where $s_k \in \mathcal{S}$ is the state of the system (collection of states of all CAVs), $r_k = R(s_k, u_k^1, \ldots, u_k^n)$ is the total cost incurred on the system at time step $k \in \mathbb{N}$, and $\alpha \in (0, 1]$ is the learning rate. Although, theoretically, this approach converges with probability 1 to the optimal action-value function, it does not scale well when the number of agents is increasing as the size of Q-table grows exponentially.

In the decentralized framework, each CAV is an *independent learner* (IL) with a corresponding Q-function. The update rule for CAV i is

$$Q^i(s_k^i, u_k^i) \leftarrow Q^i(s_k^i, u_k^i) + \alpha \left[r_k^i + \gamma \max_{u_{k+1}^i} Q^i(s_{k+1}^i, u_{k+1}^i) - Q^i(s_k^i, u_k^i) \right], \tag{2.137}$$

where $s_{k+1}^i \in \mathcal{S}^i$ is the state of CAV i at time step $k+1$. This approach has a smaller size Q-table than the centralized approach, and by increasing the number of agents, the Q-table's size does not grow exponentially. However, one of the drawbacks of this method is the lack of any coordination mechanism.

In our problem, CAVs need to coordinate to cross the intersection safely. Without a coordination mechanism, a CAV may select an optimal action, but it gets penalized due to the sub-optimal actions of other CAVs. It has been shown in [109, 197, 198], that using decentralized learning in a multi-agent framework with interacting agents leads to more oscillation in the learned policy and poorer performance compared to the centralized approach. In addition, since all CAVs are learning synchronously, the environment is not stationary anymore from the perspective of any CAV. Since past actions of some CAVs may affect the current behavior of other CAVs, the system is not Markovian. The latter implies that

convergence is not guaranteed for every single CAV [198].

Matignon *et al.* [198] first presented the hysteretic Q-learning approach to incorporate coordination among ILs in a decentralized RL framework by including two learning rates. They showed that by incorporating two learning parameters α and β, without affecting the Q-table size, the coordination among IL agents could be achieved. In addition, the performance of the system is as good as the centralized approach of multi-agent RL. The update rule is given by

$$\delta \leftarrow r_k^i + \gamma \max_{u_{k+1}^i} Q^i(s_{k+1}^i, u_{k+1}^i) - Q^i(s_k^i, u_k^i), \tag{2.138}$$

where

$$Q^i(s_k^i, u_k^i) = \begin{cases} Q^i(s_k^i, u_k^i) + \alpha\delta, & \text{if } \delta \geq 0, \\ Q^i(s_k^i, u_k^i) + \beta\delta, & \text{otherwise,} \end{cases} \tag{2.139}$$

where δ is a temporal difference (TD) error and $\beta < \alpha \in (0, 1]$. By using smaller learning rate when TD error is negative, the update results in a slower degradation of Q-value (hysteresis) associated with positive past experience. For instance, due to the sub-optimal actions of other CAVs in the environment, CAV i may get penalized by doing action u^i at state s^i, for which it received a positive reward in the past. In this case, the effects of this penalty on Q-value of agent i should be less important.

Main Elements of Proposed Framework

We adopt the hysteretic Q-learning formulation to update the Q-tables for each CAV which is an IL agent with a unique assigned index. Next, we present the main elements of our approach, including states, actions, and rewards.

At time step k, we consider that CAV i partially observes the system, and its state is $s_k^i := \langle p_k^i,\ v_k^i,\ \mathcal{X}_k^{\text{i,rear}},\ \mathcal{P}_k^{\text{i,lat}} \rangle$, where p_k^i and v_k^i are its position and speed, respectively; $\mathcal{X}_k^{\text{i,rear}} := \langle p_k^j,\ v_k^j \rangle$ consists of the position and speed of CAV j, which is immediately ahead of CAV i and $\mathcal{P}_k^{\text{i,lat}}$ consists of the position of the three closest vehicles to the exit of merging

zone that have a potential of lateral collision with CAV i; and $\mathcal{P}_k^{\text{i,lat}}$ consists of the position of the three closest vehicles to the exit of merging zone that have a potential of lateral collision with CAV i.

CAV i has to choose action u_k^i at time step k which is acceleration/deceleration from a discrete bounded set $\mathcal{U}^i$ with lower bound $u^{i,\min}$ and upper bound $u^{i,\max}$ which correspond to the minimum and maximum allowable control input of CAV i, respectively. Without loss of generality, we do not consider variation among CAVs' maximum and minimum control input. To this end, we set $u^{i,\min} = u^{\min}$ and $u^{i,\max} = u^{\max}$. In order to choose all actions in all states with nonzero probability and balance between exploration and exploitation, we employ the epsilon-greedy algorithm with a linear decay as follows

$$\rho = \max\left\{\frac{\text{total episodes} - \text{current episode}}{\text{total episodes}}, 0\right\}, \tag{2.140}$$

$$\epsilon = (\epsilon_i - \epsilon_f)\rho + \epsilon_f, \tag{2.141}$$

where ρ, ϵ_i, and ϵ_f are decay rate, initial and final ratio of exploration, respectively. In a RL framework, each episode represent a simulation, in which there is a corresponding epsilon found from (2.141). The corresponding epsilon determines the probability that an agent takes a random action at each episode. The epsilon found from (2.141) is bounded between initial and final ratio of exploration.

$$u_k^i = \begin{cases} \arg\max_{u_k^i} Q^i(s_k^i, u_k^i), & \text{with probability } 1-\epsilon, \\ \text{random action}, & \text{with probability } \epsilon, \end{cases} \tag{2.142}$$

where ϵ is a small positive number. Employing epsilon-greedy with a linear decay results in more exploration at the earlier episodes and less at the final episodes which can improve the performance of the framework. It is worth mentioning that by choosing a same value for ϵ_i and ϵ_f, the algorithm simplifies to the epsilon-greedy algorithm without decay.

CAV i takes an action u_k^i at time step k, transitions from state s_k^i to the new state s_{k+1}^i,

and receives a reward (or penalty) r_k^i based on the multi-objective cost $r_k^i = w_1 \cdot r_{\text{fuel}}^i + w_2 \cdot r_{\text{delay}}^i + w_3 \cdot r_{\text{speed}}^i + w_4 \cdot r_{\text{rear}}^i + w_5 \cdot r_{\text{lateral}}^i$, where $w_1, \ldots, w_5 \in \mathbb{R}_{\geq 0}$ are the weighting factors corresponding to the following costs.

We use the L^2-norm of the control input at each time step k as a penalty to reduce the control effort, which decreases fuel consumption.

$$r_{\text{fuel}}^i = -\frac{\|u_k^i\|^2}{(\max\{\|u^{\max}\|, \|u^{\min}\|\})^2}. \tag{2.143}$$

To improve the travel time, we define the time delay at each time step as a difference between the time that it takes for CAV i to reach its current position from the entry of the control zone and the time it would have taken for CAV i to cruise with the initial speed from the entry of the control zone until its current position. Considering CAV i at time step k, the traveled distance measured from the entry of the control zone is p_k^i, and its entry speed is denoted by v_0^i, the normalized penalty corresponding to delay is $r_{\text{delay}}^i = -\dfrac{(k\Delta t - \tau)}{\tau}$, where $\Delta t \in \mathbb{R}_{>0}$ is the time step and $\tau = \frac{p_k^i}{v_0^i}$.

For each CAV i, at each time step k, the speed is bounded by $0 \leq v^{\min} \leq v_k^i \leq v^{\max}$, where $v^{\min}, v^{\max}$ are the minimum and maximum speed limit, respectively. To ensure the speed constraint does not become active, we have

$$r_{\text{speed}}^i = \begin{cases} p_{\text{speed}}, & \text{if speed violates the constraint,} \\ 0, & \text{otherwise,} \end{cases} \tag{2.144}$$

where $p_{\text{speed}} \in \mathbb{R}_{<0}$ is the penalty for violating the speed constraint, and is decided a priori.

To ensure the absence of rear-end collision between CAV i and a preceding CAV j at time step k, we impose $p_k^j - p_k^i \geq d_{\text{safe}}$, where $d_{\text{safe}} \in \mathbb{R}_{>0}$ is a safe constant distance. The

associated penalty for violating rear-end safety at each time step k is

$$r^i_{\text{rear}} = \begin{cases} p_{\text{col}}, & \text{if } p^j_k - p^i_k < d_{\text{safe}}, \\ 0, & \text{if } p^j_k - p^i_k \geq d_{\text{safe}}, \end{cases} \tag{2.145}$$

where $p_{\text{col}} \in \mathbb{R}_{<0}$ is the penalty for violating the safety, and is decided a priori.

To guarantee lateral safety as CAVs cross the merging zone, we limit the merging zone occupancy to only one CAV at a time for CAVs with lateral collision potentials. Considering that CAVs i and j might have a lateral collision inside the merging zone, we construct the penalty according to the following two cases: Case 1: CAV i is outside the merging zone at time step k, and by taking action u^i_k, it enters the merging zone while CAV j, which previously entered the merging zone, is either still inside the merging zone, or it enters the merging zone at the same time as CAV i. In this case, CAV i receives the penalty $r^i_{\text{lateral}} = p_{\text{col}} \in \mathbb{R}_{<0}$. Case 2: CAV i is outside the merging zone at time step k, and by taking an action u^i_k, it enters the merging zone while, at the same time step k, CAV j exits the merging zone. In this case, CAV i receives no penalty.

If by the time CAV i enters the merging zone, there are more than one CAVs inside the merging zone that can cause a lateral collision with CAV i, then CAV i gets penalized for each of these CAVs separately equal to p_{col}. To encourage CAVs to have a safe pass through the intersection, each CAV receives a terminal reward equal to $n \cdot r_{\text{suc}}$ (recall that n is the total number of CAVs) when it exits the control zone, if the episode did not have any crashes, where $r_{\text{suc}} \in \mathbb{R}_{>0}$ is the success reward. Additionally, the episodes with a crash are terminated, and a new episode starts. Algorithm 4 shows the pseudocode of our decentralized coordination-aware framework for CAV i.

FIFO Queuing Policy

Here, we provide a brief overview of a common approach in motion planning of CAVs at signal-free intersections called FIFO queuing policy. By imposing a FIFO queuing

Algorithm 4 Hysteretic Q-learning Pseudocode for CAV i

Input: $\alpha,\ \beta$

Initialize $Q^i(s_k^i, u_k^i) = 0\ \ \forall s_k^i \in \mathcal{S}^i, u_k^i \in \mathcal{U}^i$
for $t = 1$: total episodes **do**
    Reset entry time and speed randomly
    for $k = 1$: maximum time step **do**
        if CRASHED **then**
            `Break`
        end if
        $s_k^i \leftarrow$ Compute current state
        $u_k^i \leftarrow$ Pick an epsilon-greedy action
        $s_{k+1}^i \leftarrow$ Simulation
        CRASHED $\leftarrow$ Did any CAVs violate the rear-end or lateral safety constraint? ▷ it is set to true, if there is any collision in the episode
        $r_k^i \leftarrow$ Compute reward
        $\delta \leftarrow r_k^i + \gamma \max_{u_{k+1}^i} Q^i(s_{k+1}^i, u_{k+1}^i) - Q^i(s_k^i, u_k^i)$
        if $\delta \geq 0$ **then**
            $Q^i(s_k^i, u_k^i) \leftarrow Q^i(s_k^i, u_k^i) + \alpha\delta$
        else
            $Q^i(s_k^i, u_k^i) \leftarrow Q^i(s_k^i, u_k^i) + \beta\delta$
        end if
    end for
end for

policy, each CAV must enter the merging zone in the same order that it entered the control zone. Let $N(t) \in \mathbb{N}$ be the total number of CAVs that have entered the control zone by the time t, $\mathcal{N}(t) = \{1, \ldots, N(t)\}$ be the queue which designates the order in which CAVs enter the merging zone, and $t_i^0,\ t_i^m \in \mathbb{R}_{>0}$ denote the time when CAV $i \in \mathcal{N}(t)$ enters the control zone and merging zone, respectively. The optimal entry time, which satisfies safety and speed constraint, can be found through the following recursive structure [65]. If $i = 1$, $t_i^{m^*} = t_i^0 + \frac{L}{v_0^i}$; if $i-1 \in$ *safe*, $t_i^{m^*} = \max\{t_{i-1}^{m^*},\ t_j^{m^*} + t_h,\ t_i^c\}$; or if $i-1 \in \{$*lateral*, *rear-end*$\}$, $t_i^{m^*} = \max\{t_{i-1}^{m^*} + t_h,\ t_i^c\}$, where based on the path of CAV $i-1$ and CAV i, CAV $i-1$ belongs to one of the following subsets: (1) *safe*, if there is no potential for collision with CAV i. (2) *lateral*, if there is a potential for lateral collision with CAV i. (3) *rear-end*, if CAV $i-1$ is the CAV immediately positioned in front of CAV i. The earliest feasible time that CAV i can reach the merging zone is denoted by t_i^c, and t_h is the safe time-headway to ensure safety at the entrance of the merging zone. If $i = 1$, CAV i cruises with the constant speed that it entered the control zone. Index j in t_j^m represents CAV

j which is physically located in front of CAV i.

Combined Hysteretic Q-learning with FIFO Framework

In our hysteretic Q-learning framework, we aimed at achieving the lateral safety through our state and reward architecture. Due to the fact that after each crash the simulation episode is terminated, an increasing number of CAVs may require a greater number of simulation episodes, which might become less applicable in the real systems. In this subsection, we introduce an enhanced framework which is a combination of FIFO and hysteretic Q-learning. In this framework, CAVs first find the optimal arrival time at merging zone recursively through a FIFO queuing policy at the start of each simulation episode. Since the lateral safety, and time-delay minimization are considered in the FIFO queuing policy [65], we need to modify the state and reward function in our Q-learning framework. The revised state of CAV i at time step k is $s_k^i := \langle p_k^i,\ v_k^i,\ \mathcal{X}_k^{\text{i,rear}}, \Delta t_i^{m^*} \rangle$, where p_k^i and v_k^i are its position and speed, respectively; and $\mathcal{X}_k^{\text{i,rear}} := \langle p_k^j,\ v_k^j \rangle$ consists of the position and speed of CAV j, which is immediately ahead of CAV i. The difference between the optimal arrival time at merging zone, and arrival time at the control zone is captured in the last element $\Delta t_i^{m^*} = t_i^{m^*} - t_i^0$, which takes value from a bounded set defined by speed limits of the roads. In the revised reward function, the weights regarding the lateral collision and delay terms are set to zero and $r_k^i = w_1' \cdot r_{\text{fuel}}^i + w_2' \cdot r_{\text{speed}}^i + w_3' \cdot r_{\text{rear}}^i + w_4' \cdot r_{\text{FIFO}}^i$, where $w_1', \ldots, w_4' \in \mathbb{R}$ are new weighting factors. To encourage CAV i to reach the merging zone at the planned arrival time $t_i^{m^*}$, we define $r_{\text{FIFO}}^i = -(\text{EAT} - t_i^{m^*})^2$ to be the negative of the normalized squared error of arrival time at the merging zone computed as the difference of the estimated arrival time (EAT) at the merging zone and the optimal arrival time. At time step k, the EAT of CAV i is approximated by assuming that CAV i cruises with a constant speed v_k^i for the rest of the path until the merging zone.

As CAV i enters the merging zone, the crossing time t_i^m is compared to the optimal arrival time $t_i^{m^*}$, and CAV i receives the last FIFO reward as $r_{\text{FIFO}}^i = p_{\text{FIFO}} \times (t_i^m - t_i^{m^*})^2$, where $p_{\text{FIFO}} \in \mathbb{R}_{<0}$ is the penalty for violating the FIFO arrival time, and is decided a priori.

After entering the merging zone, w_4' for CAV i is set to zero.

2.4.2 Simulation Setup

In our decentralized hysteretic Q-learning framework, at each time step each CAV needs to store the updated Q-value corresponding to the pair of current state and selected action. The discretization level not only directly affects the size of the Q-table, which each CAV stores, but it also influences the performance of our approach. Hence, determining proper discretization levels is a trade-off between the Q-table size and performance of the algorithm. Moreover, selecting improperly large or small values for time discretization results in poor performance, or even oscillating behavior. For instance, selecting a very small time step compared to the state discretization level leads to a situation in which a CAV takes action, but its state does not change. On the other hand, by selecting a very large time step, the system's safety might be jeopardized. The discretization level for position, speed, control input, and time are selected as $\Delta p = 2$ m, $\Delta v = 1$ m/s, $\Delta u = 0.5$ m/s^2, and $\Delta t = 0.5$ s, respectively. The rest of the parameters are set as follows: $\epsilon_i = 0.6$, $\epsilon_f = 0.01$, $\alpha = 0.4$, $\beta = 0.05$, $p_{\text{speed}} = -1$, $p_{\text{col}} = -100$, $p_{\text{FIFO}} = -10$, $r_{\text{suc}} = 10$, $w_1 = w_3 = w_4 = w_5 = 1$, $w_2 = 0.3$, and $w_i' = 1, i = \{1, \ldots, 4\}$.

At the start of each episode, the initial conditions of CAVs are reset. In order to do that, the initial speed is drawn randomly from a uniform feasible speed distribution, and the arrival time of CAV i is computed as $t_i^0 = \sum_{a=0}^{i} Y_a$, where t_i^0 is the sum of i independent and identically distributed random variable Y_a drawn from an exponential distribution with mean 2 s.

2.4.3 Simulation Results

To evaluate the effectiveness of our proposed framework, we investigate the coordination of CAVs at a signal-free intersection in two scenarios. We use the following parameters for the simulation: $d_{\text{safe}} = 4$ m, $v_{\min} = 5$ m/s, $v_{\max} = 15$ m/s, $u_{\max} = 3$ m/s^2, $u_{\min} = -3$ m/s^2.

Scenario 1: For our first scenario, we consider coordination of four CAVs using the hysteretic Q-learning framework in an intersection where the length of each road connected to the intersection is $L = 32$ m, the length of the merging zones is $D = 18$ m, and total episodes of simulation are set to $2{,}000{,}000$. CAV #1, #2, #3, #4, enter the control zone from southbound (SB), eastbound (EB), northbound (NB), and westbound (WB), respectively. Figure 2.21 shows the Cartesian norm of Q-table for each CAV and the average norm, respectively; which are computed after each 100 episodes. As it can be seen in Fig. 2.21, the norm of the Q-table for all four CAVs reaches to stable values and does not change that much in the final episodes. The difference in the converged value is due to the fact that during the earlier episodes of training, CAV #3 and #4 are more likely to cause accidents and get penalized compared to CAV #1 and CAV #2, since CAV #3 and #4 enter the control zone later. After

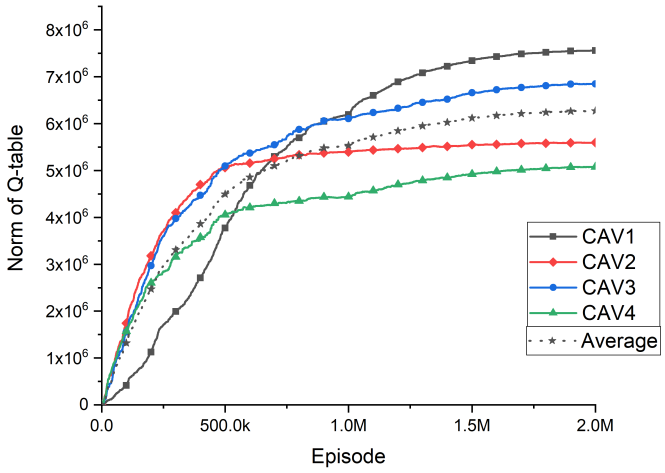

Figure 2.21: Norm of Q-table for CAVs in Scenario 1.

the training phase, we test the policies for $1{,}000$ randomly generated simulation. The same initial conditions for four CAVs are used to simulate the optimal control framework. The optimal control framework consists of throughput maximization and energy minimization problems. In the throughput maximization problem, each CAV computes its arrival time at the merging zone based on a FIFO queuing policy. By restricting CAVs to have a constant speed after entering the merging zone, each CAV derives its energy-optimal control input

from the control zone's entry until it reaches the merging zone considering speed and control constraints. Details of this approach can be found in [65]. The position trajectories of four CAVs for a randomly selected simulation is shown in Fig. 2.22 (solid lines). The major difference in the trajectories is because in the optimal control framework (dashed lines) the arrival time at merging zones for each CAV is found first, and then for each CAV, the optimal control problem is formulated from the arrival time at the control zone to the arrival time at the merging zone. On the other hand, our hysteretic Q-learning approach determines the policy with respect to the designed reward. Although trajectories resulted from our approach happen to respect the FIFO queuing policy (i.e., CAVs enter the merging zone in the same order they entered the control zone) without being enforced to, they appear to be more aggressive in minimizing the travel time. One can explore tuning w_1 and w_2 to find the trade-off between minimizing fuel consumption or delay.

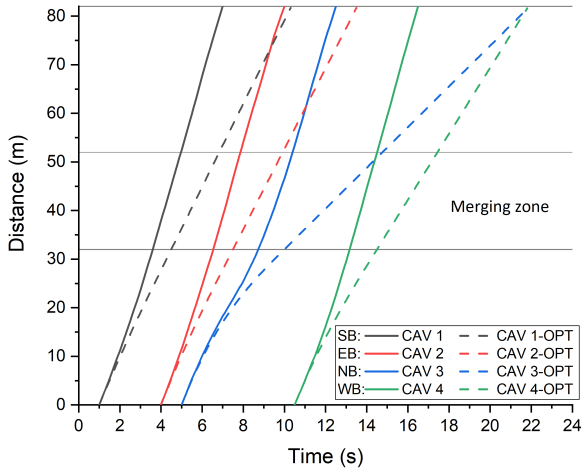

Figure 2.22: Position trajectories of CAVs in Scenario 1.

Scenario 2: For the second scenario, we consider coordination of eight CAVs using the combined hysteretic Q-learning with FIFO framework in an intersection which each road connecting to the intersection to be $L = 100$ m, the length of the merging zones to be $D = 18$ m, and total episodes of simulation are set to $400{,}000$. In this scenario, we employ the state and reward architecture based on FIFO queuing policy. This extension allows us to reduce

the state space size significantly. Namely, we are able to increase the control zone length in order to have enough space for CAVs to coordinate with each other. The position trajectories of eight CAVs for a randomly selected simulation (solid lines) along with the corresponding trajectories computed from the optimal control (dashed lines) are shown in Fig. 2.23. We note that CAVs following our combined hysteretic Q-learning with FIFO framework arrive at the merging zone at the planned arrival time with very small deviation. The trajectories for CAVs in our combined hysteretic Q-learning with FIFO framework do not deviate very much from the energy-optimal trajectories found from the optimal control techniques. Our proposed RL-based approach requires more time in the training phase compared to the classical control techniques, but after that Q-table is converged, it can be implemented in real-time. The videos from our simulation analysis can be found at the supplemental site, https://sites.google.com/view/ud-ids-lab/HQLC.

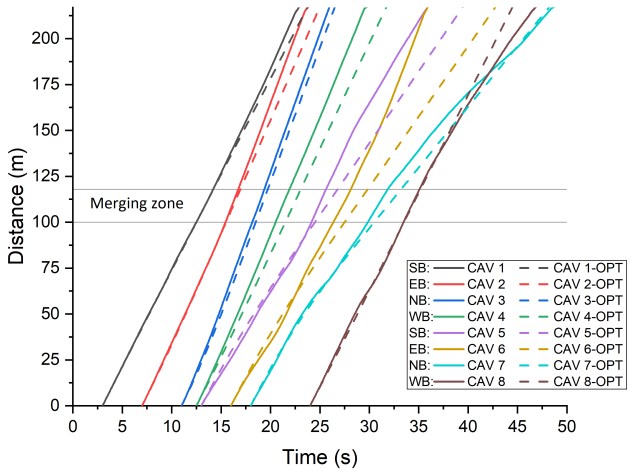

Figure 2.23: Position trajectories of CAVs in Scenario 2.

2.5 Summary

In this chapter, we established two approaches based on a bi-level architecture to coordinate CAVs at adjacent signal-free intersections consisting of the upper-level and low-level planning. In the first approach, in the upper-level planning, each CAV recursively

computes the energy-optimal arrival time at each intersection along its path, while ensuring both lateral and rear-end safety. Additionally, each CAV investigates the feasibility of a lane-changing maneuver and determines the optimal lane to occupy to the traffic throughput. Given the output of the upper-level planning, in the low-level planning, we formulated an optimal control problem for each CAV with the interior-point constraints, the solution of which yields the energy optimal control input (acceleration/deceleration). In addition, we enhanced our bi-level framework to guarantee safety in the presence of a bounded steady-state error in tracking the positions of CAVs. Finally, our proposed framework exhibited reduction in fuel-consumption, traffic delay, and improvement in the travel time compared to the baseline scenario in different traffic volumes ranging from 600 veh/h to $1{,}400$ veh/h for both symmetric and asymmetric adjacent intersections.

On the other hand, in the second approach, we focused on minimizing travel time and improving traffic throughput. Namely, in the upper level, we formulated a scheduling problem that each CAV solves upon entering the control zone. The upper-level problem's outcome becomes the input of the low-level problem, which is the tuple of optimal arrival time at each zone to avoid the lateral and rear-end collision and minimize the CAV's travel time. In the low-level control, we formulated an optimal control problem, the solution of which yields the optimal control input (acceleration/deceleration) and minimizes the transient engine operation. We derived an analytical solution for each zone that can be implemented in real time. Finally, we demonstrated the effectiveness of the proposed framework through simulation and comparison with signalized intersections, centralized scheduling, and FIFO queuing policy.

From the technical perspective, although these two approaches address a similar problem, they are different from each other on major aspects as follows:

- In Section 2.2, we considered multiple multi-lane adjacent intersections with limiting our analysis to the cases that no left/right turns are allowed. However, in Section 2.3, we considered two adjacent intersections including every possible path.
- In Section 2.2, we imposed a constant average speed inside the merging zone resulting in traveling at the merging zone with constant time. However, in Section 2.3, we partitioned the area around two adjacent intersections into different zones, and assumed

that the speed of each CAV at the boundary of zones within the merging zones was given and was equal to v_{merge}. Thus, the time that a CAV is inside each merging zone depends on the solution of the upper-level scheduling problem.

- The upper-level coordination framework in Section 2.2 is profoundly different from the one proposed in 2.3. The former is formulated to find the energy-optimal arrival time at each merging zone and optimal lane to occupy through a recursive algorithm, while the latter is concerned with finding the arrival time at each partitioned zone on the CAV's path aimed at minimizing total travel time through formulating a scheduling problem
- Although in both Sections 2.2 and 2.3, we follow Hamiltonian analysis to derive the closed-form analytical solution to the low-level problem, two major differences set the two low-level problems apart and make their Hamiltonian analysis fundamentally different. In Section 2.2, speed at the initial time is only given, while in Section 2.3, the speed at the boundaries is defined. Thus, the problem defined in Section 2.2, requires to satisfy new sets of optimality conditions due to the interior-point constraints which makes it different from the analysis in Section 2.3. Second, in contrast to Section 2.2, the rear-end safety constraint in Section 2.3 is speed dependent, which sets its Hamiltonian analysis completely apart from the minimum safe distance rear-end safety constraint discussed in Section 2.2

Finally, in this chapter, we proposed a learning-based decentralized coordination framework for CAVs at a signal-free intersection to minimize travel delay and improve fuel consumption while ensuring rear-end and lateral safety. We embedded a coordination mechanism into our decentralized learning framework by using hysteretic Q-learning to update the Q-table of each CAV. We also integrated FIFO queuing policy in our framework to improve the performance of our system. Finally, we showed the effectiveness of our proposed approach through simulation and comparison with the optimal control techniques based on Pontryagin's minimum principle.

While the proposed framework in this chapter does not consider inherent uncertainty in any real-physical system due to the disturbances, deviation from the nominal trajectory, or delay in the communication, it can be easily extended to work with the framework presented in the next chapter to consider uncertainty and react to it appropriately.

Chapter 3

A DECENTRALIZED COORDINATION FRAMEWORK FOR CONNECTED AND AUTOMATED VEHICLES IN THE PRESENCE OF UNCERTAINTY

> One who knows and knows that he knows;
> his horse of wisdom will reach the skies.
> One who knows, but doesn't know that he knows;
> he is fast asleep, so you should wake him up!
> One who doesn't know, but knows that he doesn't know;
> his limping mule will eventually get him home.
> One who doesn't know and doesn't know that he doesn't know;
> he will be eternally lost in his hopeless oblivion!
>
> Ibn Yamin, persian poet, 1286–1368 CE

Most of the existing work in optimal coordination of connected and automated vehicles (CAVs), including the framework presented in Chapter 2, have neglected any source of uncertainty in establishing their framework. This uncertainty can have a variety of sources such as deviation from the nominal strategies, disturbances from the environment, noisy observations, uncertainties in the system's dynamics, and delayed communications. Any framework for coordination of CAVs that neglects this uncertainty is prone to suboptimality and can even lead to unsafe conditions. Therefore, in order to implement optimal control strategies for coordination of CAVs in real-world scenarios, these uncertainties need to considered in the framework, or there should exists a safety layer safe-guarding the system.

After the seminal work of Athans [33] on safely coordinating vehicles at merging roadways, several research efforts have explored the benefits of coordinating CAVs in traffic scenarios using a bi-level framework such as those described in Chapter 2. The bi-level framework consists of (1) an *upper-level* optimization that yields, for each CAV, the optimal time to exit a predetermined control zone of the intersection; and (2) a *low-level* optimization that yields for the CAV its optimal control input (acceleration/deceleration) to achieve the

optimal time derived in the upper-level subject to the state, control, and safety constraints. There have been a variety of approaches in the literature to solve the upper-level optimization problem, including first-in-first-out (FIFO) queuing policy [65, 75, 199], heuristic Monte Carlo tree search methods [47, 200], centralized optimization techniques [57, 61], and job-shop scheduling [55, 176]. Given the solution of the upper-level optimization problem, the low-level optimization for each CAV addresses a constrained optimal control problem using model predictive control (MPC) [49, 61–64], or standard optimal control techniques resulting in closed-form analytical solutions [65, 78, 91, 175]. However, the latter approach leads to a system of non-linear equations that might be challenging, in some instances, to solve in real time. To address this problem, a different approach was proposed in [91], and implemented at a roundabout in [92] consisting of a single optimization level aimed at both minimizing energy consumption and improving the traffic throughput. In this approach, each CAV computes the optimal exit time of the control zone corresponding to an unconstrained energy optimal trajectory which satisfies all the state, control, and safety constraints.

In this chapter, we build upon the single-level optimization framework introduced in [91] and implemented in [92] aimed at both minimizing energy consumption and improving the traffic throughput. We first provide a general problem formulation and the single-level optimization framework for coordination of CAVs at a signal-free intersection in Section 3.1. In Section 3.2, we integrate the replanning mechanism into this single-level coordination framework for CAVs. Since unexpected changes in the presence of disturbances and uncertainties can result in deviations from the optimal planned trajectory of the CAVs, the replanning mechanism introduces feedback in the planning which can respond to these changes in the system to some extent. In addition, using the theory from the job-shop scheduling problem, we further enhance this framework by introducing a priority-aware resequencing mechanism to find the decision making sequence of the CAVs based on the minimum exit time from the traffic bottleneck. In section 3.3, we improve the single-level coordination framework for CAVs by reformulating the coordination of CAVs as a robust coordination problem. Employing Gaussian process (GP) regression, we learn the deviation of CAVs from their nominal

time trajectory and obtain confidence intervals on the unknown errors of nominal trajectories based on the noisy observations of CAVs. The obtained confidence intervals can then be used to solve the robust coordination problem using a worst-case scenario approach. In Section 3.4, using control barrier functions (CBF) for safety-critical systems [149], we integrate a safety layer into this framework to guarantee that the planned trajectory does not violate any of the constraints in the system. Particularly, since safety constraints for each CAV involve the trajectory of other CAVs, inspired by the idea of environmental CBFs [201], we consider the evolution of other relevant CAVs in constructing our CBFs. By introducing a barrier certificate as a safety middle layer between the vehicle-level tracking controller and physical vehicle, we provide a reactive mechanism to guarantee constraint satisfaction in the system. The enhanced framework results in a quadratic program (QP) that can be solved efficiently at each time step. This approach also allows us to consider more complex vehicle dynamics to ensure safety. Finally, in Section 3.5, we summarize the findings of this chapter.

The main contributions presented in this chapter are

- Section 3.2: (1) the introduction of replanning as a feedback mechanism to handle uncertainties or disturbances; and (2) the development of a priority-aware resequencing mechanism for the coordination of CAVs and relaxing the first-come-first-serve (FCFS) decision making sequence of the CAVs. The results of this section were previously presented in the following publication:
  - [178] Behdad Chalaki and Andreas A. Malikopoulos. A priority-aware replanning and resequencing framework for coordination of connected and automated vehicles. *IEEE Control Systems Letters*, 6:1772–1777, 2022
- Section 3.3: (1) the development of a robust coordination framework of CAVs at a signal-free intersection; and (2) using GP regression to learn the deviation of CAVs from their nominal time trajectory and obtain confidence intervals on the unknown errors of nominal trajectories based on the noisy observations of CAVs. The work in presented in this chapter appeared in the following publication:
  - [179] Behdad Chalaki and Andreas A Malikopoulos. Robust learning-based trajectory planning for emerging mobility systems. In *2022 American Control Conference (ACC)*, pages 2154–2159, 2022
- Section 3.4: (1) the introduction of barrier-certificate as a safety middle layer between the vehicle-level tracking controller and physical vehicle in the optimal coordination of CAVs at a signal-free intersection, and providing a reactive mechanism to guarantee

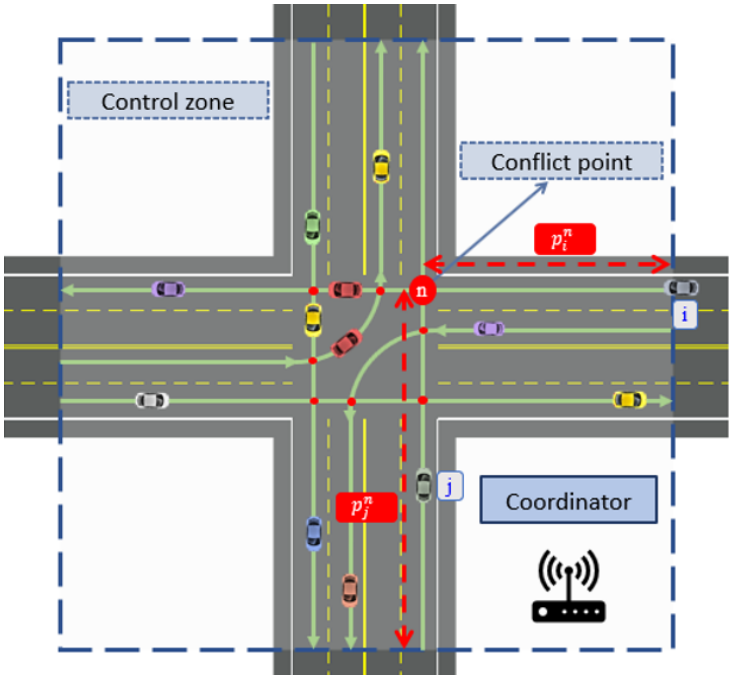

Figure 3.1: A signal free intersection with conflict points.

constraint satisfaction in the presence of uncertainty. The results of this sections is based on the material presented in:

- [180] Behdad Chalaki and Andreas A Malikopoulos. A Barrier-Certified Optimal Coordination Framework for Connected and Automated Vehicles. *arXiv:2203.16418 (in review)*, 2022

3.1 Modeling Framework

Similar to previous chapter, we consider a signal-free intersection (Fig. 3.1), which includes a *coordinator* that stores information about the intersection's geometry and CAVs' trajectories. The coordinator acts only as a database for the CAVs and does not make any decisions. The intersection includes a *control zone* inside of which the CAVs can communicate with the coordinator. We call the points inside the control zone where paths of CAVs intersect and a lateral collision may occur as *conflict points*. Let $\mathcal{Q} \subset \mathbb{N}$ index the set of conflict points, $N(t) \in \mathbb{N}$ be the total number of CAVs inside the control zone at time $t \in \mathbb{R}_{\geq 0}$, and $\mathcal{N}(t) = \{1, \ldots, N(t)\}$ be the queue that designates the order in which each CAV entered the control zone.

We model the longitudinal dynamics of each CAV $i \in \mathcal{N}(t)$ as a double integrator

$$\begin{aligned} \dot{p}_i(t) &= v_i(t), \\ \dot{v}_i(t) &= u_i(t), \end{aligned} \tag{3.1}$$

where $p_i(t) \in \mathcal{P}_i$, $v_i(t) \in \mathcal{V}_i$, and $u_i(t) \in \mathcal{U}_i$ denote position, speed, and control input at t, respectively. The sets $\mathcal{P}_i$, $\mathcal{V}_i$, and $\mathcal{U}_i$, for $i \in \mathcal{N}(t)$, are compact subsets of $\mathbb{R}$. Let $t_i^0 \in \mathbb{R}_{\geq 0}$ be the time that CAV $i \in \mathcal{N}(t)$ enters the control zone, and $t_i^f > t_i^0 \in \mathbb{R}_{\geq 0}$ be the time that CAV i exits the control zone. For each CAV $i \in \mathcal{N}(t)$, the control input and speed are bounded by

$$u_{i,\min} \leq u_i(t) \leq u_{i,\max}, \tag{3.2}$$

$$0 < v_{\min} \leq v_i(t) \leq v_{\max}, \tag{3.3}$$

where $u_{i,\min}, u_{i,\max}$ are the minimum and maximum control inputs and $v_{\min}, v_{\max}$ are the minimum and maximum speed limits, respectively.

To guarantee rear-end safety between CAV $i \in \mathcal{N}(t)$ and a preceding CAV $k \in \mathcal{N}(t) \setminus \{i\}$, we impose the following constraint,

$$p_k(t) - p_i(t) \geq \delta_i(t) = \gamma + \varphi \cdot v_i(t), \tag{3.4}$$

where $\delta_i(t)$ is the safe speed-dependent distance, while γ and $\varphi \in \mathbb{R}_{>0}$ are the standstill distance and reaction time, respectively.

Definition 3.1.1. *For CAV $i \in \mathcal{N}(t)$, the inverse function, p_i^{-1} is the time trajectory and denoted by $t_i \colon \mathcal{P}_i \to [t_i^0, t_i^f]$. The time trajectory yields the time that CAV i is at position $p_i \in \mathcal{P}_i$ inside the control zone.*

Since $0 < v_{\min} \leq v_i(t)$, the position $p_i(t)$ is a strictly increasing function. Moreover, for every element in $\mathcal{P}_i$, there is at least one element in $[t_i^0, t_i^f]$, which implies that the position $p_i(t)$ is a surjective function, and hence the inverse $t_i(\cdot) = p_i^{-1}(\cdot)$ exists [91].

CAV i may have a lateral collision with CAV $j \in \mathcal{N}(t) \setminus \{i\}$, which has already planned its trajectory, at conflict point $n \in \mathcal{Q}$ (Fig. 3.1) . We denote by p_i^n and p_j^n the distance of the conflict point n from i's and j's paths' entries, respectively (Fig. 3.1). To guarantee lateral collision avoidance, we impose the following time headway constraint

$$\left|t_i(p_i^n) - t_j(p_j^n)\right| \geq t_h, \tag{3.5}$$

where $t_h \in \mathbb{R}_{>0}$ is the minimum time headway between any two CAVs crossing conflict point n.

Proposition 3.1.2. *We can alternatively formulate the lateral safety constraint between CAV $i \in \mathcal{N}(t)$ and CAV $j \in \mathcal{N}(t) \setminus \{i\}$ in (3.5) as a constraint on the distance to the conflict point $n \in \mathcal{Q}$ as*

$$\min \left\{ \begin{array}{l} \max\limits_{t\in[t_i^0,t_j^n]} \{\delta_i(t) + p_i(t) - p_i^n\}, \\ \max\limits_{t\in[t_i^0,t_i^n]} \{\delta_j(t) + p_j(t) - p_j^n\} \end{array} \right\} \leq 0. \tag{3.6}$$

Proof. Since we do not use the FIFO queuing policy, CAV i can reach at conflict point n either after or before CAV j. In the first case, i.e., when CAV i reaches at conflict point n after CAV j, we have

$$p_i^n - p_i(t) \geq \delta_i(t), \quad \forall t \in [t_i^0, t_j^n], \tag{3.7}$$

where t_j^n is the known time that CAV j reaches at conflict point n, i.e., position p_j^n. In the second case, where CAV i reaches at the conflict point n before CAV j, we have

$$p_j^n - p_j(t) \geq \delta_j(t) = \gamma + \varphi \cdot v_j(t), \quad \forall t \in [t_i^0, t_i^n], \tag{3.8}$$

where t_i^n is determined by the trajectory planned by CAV i.

By moving all terms in (3.7) to the RHS, we get $\delta_i(t) + p_i(t) - p_i^n \leq 0$. Constraint (3.7) is satisfied, if $\max(\delta_i(t) + p_i(t) - p_i^n) \leq 0$ in the interval $[t_i^0, t_j^n]$. Likewise, if $\max(\delta_j(t) +$

$p_j(t) - p_j^n) \leq 0$ in the interval $[t_i^0, t_i^n]$ constraint (3.8) is satisfied. However, to ensure the lateral safety between CAV i and CAV j at conflict point n, either (3.7) or (3.8) must be satisfied, and thus the proof is completed. □

In this chapter, we build upon the single-level optimization framework introduced in [91] and implemented in [92] aimed at both minimizing energy consumption and improving the traffic throughput. Upon entrance the control zone, each CAV $i \in \mathcal{N}(t)$ communicates with the coordinator to access the time trajectories of CAVs which are already in the control zone. After obtaining this information, CAV i solves a time minimization problem to determine the time that it must exit the control zone, t_i^f. The time t_i^f corresponds to the unconstrained energy optimal trajectory guaranteeing that state, control, and safety constraints are satisfied. This trajectory is communicated back to the coordinator, so that the subsequent CAVs receive this information and plan their trajectories accordingly.

We first review the single-level optimization framework for coordination of CAVs. We start the exposition with the unconstrained energy optimal solution of CAV i, which has the following form [65]

$$\begin{aligned} p_i(t) &= \phi_{i,3} \cdot t^3 + \phi_{i,2} \cdot t^2 + \phi_{i,1} \cdot t + \phi_{i,0}, \\ v_i(t) &= 3\phi_{i,3} \cdot t^2 + 2\phi_{i,2} \cdot t + \phi_{i,1}, \\ u_i(t) &= 6\phi_{i,3} \cdot t + 2\phi_{i,2}, \end{aligned} \tag{3.9}$$

where $\phi_{i,3} \neq 0$ and $\phi_{i,2}, \phi_{i,1}, \phi_{i,0} \in \mathbb{R}$ are the constants of integration. CAV i must also satisfy the boundary conditions

$$p_i(t_i^0) = 0, \quad v_i(t_i^0) = v_i^0, \tag{3.10}$$

$$p_i(t_i^f) = p_i^f, \quad u_i(t_i^f) = 0, \tag{3.11}$$

where $u_i(t_i^f) = 0$ because the speed at the exit of the control zone is not specified [190]. The details of the derivation of the unconstrained solution are discussed in [65].

Using the Cardano's method [202], $t_i(p_i)$ is given by

$$t_i(p_i) = \sqrt[3]{-\frac{1}{2}\left(\omega_{i,1} + \omega_{i,2}\, p_i\right) + \sqrt{\frac{1}{4}\left(\omega_{i,1} + \omega_{i,2}\, p_i\right)^2 + \frac{1}{27}\omega_{i,0}^3}} + \sqrt[3]{-\frac{1}{2}\left(\omega_{i,1} + \omega_{i,2}\, p_i\right) - \sqrt{\frac{1}{4}\left(\omega_{i,1} + \omega_{i,2}\, p_i\right)^2 + \frac{1}{27}\omega_{i,0}^3}} + \omega_{i,3}, \qquad p_i \in \mathcal{P}_i, \quad (3.12)$$

where $\omega_{i,3}, \omega_{i,2}, \omega_{i,1}$, and $\omega_{i,0} \in \mathbb{R}$ such that $\frac{1}{4}(\omega_{i,1} + \omega_{i,2}\, p_i)^2 + \frac{1}{27}\omega_{i,0}^3 > 0$, and they are all defined in terms of $\phi_{i,3}, \phi_{i,2}, \phi_{i,1}, \phi_{i,0}$ [91]. We formally define the single-level optimization framework as follows.

Problem 3.1.3. *Each CAV $i \in \mathcal{N}(t)$ solves the following optimization problem at t_i^0, upon entering the control zone*

$$\min_{t_i^f \in \mathcal{T}_i(t_i^0)} \; t_i^f \quad (3.13)$$

$$\text{subject to: } (3.4), (3.5), (3.9) - (3.11),$$

where the compact set $\mathcal{T}_i(t_i^0) = [\underline{t}_i^{f,\tau}, \bar{t}_i^{f,\tau}]$ is the set of feasible solution of CAV $i \in \mathcal{N}(t)$ for the exit time computed at t_i^0 using the speed and control input constraints (3.2)-(3.3)*, and boundary conditions* (3.10)-(3.11).

We derive the upper and lower bounds on the exit time of the control zone for a CAV $i \in \mathcal{N}(t)$ using the speed and control constraints by exploiting two properties of the optimal trajectory. As the optimal control input is linear and satisfies $u_i(t_i^f) = 0$, it must be zero, strictly decreasing, or strictly increasing. In all three cases $u_i(t)$ achieves its extreme at t_i^0, and therefore satisfying $u_{\min} \leq u_i(t_i^0) \leq u_{\max}$ is necessary and sufficient condition to guarantee constraint satisfaction. Likewise, the speed of CAV i starts at $v_i(t_i^0) = v_i^0 \in [v_{\min}, v_{\max}]$ and must be constant, strictly increasing, or strictly decreasing inside the control zone. In all three cases $v_i(t)$ takes its extreme value at t_i^f, and thus satisfying $v_{\min} \leq v_i(t_i^f) \leq v_{\max}$ is necessary and sufficient condition to guarantee constraint satisfaction.

Next, without loss of generality, let $t_i^0 = 0$ and $p_i^0 = 0$. This implies that $p_i(t_i^0) = \phi_{i,0} = 0$ and $v_i(t_i^0) = \phi_{i,1} = v_i^0$, while $u_i(t_i^f) = 0$ implies

$$\phi_{i,3} = \frac{-\phi_{i,2}}{3t_i^f}, \tag{3.14}$$

and $p_i(t_i^f) = p_i^f$ yields

$$\phi_{i,2} = \frac{3(p_i^f - v_i^0 t_i^f)}{2(t_i^f)^2}. \tag{3.15}$$

In order to compute the lower bound on exit time of the control zone for CAV i, $\underline{t}_i^f$, there are two cases to consider:

Case L1: CAV i achieves its maximum control input at entry of the control zone, that is, $u_i(t_i^0) = u_{\max}$. In this case, evaluating optimal control input from (3.9) at $t_i^0 = 0$ yields

$$u_i(t) = 2\phi_{i,2} = u_{\max}. \tag{3.16}$$

Substituting (3.15) into (3.16) and solving for t_i^f yields the quadratic equation $u_{\max} {t_i^f}^2 + 3v_i^0 t_i^f - 3p_i^f = 0$, which has two real roots with opposite signs, since $t_{i,1}^f t_{i,2}^f = \frac{-3p_i^f}{u_{\max}} < 0$. Thus, $t_{i,u_{\max}}^f > 0$ is $t_{i,u_{\max}}^f = \frac{\sqrt{9{v_i^0}^2 + 12p_i^f u_{\max}} - 3v_i^0}{2u_{\max}}$.

Case L2: CAV i achieves its maximum speed at the end of control zone, that is, $v_i(t_i^f) = v_{\max}$. For this case, by (3.9), we have

$$v_i(t_i^f) = 3\phi_{i,3}{t_i^f}^2 + 2b_i t_i^f + v_i^0 = v_{\max}. \tag{3.17}$$

Substituting (3.14) and (3.15) into (3.17) yields

$$v_i(t_i^f) = 3\left(\frac{-\phi_{i,2}}{3t_i^f}\right){t_i^f}^2 + 2\phi_{i,2}t_i^f + v_i^0 = \phi_{i,2}t_i^f + v_i^0 = \frac{3(p_i^f - v_i^0 t_i^f)}{2t_i^f} + v_i^0 = v_{\max}, \tag{3.18}$$

which simplifies to $t_{i,v_{\max}}^f = \frac{3p_i^f}{v_i^0 + 2v_{\max}}$. Thus, our lower bound on t_i^f is given by $\underline{t}_i^f = \min\left\{t_{i,u_{\max}}^f, t_{i,v_{\max}}^f\right\}$.

The upper bound on exit time of the control zone for CAV i, $\bar{t}_i^f$ can be derived following similar steps for the lower bound, and can be broken into two cases.

Case U1: CAV i achieves its minimum control input at the entry of the control zone, that is, $u_i(t_i^0) = u_{\min}$. This implies $u_{\min}{t_i^f}^2 + 3v_i^0 t_i^f - 3p_i^f = 0$, which has two positive roots, as $t_{i,1}^f t_{i,2}^f = \frac{-3p_i^f}{u_{\min}} > 0$, from which we select the smaller one,

$$t_{i,u_{\min}}^f = \frac{\sqrt{9{v_i^0}^2 + 12p_i^f u_{\min}} - 3v_i^0}{2u_{\min}}, \tag{3.19}$$

as the speed of the vehicle should be always greater than zero. Note that when $9{v_i^0}^2 + 12p_i^f u_{\min} < 0$ there is no real value of t_i^f which satisfies all of the boundary conditions simultaneously, and therefore the constraint $u(t_i^0) = u_{\min}$ can never become active if (3.19) is complex. In that case, the upper bound must be given by Case U2.

Case U2: CAV i achieves its minimum speed at the entry of the control zone, that is, $v_i(t_i^f) = v_{\min}$. Evaluating (3.9) at t_i^f yields $v_i(t_i^f) = 3\phi_{i,3}{t_i^f}^2 + 2b_i t_i^f + v_i^0 = v_{\min}$, in which substituting (3.14) and (3.15) yields

$$v_i(t_i^f) = 3\Big(\frac{-\phi_{i,2}}{3t_i^f}\Big){t_i^f}^2 + 2\phi_{i,2}t_i^f + v_i^0 = \phi_{i,2}t_i^f + v_i^0 = \frac{3(p_i^f - v_i^0 t_i^f)}{2t_i^f} + v_i^0 = v_{\min}, \tag{3.20}$$

which simplifies to $t_{i,v_{\min}}^f = \frac{3p_i^f}{v_i^0 + 2v_{\min}}$.

Thus, the upper bound on the exit time for CAV i is

$$\bar{t}_i^f = \begin{cases} t_{i,v_{\min}}^f, & \text{if } 9{v_i^0}^2 + 12p_i^f u_{i,\min} < 0, \\ \max\{t_{i,u_{\min}}^f, t_{i,v_{\min}}^f\}, & \text{otherwise.} \end{cases} \tag{3.21}$$

where $t_{i,v_{\min}}^f = \frac{3p_i^f}{v_i^0 + 2v_{\min}}$ and $t_{i,u_{\min}}^f = \frac{\sqrt{9{v_i^0}^2 + 12p_i^f u_{\min}} - 3v_i^0}{2u_{\min}}$.

Remark 3.1.4. *The solution of Problem 3.1.3 yields a t_i^f which guarantees that none of the constraints in Problem 3.1.3 becomes active, and thus CAV i follows the unconstrained*

energy-optimal solution (3.9).

This framework implies that the CAVs do not have to come to a full stop at the intersection, thereby conserving momentum and fuel while also improving travel time. By enforcing the unconstrained energy-optimal trajectory that guarantees the satisfaction of all the state, control, and safety constraints, we avoid inherent real-time implementation difficulties in solving a constrained optimal control and piecing constrained and unconstrained arcs together [91, 92].

3.2 A Priority-Aware Replanning and Resequencing Framework for Coordination of Connected and Automated Vehicles

Deriving optimal control strategies for coordination of CAVs often requires adjusting the strategies in order to respond to unexpected changes in the presence of disturbances and uncertainties. In this section, we first extend the single-level optimization framework introduced in [91], and described in the previous section to incorporate replanning. Then, we further enhance the framework by introducing a priority-aware resequencing mechanism which designates the order of decision making of CAVs based on theory from the job-shop scheduling problem. Our enhanced framework relaxes the FCFS decision order which has been used extensively in the sequential decision making problems. We illustrate the effectiveness of our proposed approach through numerical simulations.

We structure this section as follows: In subsection 3.2.1, we offer the problem formulation and we present the priority-aware resequencing mechanism in Section 3.2.2. Finally, we provide simulation results in Section 3.2.3.

3.2.1 Problem Formulation

We consider a signal-free intersection (Fig. 3.2), and assume that CAVs do not perform any lane-change maneuver, and thus there are finite paths among which they can choose. The set of all possible paths in the control zone is given by $\mathcal{L} = \{1, \ldots, z\}$, $z \in \mathbb{N}$. The path

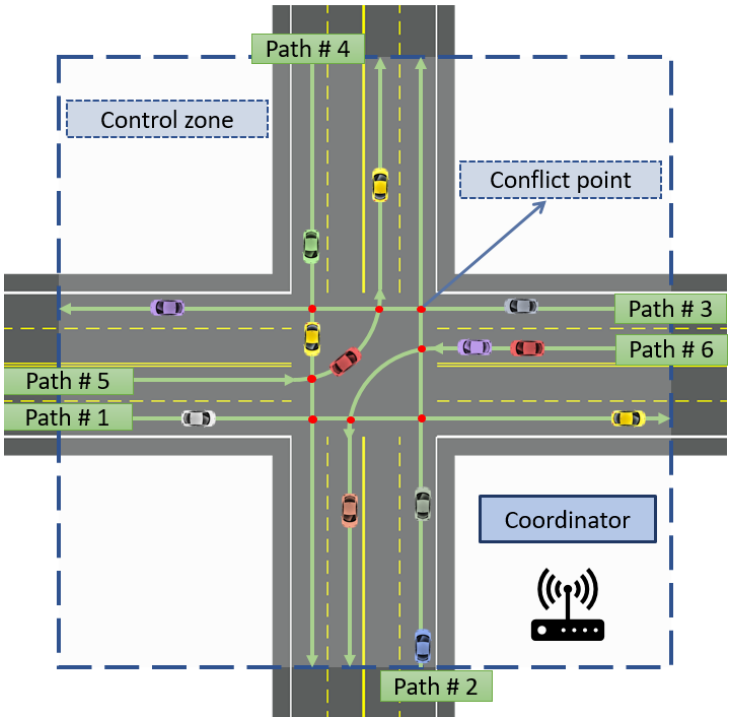

Figure 3.2: A signal free intersection with conflict points.

of the CAV $i \in \mathcal{N}(t)$ in the control zone is denoted by $\ell_i \in \mathcal{L}$ (Fig. 3.2), and is decided a priori based on some upper-level routing problem. In this section, we make the following assumption.

Assumption 3.2.1. *Each path of a CAV cannot get either split to two paths or merged by another CAV's path.*

This assumption implies that there should be separate lanes for the turning maneuvers at the intersections. This might be a strong assumption, but it simplifies the time complexity of our resequencing algorithm (formally defined next) by only considering the rear-end safety constraints for the CAVs traveling on the same path.

One of the advantages of incorporating replanning in the framework is introducing feedback in the system. Replanning can occur either periodically (i.e., at a period determined a priori) or be event-driven (i.e., based on an occurrence of a certain event such as the entrance of a new CAV in the control zone). All CAVs in the control zone observe their state at each

replanning instance and re-solve their optimization problem, discussed next, sequentially with the new initial conditions. For CAV i, let $\tau \in [t_i^0, t_i^f]$ be the replanning time, and $\tilde{\mathbf{x}}_i(\tau) = [\tilde{p}_i(\tau)\ \tilde{v}_i(\tau)]^\top$, be the measurement of the state at this time. The revised initial conditions for CAV i at this replanning instance is given by

$$p_i(\tau) = \tilde{p}_i(\tau), \quad v_i(\tau) = \tilde{v}_i(\tau). \tag{3.22}$$

To avoid abrupt changes in the control input and unnecessary acceleration, we revise the lower bound on exit time to use the maximum value between the earliest feasible exit time computed at t_i^0 (to simplify the notation denoted as $\underline{t}_i^f$), and the earliest feasible exit time computed at τ. Thus, the feasible compact set computed at τ is given by

$$\mathcal{T}_i(\tau) = \left[\max\left\{\underline{t}_i^f, \underline{t}_i^{f,\tau}\right\}, \bar{t}_i^{f,\tau}\right]. \tag{3.23}$$

Problem 3.2.2. *Each CAV $i \in \mathcal{N}(t)$ at replanning instance τ solves the following optimization problem*

$$\min_{t_i^f \in \mathcal{T}_i(\tau)} t_i^f \tag{3.24}$$

subject to:

(3.4), (3.5), (3.9), (3.11), (3.22).

To some extent, this replanning provides the CAV a feedback mechanism to react to any uncertainties.

3.2.2 A Priority-aware Resequencing

In the framework presented in [91], upon entering the control zone, CAV $i \in \mathcal{N}(t)$ solves Problem 3.2.2 at $\tau = t_i^0$ by only considering CAVs in the control zone. For the cases

in which CAVs enter the control zone simultaneously, the coordinator randomly decides the decision-making order of CAVs. Namely, the order of decision making is based on the order that CAVs entered the control zone, FCFS. We define the *decision sequence* formally as follows.

Definition 3.2.3. *The sequential decision making of $N(t)$ CAVs is based on the decision sequence that is given by the sequence $s = (s_1, s_2, \ldots, s_{N(t)})$ where $s_n \in \mathcal{N}(t)$, $n \in \{1, \ldots, N(t)\}$ is the n'th CAV in the decision making process.*

Without a resequencing mechanism, the decision sequence of the $N(t)$ CAVs is given by $s = (1, 2, 3, \ldots, N(t))$ which is imposed by the order the CAV enter the control zone, referred to as FCFS sequence. Note that this is different from the order that CAVs cross the intersection, which is determined by the lateral safety constraint (3.5) or (3.6). Next, we introduce our resequencing framework, which designates the decision sequence at each replanning instance.

Unlike our previous framework, where CAVs only solve their optimization problem upon entering the control zone, in this enhanced framework, CAVs re-solve the optimal control problem at different instances based on new observed information. The observed information of each CAV consists of position and speed of the CAV at the replanning instance, which then can be used as new initial conditions (3.22) to solve Problem 3.2.2. In this section, we introduce a priority-aware resequencing mechanism to find the sequence of decision making based on the minimum exit time from the control zone using scheduling theory.

A scheduling problem is shown by a triplet $(\alpha \mid \beta \mid \gamma)$, where α and β fields describe the machine environment and details of the processing characteristics and constraints, respectively, while γ field describes the objective function. In our problem, the control zone can be considered as *a single machine*, while different CAVs are considered as different jobs. In our problem, we also have *precedence constraint* which requires that a CAV not plan earlier than the physical CAV located in front of it, which we define formally next.

Definition 3.2.4. *The precedence constraint can be represented by a directed graph $G =$*

(V, E), where $V \coloneqq \mathcal{N}(t)$ is set of all CAVs and $E \coloneqq \{(i,j)|i,j \in V, i \to j\}$ is the set of all constraints on the order of decision making. Edge $(i,j) \in E$ shows that CAV i should plan earlier than CAV j.

Definition 3.2.5. *A non-empty subgraph $G_1 = (V_1, E_1)$, where $V_1 \subset V$ and $E_1 \subset E$ is called a **chain** if for each vertex $i \in V_1$, there exist at most a single edge $(i,j) \in E_1, j \in V_1 \setminus \{i\}$.*

In a scheduling problem, the *processing time* of a single machine on the job i is denoted by P_i, representing the time that it takes for the machine to process job i. In our case, we consider the processing time of CAV i at replanning instance t to be equal to $\min(\mathcal{T}_i(t))$, i.e., the minimum exit time from the control zone which is independent of the decision sequence. For each job i, a weight $w_i \in \mathbb{R}_{>0}$ describes the importance of job i relative to the other jobs in the system. We consider that the weight of each CAV is inversely proportional to the size of the compact set of its feasible solution. This potentially helps CAVs with smaller feasible space to generate their trajectory first.

Since our goal is to find the optimal decision sequence based on the minimum exit time of the CAVs, we consider the *total weighted completion time* of $N(t)$ CAVs denoted by $J^s = \sum_{i=1}^{N(t)} w_i \, C_i^s$ as our cost function under decision sequence s, where C_i^s is the sum of processing times of CAV i and other preceding CAVs in the decision sequence s. For example, suppose for two CAV i and j, we have $P_i < P_j$ and $w_i = w_j$. The cost functions for two different decision sequences $s = (i,j)$ and $s' = (j,i)$ are equal to $J^s = w_i \cdot P_i + w_j \cdot (P_i + P_j)$ and $J^{s'} = w_j \cdot P_j + w_i \cdot (P_j + P_i)$, respectively. It is clear that the decision sequence s, which prioritize CAV i over CAV j, has a lower total cost.

Our scheduling problem is denoted by $(1 \mid G \mid \sum_{i=1}^{N(t)} w_i \, C_i^s)$ which describes a single machine model with precedence constraint G, and the objective is to minimize the total weighted completion time by finding the optimal decision sequence s.

Lemma 3.2.6. *The precedence constraint's graph of CAVs crossing a single intersection given Assumption 3.2.1 consists of multiple disjoint chains.*

Proof. From Assumption 3.2.1, we do not have any merging or splitting paths, and thus the precedence constraint only exists among CAV i and $j \in \mathcal{N}(t)$ on the same path $\ell \in \mathcal{L}$ such that $\ell_i = \ell_j = \ell$. Thus, among CAVs on path ℓ there exist a chain denoted by $G_\ell \subset G$ such that $\bigcup_{x \in \mathcal{L}} G_x = G$. □

Definition 3.2.7. *A ρ-factor of the chain $G_\ell = (V_\ell, E_\ell)$, is denoted by $\rho\left(G_\ell\right) \in \mathbb{R}_{>0}$ and for the chain G_ℓ given by $1 \to 2 \to \cdots \to k$ is computed as*

$$\rho(G_\ell) = \max_{a \in \{1,\ldots,k\}} \left(\frac{\sum_{j=1}^{a} w_j}{\sum_{j=1}^{a} P_j} \right) = \frac{\sum_{j=1}^{a^*} w_j}{\sum_{j=1}^{a^*} P_j}, \tag{3.25}$$

where $a^* \in V_\ell \subset \mathcal{N}(t)$ is called the CAV that determines the ρ-factor of the chain G_ℓ.

The interpretation of the CAV $a^* \in V_\ell$ in the above lemma is that the ratio of weight divided by the processing time of the CAV in the chain G_ℓ increases from the first CAV in the chain until CAV a^*.

Lemma 3.2.8. *If CAV $i \in V_\ell \subset \mathcal{N}(t)$ determines the ρ-factor of chain $G_\ell = (V_\ell, E_\ell)$ given by $1 \to 2 \to \cdots \to k$, $\ell \in \mathcal{L}$, then there exist an optimal decision sequence that processes CAVs $1, \ldots, i$ one after another without any interruption by CAVs from other chains $G_{\ell'}, \ell' \in \mathcal{L} \setminus \{\ell\}$.*

Proof. The proof is by contradiction and is similar to that of [194, Lemma 3.1.3.] and follows from [194, Lemma 3.1.2.] by using the results in which it is optimal to process the chain of jobs $1 \to 2 \to \cdots \to k$ before the chain of jobs $k+1 \to \cdots \to n$ if $\frac{\sum_{j=1}^{k} w_j}{\sum_{j=1}^{k} P_j} > \frac{\sum_{j=k+1}^{n} w_j}{\sum_{j=k+1}^{n} P_j}$. □

By our resequencing mechanism, at each instance of replanning, CAV i accesses the coordinator and inquires the decision sequence computed using Algorithm 5.

Theorem 3.2.9. *Under Assumption 5, the decision sequence of $N(t)$ CAVs, which is the optimal solution to $(1 \mid G \mid \sum_{i=1}^{N(t)} w_i C_i^s)$, is computed using Algorithm 5.*

Algorithm 5 Re-sequencing Algorithm

Input: All available chains $G_\ell = (V_\ell, E_\ell)$, $\ell \in \mathcal{L}$
Output: Decision Sequence $s = (s_1, s_2, s_3 \ldots, s_N)$

1: **while** $\bigcup_{l \in \mathcal{L}} G_l$ is not empty **do**
2: Update a_ℓ and $\rho\left(G_\ell\right)$ for all $G_\ell = (V_\ell, E_\ell)$, $\ell \in \mathcal{L}$
3: $\rho_{\max}, \ell^*, a_\ell^* \leftarrow 0$
4: **for** $\ell \in \mathcal{L}$ **do**
5: **if** $\rho_{\max} < \rho\left(G_\ell\right)$ **then**
6: ▷ Find maximum ρ-factor among all chains, the corresponding chain and CAV
7: $\rho_{\max} \leftarrow \rho\left(G_\ell\right); \ell^* \leftarrow \ell; a_\ell^* \leftarrow a_\ell$
8: **end if**
9: **end for**
10: $subSequence \leftarrow \emptyset$
11: **while** `True` **do**
12: **if** $\exists\, i \in V_{\ell^*}$ such that $(i, a_\ell^*) \in E_{\ell^*}$ **then**
13: $subSequence$.PushFront(i) ▷ Add i to the front of the subsequence
14: Remove (i, a_ℓ^*) from E_{ℓ^*}
15: Remove i from V_{ℓ^*}
16: $a_\ell^* \leftarrow i$
17: **else**
18: `Break`
19: **end if**
20: **end while**
21: $sequence$.PushBack($subSequence$) ▷ Add subsequence to the back of the sequence
22: **end while**
23: **return** $sequence$

Proof. Among all the disjoint chains of all paths, let $\rho_{\max}$ and a_ℓ^* be the maximum ρ-factor and the corresponding CAV determining it, respectively. Namely, ℓ^* is the associated path with $\rho_{\max}$ and a_ℓ^*. For every $\ell \in \mathcal{L} \setminus \{\ell^*\}$, we have

$$\rho_{\max} > \frac{\sum_{j \in V_\ell}^{a_\ell} w_j}{\sum_{j \in V_\ell}^{a_\ell} P_j}, \tag{3.26}$$

where a_ℓ is the CAV determining the ρ-factor of a chain $G_\ell = (V_\ell, E_\ell)$ (lines 3-9 in the algorithm). From (3.26) and [194, Lemma 3.1.2.], the chain G_{ℓ^*}, should be processed first. From Lemma 3.2.8, all the CAVs in the chain G_{ℓ^*}, should be processed until CAV a_ℓ^* one after another without any interruption by CAVs from other chains (lines 11-20 in the algorithm). All processed CAVs get removed from their corresponding chain (lines 14 and 15 in the algorithm), and then the process will be repeated until no CAVs remained unprocessed. □

3.2.3 Simulation Results

We evaluate the effectiveness of our framework in simulation through several scenarios. In all scenarios, we consider CAVs entering the control zone from six different paths shown in Fig. 3.2, where the length of control zone for straight and turning paths are 212 m and 215 m, respectively. The CAVs enter the control zone with initial speed uniformly distributed between 12 m/s to 17 m/s from each entry with equal traffic volumes varying from 800 to 2400 veh/h. Videos from our simulation analysis can be found at the supplemental site, https://sites.google.com/view/ud-ids-lab/RPRS.

For the first scenario, we demonstrate the effects of the replanning mechanism to respond to the deviations from the previously planned trajectory. We consider 24 CAVs entering the control zone with the rate of $2,400$ veh/h per path, and replanning occurs every time the new CAVs enter the control zone. To only consider the effects of replanning, we set the decision sequence of CAVs at each replanning instance to be based on FCFS sequence. At each replanning instance, we consider CAVs to observe their current position and speed with deviation uniformly distributed in the range of $[-2, 2]$ m and $[-0.2, 0.2]$ m/s, respectively. The position trajectory of CAVs traveling from westbound to eastbound is visualized in Fig. 3.3 in the presence of deviation. The CAVs' positions in this path are denoted by solid lines, while their corresponding rear-end constraints are shown with dashed lines. The CAVs from other paths that have the potential for lateral collision with CAVs in this path are shown with a square and vertical bar showing their safety time headway. Figure 3.3 shows that by using our replanning framework, CAVs respond to the observation made at each replanning point, and they adjust their trajectory to ensure safety.

For the second scenario, we show the change in average travel time of CAVs within our proposed framework compared to the baseline case for different traffic volumes $2,400$ veh/h and $1,200$ veh/h per path. In the baseline case, CAVs only solve their optimization problem upon entering the control zone based on FCFS, while in our proposed framework, CAVs replan based on the new decision sequence as a new CAV enters the system. In this scenario, we assumed that all CAVs have the same weights, and for each traffic volume, we

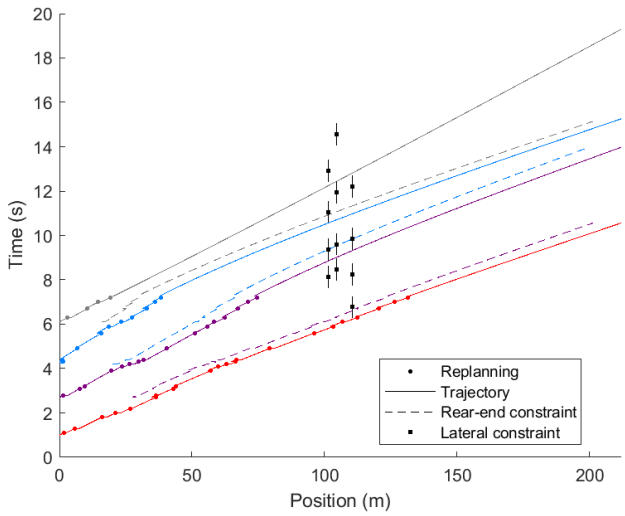

Figure 3.3: Time vs position in the presence of deviation.

performed 30 simulations with different random seeds. The results are presented in Fig. 3.4, and it can be seen how resequencing CAVs affects the average travel time. As the traffic flow increases, the change in average travel time varies more, highlighting the importance of decision sequence in influencing the traffic throughput.

For our last scenario, we demonstrate the change in weighted average travel time of CAVs within our proposed framework compared to the baseline case, at different traffic volumes $2,400$ veh/h, $1,200$ veh/h, and 800 veh/h in Fig. 3.5. Similar to the previous scenario, in our proposed framework, CAVs replan based on the new decision sequence as a new CAV enters the system. We performed 30 simulations with different random seeds for each traffic density. In this scenario, we consider that all CAVs' weights are inversely proportional to the size of their compact set of the feasible solution. After performing 30 different simulations for each traffic flow, our resequencing framework based on the minimum exit time is shown to improve the travel time on average by about 2%.

It should be noted that in 2017, congestion in urban areas across the U.S. led to drivers collectively spending an extra 8.8 billion hours on the road and purchasing an additional 3.3 billion gallons of fuel, ultimately resulting in a $166 billion expense [203]. Thus, 2% improvement on average travel time in the scale of transportation network by only changing

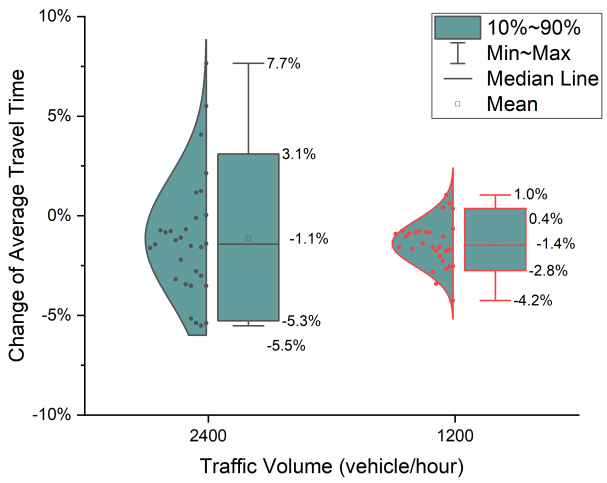

Figure 3.4: Change in average travel time compared to the FCFS decision sequence for different traffic volumes.

the decision sequence can be quite substantial. Additionally, the main benefit of our approach lies in providing a systematic framework to relax the FCFS sequence in decision making. This would be useful if one needs to prioritize some CAVs to other CAVs, such as giving higher priority to vehicles with higher passenger capacity or emergency vehicles.

By formulating the resequencing problem as a scheduling problem, we find the optimal solution to the scheduling problem. However, this optimal schedule is not the optimal solution, which minimizes the average of actual travel time of all CAVs. The actual travel time of CAVs depends on the decision sequence order, and finding this optimal sequence of decision making is a combinatorial problem, which is an NP-hard problem [81]. However, the algorithm employed in this section depends on a simple sort which can be done in $O(n \log(n))$ [194]. Thus, if the sole purpose is to improve the average travel time of all CAVs, one can find the decision sequence using our proposed framework and compare it with FCFS policy, and only choose the decision sequence based on the minimum exit time if it improves the performance.

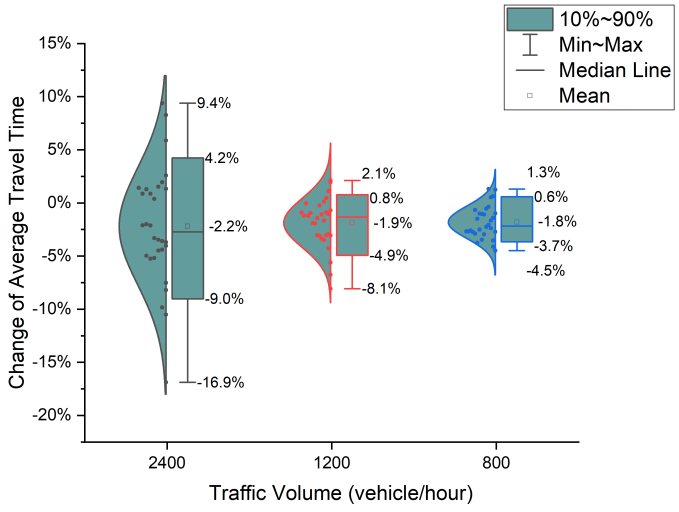

Figure 3.5: Change in weighted average travel time compared to the FCFS decision sequence for different traffic volumes.

3.3 Robust Learning-Based Trajectory Planning for Emerging Mobility Systems

In this section, we extend a framework that we described earlier in Section 3.1 for coordination of CAVs at a signal-free intersection (Fig. 3.1) to incorporate uncertainty. Using the possibly noisy observations of actual time trajectories and leveraging Gaussian process regression, we learn the bounded confidence intervals for deviations from the nominal trajectories of CAVs online. Incorporating these confidence intervals, we reformulate the trajectory planning as a robust coordination problem, the solution of which guarantees that constraints in the system are satisfied in the presence of bounded deviations from the nominal trajectories. We demonstrate the effectiveness of our extended framework through a numerical simulation.

We organize this section as follows: In subsection 3.3.1, we introduce the problem formulation, and in subsection 3.3.2, we present the solution approach. Finally, we provide simulation results in subsection 3.3.3.

3.3.1 Problem Formulation

In an earlier work [92], we showed that there is a discrepancy between the actual and planned trajectories due to the presence of uncertainty originated from errors in low-level tracking, noisy measurements, etc. In this section, to accommodate this uncertainty, we reformulate Problem 3.1.3 as a robust coordination problem, the solution of which guarantees that constraints in the system are satisfied in the presence of bounded deviations from the nominal trajectories. In this section, we make the following assumption.

Assumption 3.3.1. *The deviation from the deterministic nominal time trajectory of a real-physical CAV $i \in \mathcal{N}(t)$ is given by an unknown function $e_i : \mathcal{P}_i \to \mathcal{E}_i$, where $\mathcal{E}_i$ is an unknown bounded subset of $\mathbb{R}$.*

We consider that $e_i(p_i)$ can be approximated by a GP defined on a probability space $(\mathcal{P}_i, \mathscr{P}_i, \mathbb{P})$, where $\mathscr{P}_i$ is the associated σ-algebra and $\mathbb{P}$ is a probability measure on $(\mathcal{P}_i, \mathscr{P}_i)$. This is a reasonable approach, since GP regression has been used successfully to approximate functions in many applications [136].

Definition 3.3.2. *The actual time trajectory for CAV $i \in \mathcal{N}(t)$ is a random process defined on $(\mathcal{P}_i, \mathscr{P}_i, \mathbb{P})$, denoted by $\hat{t}_i : \mathcal{P}_i \to \mathbb{R}$, and given by*

$$\hat{t}_i(p_i) = t_i(p_i) + e_i(p_i), \tag{3.27}$$

where $t_i(p_i)$ is the nominal trajectory which is the solution of Problem 3.1.3.

From Definition 3.1.1, the time trajectory is the inverse function of the position trajectory. Having a deviation in the time trajectory also makes the deviation in the position trajectory inevitable.

Definition 3.3.3. *The actual position trajectory of CAV $i \in \mathcal{N}(t)$ is a random process denoted by $\hat{p}_i$ defined on a probability space $(\Omega_i, \mathscr{F}_i, \mathbb{P})$, $\Omega_i \in \mathbb{R}$, and given by*

$$\hat{p}_i(t) = p_i(t) + f_i(t), \tag{3.28}$$

where $f_i(t)$ is the unknown deviation from the nominal position trajectory, and it is defined on $(\Omega_i, \mathscr{F}_i, \mathbb{P})$.

Lemma 3.3.4. *The deviation in the position trajectory of CAV $i \in \mathcal{N}(t)$, $f_i(t)$, can be derived from the deviation $e_i(t)$ of its time trajectory.*

Proof. Let $p_i \in \mathcal{P}_i$ be an arbitrary known position, with $p_i = p_i(t)$. By evaluating (3.27) at p_i, we obtain the actual time $\hat{t}_i(p_i)$ that CAV $i \in \mathcal{N}(t)$ is at position p_i. Evaluating (3.28) at the actual time, we obtain

$$\hat{p}_i(\hat{t}_i(p_i)) = p_i(\hat{t}_i(p_i)) + f_i(\hat{t}_i(p_i)). \tag{3.29}$$

By definition of inverse function $(p_i \circ p_i^{-1})(x) = x$, and thus LHS in (3.29) equals to p_i. Substituting (3.27) in the first term of RHS, we have

$$\begin{aligned} p_i = \phi_{i,3} \cdot (t_i(p_i) + e_i(p_i))^3 + \phi_{i,2} \cdot (t_i(p_i) + e_i(p_i))^2 \\ + \phi_{i,1} \cdot (t_i(p_i) + e_i(p_i)) + \phi_{i,0} + f_i(\hat{t}_i(p_i)). \end{aligned} \tag{3.30}$$

Next, by expanding (3.30), we get

$$\begin{aligned} f_i(\hat{t}_i(p_i)) = -[\phi_{i,3} \cdot e_i(p_i)^3 + 3\phi_{i,3} \cdot e_i(p_i)^2 \cdot t_i(p_i) \\ + \phi_{i,2} \cdot e_i(p_i)^2 + 3\phi_{i,3} \cdot e_i(p_i) \cdot t_i(p_i)^2 \\ + 2\phi_{i,2} \cdot e_i(p_i) \cdot t_i(p_i) + \phi_{i,1} \cdot e_i(p_i)]. \end{aligned} \tag{3.31}$$

Since $p_i \in \mathcal{P}_i$ is an arbitrary known position, the above equation holds for any p_i, and the proof is complete. □

Corollary 3.3.5. *The actual speed trajectory of CAV $i \in \mathcal{N}(t)$, $\hat{v}_i(t)$ is a random process defined on probability space $(\Omega_i, \mathscr{F}_i, \mathbb{P})$, and it is found from*

$$\hat{v}_i(t) = v_i(t) + g_i(t), \tag{3.32}$$

where $g_i(t)$ is unknown deviation from nominal speed trajectory, and is defined on $(\Omega_i, \mathscr{F}_i, \mathbb{P})$.

Proof. By taking time derivative of (3.28), the result follows immediately. □

For each CAV $i \in \mathcal{N}(t)$, we formulate a robust coordination problem in the presence of uncertainty. We seek to derive the new minimum time t_i^f for CAV i to exit the control zone. This exit time corresponds to a new unconstrained energy-optimal trajectory that satisfies all the state, control, and safety constraints for all realizations of uncertainty. In what follows, let $E_i(\cdot) \subset \mathcal{E}_i$, $F_i(\cdot) \subset \mathcal{P}_i$, $G_i(\cdot) \subset \mathcal{V}_i$ denote the bounded confidence intervals of CAV i for random process $e_i(\cdot)$, $f_i(\cdot)$, and $g_i(\cdot)$, respectively.

We enhance (3.5) as follows

$$\left|\hat{t}_i(p_i^n) - \hat{t}_j(p_j^n)\right| \geq t_h, \quad \forall e_i(p_i^n) \in E_i(p_i^n), \forall e_j(p_j^n) \in E_j(p_j^n), \tag{3.33}$$

to include the CAVs' deviations from their nominal time trajectories. This constraint should be satisfied for every possible realizations of deviation from the nominal time trajectory of CAV $i \in \mathcal{N}(t)$ and CAV $j \in \mathcal{N}(t) \setminus \{i\}$. Note that for CAVs i and j, p_i^n, p_j^n are constant and they depend only on the intersection's geometry (Fig. 3.1).

Similarly, we enhance rear-end safety constraint (3.4) defined on the nominal trajectories by incorporating the deviations from nominal position trajectories (3.28) as follows

$$\begin{aligned} &\hat{p}_k(t) - \hat{p}_i(t) \geq \hat{\delta}_i(t) = \gamma + \varphi \cdot \hat{v}_i(t), \\ &\forall f_i(t) \in F_i(t),\ \forall f_k(t) \in F_k(t),\ \forall g_i(t) \in G_i(t), \end{aligned} \tag{3.34}$$

where the distance between CAV $i \in \mathcal{N}(t)$ and the preceding CAV $k \in \mathcal{N}(t) \setminus \{i\}$ has to be greater than a safe distance $\hat{\delta}_i(t)$ for every realizations of deviations from the nominal trajectories of CAV i and CAV k.

Finally, to account for the deviation of the speed of CAV i, we enhance the constraint

$$v_{\min} \leq \hat{v}_i(t) \leq v_{\max}, \quad \forall g_i(t) \in G_i(t), \tag{3.35}$$

for every realizations of deviation from the nominal speed trajectory of CAV i.

Problem 3.3.6. *For each CAV $i \in \mathcal{N}(t)$, we consider the following robust coordination problem*

$$\min_{t_i^f \in \mathcal{T}_i(t_i^0)} t_i^f \tag{3.36}$$

$$\text{subject to: (3.9), (3.12), (3.27), (3.28), (3.32) } - \text{ (3.35),}$$

$$\text{and given boundary conditions.}$$

In what follows, to simplify notation, for CAV $i \in \mathcal{N}(t)$, we denote the original nominal trajectories (resulting from the solution of Problem 3.1.3) with bar, e.g., $\bar{t}_i(p_i), \bar{p}_i(t), \bar{v}_i(t)$, and $\bar{u}_i(t)$, and reserve $t_i(p_i), p_i(t), v_i(t)$, and $u_i(t)$ for the new nominal trajectories (resulting from the solution of Problem 3.3.6).

3.3.2 Solution Approach

In our framework, upon entering the control zone, CAV $i \in \mathcal{N}(t)$ does not have any information about its uncertainty, and thus we have $E_i(\cdot) = F_i(\cdot) = G_i(\cdot) = \emptyset$. First, CAV i communicates with the coordinator and obtain trajectories and information about the uncertainty of CAVs which are already in the control zone. Using this information, CAV i computes its nominal trajectories by solving Problem 3.3.6. As CAV i travels following these nominal trajectories, it makes measurements (possibly noisy) of the actual time that it reaches to different positions $p_i \in \mathcal{P}_i$, denoted by $\tilde{t}_i(p_i) \in \mathbb{R}_{\geq 0}$, and given by $\tilde{t}_i(p_i) = \hat{t}_i(p_i) + \xi_i$, where $\xi_i \sim \mathcal{N}(0, \sigma_n^2)$ is a Gaussian noise with unknown variance σ_n^2. Next, we define the error in the time trajectory based on these measurements.

Definition 3.3.7. *The difference between the noisy measurements of the time trajectory* $\tilde{t}_i(p_i)$ *and the nominal time trajectory* $t_i(p_i)$ *is denoted by* $\tilde{e}_i(p_i) = \tilde{t}_i(p_i) - t_i(p_i)$*, which is a random process on a probability space* $(\mathcal{P}_i, \mathscr{P}_i, \mathbb{P})$.

The set of observation samples of CAV $i \in \mathcal{N}(t)$, is denoted by $\mathcal{O}_i = (\mathbf{p}_i, \tilde{\mathbf{e}}_i) = \left\{ \left(p_i^{(j)}, \tilde{e}_i(p_i^{(j)}) \right) \mid j = 1, \ldots, n \right\}$, where $\mathbf{p}_i$, $\tilde{\mathbf{e}}_i$ represent the n dimensional vector of positions and corresponding observed errors in time trajectory; respectively, and the j^{th} sample is denoted by $\left(p_i^{(j)}, \tilde{e}_i(p_i^{(j)}) \right)$. We consider that CAV i makes the noisy observations $\mathcal{O}_i$ before reaching a perfectly known landmark in the control zone called *uncertainty characterization point* denoted by $p^z \in \mathcal{P}_i$. Let t_i^z be the actual time that CAV i reaches this point. After CAV i reaches p^z, it characterizes its uncertainty in the time, position, and speed trajectories based on the observed information, $\mathcal{O}_i$. Then, CAV i communicates with the coordinator to access the trajectories of other CAVs $j < i \in \mathcal{N}(t)$ which entered the control zone earlier than CAV i. CAV i also obtains information about their deviation from their trajectories, if they have already characterized their uncertainty. After obtaining this information, CAV i solves the robust coordination problem (Problem 3.3.6), with the revised initial conditions $p_i(t_i^z) = p^z$ and $v_i(t_i^z) = \bar{v}_i(t_i^z) + g(t_i^z)$ (recall that $\bar{v}_i(t_i^z)$ is the speed of CAV i at t_i^z computed from the original nominal trajectory). CAV i communicates back these new nominal trajectories along with its characterization of uncertainty to the coordinator. Then, the coordinator broadcasts a *replanning event* for all CAVs $j > i \in \mathcal{N}(t)$ which entered the control zone after CAV i to re-plan their trajectory with this new information. These CAVs then sequentially resolve their optimization problem, and plan their trajectory accordingly. Algorithm 6 shows a psueducode of this process.

Next, we present the process for characterizing uncertainty for CAV $i \in \mathcal{N}(t)$ based on $\mathcal{O}_i$.

Algorithm 6 Robust Coordination Pseudocode

Replanning Event ←`False`
for CAV $i \in \mathcal{N}(t)$ **do**
  if $t = t_i^0$ **then**
    $E_i, F_i, G_i \leftarrow \emptyset$
    Solve Problem 3.3.6
  else if CAV i reached at p^z **then**
    $E_i, F_i, G_i \leftarrow$ Characterize uncertainty based on $\mathcal{O}_i$
    Solve Problem 3.3.6
    Replanning Event ←`True`
  else if *Replanning Event* **then**
    Solve Problem 3.3.6
  end if
end for

Modeling Uncertainty in Time Trajectory as GP

Given the observation samples, $\mathcal{O}_i$, we use GP regression to model $e_i(p_i) \sim \mathcal{GP}(m(p_i), k(p_i, p_i'))$, where $m(p_i)$ and $k(p_i, p_i')$ represents the prior mean and covariance, respectively. We assume no prior knowledge on the error is available, and thus, we set the prior mean to zero, $m(p_i) = 0$. For the covariance function, we adopt the *Matérn* $3/2$ model that is one time differentiable in the mean-square sense, and it is given by $k(p_i, p_i') = \frac{\sigma_s^2}{\Gamma(\frac{3}{2})}\left(\sqrt{3}\frac{p_i - p_i'}{\ell_s}\right)^{\frac{3}{2}} K_{\frac{3}{2}}\left(\sqrt{3}\frac{p_i - p_i'}{\ell_s}\right)$, where $K_{\frac{3}{2}}$ and Γ are modified Bessel and Gamma functions, respectively. Let σ_s^2 and ℓ_s be the process variance, the covariance function's parameter, respectively [136]. The hyperparameters are represented by $\theta = [\sigma_s^2\ \sigma_n^2\ \ell_s]^\top$, where σ_n^2 is the unknown variance of observation noise. The hyperparameters can be learned by maximizing the log marginal likelihood of the observation samples, i.e., $\theta^* = \arg\max_\theta \log \mathbb{P}(\tilde{\mathbf{e}}_i | \mathbf{p}_i, \theta)$. Given the observation samples, $\mathcal{O}_i$, the marginalized GP posterior at any arbitrary point p_i^* is a univariate normal distribution, denoted by $e_i(p_i^*) \sim \mathcal{N}(\mu_e(p_i^*), \sigma_e^2(p_i^*))$ defined with the mean $\mu_e(p_i^*) = m(p_i^*) + k^*(K + \sigma_n^2 I)^{-1}\tilde{\mathbf{e}}_i$ and variance $\sigma_e^2(p_i^*) = k(p_i^*, p_i^*) - {k^*}^\top (K + \sigma_n^2 I)^{-1} k^*$, where $K = K(\mathbf{p}_i, \mathbf{p}_i)$ denotes the $n \times n$ matrix of the covariances evaluated at all pairs of training point $\mathbf{p}_i$, and $k^* = K(\mathbf{p}_i, p_i^*)$ is the $n \times 1$ matrix of the covariances evaluated at n training points and one arbitrary point, p_i^*.

Theorem 3.3.8. *Deviation from the nominal speed trajectory of CAV $i \in \mathcal{N}(t)$, $g_i(t)$, follows a Chi-square distribution with one degree of freedom, and its posterior mean and variance*

at actual time $\hat{t}_i(p_i)$*, where CAV arrives at position* p_i *can be derived from* $\mu_g(\hat{t}_i(p_i)) = a'_1\,\mu_e + a'_2\,(\mu_e^2 + \sigma_e^2)$ *and*

$$\sigma_g^2(\hat{t}_i(p_i)) = \sigma_e^2\left({a'_1}^2 + 4\mu_e(a'_1\,a'_2 + {a'_2}^2\,\mu_e) + 2\,{a'_2}^2\,\sigma_e^2\right), \tag{3.37}$$

where $a'_1 = -2\phi_{i,2} - 6\phi_{i,3}\cdot t_i(p_i)$ *and* $a'_2 = -3\phi_{i,3}$*, and* $\mu_e = \mu_e(p_i)$*,* $\sigma_e = \sigma_e(p_i)$*.*

Proof. Let $p_i \in \mathcal{P}_i$ be an arbitrary known position, with $p_i = p_i(t)$ and $\hat{t}_i(p_i)$ be the actual time, where CAV arrives at position p_i. Following the same steps as Lemma 3.3.4, the deviation is given by $g_i(\hat{t}_i(p_i)) = -[(2\phi_{i,2} + 6\phi_{i,3}\cdot t_i(p_i))\cdot e_i(p_i) + 3\phi_{i,3}\cdot e_i(p_i)^2]$, where $e_i(p_i)$ is a univariate normal variable, and thus $g_i(\hat{t}_i(p_i))$ follows a Chi-square distribution with one degree of freedom [204]. To derive expectation and variance of $g_i(\hat{t}_i(p_i))$, we use moment-generating function and its properties. Since $e_i(p_i)$ is a normal random variable, its moment-generating function is given by $M_e(\tau) = \exp(\tau\mu_e + \frac{1}{2}\sigma_e^2\tau^2)$. The n^{th} moment of random variable $e_i(p_i)$, denoted by $\mathbb{E}[e_i(p_i)^n]$, can be derived from $\frac{d^n}{d\tau^n}M_e(\tau)\mid_{\tau=0}$. From linearity of expectation, we have $\mu_g(\hat{t}_i(p_i)) = \mathbb{E}[g_i(\hat{t}_i(p_i))] = a'_1\,\mathbb{E}[e_i(p_i)] + a'_2\,\mathbb{E}[e_i(p_i)^2]$, where the first and second moments of $e_i(p_i)$, are given by μ_e and $\mu_e^2 + \sigma_e^2$, respectively. To find the variance, we use $\sigma_g^2(\hat{t}_i(p_i)) = \mathbb{E}[g_i(\hat{t}_i(p_i))^2] - \mathbb{E}[g_i(\hat{t}_i(p_i))]^2$, where we can employ the same procedure and derive (3.37). □

Corollary 3.3.9. *The deviation* $f_i(t)$ *from the nominal position trajectory of CAV* $i \in \mathcal{N}(t)$ *follows a cubic normal distribution.*

Proof. Let $p_i \in \mathcal{P}_i$ be an arbitrary known position, with $p_i = p_i(t)$ and $\hat{t}_i(p_i)$ be the actual time, where CAV arrives at position p_i. From (3.31), we have $f_i(\hat{t}_i(p_i)) = a_3\cdot e_i(p_i)^3 + a_2\cdot e(p_i)^2 + a_1\cdot e_i(p_i)$, where $e_i(p_i)$ is a normal variable,-

$$a_1 = -3\phi_{i,3}\cdot t_i(p_i)^2 - 2\phi_{i,2}\cdot t_i(p_i) - \phi_{i,1}, \tag{3.38}$$

$$a_2 = -3\phi_{i,3}\cdot t_i(p_i) - \phi_{i,2}, \tag{3.39}$$

and $a_3 = -\phi_{i,3}$. Since a_1, a_2, and a_3 are not random variables, the proof is complete. □

Proposition 3.3.10. *For CAV $i \in \mathcal{N}(t)$, posterior mean and variance of $f_i(t)$ at actual time $\hat{t}_i(p_i)$, where vehicle arrives at position p_i can be derived from*

$$\mu_f(\hat{t}_i(p_i)) = a_1\mu_e + a_3(\mu_e^3 + 3\mu_e\sigma_e^2) + a_2(\mu_e^2 + \sigma_e^2) \tag{3.40}$$

$$\begin{aligned}\sigma_f^2(\hat{t}_i(p_i)) = \sigma_e^2[&{a_1}^2 + 4a_1a_2\mu_e + 6a_1a_3\mu_e^2 + 6a_1a_3\sigma_e^2 + \\ &4{a_2}^2\mu_e^2 + 2{a_2}^2\sigma_e^2 + 12a_2a_3\mu_e^3 + 24a_2a_3\mu_e\sigma_e^2 \\ &+9{a_3}^2\mu_e^4 + 36{a_3}^2\mu_e^2\sigma_e^2 + 15{a_3}^2\sigma_e^4],\end{aligned} \tag{3.41}$$

where $\mu_e = \mu_e(p_i)$, $\sigma_e = \sigma_e(p_i)$.

Proof. The proof is similar to Theorem 3.3.8, hence it is omitted. □

Next, we construct a bounded confidence interval for random process $e_i(p_i)$, denoted by $E_i(p_i) \subset \mathcal{E}_i$, within which $e_i(p_i)$ lies with probability P_e as follows

$$E_i(p_i) = \left[\mu_e(p_i) - z\sigma_e(p_i),\ \mu_e(p_i) + z\sigma_e(p_i)\right], \tag{3.42}$$

$$z = \sqrt{2}\,\mathrm{erf}^{-1}(P_e), \tag{3.43}$$

where $\mu_e(p_i)$ and $\sigma_e(p_i)$ are posterior mean and standard deviation of $e_i(p_i)$ at position $p_i \in \mathcal{P}_i$, respectively, and $\mathrm{erf}^{-1}(\cdot)$ is the inverse error function. Using Chebyshev's inequality, we construct a bounded confidence interval for the random process $f_i(t)$, denoted by $F_i(t) \subset \mathcal{P}_i$, within which $f_i(t)$ lies with at least probability P_f.

$$F_i(p_i) = \left[\mu_f(t) - z\sigma_f(t),\ \mu_f(t) + z\sigma_f(t)\right], \tag{3.44}$$

$$\mathbb{P}\left(f_i(t) \in F_i(t)\right) \geq P_f = 1 - \frac{1}{z^2}. \tag{3.45}$$

Deviation from speed trajectory, $g_i(t)$, follows a Chi-squared distribution which is a uni-modal distribution, i.e., its distribution permits a Lebesgue density that is non-decreasing up to a mode and non-increasing thereafter. This unimodality allows us to employ a tighter bound for the confidence interval using Vysochanskii-Petunin inequality [205]. We construct a bounded

confidence interval for the random process $g_i(t)$, denoted by $G_i(t) \subset \mathcal{V}_i$, within which $g_i(t)$ lies with at least probability P_g as follows

$$G_i(p_i) = [\mu_g(t) - z\sigma_g(t),\ \mu_g(t) + z\sigma_g(t)]\,, \tag{3.46}$$

$$\mathbb{P}\left(g_i(t) \in G_i(t)\right) \geq P_g = 1 - \frac{4}{9z^2}. \tag{3.47}$$

The solution to Problem 3.3.6 is the optimal nominal trajectories for CAV $i \in \mathcal{N}(t)$ satisfying the safety constraints in the presence of uncertainty, which is modeled through GP based on the possibly noisy observations of the time trajectory.

3.3.3 Simulation Results

To demonstrate the effectiveness of our proposed framework, we investigate the coordination of 24 CAVs at a signal-free intersection shown in Fig. 3.1. The CAVs enter the control zone from 6 different paths shown in Fig. 3.1 with the total rate of 3600 veh/hour and their initial speeds uniformly distributed between 12 m/s to 14 m/s. We use the following parameters for the simulation: $t_h = 0.5$ s, $v_{\min} = 0.25$ m/s, $v_{\max} = 30$ m/s, $u_{\max} = 2$ m/s^2, $u_{\min} = -2$ m/s^2, $\gamma = 1.5$ m, $\varphi = 0.5$ s, $p^z = 50$ m, $P_e = P_f = P_g = 95\%$. We consider the actual deviation from the nominal time trajectory for CAV $i \in \mathcal{N}(t)$ is given by function $e_i(p_i) = 0.012 \log\left(1 + p_i\right)^{1.5}$ which is not known to CAV i a priori. Videos from our simulation analysis can be found at the supplemental site, https://sites.google.com/view/ud-ids-lab/RBST.

Fig. 3.6 illustrates time trajectories of CAVs traveling from westbound to eastbound. The CAVs nominal trajectories on this path are denoted with solid lines, while their corresponding rear-end safety constraints (3.34) are visualized with dotted lines in the same color. Replanning events that are due to the change of the trajectories of other CAVs in the control zone are shown with blue asterisks, and the uncertainty characterization point at which each CAV quantifies its trajectory is shown with a black square marker. The 95% confidence bounds of the time trajectories are shown with dashed lines. Moreover, the CAVs from other

paths that have the potential for lateral collision with CAVs in this path are shown with vertical thicker lines. Their arrival times at the conflict points with 95% confidence bound are shown in red, and corresponding lateral safety constraints (3.33) are shown with vertical black lines. This figure shows that by using our robust framework, CAVs' nominal trajectories satisfy the safety constraints for every realization of the deviations from the nominal trajectories. Fig. 3.7 visualizes the case where CAVs stick to their initial planned nominal trajectories, ignoring uncertainty. It can be seen that for multiple cases, the trajectories of the CAVs with 95% confidence bounds cross the vertical lines representing the lateral constraints.

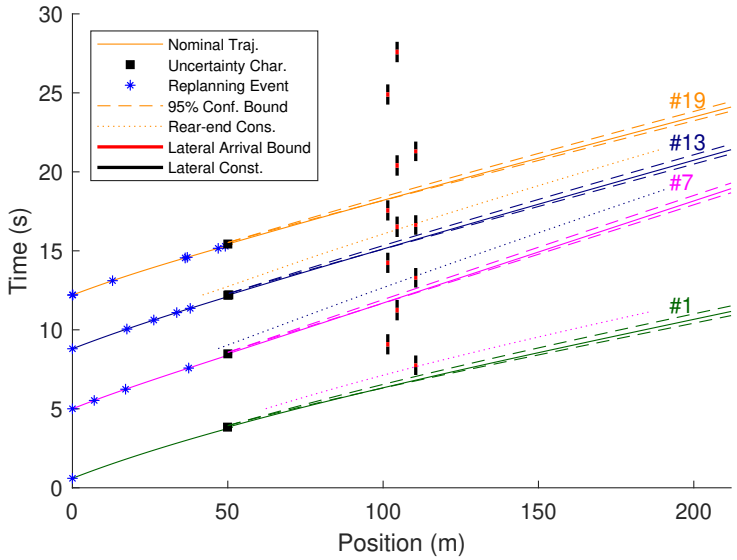

Figure 3.6: Time trajectories of CAVs under robust coordination.

We demonstrate the control input trajectory of CAV #19 traveling from westbound to eastbound under the robust coordination framework in Fig. 3.8. It can be seen that at replanning events shown with blue asterisks, CAV #19 solves Problem 3.3.6 with updated trajectories of other CAVs and new information about their uncertainty. Upon reaching the uncertainty characterization point shown with a black square, CAV #19 learns the deviation in its nominal trajectories and solves Problem 3.3.6 with this new information. It communicates back the new nominal trajectories along with its characterization of uncertainty to the coordinator. Then, the coordinator broadcasts a replanning event for all CAVs which entered the control zone after CAV #19 to replan their trajectories.

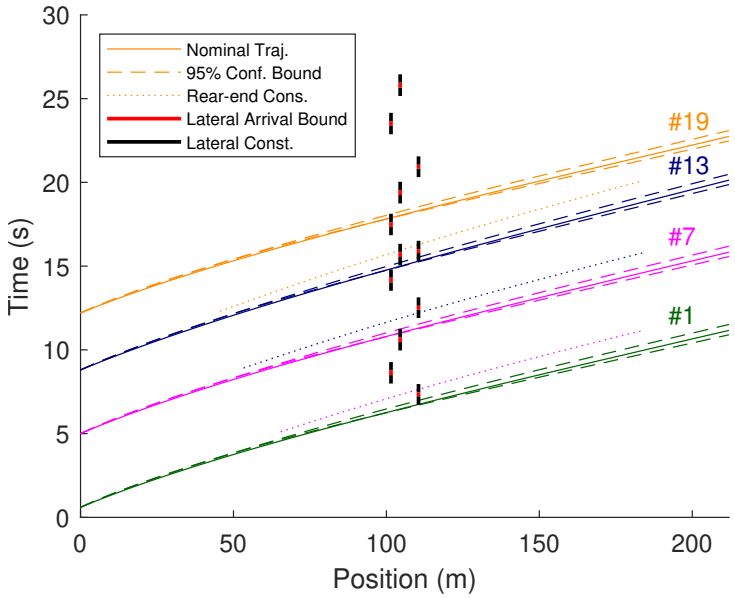

Figure 3.7: Time trajectories of CAVs under deterministic coordination.

3.4 A Barrier-Certified Optimal Coordination Framework for Connected and Automated Vehicles

In this section, we integrate a safety layer using the control barrier function into the framework that we described earlier in Section 3.1 for coordination of CAVs at a signal-free intersection. First, in our motion planning module, each CAV computes the optimal control trajectory using simple vehicle dynamics. The trajectory does not make any of the state, control, and safety constraints active. A vehicle-level tracking controller employs a combined feedforward-feedback control law to track the resulting optimal trajectory from the motion planning module. Then, a barrier-certificate module, acting as a middle layer between the vehicle-level tracking controller and physical vehicle, receives the control law from the vehicle-level tracking controller and using realistic vehicle dynamics ensures that none of the state, control, and safety constraints becomes active. The latter is achieved through a quadratic program, which can be solved efficiently in real time. We demonstrate the effectiveness of our extended framework through a numerical simulation.

We structure the rest of the section as follows: In Section 3.4.1, we introduce the general modeling framework. In Section 3.4.2, we present the motion planning, and in Section

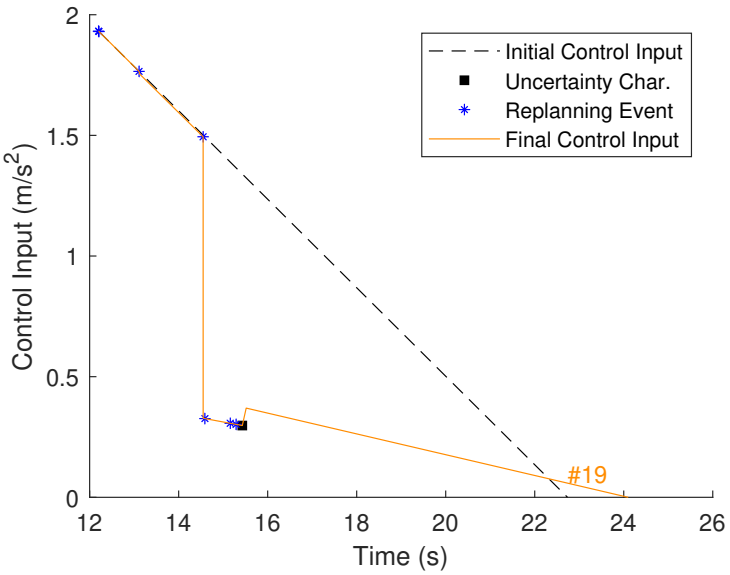

Figure 3.8: Control input trajectory of a CAV under robust coordination.

3.4.3, we introduce the barrier-certificate modules. Finally, we provide simulation results in Section 3.4.4.

3.4.1 Problem Formulation

We consider coordination of CAVs at a signal-free intersection (Fig. 3.9). Our coordination framework architecture consists of two main interconnected components called motion planning and barrier certificate (Fig. 3.10). Using the simplified dynamics of each CAV, the motion planning module which is described in Section 3.1 yields an optimal exit time from the control zone. The resulting optimal exit time corresponds to the unconstrained optimal control trajectory, derived using simple dynamics, and guarantees that none of the state, control, and safety constraints becomes active. The approach in [91] considers that a vehicle-level tracking controller can perfectly track the resulting optimal trajectory from the motion planning module. In this section, however, we no longer consider this and introduce the vehicle-level tracking controller that employs a combined feedforward-feedback control law to track the resulting optimal trajectory from the motion planning module. Then, we introduce an intermediate barrier certificate module between the vehicle-level tracking controller and physical vehicle, which takes the reference control law, and by using complex

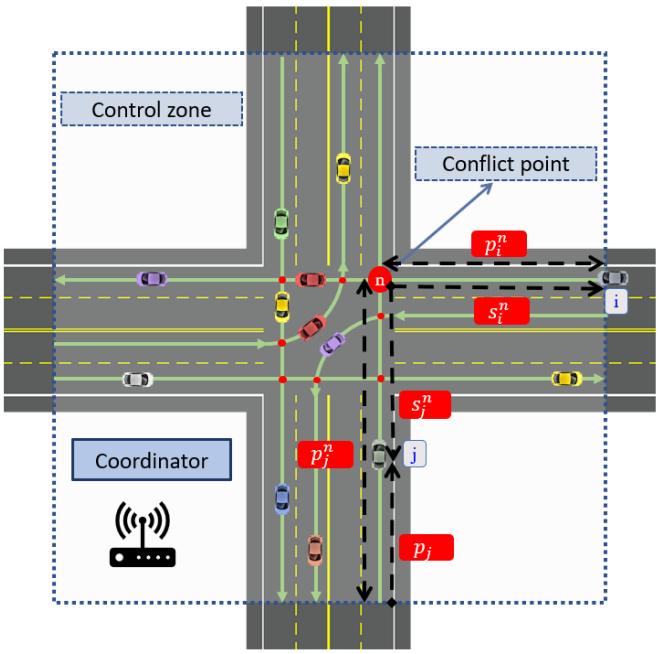

Figure 3.9: A signal free intersection with conflict points.

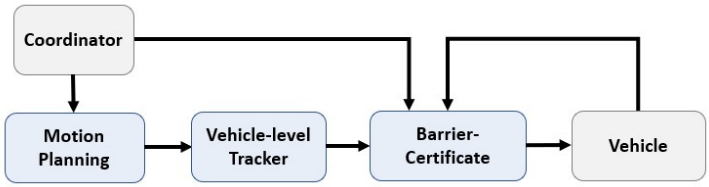

Figure 3.10: Coordination framework architecture.

vehicle dynamics, it ensures that none of the constraints in the system are violated. In particular, the barrier-certificate module yields a QP that can be solved at each time step onboard each CAV in real time.

3.4.2 Motion Planning

Definition 3.4.1. *For CAV $i \in \mathcal{N}(t)$, and a conflict point $n \in \mathcal{Q}$, $s_i^n : \mathbb{R}_{\geq 0} \to \mathbb{R}$ is the function that gives the distance between CAV i and conflict point n (Fig. 3.9), and it is given*

by

$$s_i^n(t) = p_i^n - p_i(t), \quad \forall t \in [t_i^0, t_i^f], \tag{3.48}$$

where p_i^n is the distance of the conflict point $n \in \mathcal{Q}$ from the point that CAV i enters the control zone.

We need to slightly enhance lateral safety constraint (3.6) for CAV $i \in \mathcal{N}$ to make it compatible for using CBF, since the constraint or its higher-order derivatives has to be a function of control input of CAV i. Let CAV $j \in \mathcal{N}(t) \setminus \{i\}$ be a CAV that has already planned its trajectory which might cause a lateral collision with CAV i. CAV i can reach at conflict point n either after or before CAV j. In the first case, we have

$$s_i^n(t) + s_j^n(t) \geq \delta_i(t), \quad \forall t \in [t_i^0, t_j^n], \tag{3.49}$$

where t_j^n is the known time that CAV j reaches the conflict point n, i.e., position p_j^n. The intuition in (3.49) is that at t_j^n, s_j^n is equal to zero based on Definition 3.4.1, and CAV i should maintain at least a safe distance $\delta_i(t)$ from the conflict point n. However, for $t \in [t_i^0, t_j^n)$, s_j^n is a positive number, and hence $s_i^n(t)$ needs to be greater than $\delta_i(t) - s_j^n(t)$. Similarly, in the second case, where CAV i reaches the conflict point n before CAV j, we have

$$s_i^n(t) + s_j^n(t) \geq \delta_j(t), \quad \forall t \in [t_i^0, t_i^n], \tag{3.50}$$

where t_i^n is determined by the trajectory planned by CAV i.

By moving all terms in (3.49) to the LHS, we obtain $s_i^n(t) + s_j^n(t) - \delta_i(t) \geq 0$. Constraint (3.49) is satisfied, if $\min(s_i^n(t) + s_j^n(t) - \delta_i(t)) \geq 0$ in the interval $[t_i^0, t_j^n]$. Likewise, constraint (3.50) is satisfied if $\min(s_i^n(t) + s_j^n(t) - \delta_j(t)) \geq 0$ in the interval $[t_i^0, t_i^n]$. However, to ensure the lateral safety between CAV i and CAV j at conflict point n, either (3.49) or

(3.50) must be satisfied, and thus we impose the following lateral safety constraint on CAV i

$$\max \Bigg\{ \min_{t\in[t_i^0,t_j^n]} \{s_i^n(t) + s_j^n(t) - \delta_i(t)\}, \\ \min_{t\in[t_i^0,t_i^n]} \{s_i^n(t) + s_j^n(t) - \delta_j(t)\} \Bigg\} \geq 0. \tag{3.51}$$

Next, we formally define the motion planning problem to minimize the exit time from the control zone.

Problem 3.4.2. *Each CAV $i \in \mathcal{N}(t)$ solves the following optimization problem at t_i^0, upon entering the control zone*

$$\min_{t_i^f \in \mathcal{T}_i(t_i^0)} t_i^f \tag{3.52}$$
$$\text{subject to: (3.4), (3.9)} - \text{(3.11), (3.51)}.$$

Solving Problem 3.4.2, CAV i derives the optimal exit time, t_i^f, corresponding to an optimal trajectory, $\bar{u}_i(t), \bar{v}_i(t)$ and $\bar{p}_i(t)$, which satisfies all the state, control, and safety constraints.

A vehicle-level tracking controller employs a combined feedforward-feedback control law u_i^{ref} to track the resulting optimal trajectory from the motion planning module as follows

$$u_i^{ref}(t) = \bar{u}_i(t) + k_p \cdot (\bar{p}_i(t) - p_i(t)) + k_v \cdot (\bar{v}_i(t) - v_i(t)), \tag{3.53}$$

where $p_i(t)$ and $v_i(t)$ are current observed position and speed of CAV i; respectively, while $k_p, k_v \in \mathbb{R}_{>0}$ are feedback control gains.

Remark 3.4.3. *In this section, we consider that CAVs solve Problem 3.4.2 upon entering the control zone. However, one can consider the case in which CAVs re-solve their motion planning problem either periodically or based on an occurrence of a certain event such as the entrance of a new CAV in the control zone as described in Section 3.2 [178].*

3.4.3 Barrier-certificate

In this subsection, we present our barrier-certificate module which is a middle layer between the vehicle-level tracking controller and physical vehicle. In this module, we consider more realistic model to describe the dynamics of each CAV $i \in \mathcal{N}(t)$ as follows

$$\begin{aligned} \dot{p}_i(t) &= v_i(t), \\ \dot{v}_i(t) &= u_i(t) - \frac{F_r(v_i(t))}{m_i}. \end{aligned} \tag{3.54}$$

Let $F_r \in \mathbb{R}_{\geq 0}$ correspond to all resisting forces including longitudinal aerodynamic drag force and rolling resistance force at tires, while $m_i \in \mathbb{R}_{\geq 0}$ is the mass of CAV [206, 207]. The net resisting force typically is approximated as a quadratic function of the CAV's speed [206, Chapter 2], i.e.,

$$F_r(v_i(t)) = \beta_0 + \beta_1\, v_i(t) + \beta_2\, v_i^2(t), \tag{3.55}$$

where $\beta_0, \beta_1, \beta_2 \in \mathbb{R}_{\geq 0}$ are all constant parameters that can be computed empirically. We write (3.54) in a control-affine, vector form as

$$\dot{\mathbf{x}}_i(t) = \underbrace{\begin{bmatrix} v_i(t) \\ -\frac{F_r(v_i(t))}{m_i} \end{bmatrix}}_{\mathbf{f}_i(\mathbf{x}_i(t))} + \underbrace{\begin{bmatrix} 0 \\ 1 \end{bmatrix}}_{\mathbf{g}_i(\mathbf{x}_i(t))} u_i(t), \tag{3.56}$$

where $\mathbf{x}_i(t) = [p_i(t), v_i(t)]^\top \in \mathcal{P}_i \times \mathcal{V}_i$ denotes the state of the CAV i at t. Note that $\mathbf{f}_i$ and $\mathbf{g}_i$ are globally Lipschitz functions, which results in global existence and uniqueness of the solution of (3.56) if u_i is also globally Lipschitz [206, Chapter 3].

Background Materials

Here, we review some basic definitions and results from [149, 154] adapted appropriately to reflect our notation. Inspired by the idea of environmental CBFs [201], we construct

a CBF for the cases in which the constraint of the CAV is coupled to the dynamics of other CAVs, such as lateral safety and rear-end safety constraints. To simplify notation, we discard the argument of time in our state and control variables whenever it does not create confusion.

Next, we define the safe set of a constraint that depends only on the state of a CAV.

Definition 3.4.4. *For CAV $i \in \mathcal{N}(t)$, the safe set $\mathcal{C}$ is a zero-superlevel set of a continuously differentiable function $h : \mathcal{P}_i \times \mathcal{V}_i \to \mathbb{R}$,*

$$\mathcal{C} = \{\mathbf{x}_i \in \mathcal{P}_i \times \mathcal{V}_i : h(\mathbf{x}_i) \geq 0\}. \tag{3.57}$$

For those cases where a constraint of CAV i also depends on another CAV j, i.e., in rear-end safety and lateral safety constraints, we define the coupled safe set next.

Definition 3.4.5. *For CAV $i \in \mathcal{N}(t)$, the coupled safe set $\mathcal{C}'$ with CAV $j \in \mathcal{N}(t)$ is a zero-superlevel set of a continuously differentiable function $z : D \subseteq (\mathcal{P}_i \times \mathcal{V}_i) \times (\mathcal{P}_j \times \mathcal{V}_j) \to \mathbb{R}$,*

$$\mathcal{C}' = \{(\mathbf{x}_i, \mathbf{x}_j) \in D : z(\mathbf{x}_i, \mathbf{x}_j) \geq 0\}. \tag{3.58}$$

Next, we define the safety of the CAV i, with longitudinal dynamics (3.56), with respect to the safe set $\mathcal{C}$.

Definition 3.4.6. *CAV i with the longitudinal dynamics given by (3.56) is safe with respect to the safe set $\mathcal{C}$ if the set $\mathcal{C}$ is forward-invariant, namely, if $\mathbf{x}_i(t_i^0) \in \mathcal{C}$, $\mathbf{x}_i(t) \in \mathcal{C}$ for all $t \geq t_i^0$.*

Similarly, we define safety with respect to the coupled safe set $\mathcal{C}'$.

Definition 3.4.7. *CAV i with longitudinal dynamics given by (3.56) is safe with respect to the coupled safe set $\mathcal{C}'$ with CAV j, if the set $\mathcal{C}'$ is forward-invariant, namely, if $(\mathbf{x}_i(t_i^0), \mathbf{x}_j(t_i^0)) \in \mathcal{C}'$, $(\mathbf{x}_i(t), \mathbf{x}_j(t)) \in \mathcal{C}'$ for all $t \geq t_i^0$.*

Next, we need to define the extended class $\mathcal{K}_\infty$ function.

Definition 3.4.8. *A strictly increasing function $\alpha : \mathbb{R} \to \mathbb{R}$ with $\alpha(0) = 0$, is an extended class $\mathcal{K}_\infty$ function.*

Definition 3.4.9 ([149])**.** *Let $\mathcal{C}$ be a safe set for CAV $i \in \mathcal{N}(t)$ for a continuously differentiable function $h : \mathcal{P}_i \times \mathcal{V}_i \to \mathbb{R}$. The function h is a CBF if there exists an extended class $\mathcal{K}_\infty$ function $\alpha(\cdot)$ such that for all $\mathbf{x}_i \in \mathcal{C}$*

$$\sup_{u_i \in \mathcal{U}_i} \dot{h}(\mathbf{x}_i, u_i) \geq -\alpha(h(\mathbf{x}_i)), \tag{3.59}$$

where

$$\dot{h}(\mathbf{x}_i, u_i) = \nabla h(\mathbf{x}_i) \cdot \dot{\mathbf{x}}_i, \tag{3.60}$$

and $\dot{\mathbf{x}}_i$ is given by (3.56).

Remark 3.4.10. *We can also write (3.60) in terms of Lie derivatives as follows*

$$\dot{h}(\mathbf{x}_i, u_i) = L_{\mathbf{f}_i} h(\mathbf{x}_i) + L_{\mathbf{g}_i} h(\mathbf{x}_i) u_i, \tag{3.61}$$

where

$$L_{\mathbf{f}_i} h(\mathbf{x}_i) = \left[\frac{\partial h(\mathbf{x}_i)}{\partial p_i}, \frac{\partial h(\mathbf{x}_i)}{\partial v_i} \right]^\top \cdot \mathbf{f}_i(\mathbf{x}_i), \tag{3.62}$$

$$L_{\mathbf{g}_i} h(\mathbf{x}_i) = \left[\frac{\partial h(\mathbf{x}_i)}{\partial p_i}, \frac{\partial h(\mathbf{x}_i)}{\partial v_i} \right]^\top \cdot \mathbf{g}_i(\mathbf{x}_i). \tag{3.63}$$

Theorem 3.4.11 ([149])**.** *Let $\mathcal{C}$ be a safe set for CAV $i \in \mathcal{N}(t)$ for a continuously differentiable function $h : \mathcal{P}_i \times \mathcal{V}_i \to \mathbb{R}$. If h is a CBF on $\mathcal{P}_i \times \mathcal{V}_i$, then any Lipschitz continuous controller $u_i : \mathcal{P}_i \times \mathcal{V}_i \to \mathcal{U}_i$ such that $u_i(\mathbf{x}_i) \in \mathcal{A}_h(\mathbf{x}_i)$ renders the safe set $\mathcal{C}$ forward invariant, where*

$$\mathcal{A}_h(\mathbf{x}_i) = \{u_i \in \mathcal{U}_i : \nabla h(\mathbf{x}_i) \cdot \dot{\mathbf{x}}_i \geq -\alpha(h(\mathbf{x}_i))\}. \tag{3.64}$$

Inspired by the idea of environmental CBF [201], which considers the evolution of

environment state in analyzing safety, we consider the evolution of other relevant CAVs in constructing the CBF for CAV i.

Definition 3.4.12. *Let $\mathcal{C}'$ be a coupled safe set for CAV i and $j \in \mathcal{N}(t)$ for a continuously differentiable function $z : D \subseteq (\mathcal{P}_i \times \mathcal{V}_i) \times (\mathcal{P}_j \times \mathcal{V}_j) \to \mathbb{R}$. The function z is a CBF if there exists an extended class $\mathcal{K}_\infty$ function $\alpha(\cdot)$ such that for all $(\mathbf{x}_i, \mathbf{x}_j) \in \mathcal{C}'$*

$$\sup_{u_i \in \mathcal{U}_i} \dot{z}(\mathbf{x}_i, u_i, \mathbf{x}_j, u_j) \geq -\alpha(z(\mathbf{x}_i, \mathbf{x}_j)), \tag{3.65}$$

where

$$\begin{aligned}\dot{z}(\mathbf{x}_i, u_i, \mathbf{x}_j, u_j) = \nabla_{\mathbf{x}_i} z(\mathbf{x}_i, \mathbf{x}_j) \cdot \underbrace{(\mathbf{f}_i(\mathbf{x}_i) + \mathbf{g}_i(\mathbf{x}_i)u_i)}_{\dot{\mathbf{x}}_i} \\ + \nabla_{\mathbf{x}_j} z(\mathbf{x}_i, \mathbf{x}_j) \cdot \underbrace{(\mathbf{f}_j(\mathbf{x}_j) + \mathbf{g}_j(\mathbf{x}_j)u_j)}_{\dot{\mathbf{x}}_j},\end{aligned} \tag{3.66}$$

$$\nabla_{\mathbf{x}_i} z(\mathbf{x}_i, \mathbf{x}_j) = \left[\frac{\partial z(\mathbf{x}_i, \mathbf{x}_j)}{\partial p_i}, \frac{\partial z(\mathbf{x}_i, \mathbf{x}_j)}{\partial v_i}\right]^\top, \tag{3.67}$$

$$\nabla_{\mathbf{x}_j} z(\mathbf{x}_i, \mathbf{x}_j) = \left[\frac{\partial z(\mathbf{x}_i, \mathbf{x}_j)}{\partial p_j}, \frac{\partial z(\mathbf{x}_i, \mathbf{x}_j)}{\partial v_j}\right]^\top. \tag{3.68}$$

Remark 3.4.13. *Note that in our decentralized coordination framework, CAV $i \in \mathcal{N}(t)$ plans its trajectory after CAV $j \in \mathcal{N}(t)$, which means that $\mathbf{x}_j$ and u_j are available to CAV i through the coordinator.*

Theorem 3.4.14. *Let $\mathcal{C}'$ be a coupled safe set for CAV $i \in \mathcal{N}(t)$ and $j \in \mathcal{N}(t)$ for a continuously differentiable function $z : D \subseteq (\mathcal{P}_i \times \mathcal{V}_i) \times (\mathcal{P}_j \times \mathcal{V}_j) \to \mathbb{R}$. If z is a CBF on D, then any Lipschitz continuous controller $u_i : D \to \mathcal{U}_i$ such that $u_i(\mathbf{x}_i, \mathbf{x}_j) \in \mathcal{A}_z(\mathbf{x}_i, \mathbf{x}_j)$ renders the coupled safe set $\mathcal{C}'$ forward invariant, where*

$$\mathcal{A}_z(\mathbf{x}_i, \mathbf{x}_j) = \{u_i \in \mathcal{U}_i : \nabla_{\mathbf{x}_i} z(\mathbf{x}_i, \mathbf{x}_j) \cdot \dot{\mathbf{x}}_i + \nabla_{\mathbf{x}_j} z(\mathbf{x}_i, \mathbf{x}_j) \cdot \dot{\mathbf{x}}_j \geq -\alpha(z(\mathbf{x}_i, \mathbf{x}_j))\}. \tag{3.69}$$

Proof. The proof is similar to the one in [201, Theorem 2]. By considering the new state $\mathbf{X}_{i,j}$ as stacked state of $\mathbf{x}_i$ and $\mathbf{x}_j$, and applying Theorem 3.4.11, the result follows. □

Constructing CBFs

Using CBFs, we can map all of the constraints from the states for CAV $i \in \mathcal{N}(t)$ to the control input. For the speed constraint (3.3) of CAV i, we consider

$$h_1(\mathbf{x}_i) = v_{\max} - v_i, \tag{3.70}$$

$$h_2(\mathbf{x}_i) = v_i - v_{\min}. \tag{3.71}$$

From Definition 3.4.9 and choosing $\alpha_q(x) = \lambda_q x,\ \lambda_q \in \mathbb{R}_{>0}, q \in \{1, 2\}$, we have $h_1(\mathbf{x}_i)$ and $h_2(\mathbf{x}_i)$ as CBFs to ensure satisfying the speed limit constraint. Then, from Theorem 3.4.11, any control input u_i should satisfy the following

$$u_i \leq \frac{F_r(v_i)}{m_i} + \lambda_1(v_{\max} - v_i), \tag{3.72}$$

$$u_i \geq \frac{F_r(v_i)}{m_i} - \lambda_2(v_i - v_{\min}). \tag{3.73}$$

Rear-end safety constraint depends on both states of CAV i and $k \in \mathcal{N}(t)$, and thus we have

$$z_1(\mathbf{x}_i, \mathbf{x}_k) = p_k - p_i - (\gamma + \varphi \cdot v_i). \tag{3.74}$$

From Definition 3.4.12 and choosing $\alpha_3(x) = \lambda_3 x,\ \lambda_3 \in \mathbb{R}_{>0}$, we have $z_1(\mathbf{x}_i, \mathbf{x}_k)$ as a CBF to guarantee satisfying the rear-end safety constraint. Next, we use the result of Theorem 3.4.11 to derive the condition on control input that needs to be satisfied. The gradient of z_1 is

$$\nabla_{\mathbf{x}_i} z_1(\mathbf{x}_i, \mathbf{x}_k) = [-1, -\varphi]^\top, \tag{3.75}$$

$$\nabla_{\mathbf{x}_k} z_1(\mathbf{x}_i, \mathbf{x}_k) = [1, 0]^\top. \tag{3.76}$$

Taking the dot product of (3.75) and (3.76) with $\dot{\mathbf{x}}_i$ and $\dot{\mathbf{x}}_k$; respectively, yields

$$\nabla_{\mathbf{x}_i} z_1(\mathbf{x}_i, \mathbf{x}_k) \cdot \dot{\mathbf{x}}_i = -v_i - \varphi(-\frac{F_r(v_i)}{m_i} + u_i), \tag{3.77}$$

$$\nabla_{\mathbf{x}_k} z_1(\mathbf{x}_i, \mathbf{x}_k) \cdot \dot{\mathbf{x}}_k = v_k. \tag{3.78}$$

Using the result of Theorem 3.4.14, the control input u_i should satisfy the following condition in order to satisfy the rear-end safety constraint,

$$u_i \leq \frac{1}{\varphi}\left[\lambda_3(p_k - p_i - (\gamma + \varphi v_i)) + v_k - v_i\right] + \frac{F_r(v_i)}{m_i}. \tag{3.79}$$

For the lateral-safety constraint (3.49), when $t_i^n > t_j^n$, we have

$$\begin{aligned} z_2(\mathbf{x}_i, \mathbf{x}_j) &= s_i^n + s_j^n - \delta_i \\ &= (p_i^n - p_i) + (p_j^n - p_j) - (\gamma + \varphi \cdot v_i). \end{aligned} \tag{3.80}$$

By choosing $\alpha_4(x) = \lambda_4 x,\ \lambda_4 \in \mathbb{R}_{>0}$, $z_2(\mathbf{x}_i, \mathbf{x}_j)$ is a CBF to guarantee satisfying the lateral safety constraint, which implies

$$\nabla_{\mathbf{x}_i} z_2(\mathbf{x}_i, \mathbf{x}_j) = \left[-1, -\varphi\right]^\top, \tag{3.81}$$

$$\nabla_{\mathbf{x}_j} z_2(\mathbf{x}_i, \mathbf{x}_j) = \left[-1, 0\right]^\top. \tag{3.82}$$

Taking the dot product of above equations with $\dot{\mathbf{x}}_i$ and $\dot{\mathbf{x}}_j$; respectively, yields

$$\nabla_{\mathbf{x}_i} z_2(\mathbf{x}_i, \mathbf{x}_j) \cdot \dot{\mathbf{x}}_i = -v_i - \varphi(-\frac{F_r(v_i)}{m_i} + u_i), \tag{3.83}$$

$$\nabla_{\mathbf{x}_j} z_2(\mathbf{x}_i, \mathbf{x}_j) \cdot \dot{\mathbf{x}}_j = -v_j. \tag{3.84}$$

For this case, the control input u_i should satisfy the following condition in order to satisfy constraint (3.49),

$$u_i \leq \frac{1}{\varphi}\left[\lambda_4(s_i^n + s_j^n - \delta_i) - (v_i + v_j)\right] + \frac{F_r(v_i)}{m_i}. \tag{3.85}$$

For the lateral-safety constraint (3.50), we have

$$\begin{aligned} z_3(\mathbf{x}_i, \mathbf{x}_j) &= s_i^n + s_j^n - \delta_j \\ &= (p_i^n - p_i) + (p_j^n - p_j) - (\gamma + \varphi \cdot v_j). \end{aligned} \tag{3.86}$$

However, since $\dot{z}_3$ does not depend on u_i, (3.86) cannot be a valid CBF for CAV i. These type of constraints are called constraints with higher relative degree $r > 1$. For example, the relative degree of (3.50) is equal to 2. A complete analysis of handling higher relative degree constraints in general cases is given in [153].

Next, we use a higher order CBF based on [153, Definition 7, Theorem 5], and extend it to our case with coupled constraints. We first form a series of functions $\psi_q : D \subseteq (\mathcal{P}_i \times \mathcal{V}_i) \times (\mathcal{P}_j \times \mathcal{V}_j) \to \mathbb{R}$, $q = \{0, 1, 2\}$ as

$$\begin{aligned} \psi_0(\mathbf{x}_i, \mathbf{x}_j) &= z_3(\mathbf{x}_i, \mathbf{x}_j), \\ \psi_1(\mathbf{x}_i, \mathbf{x}_j) &= \dot{\psi}_0(\mathbf{x}_i, \mathbf{x}_j) + \alpha_5(\psi_0(\mathbf{x}_i, \mathbf{x}_j)), \\ \psi_2(\mathbf{x}_i, \mathbf{x}_j) &= \dot{\psi}_1(\mathbf{x}_i, \mathbf{x}_j) + \alpha_6(\psi_1(\mathbf{x}_i, \mathbf{x}_j)), \end{aligned} \tag{3.87}$$

where $\alpha_5(\cdot)$ and $\alpha_6(\cdot)$ are extended class $\mathcal{K}_\infty$ functions. The zero-superlevel sets of ψ_0 and ψ_1 are given by

$$\mathcal{C}_1' = \{(\mathbf{x}_i, \mathbf{x}_j) \in D : \psi_0(\mathbf{x}_i, \mathbf{x}_j) \geq 0\}, \tag{3.88}$$

$$\mathcal{C}_2' = \{(\mathbf{x}_i, \mathbf{x}_j) \in D : \psi_1(\mathbf{x}_i, \mathbf{x}_j) \geq 0\}. \tag{3.89}$$

Based on [153, Definition 7], if there exist extended class $\mathcal{K}_\infty$ functions $\alpha_5(\cdot)$ and $\alpha_6(\cdot)$ such that $\psi_2(\mathbf{x}_i, \mathbf{x}_j) \geq 0$ for all $(\mathbf{x}_i, \mathbf{x}_j) \in \mathcal{C}_1' \cap \mathcal{C}_2'$, $z_3(\mathbf{x}_i, \mathbf{x}_j)$ is a higher order CBF. From [153, Theorem 5], if $(\mathbf{x}_i(t_i^0), \mathbf{x}_j(t_i^0)) \in \mathcal{C}_1' \cap \mathcal{C}_2'$, then any Lipschitz continuous controller $u_i : D \to \mathbb{R}$ such that $u_i(\mathbf{x}_i, \mathbf{x}_j) \in \mathcal{A}_\psi(\mathbf{x}_i, \mathbf{x}_j)$ renders the set $\mathcal{C}_1' \cap \mathcal{C}_2'$ forward invariant, where

$$\mathcal{A}_\psi(\mathbf{x}_i, \mathbf{x}_j) = \{u_i \in \mathcal{U}_i : \psi_2(\mathbf{x}_i, \mathbf{x}_j) \geq 0\}. \tag{3.90}$$

Theorem 3.4.15. *The allowable set of control actions that renders the set $\mathcal{C}_1' \cap \mathcal{C}_2'$ forward*

invariant, $\mathcal{A}_\psi$, is given by

$$u_i \leq -\lambda_5(v_i + v_j) + \frac{F_r(v_i)}{m_i} + \frac{F_r(v_j)}{m_j} - \frac{\varphi\beta_1 F_r(v_j)}{m_j^2} - \frac{2\varphi\beta_2 v_j F_r(v_j)}{m_j^2} + (\frac{\varphi\beta_1 + 2\varphi\beta_2 v_j}{m_j} - \lambda_5\varphi - 1)u_j - \varphi\dot{u}_j + \lambda_6\,\psi_1. \tag{3.91}$$

Proof. By choosing $\alpha_q(x) = \lambda_q x,\ \lambda_q \in \mathbb{R}_{>0}, q \in \{5, 6\}$, we have

$$\psi_1(\mathbf{x}_i, \mathbf{x}_j) = \nabla_{\mathbf{x}_i} z_3(\mathbf{x}_i, \mathbf{x}_j) \cdot \dot{\mathbf{x}}_i + \nabla_{\mathbf{x}_j} z_3(\mathbf{x}_i, \mathbf{x}_j) \cdot \dot{\mathbf{x}}_j + \lambda_5 z_3(\mathbf{x}_i, \mathbf{x}_j), \tag{3.92}$$

where

$$\nabla_{\mathbf{x}_i} z_3(\mathbf{x}_i, \mathbf{x}_j) \cdot \dot{\mathbf{x}}_i = -v_i, \tag{3.93}$$

$$\nabla_{\mathbf{x}_j} z_3(\mathbf{x}_i, \mathbf{x}_j) \cdot \dot{\mathbf{x}}_j = -v_j + \varphi\frac{F_r(v_j)}{m_j} - \varphi u_j. \tag{3.94}$$

Substituting (3.86),(3.93), and (3.94) in (3.92) yields

$$\psi_1(\mathbf{x}_i, \mathbf{x}_j, u_j, F_r(v_j)) = -v_i - v_j + \varphi\frac{F_r(v_j)}{m_j} - \varphi u_j + \lambda_5[p_i^n - p_i + p_j^n - p_j - \gamma - \varphi \cdot v_j]. \tag{3.95}$$

Next, we derive the full time derivative of (3.95) in order to construct $\psi_2(\mathbf{x}_i, \mathbf{x}_j)$ in (3.87),

$$\dot{\psi}_1(\mathbf{x}_i, \mathbf{x}_j) = \nabla_{\mathbf{x}_i}\psi_1 \cdot \dot{\mathbf{x}}_i + \nabla_{\mathbf{x}_j}\psi_1 \cdot \dot{\mathbf{x}}_j + \frac{\partial\psi_1}{\partial u_j}\,\dot{u}_j + \frac{\partial\psi_1}{\partial F_r(v_j)}\frac{\partial F_r(v_j)}{\partial v_j}\dot{v}_j, \tag{3.96}$$

where

$$\nabla_{\mathbf{x}_i}\psi_1 \cdot \dot{\mathbf{x}}_i = -\lambda_5 v_i + \frac{F_r(v_i)}{m_i} - u_i, \tag{3.97}$$

$$\nabla_{\mathbf{x}_j}\psi_1 \cdot \dot{\mathbf{x}}_j = -\lambda_5 v_j + \frac{F_r(v_j)}{m_j} + \lambda_5\varphi\frac{F_r(v_j)}{m_j} - u_j - \lambda_5 u_j, \tag{3.98}$$

$$\frac{\partial\psi_1}{\partial u_j}\,\dot{u}_j = -\varphi\,\dot{u}_j, \tag{3.99}$$

$$\frac{\partial\psi_1}{\partial F_r(v_j)}\frac{\partial F_r(v_j)}{\partial v_j}\dot{v}_j = \frac{\varphi}{m_j}(\beta_1 + 2\beta_2 v_j)\cdot(-\frac{F_r(v_j)}{m_j} + u_j). \tag{3.100}$$

By substituting (3.96)-(3.100) into (3.87), we derive $\psi_2(\mathbf{x}_i, \mathbf{x}_j)$ from (3.87), which can then be used to construct the condition for the control input u_i based on (3.90), and the proof is complete. □

As described in Section 3.4.2, to guarantee the lateral safety between CAV $i \in \mathcal{N}(t)$ and CAV $j \in \mathcal{N}(t)$ at conflict point $n \in \mathcal{Q}$, either (3.49) or (3.50) must be satisfied. Thus, depending on the the arrival time at conflict point n for CAV i and j (t_i^n and t_j^n, respectively), we must satisfy (3.85) or (3.91) as follows

$$\begin{cases} u_i \le A, & \text{if } t_i^n > t_j^n \\ u_i \le B, & \text{if } t_i^n < t_j^n \end{cases}, \tag{3.101}$$

where

$$A = \frac{1}{\varphi}\left[\lambda_4(s_i^n + s_j^n - \delta_i) - (v_i + v_j)\right] + \frac{F_r(v_i)}{m_i}, \tag{3.102}$$

$$\begin{aligned} B = {} & \lambda_5(v_i + v_j) + \frac{F_r(v_i)}{m_i} + \frac{F_r(v_j)}{m_j} - \frac{\varphi\beta_1 F_r(v_j)}{m_j^2} \\ & - \frac{2\varphi\beta_2 v_j F_r(v_j)}{m_j^2} + (\frac{\varphi\beta_1 + 2\varphi\beta_2 v_j}{m_j} - \lambda_5\varphi - 1)u_j \\ & - \varphi\dot{u}_j + \lambda_6\,\psi_1. \end{aligned} \tag{3.103}$$

Next, we formulate an optimization problem based on QP for our barrier-certificate

module. This QP can be solved at discrete time step to verify the reference control input $u_i^{ref}(t)$, resulting from the vehicle-level tracking controller. In case of a potential violation, QP minimally modifies the control input to guarantee the satisfaction of all constraints.

Problem 3.4.16. *Each CAV $i \in \mathcal{N}(t)$ at time t observes its state $\mathbf{x}_i$ and accesses the states and control inputs, $\mathbf{x}_j$ and u_j, respectively, of neighbour CAVs. Then, i solves the following optimization problem to find the safe control input.*

$$u_i^*(t) = \arg\min_{u_i(t)} \frac{1}{2}\|u_i(t) - u_i^{ref}(t)\|^2 \tag{3.104}$$

subject to:

$$(3.2), (3.72), (3.73), (3.79), (3.101),$$

where each pertaining constraint (3.3)-(3.50) *for CAV i are mapped to the control input constraint using the appropriate CBFs* (3.64)*,* (3.69)*, or* (3.90)*. Note that $u_i^{ref}(t)$ is the combined feedforward-feedback control law to track the resulting optimal trajectory from the motion planning module 3.4.2.*

Since the control input is bounded, the feasibility of the QP in Problem 3.4.16 can be ensured by choosing appropriate $\lambda_q \in \mathbb{R}_{\geq 0}$ for class $\mathcal{K}_\infty$ functions $\alpha_q(x) = \lambda_q x$, $q \in \mathbb{N}$. Note that in this section, we chose linear class $\mathcal{K}_\infty$ functions; however, one may decide to choose a different form for their class $\mathcal{K}_\infty$.

3.4.4 Simulation Results

To show the performance of our barrier-certified coordination framework, we investigate the coordination of 24 CAVs at a signal-free intersection shown in Fig.3.9. The CAVs enter the control zone from 6 different paths (Fig. 3.9) with a total rate of 3600 veh/hour while their initial speed is uniformly distributed between 12 m/s and 14 m/s. We consider the length of the control zone and road width to be 212 m and 3 m, respectively. The rest of the parameters for the simulation are $v_{\min} = 0.2$ m/s, $v_{\max} = 20$ m/s,

$u_{\max} = 2$ m/s^2, $u_{\min} = -2$ m/s^2, $\gamma = 2.5$ m, $\varphi = 0.5$ s $k_p = k_v = 1.5$, $\Delta t = 0.1$ s. We used `lsqlin` in Matlab to solve Problem 3.4.16 and `ODE45` to integrate the vehicle dynamics. Videos from our simulation can be found at the supplemental site, https://sites.google.com/view/ud-ids-lab/BCOCF.

Figs. 3.11-3.13 demonstrate the control input, position, and speed for a selected CAV in the simulation. The blue line in Fig. 3.11 shows the reference control input from the feedforward-feedback control law (3.53), and the dashed red line denotes the resulting optimal control trajectory from the motion planning module. The black line shows the applied control input at each time step resulting from the Solution of Problem 3.4.16. It can be seen that at around 16.5 s the barrier-certificate module overrides the reference control input in order to satisfy the speed limit constraint. The actual trajectory of the vehicle in Figs. 3.12 and 3.13 is computed by integrating the realistic vehicle dynamics (3.56) and applying the solution of Problem 3.4.16 at each time step. Our proposed framework tracks the resulting optimal trajectory from the motion planning module, while it ensures that none of the state, control, and safety constraints becomes active.

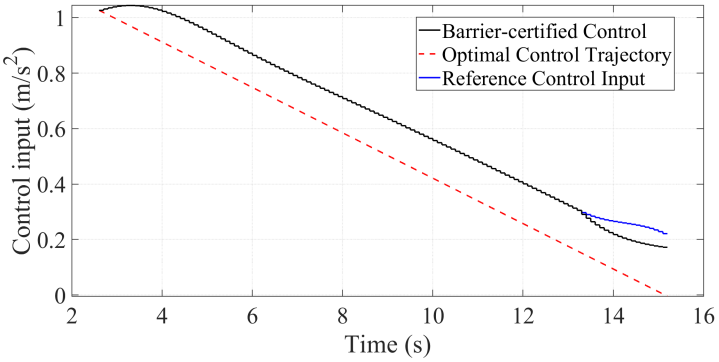

Figure 3.11: Control input for a selected CAV.

The mean and standard deviation of computation times of the motion planning and barrier-certificate modules in our proposed framework are listed in Table 3.1. It shows that our framework is computationally feasible.

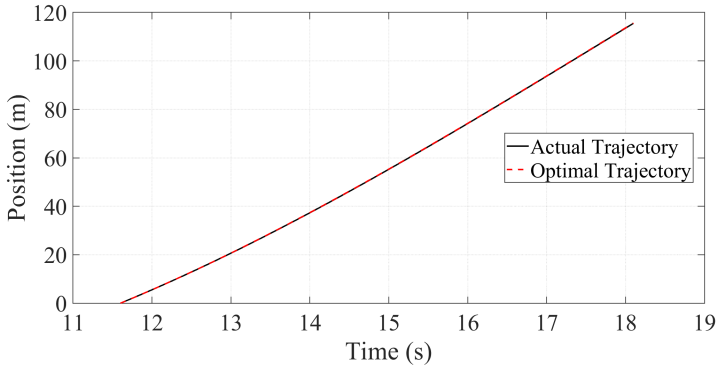

Figure 3.12: Actual and optimal position trajectory for a selected CAV.

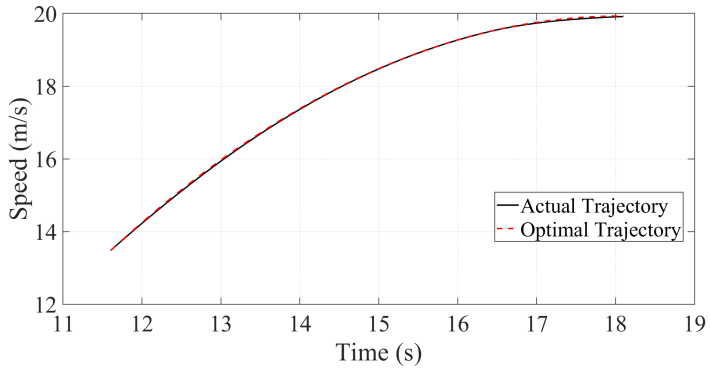

Figure 3.13: Actual and optimal speed trajectory for a selected CAV.

3.5 Summary

In this chapter, we first reviewed a single-level coordination framework for CAVs proposed in [91], and implemented at a roundabout in [92]. Utilizing the proposed framework, each CAV computes the optimal unconstrained control trajectory without activating any of the state, control, and safety constraints. One direct benefit of this framework is that it avoids the inherent implementation challenges in solving a constrained optimal control problem in real time described in Chapter 2.

In this chapter, we provided three different approaches to make our coordination framework uncertainty-aware. First, we integrated a replanning mechanism into our coordination framework, which can be implemented in a time-driven or event-driven manner. This embedded replanning aims at introducing indirect feedback into the coordination framework to respond to the unexpected changes in the system to some extent. Additionally, using the

Table 3.1: The mean and standard deviation of computation times for each module.

	Mean (s)	Standard deviation (s)
Motion planning	0.029	0.0331
Barrier-certificate	0.0063	0.0026

theory of the job-shop scheduling problem, we further enhanced our decentralized coordination framework by introducing a priority-aware resequencing mechanism, which designates the order of decision making. This enhancement advances the state of the art in a way that relaxes the FCFS decision making sequence of the CAVs. Moreover, in our resequencing framework, we can have different weights representing the priorities for CAVs based on the application. Here, we chose the weights of the CAVs to be inversely proportional to the size of their compact set of feasible solutions.

Second, we reformulated the motion-planning framework for CAVs at a signal-free intersection as a robust coordination problem by including the deviations from the nominal trajectories as uncertainty. We adopted the data-driven approach, GP regression, to learn the uncertainty from the possibly noisy observation of CAVs' time trajectories. After obtaining the statistical knowledge about the deviation from nominal trajectories, we constructed the confidence interval for time, position, and speed trajectories using the inverse error function, Chebyshev's inequality, and Vysochanskii-Petunin inequality, respectively.

Finally, we enhanced the motion planning framework for coordination of CAVs at a signal-free intersection through employing CBFs to provide an additional safety layer and ensure the satisfaction of all constraints in the system. By using the proposed framework in the motion planning module, each CAV first uses simple longitudinal dynamics to derive the optimal control trajectory without activating any constraint. In a real physical system, we require a vehicle-level controller to track the resulting optimal trajectory. However, due to the inherent deviations between the actual trajectory and the planned trajectory, the system's constraints may become active. We addressed this issue by introducing a barrier-certificate module based on a more realistic dynamics as a safety middle layer between the vehicle-level tracking controller and physical vehicle to provide a reactive mechanism to guarantee

constraint satisfaction in the system.

Next, we introduce our scaled smart city to validate the coordination framework of CAVs in a safe and controlled environment, and to prove the concepts beyond the simulation.

Chapter 4

EXPERIMENTAL VALIDATION OF CONNECTED AND AUTOMATED VEHICLES AT A SCALED ENVIRONMENT

> Two men took useless trouble and strove without any profit, when one of them accumulated property without enjoying it, and the other learned without practicing what he had learned.
>
> Saadi Shirazi, *The Gulistan of Saadi (1258 CE)*

Commercial simulation platforms are currently available for testing and validating control algorithms for connected and automated vehicles (CAVs) in a safe and cost-efficient setting. Simulation can help us gather key information about how the system performs in an idealized environment. However, evaluating the performance of CAVs in a simulation environment imposes limitations since modeling the exact vehicle dynamics and driving behavior is not feasible. Capturing the complexities arising from data loss and transmission latency associated with connectivity and communication networks can also be challenging. As Grim et al. [164] stated, "*the problem with simulations is that they are doomed to succeed.*" Although there have been several studies reporting on the impact of coordination of CAVs in traffic scenarios, e.g., intersections, merging at roadways and roundabouts, the effectiveness of these approaches has been mostly shown in simulation. Therefore, validating control approaches for CAVs in a physical testbed is of great importance.

In this chapter, we first provide a description of the hardware and software architecture of the Information and Decision Science Lab's Scaled Smart City (IDS^{3}C) in Section 4.1. Then, in Section 4.2, we show a tutorial of the coordination of CAVs at multi-lane roundabout in IDS^{3}C using 9 CAVs. Next, in Section 4.3, we show how we can improve traffic throughput along a transportation corridor consisting of a roundabout, an intersection, and a merging

roadway by using a fleet of 15 CAVs. Finally, in Section 4.4, we provide a summary of the chapter.

The main contributions presented in this chapter are

- (1) The development of a robotic scaled (1:25) testbed to validate control approaches beyond simulation in applications related to emerging mobility systems; (2) validating the control framework for coordination of CAVs at a multi-lane roundabout in real time; and (3) demonstrating the scalability of the control framework at a transportation corridor using a fleet of 15 CAVs. The results of this section were previously presented in the following publications:
  - [93] Behdad Chalaki, Logan E. Beaver, A M Ishtiaque Mahbub, Heeseung Bang, and Andreas A. Malikopoulos. A research and educational robotic testbed for real-time control of emerging mobility systems: From theory to scaled experiments. *IEEE Control Systems Magazine*, 2022 (in press)
  - [92] Behdad Chalaki, Logan E Beaver, and Andreas A Malikopoulos. Experimental validation of a real-time optimal controller for coordination of cavs in a multi-lane roundabout. In *31st IEEE Intelligent Vehicles Symposium (IV)*, pages 504–509, 2020

4.1 Information and Decision Science Lab's Scaled Smart City

IDS^{3}C (Fig. 4.1) is a 1:25 scaled testbed spanning over 400 square feet, and it is capable of replicating real-world traffic scenarios in a small and controlled environment using 50 ground and 10 aerial vehicles. IDS^{3}C provides the opportunity to prove concepts beyond simulations and to understand the implications of errors and delays in the vehicle-to-vehicle and vehicle-to-infrastructure communication as well as their impact on energy usage. IDS^{3}C can also be used to understand the implications of emerging mobility systems, consisting of CAVs, electric vehicles, and shared mobility, on energy consumption and transportation efficiency. Another facet of research that can be explored using IDS^{3}C is complex missions that include the cooperation of aerial and ground vehicles for logistic problems, such as last-mile delivery. IDS^{3}C has six driver emulation stations interfaced directly with the robotic cars which also allow us to explore human driving behavior.

IDS^{3}C is equipped with a VICON motion capture system and uses eight cameras to track the position of each vehicle with sub-millimeter accuracy. The testbed contains a

Figure 4.1: A view of the IDS Lab's Scaled Smart City.

dozen traffic bottlenecks, including merging roadways, multi-lane roundabouts, adjacent intersections, multi-lane intersections, lane-drops, and speed reduction zones. A central mainframe computer (Processor: Intel Core i7-6950X CPU @ 3.00 GHz x 20, Memory: 128 GB) stores a map of the IDS^{3}C as a database of line and arc segments that make up the road network. Coordination of the CAVs within the IDS^{3}C is achieved using a multi-level control framework spanning the mainframe computer and the individual CAVs in an experiment; a schematic of this multi-level framework is shown in Fig. 4.2.

At the start of the experiment, each CAV sets its temporal baseline from which it measures all later times; this avoids the problem of synchronizing CAV clocks, as all information is calculated relative to the experiment start time. High-level trajectory generation is achieved by a multi-threaded C++ program on the mainframe computer, which allocates a thread to each CAV in the experiment. Each CAV is given its own thread on the mainframe, which it uses to receive position information from VICON and generate its trajectory. This is equivalent to other decentralized control architectures, where routing is performed on supplementary external hardware [171]. The only difference is that our external hardware shares a single physical processor. This approach replicates the decentralized structure of traffic coordination problems. The control strategy for each CAV is defined for each zone in the experiment (for example, optimal control in the control zone and the intelligent driver model everywhere else). The mainframe computer transmits the current state of the CAV as

well as reference trajectory data to each CAV through WiFi.

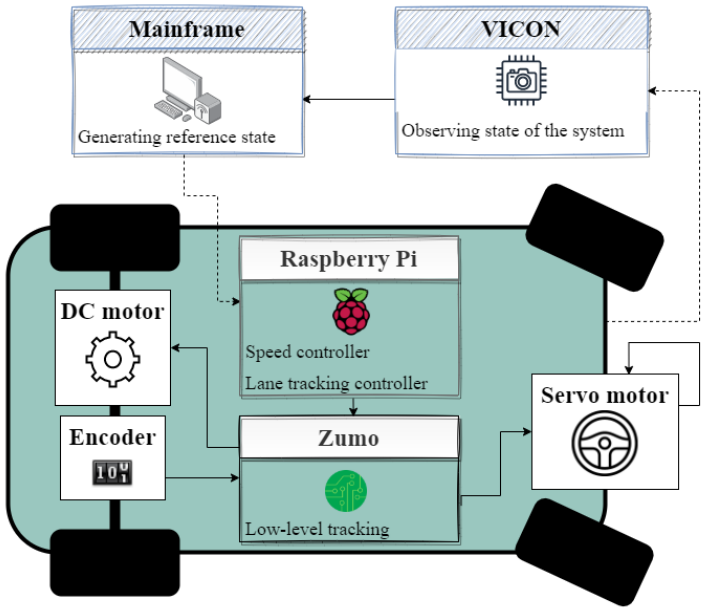

Figure 4.2: Diagram of the high, medium, and low-level control loops. This schematic shows the high-level (mainframe), medium-level (Raspberry Pi) and low-level (Zumo) control loops in IDS^{3}C and communication structure for each CAV.

Lane and reference trajectory tracking are accomplished onboard each CAV in a purely distributed manner. Using state and trajectory data from its reserved thread on the mainframe, each CAV updates its lateral, heading, and distance error at a rate of 50 Hz. Each CAV can operate in one of three modes depending on its control strategy. In *trajectory tracking* mode, i.e., optimal planning, the CAV uses a modified Stanley controller [208] for lane tracking while a feedforward-feedback PID controller [209] tracks the desired longitudinal speed and position. In *lane tracking* mode, that is, reactive control, the modified Stanley controller is used to control the steering angle, while the desired speed is transmitted directly to the CAV. Finally, in *human driver* mode, the CAV directly receives a steering angle and wheel speed command from a driving base station and transmits back a live feed from the onboard Pi camera.

The CAVs of IDS^{3}C have been designed using off-the-shelf electrical components and 3D printed parts that we designed in house. The primary microcontroller on the CAV

is a Raspberry Pi 3B+ running Ubuntu Mate and ROS Kinetic. The Raspberry Pi tracks the reference trajectory and passes a desired motor speed and steering angle to a Pololu Zumo 32U4 for low-level control. The Zumo applies PID control to track the desired motor speed while acting as an ad-hoc analog to digital converter for sensors.

The CAVs are equipped with a Pi Camera, accelerometer, gyroscope, and compass to collect experimental data and to allow for some degree of onboard localization. With this hardware configuration, each CAV is able to run and collect experimental data at 20 Hz for approximately 2 hours.

We designed IDS^{3}C with the capacity to experimentally validate a wide variety of urban traffic scenarios. This includes eco-routing, mixed traffic [71], ride-sharing [5], last-mile delivery [183], and air-ground coordination [210]. In several recent efforts, we have used IDS^{3}C to implement and validate control algorithms for coordinating CAVs at traffic scenarios, such as merging roadways [74], roundabouts [92], intersections [90], adjacent intersections [69, 175, 176], and corridors [75]. We have used IDS^{3}C to generate control actions from neural networks [184, 185] and handle the stochasticity that arises in physical systems [179]. IDS^{3}C also provides a means for user interaction through a mobile application, which enables them to submit origin and destination pairs for dynamic routing in shared mobility and last-mile delivery scenarios.

Recently, we introduced a Unity-based virtual simulation environment for emerging mobility systems, called the IDS 3D City, intended to operate alongside its physical peer, IDS^{3}C, and interface with its existing control framework. The IDS 3D City is a digital replica of the IDS^{3}C using AirSim and Unity. We have designed the IDS 3D City to integrate the control framework used in IDS^{3}C to simulate virtual vehicles. The IDS 3D City enables users to rapidly iterate their control algorithms and experiment parameters before deploying it to IDS^{3}C. A schematic of how the IDS 3D City interacts with IDS^{3}C is shown in Fig. 4.3. The end result is a transition between the physical and virtual environments with minimal changes to input files, as well as the capability to mix physical and virtual vehicles.

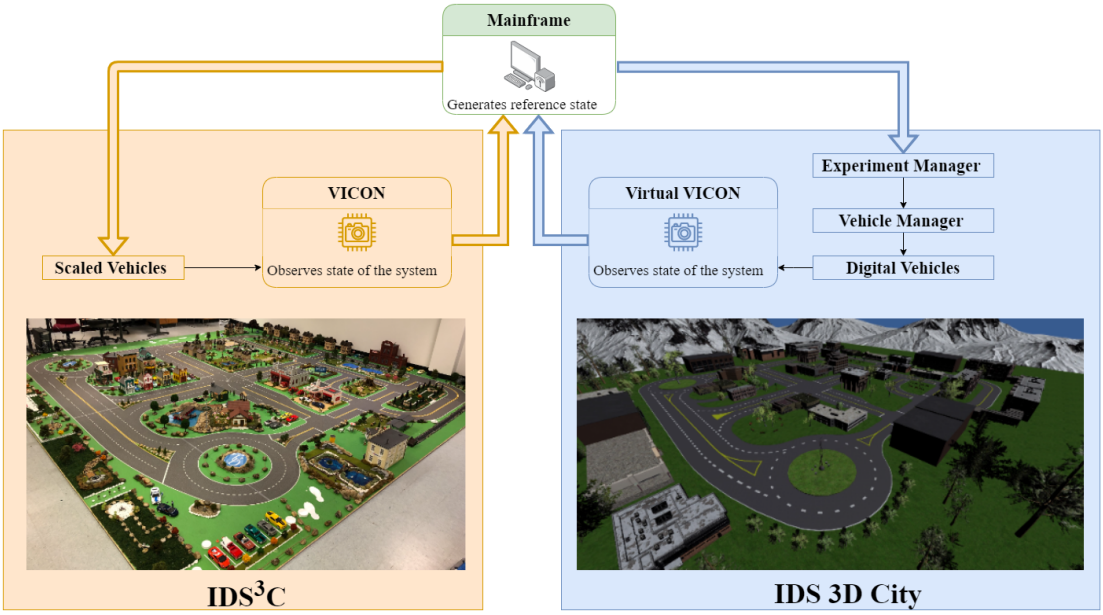

Figure 4.3: The physical and virtual city environments. The mainframe computer can switch between physical and virtual experiment.

4.2 Tutorial: Roundabout Case Study

We performed experiments in the multi-lane roundabout shown in Fig. 4.4 using three CAVs per path in IDS^{3}C to illustrate the implementation of the single-level coordination framework described in 3.1. Fig. 4.4 shows three paths with three conflict points that have a potential for lateral collisions, which we denote as lateral nodes. The length of the control zone for paths are 5.3 m, 5.8 m, and 3.8 m (132.5 m, 145 m, 95 m scaled), respectively. The CAVs initially follow the intelligent driver model controller [211], and switch to our proposed optimal control framework when entering the control zone. Each CAV then determines its optimal trajectory by solving 3.1.3 numerically. The CAV follows this optimal trajectory through the control zone. Upon exiting the control zone, it reverts to the intelligent driver model and loops back around toward the control zone entrance.

To facilitate data collection and fast analysis, we define a finite state machine for the experiment consisting of three states: *Starting*, *Running*, and *Waiting*. In the Starting state of the experiment, CAVs are released upstream of the considered traffic scenario (that is, roundabout) and drive towards the control zone. Once the first CAV enters the control zone,

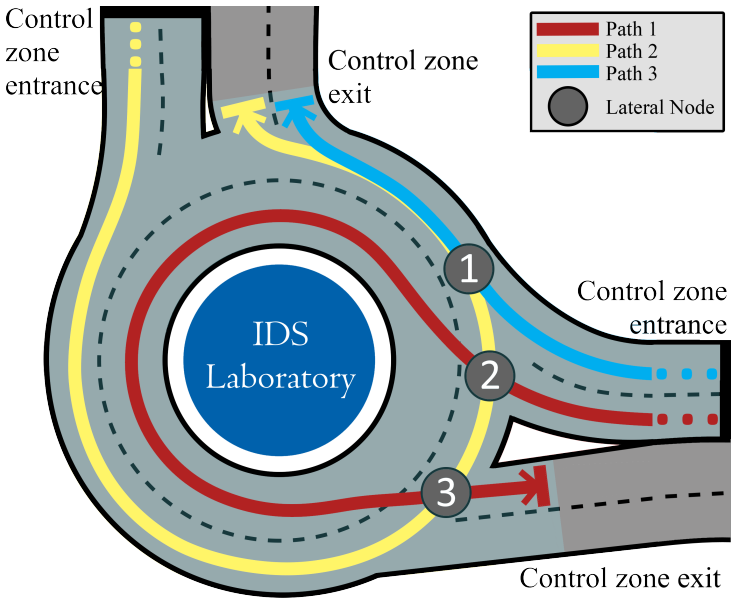

Figure 4.4: A schematic of the roundabout scenario. The highlighted control zone continues upstream from the roundabout at both entrances.

we log the current time and the state machine transitions to Running. In the Running state, we track the planned exit time and trajectory coefficients of each CAV that enters the control zone. Simultaneously, we log the state information of each CAV inside the control zone with a corresponding timestamp. Finally, when a CAV exits the control zone, we log the actual exit time, and, if it is the last CAV to exit the experiment, the state machine transitions to Waiting. Once all of the CAVs have exited the experiment and a sufficient number of CAVs have circled around to their initial positions, a user-specified countdown begins before the CAVs are released to start another experiment.

To automate the testing procedure, we developed a *queue sign*, which is analogous to a ramp metering signal. We use queue signs to precisely time the release of CAVs on each path during an experiment. The number of CAVs released by each queue sign is determined by user input, and it can be fixed or drawn from a discrete uniform distribution for each experiment. Once the required number of CAVs have formed a queue behind a queue sign, the experiment state machine is notified that it is ready for the experiment to begin. A schematic showing the behavior of the experiment and queue signs, as well as their connections, is

shown in Fig. 4.5. Once all queue signs have a sufficient number of CAVs accumulated, the state machine can transition from Waiting to Starting, wherein it will notify all queue signs to release CAVs. Each queue sign has a user-specified initial delay, which allows the arrival time of CAV to the control zone to be precisely selected. The initial delay can either be a fixed number or drawn from a user-supplied uniform distribution. Similarly, the time delay between the release of each CAV from a particular queue sign can be set to a fixed number or a uniform distribution. Once the queue sign has released the appropriate number of CAVs, it waits for the experiment to complete, and at that point, it selects the number of CAVs for the next experiment. This allows for little to no delay between experiments if the number of CAVs physically present in the testbed is greater than the number of CAVs required for any single experiment—potentially doubling the rate of data collection.

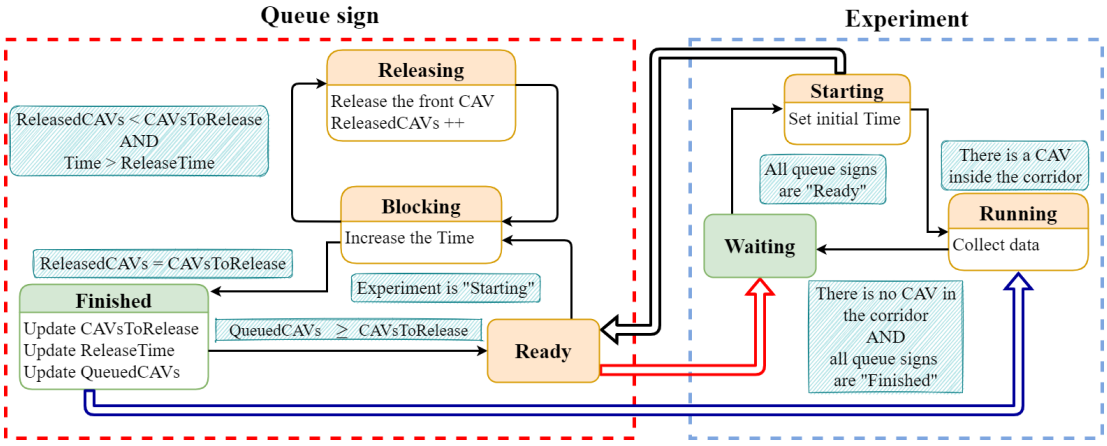

Figure 4.5: State machine diagrams of the experiment and queue sign. The starting states for experiment and queue sign state machines are colored green. Solid lines correspond to state transitions, and hollow lines correspond to communication between state machines.

For the roundabout experiments we used the following parameters: $v_{\max} = 0.5$ m/s (28 mph full scale), $v_{\min} = 0.15$ m/s (8.4 mph full scale), $u_{\max} = 0.45$ m/s^2 (11 m/s^2 full scale), and $u_{\min} = -u_{\max}$. To ensure safety, we select a time gap of 1.0 s and a minimum standstill distance of 0.07 m (approx. 1 car length). Our coordination framework has an average computation time of 2.14 ms, with a maximum of 3.4 ms when a CAV plans its trajectory. To quantify the effect of noise and disturbances acting on the system, we repeated

the experiment five times. Furthermore, we precisely timed the release of the CAVs into the roundabout such that lateral collisions would occur without intervention. Supplementary videos of the roundabout experiment can be found at https://sites.google.com/view/ud-ids-lab/csm.

Minimum and average speed and travel time results for the five experiments are summarized in Table 4.1. Note that the minimum speed of all CAVs is 0.12 m/s (7 mph at full scale) across all optimal control experiments, which demonstrates that stop and go driving has been completely eliminated. Additionally, the average speed of CAVs is 0.42 m/s (24 mph at full scale), which implies that most CAVs travel near $v_{\max} = 0.5$ m/s. The error between desired and actual exit time varies between $2 - 4\%$, which comes from the tracking error in the CAV's low-level controller.

Table 4.1: Minimum and average speed and travel time results for the 5 experiments. The root mean square error (RMSE) of the actual exit time compared to the desired exit time from the control zone averaged over all CAVs in each experiment is provided.

Experiment	$v_{\min}$ [m/s]	v_{avg} [m/s]	Travel Time RMSE
1	0.16	0.41	2.71 %
2	0.27	0.45	1.54 %
3	0.18	0.41	4.03 %
4	0.12	0.43	1.92 %
5	0.21	0.42	1.38 %

The exit time data for each CAV is visualized in Fig. 4.6, which demonstrates the variation between the simulated and actual behavior of each CAV. The grey bars represent the feasible space of t_i^f, the wide black bars correspond with the planned value of t_i^f, and the thin red bars show the actual value of t_i^f achieved by each CAV. This effect of tracking error is visible in Table 4.1, where the minimum achieved speed is slightly lower than the minimum speed imposed on the reference trajectory. Fig. 4.6 also demonstrates how some scenarios can lead to a very small feasible space, i.e., an exit time near the maximum. This can be seen in vehicles $17, 18$, and 27. This motivates the introduction of a regularization zone upstream, which could influence the initial state of each CAV in the control zone to enlarge its feasible space.

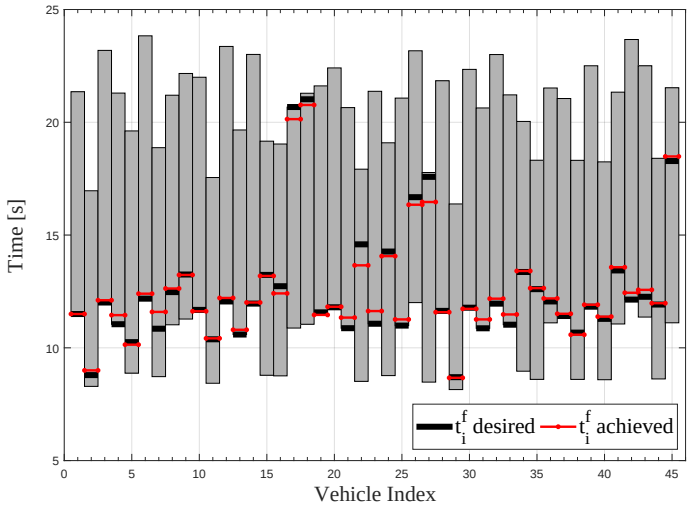

Figure 4.6: Planned and achieved exit time for each vehicle over all experiments. The grey bars shows the range of admissible t_i^f from the state and control constraints. Every 9 vehicles corresponds to a single experiment; they are sorted in ascending order by departure time from the control zone.

The position trajectory of an ego-CAV, which is selected to be the last CAV following path 2, is given in Fig. 4.7. The ego-CAV's position is denoted by the dashed red line, while the positions of two other CAVs are represented by dotted black lines. The lateral collision constraints are denoted by vertical black bars, and the rear-end safety constraint is the hashed region on the graph. There are two other CAVs shown; one is on path 3 and merges in front of the ego-CAV at node 1 (see Fig. 4.4) and a second CAV leads the ego-CAV on path 2. Fig. 4.7 demonstrates that, in a physical testbed, noise and disturbances play a significant role in the actual trajectory of the CAVs. The trajectory generated by the ego-vehicle did not lead to a physical collision, but it does violate the rear-end safety constraint by a car length. However, at that speed, the rear-end safety constraint required a three-car length gap, so a robust control formulation of 3.1.3 similar to 3.3.6 could likely guarantee collision avoidance. This can also be seen in the lateral collision avoidance constraint in Fig. 4.7, where a CAV later in the sequence crosses node 3 in a way that violates the time headway constraint (again, without leading to an actual collision). This further demonstrates the value of performing scaled experiments, where external physical factors, such as unmodeled dynamics and slip, can inform new research directions without the cost and risk associated with full-scale testing.

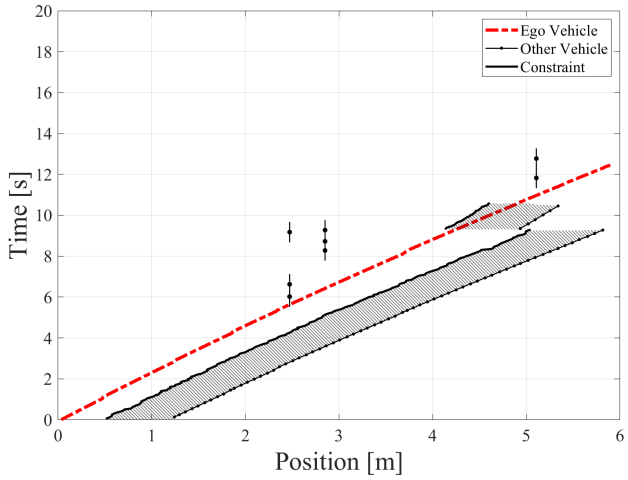

Figure 4.7: Position trajectory for the third vehicle entering from path 2 in the 5th experiment. The lateral constraints are shown as vertical lines, and the rear-end safety constraint is the hashed region.

Finally, the average, maximum, and minimum speed for each CAV across all experiments are given in Fig. 4.8. Each figure corresponds to a single path (see Fig. 4.4) and considers 15 CAVs (3 CAVs per path over five experiments). The CAVs' positions are taken directly from VICON and numerically derived using a first-order method. From Fig. 4.8, the average speed for CAVs on each path is very close to constant. Path 1 shows the most variance, which is due to the distance between collision nodes 2 and 3 on path 1 (see Fig. 4.4). In order for a CAV $i \in \mathcal{N}(t)$ that is traveling along path 1 to reduce its arrival time at node 2, it must make a proportionally larger reduction in the value of t_i^f. This is a side effect of enforcing the unconstrained trajectory on each CAV over the entire control zone. Additionally, the entrance to the control zone along path 3 follows a sharp right turn. This results in a relatively lower average speed in Fig. 4.8(c), as the dynamics of the CAVs reduce their speed while turning, causing them to enter the control zone at a lower initial speed. Finally, there are instances in Fig. 4.8(b) where the maximum vehicle speed surpasses the speed limit. This is a result of stochasticity in the vehicle dynamics and sensing equipment, as well as environmental disturbances, on our deterministic controller. This analysis motivates an enhanced trajectory generation framework that accounts for noise, disturbances, communication delay, and low-level tracking errors in the CAVs [175, 179].

Next, we present a high-level overview and analysis of our framework for a full transportation corridor in IDS^{3}C .

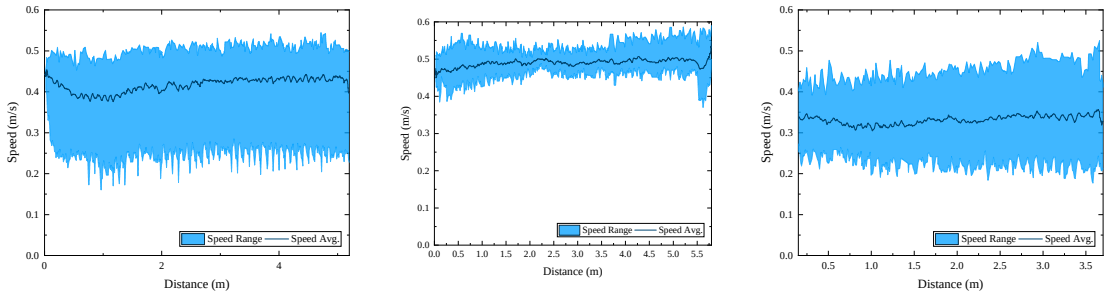

(a) (b) (c)

Figure 4.8: Speed range and average for all CAVs on (a) path 1, (b) path 2, and (c) path 3 across all experiments in the multi-lane roundabout.

4.3 Transportation Corridor

To demonstrate the single-level optimal coordination framework described in 3.1 for a transportation corridor in IDS^{3}C, we use a fleet of 15 CAVs. The corridor is shown in Fig. 4.9, where 3 ego-CAVs are released along the red path (starting in the northeast of the IDS^{3}C) and travel through a roundabout, an intersection, and a merging roadway. At each traffic scenario, we release 3 additional CAVs per path (as indicated in Fig. 4.9) to create congestion. The traffic scenarios were specifically selected so that upon entering the control zone, each CAV would have approximately 3 m (75 m scaled) to adjust their speed before reaching a conflict point. This also allowed us to consider each coordinator and control zone independently, as the control zone length was sufficiently long to neglect the influence of another upstream control zone.

In the baseline case, we replaced the roundabout and merging zone coordinators with yield signs. In both scenarios, the merging vehicles yield to any vehicle within 0.4 m of the merging zone (10 m scaled, approx. 4 car lengths). To manage the intersection, we implemented a four-way stop with a FIFO queue, that is, whenever a vehicle enters a line segment leading up to the intersection, it is added to the queue. When the merging zone

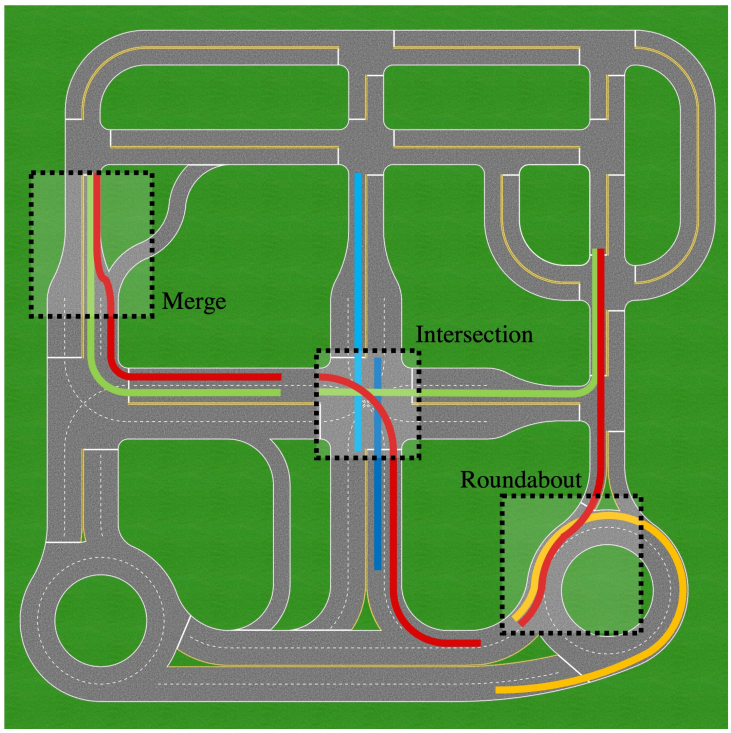

Figure 4.9: Corridor experiment where the ego-CAVs (red path) must navigate a roundabout, intersection, and merging roadway. The paths are only colored where they pass through a control zone, and the segments belonging to the same path have a shared color.

contains no vehicles, if the front vehicle has come to a complete stop, it is removed from the queue and allowed to pass through the merging zone. We have taken this approach to the intersection in order to avoid any bias that may be introduced into our results by the timing of a traffic light.

Finally, to ensure a fair comparison, we set the speed limit for the entire city to 0.5 m/s (approximately 30 mph scaled) in both tests. In our framework, we impose a maximum speed of 0.3 m/s (approx. 15 mph scaled) outside of the control zone. This ensures that the vehicles enter the control zone at a speed lower than $v_{\max}$, and gives them the opportunity to accelerate through the control zone. This decision was an insight from previous experiments in the IDS^{3}C. Reducing the initial speed of the vehicles below $v_{\max}$ at the entrance of the control zone generally leads to an larger feasible space for t_i^f.

Fig. 4.10 shows that despite the apparent advantage of the baseline case's higher

speed limit, the ego-CAV maintains a higher average speed in the optimal control case, and stop-and-go driving has been completely eliminated. Furthermore, Fig. 4.11 shows that the ego-CAVs do not activate any safety constraints throughout the experiment. Additional videos and figures of the experiment can be found at https://sites.google.com/view/ud-ids-lab/csm.

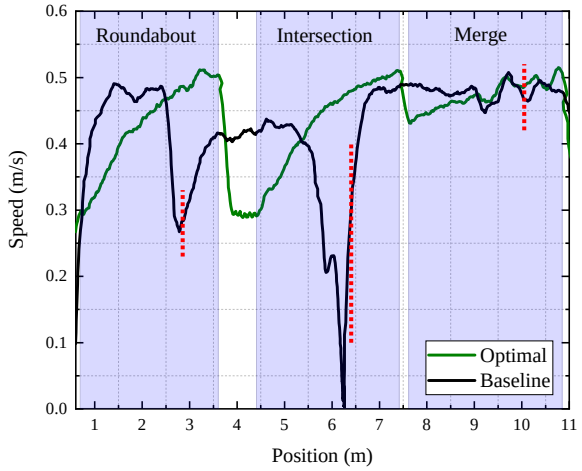

Figure 4.10: Speed vs position graph for the front ego vehicles in the optimal control and baseline cases. Blue highlighted areas are within each of the control zones in the optimal case, and the vertical dashed lines correspond to the location of stop and yield signs in the baseline case.

4.4 Summary

In this chapter, we first introduced the IDS^{3}C, a robotic scaled (1:25) testbed capable of safely validating control approaches beyond simulation in applications related to emerging mobility systems such as coordination of CAVs. Then, we demonstrated the effectiveness of coordination of CAVs at a multi-lane roundabout and we showed its scalability in a corridor consisting of a roundabout, an intersection, and a merging roadway.

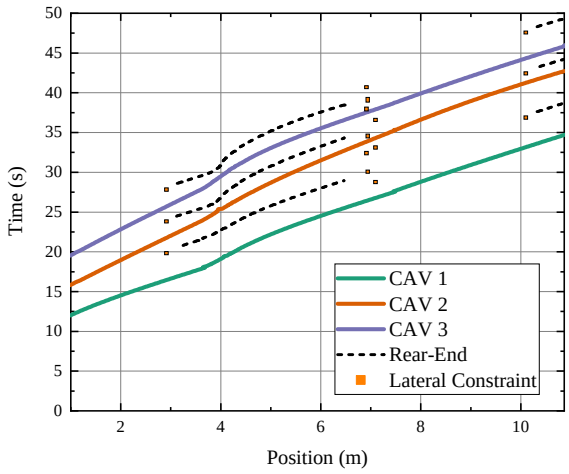

Figure 4.11: Time vs position graph for the ego CAVs in the optimal control case. Solid lines correspond to the CAV trajectories, dashed lines correspond to CAVs that merge onto the ego-path, and orange boxes correspond to time intervals when a lateral conflict point is occupied by another CAV.

Chapter 5

CONCLUSIONS AND FUTURE WORK

> If your tree bears the fruit of knowledge;
> you can govern the stars yourself.
>
> Naser Khosrow, *Diwan*, 1004–1088 CE

In Chapter 1, we completed the literature review and presented some major research gaps in the literature. In Chapter 2, we developed two different bi-level approaches for coordinating CAVs at adjacent signal-free intersections consisting of the upper-level and low-level planning. In the first approach, in the upper-level planning, each CAV recursively computes the energy-optimal arrival time at each intersection along its path, while ensuring both lateral and rear-end safety. Additionally, each CAV investigates the feasibility of a lane-changing maneuver and determines the optimal lane to occupy to the traffic throughput. Given the output of the upper-level planning, in the low-level planning, we formulated an optimal control problem for each CAV with the interior-point constraints, the solution of which yields the energy optimal control input (acceleration/deceleration). In addition, we enhanced our bi-level framework to guarantee safety in the presence of a bounded steady-state error in tracking the positions of CAVs. Finally, our proposed framework exhibited a reduction in fuel-consumption, traffic delay, and improvement in the travel time compared to the baseline scenario in different traffic volumes ranging from 600 veh/h to $1{,}400$ veh/h for both symmetric and asymmetric adjacent intersections.

Focusing on minimizing travel time and improving traffic throughput, in the second approach, we formulated the upper-level problem as a scheduling problem that each CAV solves upon entering the control zone. The upper-level problem's outcome becomes the input of the low-level problem, which is the tuple of optimal arrival time at each zone to avoid the

lateral and rear-end collision and minimize the CAV's travel time. In the low-level control, we formulated an optimal control problem, the solution of which yields the optimal control input and minimizes the transient engine operation. We derived an analytical solution for each zone that can be implemented in real time. Finally, we demonstrated the effectiveness of the proposed framework through simulation and comparison with signalized intersections, centralized scheduling, and FIFO queuing policy. Finally, in the last section of Chapter 2, we proposed a learning-based decentralized coordination framework for CAVs at a signal-free intersection to minimize travel delay and improve fuel consumption while ensuring rear-end and lateral safety. We introduced a coordination mechanism into our decentralized learning framework by using hysteretic Q-learning to update the Q-table of each CAV. We also integrated FIFO queuing policy in our framework to improve the performance of our system. Finally, we showed the effectiveness of our proposed approach through simulation and comparison with the optimal control techniques based on Pontryagin's minimum principle.

In Chapter 3, after reviewing a single-level coordination framework for CAVs proposed in [91], we provided three different approaches to enhance this framework in the presence of uncertainty. First, we integrated a replanning mechanism into our coordination framework, which can be implemented in a time-driven or event-driven manner. This embedded replanning aims at introducing indirect feedback into the coordination framework to respond to the unexpected changes in the system to some extent. Additionally, using the theory of the job-shop scheduling problem, we further enhanced our decentralized coordination framework by introducing a priority-aware resequencing mechanism, which designates the order of decision making. This enhancement advances the state of the art in a way that relaxes the FCFS decision making sequence of the CAVs. Second, we reformulated the motion-planning framework for CAVs at a signal-free intersection as a robust coordination problem by including the deviations from the nominal trajectories as uncertainty. We adopted the data-driven approach, GP regression, to learn the uncertainty from the possibly noisy observation of CAVs' time trajectories. After obtaining the statistical knowledge about the deviation from nominal trajectories, we constructed the confidence interval for time, position, and speed trajectories

using the inverse error function, Chebyshev's inequality, and Vysochanskii-Petunin inequality, respectively. Finally, we enhanced the motion planning framework for coordination of CAVs at a signal-free intersection through employing control barrier functions (CBFs) to provide an additional safety layer and ensure the satisfaction of all constraints in the system. By using the proposed framework in the motion planning module, each CAV first uses simple longitudinal dynamics to derive the optimal control trajectory without activating any constraint. In a real physical system, we require a vehicle-level controller to track the resulting optimal trajectory. However, due to the inherent deviations between the actual trajectory and the planned trajectory, the system's constraints may become active. We addressed this issue by introducing a barrier-certificate module based on a more realistic dynamics as a safety middle layer between the vehicle-level tracking controller and physical vehicle to provide a reactive mechanism to guarantee constraint satisfaction in the system.

In Chapter 4, we introduced Information and Decision Science Lab's Scaled Smart City (IDS^{3}C), a robotic scaled (1:25) testbed capable of safely validating control approaches beyond simulation in applications related to emerging mobility systems such as coordination of CAVs. Then, we demonstrated the effectiveness of coordination of CAVs at a multi-lane roundabout and we showed its scalability in a corridor consisting of a roundabout, an intersection, and a merging roadway.

The contributions of this dissertation are summarized as follows:

1. Development of a bi-level coordination framework for CAVs at multiple adjacent multi-lane signal-free intersections closely distanced from each other aimed at improving traffic throughput and minimizing energy consumption (Chapter 2).
2. Establishment of a decentralized coordination framework for CAVs at a signal-free intersection through combining FIFO queuing policy and hysteretic Q-learning (Chapter 2).
3. Integrating replanning and resequencing mechanisms into the coordination framework to introduce feedback and relax FCFS decision sequence (Chapter 3).
4. Development of a robust coordination framework by learning deviation from the nominal trajectory online using Gaussian process (Chapter 3).

5. Introducing a safety-layer into the coordination framework of CAVs at a signal-free intersection using CBFs (Chapter 3).
6. Validating the coordination framework for CAVs at different traffic scenarios in a scaled environment (Chapter 4).

These research contributions together result in a mathematically rigorous framework for the online coordination of CAVs in different traffic scenarios. This dissertation advances the state of the art in utilizing CAVs in real-world traffic scenarios to alleviate congestion, improve traffic throughput, and increase passenger safety.

5.1 Future Work

Several studies have developed eco-driving approaches for signalized intersections under mixed-traffic scenarios [212–214]. However, coordination for mixed-traffic scenarios and the interaction of human-driven vehicles and CAVs are still open research questions and potential directions for future research. A recent approach proposed in [26, 28] explored forming platoons using CAVs to indirectly control human-driven vehicles. Future studies should investigate the coordination of platoons of mixed-vehicle in traffic scenarios. Another possible direction is to model human-driven vehicles as uncertainty or disturbances for the CAVs and extend the coordination framework to consider this uncertainty.

Our proposed RL-based coordination framework for CAVs at a signal-free intersection through combining FIFO queuing policy and hysteretic Q-learning can be extended in several ways. Future research should examine exploring the convergence properties of the proposed learning framework. Another future direction is integrating a safety layer based on CBFs into the RL-based coordination framework to ensure safety during the training and after deployment.

This dissertation assumed that CAVs can communicate with other CAVs and the coordinator without errors, communication delays, or packet loss. For a scenario of vehicle platooning at a highway on-ramp merging, we explored the effect of delayed communication among the CAV platoons and proposed a robust framework in the presence of bounded delays

[30]. A potential future direction would be to extend the proposed coordination framework in this dissertation to be robust in the presence of communication delay or packet loss. Future research should also investigate online learning techniques to characterize the bounds of communication delays. Another potential direction is to explore other communication structures, such as word-of-mouth communication [215], where each CAV may directly communicate only with a subset of CAVs in the control zone or nested information structure [216–218], where information flow among CAVs is not bidirectional.

In our resequencing framework, we assumed that each path of a CAV cannot get either split into two paths or merged by another CAV's path. One can investigate relaxing this assumption and establish a computationally efficient algorithm for the general case in future work. Additionally, the main benefit of our resequencing framework lies in providing a systematic framework to relax the FCFS sequence in decision making. This would be useful if one needs to prioritize some CAVs over other CAVs, such as giving higher priority to vehicles with higher passenger capacity or emergency vehicles. One future direction is to explore the implications of the resequencing framework to incentivize people to use other modes of transportation through mechanism design [219–222].

BIBLIOGRAPHY

[1] United Nations. 2018 revision of world urbanization prospects, 2018.

[2] D. Schrank, B. Eisele, L. Albert, and T Lomax. 2021 Urban Mobility Scorecard. Technical report, Texas A& M Transportation Institute, 2021.

[3] Timothy Stewart. Overview of motor vehicle crashes in 2020. Technical Report DOT HS 813 266, National Center for Statistics and Analysis, March, 2022.

[4] Santokh Singh. Critical reasons for crashes investigated in the national motor vehicle crash causation survey (traffic safety facts crash stats.). Technical Report DOT HS 812 506, National Highway Traffic Safety Administration, March, 2018.

[5] Liuhui Zhao and Andreas A Malikopoulos. Enhanced mobility with connectivity and automation: A review of shared autonomous vehicle systems. *IEEE Intelligent Transportation Systems Magazine*, 14(1):87–102, 2022.

[6] Dimitris Milakis, Laura Gedhardt, Daniel Ehebrecht, and Barbara Lenz. Is micro-mobility sustainable? an overview of implications for accessibility, air pollution, safety, physical activity and subjective wellbeing. *Handbook of sustainable transport*, 2020.

[7] Xiaopeng Shaw Li, Xiaobo Qu, Joseph YJ Chow, Monica Menendez, and Zhen Sean Qian. Emerging mobility systems [guest editorial]. *IEEE Intelligent Transportation Systems Magazine*, 11(3):8–11, 2019.

[8] Zia Wadud, Don MacKenzie, and Paul Leiby. Help or hindrance? the travel, energy and carbon impacts of highly automated vehicles. *Transportation Research Part A: Policy and Practice*, 86:1–18, 2016.

[9] Ido Klein and Eran Ben-Elia. Emergence of cooperation in congested road networks using ICT and future and emerging technologies: A game-based review. *Transportation Research Part C: Emerging Technologies*, 72:10–28, 2016.

[10] Sandra Melo, Joaquim Macedo, and Patrícia Baptista. Guiding cities to pursue a smart mobility paradigm: An example from vehicle routing guidance and its traffic and operational effects. *Research in Transportation Economics*, 65:24–33, 2017.

[11] Danyang Tian, Guoyuan Wu, Kanok Boriboonsomsin, and Matthew J Barth. Performance measurement evaluation framework and co-benefit/tradeoff analysis for connected and automated vehicles (cav) applications: A survey. *IEEE Intelligent Transportation Systems Magazine*, 10(3):110–122, 2018.

[12] Kevin Spieser, Kyle Treleaven, Rick Zhang, Emilio Frazzoli, Daniel Morton, and Marco Pavone. Toward a systematic approach to the design and evaluation of automated mobility-on-demand systems: A case study in singapore. In *Road vehicle automation*, pages 229–245. Springer, 2014.

[13] S. E. Shladover, C. A. Desoer, J. K. Hedrick, M. Tomizuka, J. Walrand, W.-B. Zhang, D. H. McMahon, H. Peng, S. Sheikholeslam, and N. McKeown. Automated vehicle control developments in the PATH program. *IEEE Transactions on Vehicular Technology*, 40(1):114–130, 1991.

[14] Pravin Varaiya. Smart cars on smart roads: problems of control. *IEEE Transactions on automatic control*, 38(2):195–207, 1993.

[15] R. Rajamani, H.-S. Tan, B. K. Law, and W.-B. Zhang. Demonstration of integrated longitudinal and lateral control for the operation of automated vehicles in platoons. *IEEE Transactions on Control Systems Technology*, 8(4):695–708, 2000.

[16] Sebastian Van De Hoef, Karl Henrik Johansson, and Dimos V Dimarogonas. Fuel-efficient en route formation of truck platoons. *IEEE Transactions on Intelligent Transportation Systems*, 19(1):102–112, 2017.

[17] Ziran Wang, Guoyuan Wu, Peng Hao, Kanok Boriboonsomsin, and Matthew Barth. Developing a platoon-wide eco-cooperative adaptive cruise control (cacc) system. In *2017 ieee intelligent vehicles symposium (iv)*, pages 1256–1261. IEEE, 2017.

[18] Alexander Johansson, Ehsan Nekouei, Karl Henrik Johansson, and Jonas Mårtensson. Multi-fleet platoon matching: A game-theoretic approach. In *2018 21st International Conference on Intelligent Transportation Systems (ITSC)*, pages 2980–2985. IEEE, 2018.

[19] Sogand Karbalaieali, Osama A Osman, and Sherif Ishak. A dynamic adaptive algorithm for merging into platoons in connected automated environments. *IEEE Transactions on Intelligent Transportation Systems*, 21(10):4111–4122, 2019.

[20] Shengyue Yao and Bernard Friedrich. Managing connected and automated vehicles in mixed traffic by human-leading platooning strategy: a simulation study. In *2019 IEEE Intelligent Transportation Systems Conference (ITSC)*, pages 3224–3229. IEEE, 2019.

[21] Xi Xiong, Erdong Xiao, and Li Jin. Analysis of a stochastic model for coordinated platooning of heavy-duty vehicles. In *2019 IEEE 58th Conference on Decision and Control (CDC)*, pages 3170–3175. IEEE, 2019.

[22] Nadia Pourmohammad-Zia, Frederik Schulte, and Rudy R Negenborn. Platform-based platooning to connect two autonomous vehicle areas. In *2020 IEEE 23rd International Conference on Intelligent Transportation Systems (ITSC)*, pages 1–6. IEEE, 2020.

[23] Tyler Ard, Faraz Ashtiani, Ardalan Vahidi, and Hoseinali Borhan. Optimizing gap tracking subject to dynamic losses via connected and anticipative mpc in truck platooning. In *2020 American Control Conference (ACC)*, pages 2300–2305. IEEE, 2020.

[24] S.D. Kumaravel, Andreas A Malikopoulos, and R. Ayyagari. Decentralized cooperative merging of platoons of connected and automated vehicles at highway on-ramps. In *2021 American Control Conference (ACC)*, pages 2055–2060, 2021. ISBN 2378-5861.

[25] S.D. Kumaravel, Andreas A Malikopoulos, and R. Ayyagari. Optimal coordination of platoons of connected and automated vehicles at signal-free intersections. *IEEE Transactions on Intelligent Vehicles*, pages 1–1, 2021.

[26] A M Ishtiaque Mahbub and Andreas A Malikopoulos. A Platoon Formation Framework in a Mixed Traffic Environment. *IEEE Control Systems Letters (LCSS)*, 6:1370–1375, 2021.

[27] Anirudh Kishore Bhoopalam, Niels Agatz, and Rob Zuidwijk. Planning of truck platoons: A literature review and directions for future research. *Transportation research part B: methodological*, 107:212–228, 2018.

[28] A M Ishtiaque Mahbub and Andreas A. Malikopoulos. Platoon Formation in a Mixed Traffic Environment: A Model-Agnostic Optimal Control Approach. *Proceedings of 2022 American Control Conference (ACC)*, pages 4746–4751, 2022.

[29] Logan E. Beaver and Andreas A. Malikopoulos. Constraint-driven optimal control of multi-agent systems: A highway platooning case study. *IEEE Control Systems Letters*, 6:1754–1759, 2022.

[30] A M Ishtiaque Mahbub, Behdad Chalaki, and Andreas A Malikopoulos. A constrained optimal control framework for vehicle platoons with delayed communication. *Network and Heterogeneous Media, Special Issue: Traffic and Autonomy*, 2022 (accepted).

[31] Raphael E Stern, Shumo Cui, Maria Laura Delle Monache, Rahul Bhadani, Matt Bunting, Miles Churchill, Nathaniel Hamilton, Hannah Pohlmann, Fangyu Wu, Benedetto Piccoli, et al. Dissipation of stop-and-go waves via control of autonomous vehicles: Field experiments. *Transportation Research Part C: Emerging Technologies*, 89:205–221, 2018.

[32] W.S. Levine and M. Athans. On the optimal error regulation of a string of moving vehicles. *IEEE Transactions on Automatic Control*, 11(3):355–361, 1966.

[33] Michael Athans. A unified approach to the vehicle-merging problem. *Transportation Research*, 3(1):123–133, 1969.

[34] Jackeline Rios-Torres and Andreas A. Malikopoulos. A Survey on Coordination of Connected and Automated Vehicles at Intersections and Merging at Highway On-Ramps. *IEEE Transactions on Intelligent Transportation Systems*, 18(5):1066–1077, 2017.

[35] K. Dresner and P. Stone. Multiagent traffic management: a reservation-based intersection control mechanism. In *Proceedings of the Third International Joint Conference on Autonomous Agents and Multiagents Systems*, pages 530–537, 2004.

[36] Kurt Dresner and Peter Stone. A Multiagent Approach to Autonomous Intersection Management. *Journal of Artificial Intelligence Research*, 31:591–653, 2008.

[37] Matthew Hausknecht, Tsz-Chiu Au, and Peter Stone. Autonomous intersection management: Multi-intersection optimization. In *2011 IEEE/RSJ International Conference on Intelligent Robots and Systems*, pages 4581–4586. IEEE, 2011.

[38] Qiu Jin, Guoyuan Wu, Kanok Boriboonsomsin, and Matthew Barth. Multi-agent intersection management for connected vehicles using an optimal scheduling approach. In *2012 International Conference on Connected Vehicles and Expo (ICCVE)*, pages 185–190. IEEE, 2012.

[39] Michael W Levin, Hagen Fritz, and Stephen D Boyles. On optimizing reservation-based intersection controls. *IEEE Transactions on Intelligent Transportation Systems*, 18(3):505–515, 2016.

[40] Shan Huang, Adel W. Sadek, and Yunjie Zhao. Assessing the Mobility and Environmental Benefits of Reservation-Based Intelligent Intersections Using an Integrated Simulator. *IEEE Transactions on Intelligent Transportation Systems*, 13(3):1201–1214, 2012.

[41] Arnaud de La Fortelle. Analysis of reservation algorithms for cooperative planning at intersections. *13th International IEEE Conference on Intelligent Transportation Systems*, pages 445–449, September 2010.

[42] Aleksandar Stevanovic and Nikola Mitrovic. Combined alternate-direction lane assignment and reservation-based intersection control. In *2018 21st International Conference on Intelligent Transportation Systems (ITSC)*, pages 14–19. IEEE, 2018.

[43] Joyoung Lee and Byungkyu Park. Development and evaluation of a cooperative vehicle intersection control algorithm under the connected vehicles environment. *IEEE Transactions on Intelligent Transportation Systems*, 13(1):81–90, 2012.

[44] Joyoung Lee, Byungkyu Brian Park, Kristin Malakorn, and Jaehyun Jason So. Sustainability assessments of cooperative vehicle intersection control at an urban corridor. *Transportation Research Part C: Emerging Technologies*, 32:193–206, 2013.

[45] Jean Gregoire, Silvere Bonnabel, and Arnaud De La Fortelle. Priority-based intersection management with kinodynamic constraints. In *2014 European Control Conference (ECC)*, pages 2902–2907. IEEE, 2014.

[46] Youssef Bichiou and Hesham A Rakha. Developing an optimal intersection control system for automated connected vehicles. *IEEE Transactions on Intelligent Transportation Systems*, 20(5):1908–1916, 2018.

[47] Huile Xu, Yi Zhang, Li Li, and Weixia Li. Cooperative driving at unsignalized intersections using tree search. *IEEE Transactions on Intelligent Transportation Systems*, 21(11):4563–4571, 2019.

[48] John Borek, Ben Groelke, Christian Earnhardt, and Chris Vermillion. Economic optimal control for minimizing fuel consumption of heavy-duty trucks in a highway environment. *IEEE Transactions on Control Systems Technology*, 28(5):1652–1664, 2019.

[49] Zhiyuan Du, Baisravan HomChaudhuri, and Pierluigi Pisu. Hierarchical distributed coordination strategy of connected and automated vehicles at multiple intersections. *Journal of Intelligent Transportation Systems*, 22(2):144–158, 2018.

[50] Md Abdus Samad Kamal, Jun-ichi Imura, Tomohisa Hayakawa, Akira Ohata, and Kazuyuki Aihara. A vehicle-intersection coordination scheme for smooth flows of traffic without using traffic lights. *IEEE Transactions on Intelligent Transportation Systems*, 16(3):1136–1147, 2014.

[51] Alessandro Colombo and Domitilla Del Vecchio. Least restrictive supervisors for intersection collision avoidance: A scheduling approach. *IEEE Transactions on Automatic Control*, 60(6):1515–1527, 2014.

[52] Heejin Ahn, Alessandro Colombo, and Domitilla Del Vecchio. Supervisory control for intersection collision avoidance in the presence of uncontrolled vehicles. In *2014 American Control Conference*, pages 867–873. IEEE, 2014.

[53] Gabriel Rodrigues De Campos, Fabio Della Rossa, and Alessandro Colombo. Optimal and least restrictive supervisory control: Safety verification methods for human-driven vehicles at traffic intersections. *Proceedings of the IEEE Conference on Decision and Control*, pages 1707–1712, 2015.

[54] Heejin Ahn and Domitilla Del Vecchio. Semi-autonomous Intersection Collision Avoidance through Job-shop Scheduling. *Proceedings of the 19th International Conference on Hybrid Systems: Computation and Control - HSCC '16*, pages 185–194, 2016.

[55] Seyed Alireza Fayazi and Ardalan Vahidi. Mixed-integer linear programming for optimal scheduling of autonomous vehicle intersection crossing. *IEEE Transactions on Intelligent Vehicles*, 3(3):287–299, 2018.

[56] Chunhui Yu, Yiheng Feng, Henry X Liu, Wanjing Ma, and Xiaoguang Yang. Corridor level cooperative trajectory optimization with connected and automated vehicles. *Transportation Research Part C: Emerging Technologies*, 105:405–421, 2019.

[57] Mehmet Ali Guney and Ioannis A Raptis. Scheduling-based optimization for motion coordination of autonomous vehicles at multilane intersections. *Journal of Robotics*, 2020, 2020.

[58] Laleh Makarem and Denis Gillet. Fluent coordination of autonomous vehicles at intersections. *2012 IEEE International Conference on Systems, Man, and Cybernetics (SMC)*, pages 2557–2562, October 2012.

[59] Weigang Wu, Jiebin Zhang, Aoxue Luo, and Jiannong Cao. Distributed mutual exclusion algorithms for intersection traffic control. *IEEE Transactions on Parallel and Distributed Systems*, 26(1):65–74, 2014.

[60] Reza Azimi, Gaurav Bhatia, Ragunathan Raj Rajkumar, and Priyantha Mudalige. STIP: Spatio-temporal intersection protocols for autonomous vehicles. In *2014 ACM/IEEE International Conference on Cyber-Physical Systems (ICCPS)*, pages 1–12. IEEE, 2014.

[61] Robert Hult, Mario Zanon, Sebastien Gros, and Paolo Falcone. Optimal coordination of automated vehicles at intersections: Theory and experiments. *IEEE Transactions on Control Systems Technology*, 27(6):2510–2525, 2018.

[62] Kyoung-Dae Kim and Panganamala Ramana Kumar. An MPC-based approach to provable system-wide safety and liveness of autonomous ground traffic. *IEEE Transactions on Automatic Control*, 59(12):3341–3356, 2014.

[63] Gabriel R Campos, Paolo Falcone, Henk Wymeersch, Robert Hult, and Jonas Sjöberg. Cooperative receding horizon conflict resolution at traffic intersections. In *53rd IEEE Conference on Decision and Control*, pages 2932–2937. IEEE, 2014.

[64] Maximilian Kloock, Patrick Scheffe, Sascha Marquardt, Janis Maczijewski, Bassam Alrifaee, and Stefan Kowalewski. Distributed model predictive intersection control of multiple vehicles. In *2019 IEEE Intelligent Transportation Systems Conference (ITSC)*, pages 1735–1740. IEEE, 2019.

[65] A A Malikopoulos, Christos G Cassandras, and Y Zhang. A decentralized energy-optimal control framework for connected automated vehicles at signal-free intersections. *Automatica*, 93:244–256, 2018.

[66] J. Rios-Torres, Andreas A Malikopoulos, and Pierluigi Pisu. Online Optimal Control of Connected Vehicles for Efficient Traffic Flow at Merging Roads. In *2015 IEEE 18th International Conference on Intelligent Transportation Systems*, pages 2432–2437, 2015.

[67] Jackeline Rios-Torres and Andreas A Malikopoulos. Automated and Cooperative Vehicle Merging at Highway On-Ramps. *IEEE Transactions on Intelligent Transportation Systems*, 18(4):780–789, 2017.

[68] Ioannis A Ntousakis, Ioannis K Nikolos, and Markos Papageorgiou. Optimal vehicle trajectory planning in the context of cooperative merging on highways. *Transportation Research Part C: Emerging Technologies*, 71:464–488, 2016.

[69] A M Ishtiaque Mahbub, Liuhui Zhao, Dimitris Assanis, and Andreas A Malikopoulos. Energy-Optimal Coordination of Connected and Automated Vehicles at Multiple Intersections. In *Proceedings of 2019 American Control Conference*, pages 2664–2669, 2019.

[70] Behdad Chalaki and Andreas A Malikopoulos. An optimal coordination framework for connected and automated vehicles in two interconnected intersections. In *2019 IEEE Conference on Control Technology and Applications (CCTA)*, pages 888–893. IEEE, 2019.

[71] Liuhui Zhao, Andreas A Malikopoulos, and Jackeline Rios-Torres. Optimal control of connected and automated vehicles at roundabouts: An investigation in a mixed-traffic environment. In *15th IFAC Symposium on Control in Transportation Systems*, pages 73–78, 2018.

[72] A M Ishtiaque Mahbub, Andreas A Malikopoulos, and L. Zhao. Impact of connected and automated vehicles in a corridor. In *Proceedings of 2020 American Control Conference, 2020*, pages 1185–1190. IEEE, 2020.

[73] AM Ishtiaque Mahbub, Andreas A Malikopoulos, and Liuhui Zhao. Decentralized optimal coordination of connected and automated vehicles for multiple traffic scenarios. *Automatica*, 117(108958), 2020.

[74] Adam Stager, L. Bhan, Andreas A Malikopoulos, and Liuhui Zhao. A scaled smart city for experimental validation of connected and automated vehicles. In *15th IFAC Symposium on Control in Transportation Systems*, pages 130–135, 2018.

[75] Logan E Beaver, Behdad Chalaki, A M Mahbub, Liuhui Zhao, Ray Zayas, and Andreas A Malikopoulos. Demonstration of a Time-Efficient Mobility System Using a Scaled Smart City. *Vehicle System Dynamics*, 58(5):787–804, 2020.

[76] A M Ishtiaque Mahbub, V. Karri, Darshil Parikh, S. Jade, and Andreas A Malikopoulos. A decentralized time- and energy-optimal control framework for connected automated

vehicles: From simulation to field test. In *SAE Technical Paper 2020-01-0579*. SAE International, 2020.

[77] Andreas A Malikopoulos and Liuhui Zhao. A closed-form analytical solution for optimal coordination of connected and automated vehicles. In *2019 American Control Conference (ACC)*, pages 3599–3604. IEEE, 2019.

[78] Yue Zhang and Christos G Cassandras. Decentralized optimal control of connected automated vehicles at signal-free intersections including comfort-constrained turns and safety guarantees. *Automatica*, 109:108563, 2019.

[79] Y. Zhang and C. G. Cassandras. Joint time and energy-optimal control of connected automated vehicles at signal-free intersections with speed-dependent safety guarantees. In *2019 IEEE 58th Conference on Decision and Control (CDC)*, pages 329–334, 2019.

[80] Wei Xiao and Christos G Cassandras. Decentralized optimal merging control for connected and automated vehicles with safety constraint guarantees. *Automatica*, 123: 109333, 2021.

[81] Gabriel Rodrigues de Campos, Paolo Falcone, and Jonas Sjöberg. Autonomous cooperative driving: a velocity-based negotiation approach for intersection crossing. In *16th International IEEE Conference on Intelligent Transportation Systems (ITSC 2013)*, pages 1456–1461. IEEE, 2013.

[82] Bassam Alrifaee, Frank-Josef Heßeler, and Dirk Abel. Coordinated non-cooperative distributed model predictive control for decoupled systems using graphs. *IFAC-PapersOnLine*, 49(22):216–221, 2016.

[83] Yue Zhang and Christos G Cassandras. A decentralized optimal control framework for connected automated vehicles at urban intersections with dynamic resequencing. In *2018 IEEE Conference on Decision and Control (CDC)*, pages 217–222. IEEE, 2018.

[84] Wei Xiao and Christos G Cassandras. Decentralized optimal merging control for connected and automated vehicles with optimal dynamic resequencing. In *2020 American Control Conference (ACC)*, pages 4090–4095. IEEE, 2020.

[85] A M Ishtiaque Mahbub and Andreas A Malikopoulos. Conditions for state and control constraint activation in coordination of connected and automated vehicles. *Proceedings of 2020 American Control Conference*, pages 436–441, 2020.

[86] A M Ishtiaque Mahbub and Andreas A Malikopoulos. Conditions to Provable System-Wide Optimal Coordination of Connected and Automated Vehicles. *Automatica*, 131 (109751), 2021.

[87] A. A. Malikopoulos, S. Hong, B. B. Park, J. Lee, and S. Ryu. Optimal control for speed harmonization of automated vehicles. *IEEE Transactions on Intelligent Transportation Systems*, 20(7):2405–2417, 2019.

[88] Wei Xiao and Christos G Cassandras. Decentralized optimal merging control for connected and automated vehicles. In *2019 American Control Conference (ACC)*, pages 3315–3320. IEEE, 2019.

[89] Wei Xiao and Christos G Cassandras. Conditions for improving the computational efficiency of decentralized optimal merging controllers for connected and automated vehicles. In *2019 IEEE 58th Conference on Decision and Control (CDC)*, pages 3158–3163. IEEE, 2019.

[90] Andreas A Malikopoulos and Liuhui Zhao. Optimal path planning for connected and automated vehicles at urban intersections. In *Proceedings of the 58th IEEE Conference on Decision and Control, 2019*, pages 1261–1266. IEEE, 2019.

[91] Andreas A Malikopoulos, Logan E Beaver, and Ioannis Vasileios Chremos. Optimal time trajectory and coordination for connected and automated vehicles. *Automatica*, 125(109469), 2021.

[92] Behdad Chalaki, Logan E Beaver, and Andreas A Malikopoulos. Experimental validation of a real-time optimal controller for coordination of cavs in a multi-lane roundabout. In *31st IEEE Intelligent Vehicles Symposium (IV)*, pages 504–509, 2020.

[93] Behdad Chalaki, Logan E. Beaver, A M Ishtiaque Mahbub, Heeseung Bang, and Andreas A. Malikopoulos. A research and educational robotic testbed for real-time control of emerging mobility systems: From theory to scaled experiments. *IEEE Control Systems Magazine*, 2022 (in press).

[94] Amir Mirheli, Mehrdad Tajalli, Leila Hajibabai, and Ali Hajbabaie. A consensus-based distributed trajectory control in a signal-free intersection. *Transportation research part C: emerging technologies*, 100:161–176, 2019.

[95] Enrique Onieva, Vicente Milanés, Jorge Villagra, Joshué Pérez, and Jorge Godoy. Genetic optimization of a vehicle fuzzy decision system for intersections. *Expert Systems with Applications*, 39(18):13148–13157, 2012.

[96] David Miculescu and Sertac Karaman. Polling-systems-based control of high-performance provably-safe autonomous intersections. In *Decision and Control (CDC), 2014 IEEE 53rd Annual Conference on*, pages 1417–1423. IEEE, 2014.

[97] Ismail H Zohdy and Hesham Rakha. Game theory algorithm for intersection-based cooperative adaptive cruise control (cacc) systems. In *Intelligent Transportation Systems (ITSC), 2012 15th International IEEE Conference on*, pages 1097–1102. IEEE, 2012.

[98] Jacopo Guanetti, Yeojun Kim, and Francesco Borrelli. Control of connected and automated vehicles: State of the art and future challenges. *Annual Reviews in Control*, 45:18–40, 2018.

[99] Richard S Sutton and Andrew G Barto. *Reinforcement learning: An introduction*. MIT press, 2018.

[100] Bahare Kiumarsi, Kyriakos G Vamvoudakis, Hamidreza Modares, and Frank L Lewis. Optimal and autonomous control using reinforcement learning: A survey. *IEEE transactions on neural networks and learning systems*, 29(6):2042–2062, 2017.

[101] Christopher John Cornish Hellaby Watkins. *Learning from Delayed Rewards*. PhD thesis, King's College, Cambridge, UK, May 1989. URL http://www.cs.rhul.ac.uk/~chrisw/new_thesis.pdf.

[102] Samah El-Tantawy and Baher Abdulhai. An agent-based learning towards decentralized and coordinated traffic signal control. In *13th International IEEE Conference on Intelligent Transportation Systems*, pages 665–670. IEEE, 2010.

[103] Xiaofeng Ji and Zenghui He. An optimal control method for expressways entering ramps metering based on q-learning. In *2009 Second International Conference on Intelligent Computation Technology and Automation*, volume 1, pages 739–741. IEEE, 2009.

[104] Céline Jacob and Baher Abdulhai. Integrated traffic corridor control using machine learning. In *2005 IEEE International Conference on Systems, Man and Cybernetics*, volume 4, pages 3460–3465. IEEE, 2005.

[105] Mohsen Davarynejad, Andreas Hegyi, Jos Vrancken, and Jan van den Berg. Motorway ramp-metering control with queuing consideration using q-learning. In *2011 14th International IEEE Conference on Intelligent Transportation Systems (ITSC)*, pages 1652–1658. IEEE, 2011.

[106] Edouard Ivanjko, Daniela Koltovska Nečoska, Martin Gregurić, Miroslav Vujić, Goran Jurković, and Sadko Mandžuka. Ramp metering control based on the q-learning algorithm. *Cybernetics and Information Technologies*, 15(5):88–97, 2015.

[107] Long Wang, Fangmin Ye, Yibing Wang, Jingqiu Guo, Ioannis Papamichail, Markos Papageorgiou, Simon Hu, and Lihui Zhang. A q-learning foresighted approach to ego-efficient lane changes of connected and automated vehicles on freeways. In *2019 IEEE Intelligent Transportation Systems Conference (ITSC)*, pages 1385–1392. IEEE, 2019.

[108] Daniel Chi Kit Ngai and Nelson Hon Ching Yung. A multiple-goal reinforcement learning method for complex vehicle overtaking maneuvers. *IEEE Transactions on Intelligent Transportation Systems*, 12(2):509–522, 2011.

[109] Yuanyuan Wu, Haipeng Chen, and Feng Zhu. Dcl-aim: Decentralized coordination learning of autonomous intersection management for connected and automated vehicles. *Transportation Research Part C: Emerging Technologies*, 103:246–260, 2019.

[110] Volodymyr Mnih, Koray Kavukcuoglu, David Silver, Alex Graves, Ioannis Antonoglou, Daan Wierstra, and Martin Riedmiller. Playing atari with deep reinforcement learning. *arXiv preprint arXiv:1312.5602*, 2013.

[111] Salaheldeen MS Seliman, Adel W Sadek, and Qing He. Automated vehicle control at freeway lane-drops: a deep reinforcement learning approach. *Journal of Big Data Analytics in Transportation*, pages 1–20, 2020.

[112] David Isele and Akansel Cosgun. To go or not to go: a case for q-learning at unsignalized intersections. *International Conference on Machine Learning (ICML)*, 2017.

[113] Tommy Tram, Anton Jansson, Robin Grönberg, Mohammad Ali, and Jonas Sjöberg. Learning negotiating behavior between cars in intersections using deep q-learning. In *2018 21st International Conference on Intelligent Transportation Systems (ITSC)*, pages 3169–3174. IEEE, 2018.

[114] Dingbo He, Yuan Zou, Jinlong Wu, Xudong Zhang, Zhigang Zhang, and Ruizhi Wang. Deep q-learning based energy management strategy for a series hybrid electric tracked vehicle and its adaptability validation. In *2019 IEEE Transportation Electrification Conference and Expo (ITEC)*, pages 1–6. IEEE, 2019.

[115] Xin Ma, Yuanchang Xie, and Chunxiao Chigan. Meta-deep q-learning for eco-routing. In *2019 IEEE 2nd Connected and Automated Vehicles Symposium (CAVS)*, pages 1–5. IEEE, 2019.

[116] Max Peter Ronecker and Yuan Zhu. Deep q-network based decision making for autonomous driving. In *2019 3rd International Conference on Robotics and Automation Sciences (ICRAS)*, pages 154–160. IEEE, 2019.

[117] Pin Wang and Ching-Yao Chan. Formulation of deep reinforcement learning architecture toward autonomous driving for on-ramp merge. In *2017 IEEE 20th International Conference on Intelligent Transportation Systems (ITSC)*, pages 1–6. IEEE, 2017.

[118] Tomoki Nishi, Prashant Doshi, and Danil Prokhorov. Merging in congested freeway traffic using multipolicy decision making and passive actor-critic learning. *IEEE Transactions on Intelligent Vehicles*, 4(2):287–297, 2019.

[119] Omar Nassef, Luis Sequeira, Elias Salam, and Toktam Mahmoodi. Building a lane merge coordination for connected vehicles using deep reinforcement learning. *IEEE Internet of Things Journal*, 8(4):2540–2557, 2020.

[120] Tianzhu Ren, Yuanchang Xie, and Liming Jiang. Cooperative highway work zone merge control based on reinforcement learning in a connected and automated environment. *Transportation research record*, 2674(10):363–374, 2020.

[121] Sampo Kuutti, Richard Bowden, Yaochu Jin, Phil Barber, and Saber Fallah. A survey of deep learning applications to autonomous vehicle control. *IEEE Transactions on Intelligent Transportation Systems*, 2020.

[122] Nahid Parvez Farazi, Tanvir Ahamed, Limon Barua, and Bo Zou. Deep reinforcement learning and transportation research: A comprehensive review. *arXiv preprint arXiv:2010.06187*, 2020.

[123] Yang Zhou, Soyoung Ahn, Madhav Chitturi, and David A Noyce. Rolling horizon stochastic optimal control strategy for acc and cacc under uncertainty. *Transportation Research Part C: Emerging Technologies*, 83:61–76, 2017.

[124] Michael P Vitus and Claire J Tomlin. A probabilistic approach to planning and control in autonomous urban driving. In *52nd IEEE Conference on Decision and Control*, pages 2459–2464. IEEE, 2013.

[125] Yulong Gao, Frank J Jiang, Karl H Johansson, and Lihua Xie. Stochastic Modeling and Optimal Control for Automated Overtaking. In *58th Conference on Decision and Control*, pages 1273–1278. IEEE, 2019.

[126] Ashwin Carvalho, Stéphanie Lefévre, Georg Schildbach, Jason Kong, and Francesco Borrelli. Automated driving: The role of forecasts and uncertainty—a control perspective. *European Journal of Control*, 24:14–32, 2015.

[127] Changchun Liu, Ashwin Carvalho, Georg Schildbach, and J Karl Hedrick. Stochastic predictive control for lane keeping assistance systems using a linear time-varying model. In *2015 American Control Conference (ACC)*, pages 3355–3360. IEEE, 2015.

[128] Ashwin Carvalho, Yiqi Gao, Stéphanie Lefevre, and Francesco Borrelli. Stochastic predictive control of autonomous vehicles in uncertain environments. In *12th International Symposium on Advanced Vehicle Control*, pages 712–719, 2014.

[129] Alexander Katriniok, Stefan Kojchev, Erjen Lefeber, and Henk Nijmeijer. A stochastic model predictive control approach for driver-aided intersection crossing with uncertain driver time delay. In *2019 18th European Control Conference (ECC)*, pages 243–249. IEEE, 2019.

[130] Damion D Dunlap, Emmanuel G Collins Jr, and Charmane V Caldwell. Sampling based model predictive control with application to autonomous vehicle guidance. In *Florida Conference on Recent Advances in Robotics*, 2008.

[131] Karl Berntorp and Stefano Di Cairano. Joint decision making and motion planning for road vehicles using particle filtering. *IFAC-PapersOnLine*, 49(11):175–181, 2016.

[132] Karl Berntorp, Tru Hoang, and Stefano Di Cairano. Motion planning of autonomous road vehicles by particle filtering. *IEEE Transactions on Intelligent Vehicles*, 4(2): 197–210, 2019.

[133] Georg Schildbach and Francesco Borrelli. Scenario model predictive control for lane change assistance on highways. In *2015 IEEE Intelligent Vehicles Symposium (IV)*, pages 611–616. IEEE, 2015.

[134] Ashwin Mark Carvalho. *Predictive Control under Uncertainty for Safe Autonomous Driving: Integrating Data-Driven Forecasts with Control Design*. PhD thesis, UC Berkeley, 2016.

[135] Tim Brüdigam, Michael Olbrich, Dirk Wollherr, and Marion Leibold. Stochastic model predictive control with a safety guarantee for automated driving. *IEEE Transactions on Intelligent Vehicles*, 2021.

[136] Carl Edward Rasmussen. Gaussian processes in machine learning. In *Summer School on Machine Learning*, pages 63–71. Springer, 2003.

[137] Achin Jain, Truong Nghiem, Manfred Morari, and Rahul Mangharam. Learning and control using gaussian processes. In *2018 ACM/IEEE 9th International Conference on Cyber-Physical Systems (ICCPS)*, pages 140–149. IEEE, 2018.

[138] Torsten Koller, Felix Berkenkamp, Matteo Turchetta, and Andreas Krause. Learning-based model predictive control for safe exploration. In *2018 IEEE conference on decision and control (CDC)*, pages 6059–6066. IEEE, 2018.

[139] Felix Berkenkamp and Angela P Schoellig. Safe and robust learning control with gaussian processes. In *2015 European Control Conference (ECC)*, pages 2496–2501. IEEE, 2015.

[140] Tim Brüdigam, Alexandre Capone, Sandra Hirche, Dirk Wollherr, and Marion Leibold. Gaussian process-based stochastic model predictive control for overtaking in autonomous racing. *arXiv preprint arXiv:2105.12236*, 2021.

[141] Lukas Hewing, Alexander Liniger, and Melanie N Zeilinger. Cautious nmpc with gaussian process dynamics for autonomous miniature race cars. In *2018 European Control Conference (ECC)*, pages 1341–1348. IEEE, 2018.

[142] Juraj Kabzan, Lukas Hewing, Alexander Liniger, and Melanie N Zeilinger. Learning-based model predictive control for autonomous racing. *IEEE Robotics and Automation Letters*, 4(4):3363–3370, 2019.

[143] Chris J Ostafew, Angela P Schoellig, Timothy D Barfoot, and Jack Collier. Learning-based nonlinear model predictive control to improve vision-based mobile robot path tracking. *Journal of Field Robotics*, 33(1):133–152, 2016.

[144] Chris J Ostafew, Angela P Schoellig, and Timothy D Barfoot. Robust constrained learning-based nmpc enabling reliable mobile robot path tracking. *The International Journal of Robotics Research*, 35(13):1547–1563, 2016.

[145] Jaime F Fisac, Anayo K Akametalu, Melanie N Zeilinger, Shahab Kaynama, Jeremy Gillula, and Claire J Tomlin. A general safety framework for learning-based control in uncertain robotic systems. *IEEE Transactions on Automatic Control*, 64(7):2737–2752, 2018.

[146] Anayo K Akametalu, Jaime F Fisac, Jeremy H Gillula, Shahab Kaynama, Melanie N Zeilinger, and Claire J Tomlin. Reachability-based safe learning with gaussian processes. In *53rd IEEE Conference on Decision and Control*, pages 1424–1431. IEEE, 2014.

[147] H Rong, AP Teixeira, and C Guedes Soares. Ship trajectory uncertainty prediction based on a gaussian process model. *Ocean Engineering*, 182:499–511, 2019.

[148] Truong X Nghiem and Colin N Jones. Data-driven demand response modeling and control of buildings with gaussian processes. In *2017 American Control Conference (ACC)*, pages 2919–2924. IEEE, 2017.

[149] Aaron D Ames, Xiangru Xu, Jessy W Grizzle, and Paulo Tabuada. Control barrier function based quadratic programs for safety critical systems. *IEEE Transactions on Automatic Control*, 62(8):3861–3876, 2016.

[150] Aaron D Ames, Jessy W Grizzle, and Paulo Tabuada. Control barrier function based quadratic programs with application to adaptive cruise control. In *53rd IEEE Conference on Decision and Control*, pages 6271–6278. IEEE, 2014.

[151] Aakar Mehra, Wen-Loong Ma, Forrest Berg, Paulo Tabuada, Jessy W Grizzle, and Aaron D Ames. Adaptive cruise control: Experimental validation of advanced controllers on scale-model cars. In *2015 American control conference (ACC)*, pages 1411–1418. IEEE, 2015.

[152] Quan Nguyen and Koushil Sreenath. Exponential control barrier functions for enforcing high relative-degree safety-critical constraints. In *2016 American Control Conference (ACC)*, pages 322–328. IEEE, 2016.

[153] Wei Xiao and Calin Belta. Control barrier functions for systems with high relative degree. In *2019 IEEE 58th conference on decision and control (CDC)*, pages 474–479. IEEE, 2019.

[154] Aaron D Ames, Samuel Coogan, Magnus Egerstedt, Gennaro Notomista, Koushil Sreenath, and Paulo Tabuada. Control barrier functions: Theory and applications. In *2019 18th European control conference (ECC)*, pages 3420–3431. IEEE, 2019.

[155] Wei Xiao, Christos G Cassandras, and Calin A Belta. Bridging the gap between optimal trajectory planning and safety-critical control with applications to autonomous vehicles. *Automatica*, 129:109592, 2021.

[156] Wei Xiao, Calin Belta, and Christos G Cassandras. Decentralized merging control in traffic networks: A control barrier function approach. In *Proceedings of the 10th ACM/IEEE International Conference on Cyber-Physical Systems*, pages 270–279, 2019.

[157] Manuel Rodriguez and Hosam Fathy. Vehicle and traffic light control through gradient-based coordination and control barrier function safety regulation. *Journal of Dynamic Systems, Measurement, and Control*, 144(1), 2022.

[158] Samaa Khaled, Omar M Shehata, and Elsayed I Morgan. Intersection control for autonomous vehicles using control barrier function approach. In *2020 2nd Novel Intelligent and Leading Emerging Sciences Conference (NILES)*, pages 479–485. IEEE, 2020.

[159] Kaiyuan Xu, Wei Xiao, and Christos G Cassandras. Feasibility guaranteed traffic merging control using control barrier functions. *arXiv preprint arXiv:2203.04348*, 2022.

[160] Shashwat Shivam, Yorai Wardi, Magnus Egerstedt, Aris Kanellopoulos, and Kyriakos G Vamvoudakis. Intersection-traffic control of autonomous vehicles using newton-raphson flows and barrier functions. *IFAC-PapersOnLine*, 53(2):15733–15738, 2020.

[161] Alexander Katriniok. Control-sharing control barrier functions for intersection automation under input constraints. *arXiv preprint arXiv:2111.10205*, 2021.

[162] Wei Xiao, Calin A Belta, and Christos G Cassandras. Sufficient conditions for feasibility of optimal control problems using control barrier functions. *Automatica*, 135: 109960, 2022.

[163] Haoji Liu, Weichao Zhuang, Guodong Yin, Rongcan Li, Chang Liu, and Shanxing Zhou. Decentralized on-ramp merging control of connected and automated vehicles in the mixed traffic using control barrier functions. In *2021 IEEE International Intelligent Transportation Systems Conference (ITSC)*, pages 1125–1131. IEEE, 2021.

[164] Patrick Grim, Robert Rosenberger, Adam Rosenfeld, Brian Anderson, and Robb E Eason. How simulations fail. *Synthese*, 190(12):2367–2390, 2013.

[165] Mitra Pahlavan, Marina Papatriantafilou, and Elad M Schiller. Gulliver: a test-bed for developing, demonstrating and prototyping vehicular systems. In *Proceedings of the 9th ACM international symposium on Mobility management and wireless access*, pages 1–8, 2011.

[166] Jakob Axelsson, Avenir Kobetski, Ze Ni, Shuzhou Zhang, and Eilert Johansson. Moped: A mobile open platform for experimental design of cyber-physical systems. In *2014 40th EUROMICRO Conference on Software Engineering and Advanced Applications*, pages 423–430. IEEE, 2014.

[167] Liam Paull, Jacopo Tani, Heejin Ahn, Javier Alonso-Mora, Luca Carlone, Michal Cap, Yu Fan Chen, Changhyun Choi, Jeff Dusek, and ... Duckietown: An open, inexpensive and flexible platform for autonomy education and research. In *Proceedings of the IEEE International Conference on Robotics and Automation*, pages 1497–1504, 2017.

[168] Shenbagaraj Kannapiran and Spring Berman. Go-chart: A miniature remotely accessible self-driving car robot. In *2020 IEEE/RSJ International Conference on Intelligent Robots and Systems (IROS)*, pages 2265–2272, 2020.

[169] Nicholas Hyaldmar, Yijun He, and Amanda Porok. A fleet of miniature cars for experiments in cooperative driving. In *Proceedings of the IEEE International Conference on Robotics and Automation*, 2019.

[170] Sean Wilson, Paul Glotfelter, Li Wang, Siddharth Mayya, Gennaro Notomista, Mark Mote, and Magnus Egerstedt. The robotarium: Globally impactful opportunities, challenges, and lessons learned in remote-access, distributed control of multirobot systems. *IEEE Control Systems Magazine*, 40(1):26–44, 2020.

[171] Maximilian Kloock, Patrick Scheffe, Janis Maczijewski, Alexandru Kampmann, Armin Mokhtarian, Stefan Kowalewski, and Bassam Alrifaee. Cyber-physical mobility lab: An open-source platform for networked and autonomous vehicles. In *2021 European Control Conference (ECC)*, pages 1937–1944. IEEE, 2021.

[172] Adrián Jiménez-González, Jose Ramiro Martinez-de Dios, and Anibal Ollero. Testbeds for ubiquitous robotics: A survey. *Robotics and Autonomous Systems*, 61(12):1487–1501, 2013.

[173] Alessandro Colombo. A mathematical framework for cooperative collision avoidance of human-driven vehicles at intersections. In *2014 11th International Symposium on Wireless Communications Systems, ISWCS 2014 - Proceedings*, 2014. ISBN 9781479958634.

[174] Jean Gregoire, Silvere Bonnabel, and Arnaud De La Fortelle. Priority-based intersection management with kinodynamic constraints. *2014 European Control Conference, ECC 2014*, pages 2902–2907, 2014.

[175] Behdad Chalaki and Andreas A Malikopoulos. Optimal control of connected and automated vehicles at multiple adjacent intersections. *IEEE Transactions on Control Systems Technology*, 30(3):972–984, 2022.

[176] Behdad Chalaki and Andreas A Malikopoulos. Time-optimal coordination for connected and automated vehicles at adjacent intersections. *IEEE Transactions on Intelligent Transportation Systems*, 2021.

[177] Behdad Chalaki and Andreas A Malikopoulos. A hysteretic q-learning coordination framework for emerging mobility systems in smart cities. In *2021 European Control Conferences (ECC)*, pages 17–22, 2021.

[178] Behdad Chalaki and Andreas A. Malikopoulos. A priority-aware replanning and resequencing framework for coordination of connected and automated vehicles. *IEEE Control Systems Letters*, 6:1772–1777, 2022.

[179] Behdad Chalaki and Andreas A Malikopoulos. Robust learning-based trajectory planning for emerging mobility systems. In *2022 American Control Conference (ACC)*, pages 2154–2159, 2022.

[180] Behdad Chalaki and Andreas A Malikopoulos. A Barrier-Certified Optimal Coordination Framework for Connected and Automated Vehicles. *arXiv:2203.16418 (in review)*, 2022.

[181] Raymond M. Zayas, Logan E. Beaver, Behdad Chalaki, Heeseung Bang, and Andreas A. Malikopoulos. A digital smart city for emerging mobility systems. *arXiv:2109.02811*, 2021.

[182] Heeseung Bang, Behdad Chalaki, and Andreas A Malikopoulos. Combined Optimal Routing and Coordination of Connected and Automated Vehicles. *IEEE Control Systems Letters*, 6:2749–2754, 2022.

[183] Meera Ratnagiri, Clare O'Dwyer, Logan E. Beaver, Behdad Chalaki, Heeseung Bang, and Andreas A. Malikopoulos. A scalable last-mile delivery service: From simulation to scaled experiment. *arXiv:2109.05995*, 2021.

[184] Behdad Chalaki, Logan E Beaver, Ben Remer, Kathy Jang, Eugene Vinitsky, Alexandre Bayen, and Andreas A Malikopoulos. Zero-shot autonomous vehicle policy transfer: From simulation to real-world via adversarial learning. In *IEEE 16th International Conference on Control & Automation (ICCA)*, pages 35–40, 2020.

[185] Kathy Jang, Eugene Vinitsky, Behdad Chalaki, Ben Remer, Logan Beaver, Andreas A Malikopoulos, and Alexandre Bayen. Simulation to scaled city: zero-shot policy transfer for traffic control via autonomous vehicles. In *Proceedings of the 10th ACM/IEEE International Conference on Cyber-Physical Systems*, pages 291–300, 2019.

[186] Federal Highway Administration. Department of Transportation. www.safety.fhwa.dot.gov/intersection, online.

[187] A. A. Malikopoulos. Stochastic optimal control for series hybrid electric vehicles. *2013 American Control Conference*, pages 1189–1194, 2013.

[188] Andreas A Malikopoulos, Panos Y Papalambros, and Dennis N Assanis. Online identification and stochastic control for autonomous internal combustion engines. *Journal of dynamic systems, measurement, and control*, 132(2):024504, 2010.

[189] A. A. Malikopoulos, P.Y. Papalambros, and D.N. Assanis. Optimal engine calibration for individual driving styles. In *SAE Congress*, 2008.

[190] Arthur Earl Bryson and YU Chi Ho. *Applied optimal control: optimization, estimation and control*. CRC Press, 1975.

[191] *PTV VISSIM 11 User manual*. Planung Transport Verkehr AG,, Karlsruhe, Germany, 2018.

[192] Rainer Wiedemann. *Simulation des Strassenverkehrsflusses*. PhD thesis, Universität Karlsruhe, 1974.

[193] Md Abdus Samad Kamal, Masakazu Mukai, Junichi Murata, and Taketoshi Kawabe. Model predictive control of vehicles on urban roads for improved fuel economy. *IEEE Transactions on control systems technology*, 21(3):831–841, 2012.

[194] Michael L Pinedo. *Scheduling: theory, algorithms, and systems*. Springer, 2016.

[195] Ignacio E Grossmann and Juan P Ruiz. Generalized disjunctive programming: A framework for formulation and alternative algorithms for minlp optimization. In *Mixed Integer Nonlinear Programming*, pages 93–115. Springer, 2012.

[196] *IBM ILOG CPLEX Optimization Studio V12.10.0 documentation*. International Business Machines Corporation, Armonk, NY, 2019.

[197] Li Meng-Lin, Chen Shao-Fei, and Chen Jing. Adaptive learning: A new decentralized reinforcement learning approach for cooperative multiagent systems. *IEEE Access*, 2020.

[198] Laëtitia Matignon, Guillaume J Laurent, and Nadine Le Fort-Piat. Hysteretic q-learning: an algorithm for decentralized reinforcement learning in cooperative multi-agent teams. In *2007 IEEE/RSJ International Conference on Intelligent Robots and Systems*, pages 64–69. IEEE, 2007.

[199] Jackeline Rios-Torres and Andreas A. Malikopoulos. Automated and Cooperative Vehicle Merging at Highway On-Ramps. *IEEE Transactions on Intelligent Transportation Systems*, 18(4):780–789, 2017.

[200] Huile Xu, Yi Zhang, Christos G Cassandras, Li Li, and Shuo Feng. A bi-level cooperative driving strategy allowing lane changes. *Transportation research part C: emerging technologies*, 120:102773, 2020.

[201] Tamas G Molnar, Adam K Kiss, Aaron D Ames, and Gábor Orosz. Safety-critical control with input delay in dynamic environment. *arXiv preprint arXiv:2112.08445*, 2021.

[202] Girolamo Cardano, T Richard Witmer, and Oystein Ore. *The rules of algebra: Ars Magna*, volume 685. Courier Corporation, 2007.

[203] D. Schrank, B. Eisele, and T Lomax. 2019 Urban Mobility Scorecard. Technical report, Texas A& M Transportation Institute, 2019.

[204] Allen I Fleishman. A method for simulating non-normal distributions. *Psychometrika*, 43(4):521–532, 1978.

[205] Friedrich Pukelsheim. The three sigma rule. *The American Statistician*, 48(2):88–91, 1994.

[206] Hassan K Khalil. Nonlinear systems third edition. *Patience Hall*, 115, 2002.

[207] Rajesh Rajamani. *Vehicle dynamics and control*. Springer Science & Business Media, 2011.

[208] Sebastian Thrun, Mike Montemerlo, Hendrik Dahlkamp, David Stavens, Andrei Aron, James Diebel, Philip Fong, John Gale, Morgan Halpenny, Gabriel Hoffmann, Kenny Lau, Celia Oakley, Mark Palatucci, Vaughan Pratt, Pascal Stang, Sven Strohband, Cedric Dupont, Lars Erik Jendrossek, Christian Koelen, Charles Markey, Carlo Rummel, Joe van Niekerk, Eric Jensen, Philippe Alessandrini, Gary Bradski, Bob Davies, Scott Ettinger, Adrian Kaehler, Ara Nefian, and Pamela Mahoney. Stanley: The robot that won the DARPA Grand Challenge. *Springer Tracts in Advanced Robotics*, 2007.

[209] Mark W Spong and Mathukumalli Vidyasagar. *Robot dynamics and control*. John Wiley & Sons, 2008.

[210] Ben Remer and Andreas A Malikopoulos. The multi-objective dynamic traveling salesman problem: Last mile delivery with unmanned aerial vehicles assistance. In *2019 American Control Conference (ACC)*, pages 5304–5309. IEEE, 2019.

[211] Martin Treiber, Ansgar Hennecke, and Dirk Helbing. Congested traffic states in empirical observations and microscopic simulations. *Physical review E*, 62(2):1805, 2000.

[212] Ziran Wang, Guoyuan Wu, and Matthew J Barth. Cooperative eco-driving at signalized intersections in a partially connected and automated vehicle environment. *IEEE Transactions on Intelligent Transportation Systems*, 21(5):2029–2038, 2019.

[213] Zhen Yang, Yiheng Feng, and Henry X Liu. A cooperative driving framework for urban arterials in mixed traffic conditions. *Transportation Research Part C: Emerging Technologies*, 124:102918, 2021.

[214] H. Yang, F. Almutairi, and H. Rakha. Eco-driving at signalized intersections: A multiple signal optimization approach. *IEEE Transactions on Intelligent Transportation Systems*, pages 1–13, 2020.

[215] Aditya Dave and Andreas A Malikopoulos. Structural results for decentralized stochastic control with a word-of-mouth communication. In *2020 American Control Conference (ACC)*, pages 2796–2801. IEEE, 2020.

[216] Aditya Dave and Andreas A Malikopoulos. Decentralized Stochastic Control in Partially Nested Information Structures. In *IFAC-PapersOnLine*, volume 52, pages 97–102, Chicago, IL, USA, 2019.

[217] Aditya Dave, Nishanth Venkatesh, and Andreas A Malikopoulos. On decentralized minimax control with nested subsystems. pages 3437–3444, 2022.

[218] Aditya Dave, Nishanth Venkatesh, and Andreas A Malikopoulos. On decentralized control of two agents with nested accessible information. pages 3423–3430, 2022.

[219] Ioannis Vasileios Chremos and Andreas A. Malikopoulos. Social resource allocation in a mobility system with connected and automated vehicles: A mechanism design problem. In *Proceedings of the 59th IEEE Conference on Decision and Control (CDC), 2020*, pages 2642–2647, 2020.

[220] Ioannis Vasileios Chremos, Logan E. Beaver, and Andreas A. Malikopoulos. A game-theoretic analysis of the social impact of connected and automated vehicles. In *2020 23rd International Conference on Intelligent Transportation Systems (ITSC)*, pages 2214–2219. IEEE, 2020.

[221] Ioannis Vasileios Chremos and Andreas A. Malikopoulos. An analytical study of a two-sided mobility game. In *2022 American Control Conference (ACC)*, pages 1254–1259, 2022.

[222] Ioannis Vasileios Chremos and Andreas A. Malikopoulos. Design and stability analysis of a shared mobility market. In *2021 European Control Conference (ECC)*, pages 375–380, 2021.

Appendix

PERMISSIONS

Thesis / Dissertation Reuse

The IEEE does not require individuals working on a thesis to obtain a formal reuse license, however, you may print out this statement to be used as a permission grant:

Requirements to be followed when using any portion (e.g., figure, graph, table, or textual material) of an IEEE copyrighted paper in a thesis:

1) In the case of textual material (e.g., using short quotes or referring to the work within these papers) users must give full credit to the original source (author, paper, publication) followed by the IEEE copyright line © 2011 IEEE.
2) In the case of illustrations or tabular material, we require that the copyright line © [Year of original publication] IEEE appear prominently with each reprinted figure and/or table.
3) If a substantial portion of the original paper is to be used, and if you are not the senior author, also obtain the senior author's approval.

Requirements to be followed when using an entire IEEE copyrighted paper in a thesis:

1) The following IEEE copyright/ credit notice should be placed prominently in the references: © [year of original publication] IEEE. Reprinted, with permission, from [author names, paper title, IEEE publication title, and month/year of publication]
2) Only the accepted version of an IEEE copyrighted paper can be used when posting the paper or your thesis on-line.
3) In placing the thesis on the author's university website, please display the following message in a prominent place on the website: In reference to IEEE copyrighted material which is used with permission in this thesis, the IEEE does not endorse any of [university/educational entity's name goes here]'s products or services. Internal or personal use of this material is permitted. If interested in reprinting/republishing IEEE copyrighted material for advertising or promotional purposes or for creating new collective works for resale or redistribution, please go to http://www.ieee.org/publications_standards/publications/rights/rights_link.html to learn how to obtain a License from RightsLink.

If applicable, University Microfilms and/or ProQuest Library, or the Archives of Canada may supply single copies of the dissertation.